Analysis and Description of High-Cycle Fatigue in Steel

Gansted-Mortensen, Lise

Publication date:
1991

Document Version
Publisher's PDF, also known as Version of record

INSTITUTTET FOR BYGNINGSTEKNIK
DEPT. OF BUILDING TECHNOLOGY AND STRUCTURAL ENGINEERING
AALBORG UNIVERSITETSCENTER • AUC • AALBORG • DANMARK

Ph.D.-Thesis defended publicly at the University of Aalborg
November 8, 1991

LISE GANSTED
ANALYSIS AND DESCRIPTION OF
HIGH-CYCLE STOCHASTIC FATIGUE IN STEEL
NOVEMBER 1991 **ISSN 0902-7513 R9135**

ANALYSIS AND DESCRIPTION OF HIGH-CYCLE STOCHASTIC FATIGUE IN STEEL

by

Lise Gansted

Department of Building Technology
and
Structural Engineering

University of Aalborg
Sohngaardsholmsvej 57
DK-9000 Aalborg
Denmark

ABSTRACT

Analysis of structures subjected to dynamic load has a still increasing influence on structural design due to increased demands on size of structures and requirements for minimum use of material. These and other factors as e.g. thermal loading and corrosive environments, give an increased risk of fatigue failure in structures or structural members. In relation to civil engineering, steel is of special interest because this material is used extensively in offshore structures, large bridges etc.

This is some of the background for the present thesis. A more detailed description and the scope of the thesis are given in chapter 1. The main question is: "Is it possible to establish a simple, numerical fatigue crack growth model in which all model parameters can be regarded as characteristic of the material and in which existing knowledge of fatigue are included ?"

The basic aspects of fatigue due to dynamic loads are described in chapter 2. The focus of interest is to give a physical understanding of the fatigue phenomenon and to introduce the two most well-known approaches to description of fatigue. Further, the different types of dynamic load and their effects on the fatigue process are described.

Existing empirically based fatigue models and their applications are discussed in chapter 3. Only the most important (most typical) models are included. The result of the state-of-the-art is that none of the models is able to describe the fatigue progress under any type of load in a satisfactory way.

An alternative is to use numerical models of which one of the most well-known (the B-model) is described and evaluated in chapter 4. It turns out that the basic principle of the model is good, but that the relation to the physical knowledge of fatigue is not directly used. Further, it is difficult to determine the model parameters.

On the basis of the numerical model in chapter 4, a new numerical model incorporating the physical knowledge of fatigue crack propagation is developed. The model is based on the assumption that the crack propagation progress can be described by a discrete space Markov theory. The model, which is described in chapter 5, is applicable to deterministic as well as to random loading. Once the model parameters for a given material have been determined, the results can be used for any structure as soon as the geometric function is known.

Introduction of a new model requires that it is tested in order to evaluate its applicability. Two tests have been performed, one using existing crack growth data for an aluminium alloy (chapter 6) and one using mild steel for which the crack growth data have been experimentally established in connection with the project, see chapter 7.

The analyses of the simulated crack growth data compared to the exsisting data in chapter 6 show that for adequate choice of the model parameters, good agreement is obtained. The comparison is based on qualitative as well as quantitative demands such as the form of the curves and statistical properties. The latter is compared on the basis of a norm, and a discussion which property is the most important is performed.

Similar analyses of the qualitative and statistical properties of the experimentally established fatigue crack growth data compared with simulated data are performed in chapter 7 and give the same results.

Thus, it should be possible for a given material, for which only a few material parameters must be experimentally determined, to apply the developed model to simulation of fatigue crack growth data.

Finally, in chapter 8 it is concluded that the results of the thesis are: On the basis of existing knowledge of fatigue and fatigue models, a new, simple, numerical fatigue crack growth model has been established and tested with a satisfactory result; a large number of fatigue data for mild steel have been established experimentally and the work has potentials for further research.

Appendix A contains an introduction to linear elastic fracture mechanics including derivation of stress and displacement fields.

Comparison of two cycle counting methods is performed in appendix B in the form of an illustrative example.

Appendix C gives an overview of the programs developed in connection with the thesis.

The simulated fatigue crack growth curves used in chapter 6 are shown in appendix D. Only one typical plot from each simulation series is included. Remaining curves are obtainable from the author.

In appendix E, the simulated fatigue crack growth curves based on the experimentally established parameters in chapter 7 are shown.

KEYWORDS

Fatigue process mechanisms, fracture mechanics, constant-amplitude load, variable-amplitude load, random load, fatigue crack growth models, improved numerical fatigue crack growth model, Markov assumptions, random material properties, numerical tests, experimental tests.

PREFACE

The present thesis has been carried out at the Department of Building Technology and Structural Engineering at the University of Aalborg, Denmark from August 1987 to August 1991 as part of a project on "Random Fatigue" supported by the Danish Technical Research Council (STVF).

The thesis consists of 8 chapters and 5 appendices. The figures/tables as well as the formulas are numbered successively within a chapter. The references, which are stated: [Author(s); Year, p./ch.] in the text (p. = page, ch. = chapter), appear alphabetically in **REFERENCES** p. 129-139. Sources used as a basis for the thesis - but without a direct reference - are located separately in **OTHER LITERATURE** p. 141-143.

ACKNOWLEDGEMENTS

The thesis has been made under the supervision of associate professor Lars Pilegaard Hansen and senior lecturer Rune Brincker to whom I am very grateful for good inspiration and cooperation.

Furthermore, I would like to express my gratitude to the staff at the Laboratory of Structural Engineering, led by engineering assistent Henning Andersen, for careful performance of test specimens and test equipment.

The preparation of the figures for the thesis has been carried out by draughtsman Mrs. Norma Hornung and skilful proofreading of the manuscript by senior secretary Mrs. Kirsten Aakjær. Their work is greatly appriciated.

In addition, thanks to professor B.M. Hillberry, Purdue University, Indiana (USA), for giving his permission to use the Virkler data in the tests of the fatigue model, which is developed in this thesis.

Finally, I thank the Danish Technical Research Council, without their support I would have been unable to prepare this thesis.

Aalborg, October 11, 1991

Lise Gansted

LIST OF CONTENTS

1. INTRODUCTION

A structure is said to have failed when it no longer serves its purpose. Failure of a structure is caused by loss of the static or dynamic load-carrying or by damage accumulation exceeding some limit. The former is known as static failure and as dynamic failure, whereas the latter is also known as fatigue. Static failure as well as the dynamic failure are characterized by the structure being influenced by low-frequency action, whereas fatigue results from high-frequency action.

Fatigue failure is often defined as fracture due to initiation and propagation of a crack as a result of an alternating uniaxial stress less than the yield or ultimate stress. Thus, the resistance of a given structure against static stress can be sufficient, whereas a dynamic stress may lead to fracture for a stress range much less than the static stress. The stress range is the difference between the maximum stress and the minimum stress in a load cycle.

The static failure modes as yielding, buckling, fracture or the dynamic failure mode in the form of unacceptable deformations due to dynamic amplification can - at a reasonable probability - be avoided using the design and safety codes in the design and performance of structures. These codes are based on the knowledge of appropriate solutions to the static and dynamic failure modes and give a sufficient/acceptable reliability of the structures, provided they are used for their intents.

Some of the consequences for a structure not serving its purpose are inconveniences for the users, loss of human life and great economic costs.

Fatigue failure can appear in any part of a structure, but empirical experience shows that connections form a special weak part.

Generally, the design and safety codes only include empirical rules in order to avoid fatigue failure. This gives occasion for the following question: "Is it possible to give an estimate of the fatigue crack growth process in a structure of arbitrary geometry in a given material by use of a simple, numerical model ?"

This initiating problem is concretized by analysis of which factors influence a fatigue failure.

As mentioned earlier, dynamic stress has a large influence. The characterization of the alternating stress depends on the type of the dynamic load. It is common to distinguish between

- deterministic, cyclic, constant-amplitude load
- deterministic, cyclic, variable-amplitude load
- random load

see also figure 1.1. Multiaxial load cases will not be considered in the present thesis.

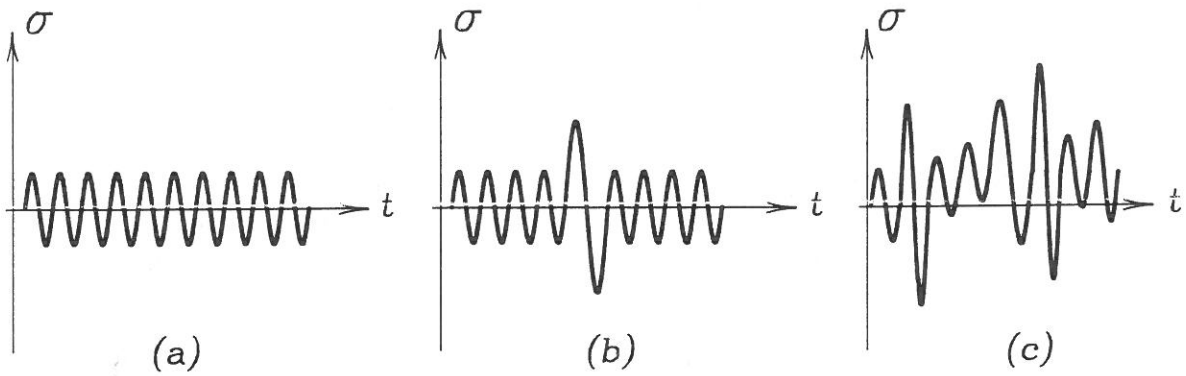

Figure 1.1: Different types of load. (a) deterministic, cyclic, constant-amplitude load. (b) deterministic, cyclic, variable-amplitude load. (c) random load.

In addition to the dynamic load, the damage accumulation is influenced by the material properties, the geometry of the structure, the loading frequency and the environments (e.g. corrosive environment and thermal loading). The two last-mentioned items will not be further discussed in the present thesis.

The material properties are characterized by the material parameters - in the form of Young's modulus E, Poisson's ratio ν, yield stress f_y, ultimate stress f_u and fracture toughness K_c - and by the possible inclusions and defects.

The geometry of the structure influences the stress state in the structure. Especially, sudden changes in geometry, such as notches and other discontinuities, have a significant influence on damage accumulation.

Depending upon the stress level which the dynamic load causes in a structure a distinction between low-cycle fatigue and high-cycle fatigue is made. Fatigue failure occurring after only $\approx 10^4$ cycles caused by a high stress level is denoted low-cycle fatigue, whereas a low stress level allowing $\approx 10^6$ cycles or even more before fatigue failure occurs is denoted high-cycle fatigue. Only the latter case will be discussed, because high-cycle fatigue is that type of fatigue, which most frequently occurs in civil engineering structures.

An analysis of the resistance of a structure against damage accumulation demands an understanding of the mechanisms of fatigue; description of fatigue damage process; how to avoid, survey, detect and repair fatigue damage.

A physical understanding of the mechanisms of fatigue is a necessity in order to be able to fulfil the other subjects in the analysis. Based on this physical knowledge of fatigue the fatigue damage process is described in order to predict when the damage becomes critical. Further, criteria of crack growth, failure and fracture have to be established.

To avoid damage, rational design is required, but since it is possible to have stress levels exceeding the maximum stress used in the design, surveillance is necessary. Regular inspection of the most critical parts of the structure, i.e. typically parts with large stress gradients such as joints and roots of notches, is in many cases the

most simple form of control. Detection of fatigue damage in a structure can be performed in different ways. The most appropriate is to use a non-destructive test, e.g. visual observation or X-ray scanning. The subject of damage detection will not be further discussed. In case failure of a component in a structure (local failure) does not lead to failure of the structure (global failure), repair or replacement of the component might take place.

The still increasing demands on size and slimness of structures in civil engineering (off-shore platforms, bridges etc.), and the fact that, apart from being influenced by static load, far the most structures in civil engineering are influenced by dynamic load, have increased the necessity for failure analysis with regard to dynamic load, i.e. fatigue analysis.

All types of material used in civil engineering (e.g. steel, concrete, wood) are of interest in fatigue analysis, but in the present thesis the scope is restricted to mild steel because this material is used extensively and because structures of this material have caused lots of fatigue failures - especially in connections.

On the basis of the analysis of the problem, the initiating problem is re-formulated to "Is it possible to establish a simple, numerical fatigue crack growth model in which all model parameters can be regarded as characteristic of the material and in which existing knowledge of fatigue are included ?"

The model must give a satisfactory estimate of the fatigue crack growth process in a structure of arbitrary geometry in a given material. The scope of the thesis includes

- description of the basic aspects of fatigue for the purpose of obtaining knowledge and understanding of the phenomenon "fatigue", (chapter 2),
- information of existing empirically based fatigue models and their applications, given as a state-of-the-art, (chapter 3),
- description of a numerical fatigue model recently developed, (chapter 4).

where these subjects are investigated in order to serve as a basis for

- establishment of an improved fatigue model in which all parameters are assumed to be characteristic of the material. Provided that this assumption is fulfilled the model can be used for any geometry (given the geometry function) in a given steel material, (chapter 5).

The model will be tested in two ways:

- Numerical tests in the form of simulations which are compared with existing data, (chapter 6).
- Experimental tests in which the model parameters are determined and the results are compared with the model, (chapter 7).

Finally,

- the conclusions and objects for further research are given in chapter 8.

2. BASIC ASPECTS OF FATIGUE

The purpose of this chapter is to obtain knowledge and understanding of the basic aspects of fatigue in order to establish an improved fatigue model, as stated in chapter 1.

Emphasizing the process of fatigue, a qualitative description of the properties of fatigue is given in section 2.1. Micro level as well as macro level are included. Different approaches to quantitative description of fatigue at macro level are described in section 2.2, and a discussion of which approach is the most appropriate is performed. Characterization of the different types of dynamic load mentioned in chapter 1 is given in section 2.3. Further, it is described how the number of load cycles can be counted. The effects on the progress of fatigue from the loads described in section 2.3 are investigated in section 2.4, including the possible causes of the effects.

Finally, some concluding remarks on the basic aspects of fatigue are given in section 2.5.

2.1 THE PROCESS OF FATIGUE

The purpose of the description of the process of fatigue performed in this section is to give an overview of the different stages occurring during damage accumulation (i.e. the irreversible accumulation of damage through lifetime which ultimately causes failure) and the mechanisms which lead to the fatigue failure.

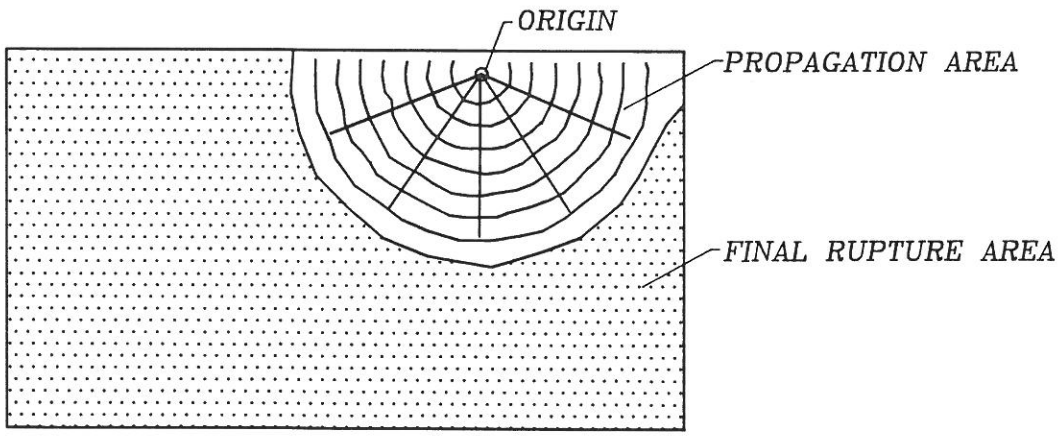

Figure 2.1: Typical fatigue fracture surface.
Based on [Gurney, T.R.; 1979, p.5].

Studying the surface of a fatigue fracture, three characteristic areas are observed: the origin, the propagation area and the area of final rupture, occurring when the remaining area is insufficient to support the applied load. A typical fatigue fracture surface is shown in figure 2.1.

The point of origin is often located on the surface of the structure in the region of the highest strain concentration. An important exception is welds in which the origin sometimes is inside the weld material. The propagating area, where stable crack growth takes place, is characterized by a smooth surface on which concentric circles and radial lines appear with the point of origin as centre. The circles are striation marks formed by the propagating crack as a result of a step-by-step plastic blunting process (described in figure 2.4). The radial lines indicate the propagation directions. If the stresses are low, but large enough to cause fatigue crack growth, the propagation area is large compared with the final rupture area and vice versa. The direction of propagation is perpendicular to the stresses causing the crack propagation. The appearance of the final rupture area, i.e. where unstable crack growth takes place, depends on the nature of the material, i.e. if the material is brittle or ductile, see also [Gurney, T.R.; 1979, p.4-7] and [Hellan, K.; 1985, p.167-168].

A fracture in a brittle material is characterized by the cleavage of the grains and/or the separation along grain boundaries, also known as transcrystalline fracture and intercrystalline fracture, respectively. Thus, the grain structure is clearly seen.

If a ductile material possesses yielding ability it can sustain large deformations before fracture occurs. The deformations are due to initiation and coalescence of voids, formed around inclusions. The fracture surface has a characteristic fibrous appearance.

Due to the observations mentioned above, it is common to subdivide the process of fatigue into three main stages: initiation of crack(s), crack propagation and failure, see figure 2.2.

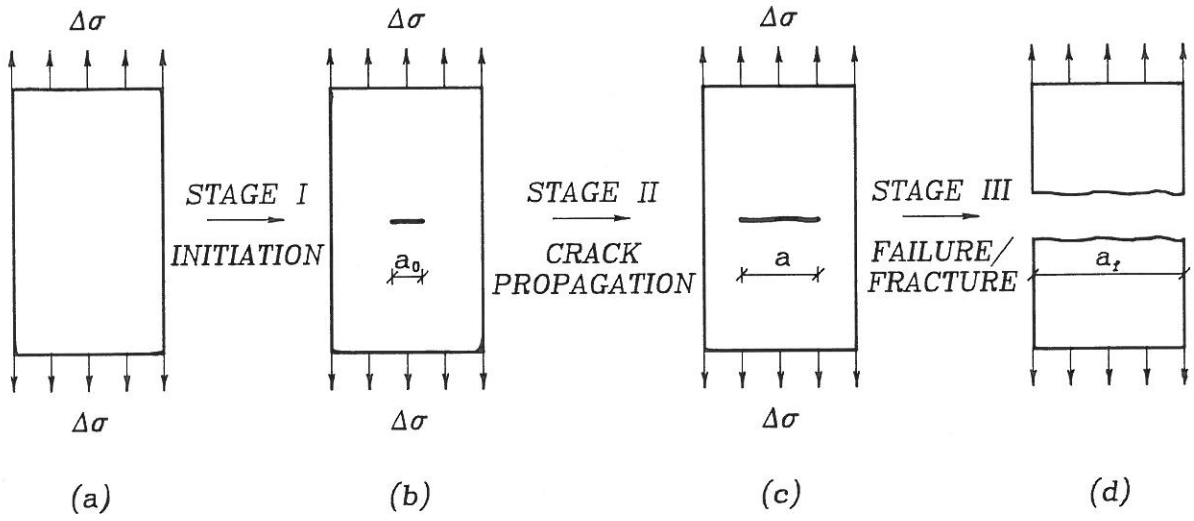

Figure 2.2: Process of fatigue. $\Delta\sigma$ = applied stress range. (a) Uncracked specimen. (b) Initial crack length a_0. (c) Macro crack length a. (d) Failure crack length a_f/critical crack length a_c.

The three stages will be further described in the following.

Besides cracks starting from macroscopic precracks (e.g. notches), cracks may develop from originally uncracked structures. From a microscopic point of view, crack initiation often occurs in slip planes near the surface of the structure or near internal material inhomogeneities as voids and inclusions. Otherwise, cracks may be initiated in the grain boundaries.

Initiation of a micro crack is due to slip, generated as a result of localized plastic deformation occurring by movement of dislocations. Slip is regarded as bands separated by slip planes, i.e. planes of maximum shear stress. Thus, the slip generated micro crack propagates at an angle of $\pm 45°$ with respect to the first principal axis, and this crack growth along the slip planes is named *stage I* or *shear mode propagation.*

[Gdoutos, E.E. and G. Papakaliatakis; 1987] propose that the strain energy dissipation density can be used as a damage initiation criterion, i.e. when the strain energy density reaches a critical value, the plastic deformation results in micro cracking.

The theories of slip and dislocation are further discussed in [Mughrabi, H., R. Wang, K. Differt and U. Essmann; 1983] and [Ewalds, H.L. and R.J.H. Wanhill; 1984, p.232-235].

The extent of the micro crack is rather small, e.g. [Lemaitre, J.; 1986] has estimated a value of 0.1 mm in metals. The number of load cycles spent in *stage I* is strongly dependent on the material micro structure, the load sequence and the geometry of the structure.

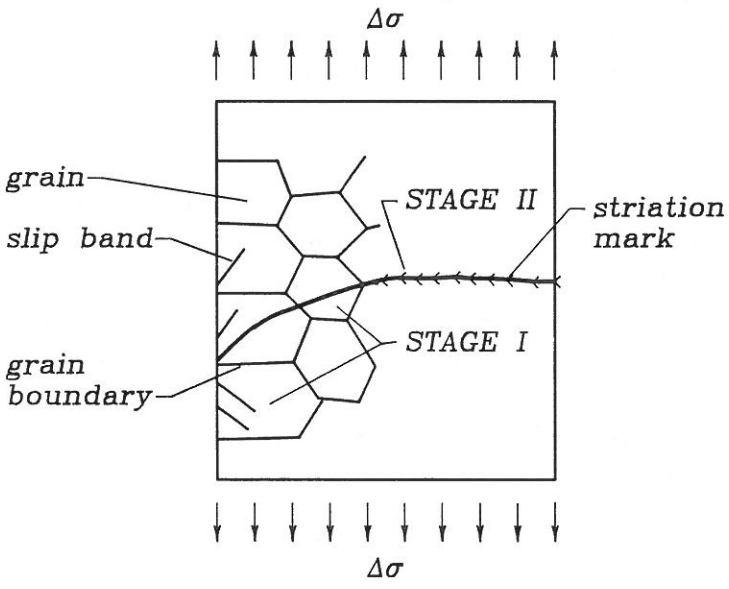

Figure 2.3: Illustration of *stage I* and *stage II* propagation.
From [Laird, C.; 1967].

As illustrated in figure 2.3, *stage II* propagation succeeds *stage I.* The transition from *stage I* to *stage II* propagtion takes place when the dislocation movements become large in magnitude as well as in number. At *stage II*, the macro crack propagates normally to the maximum tensile direction, which is the reason why this stage is also

denoted *tensile mode propagation.*

According to [Laird, C.; 1967], crack propagation at *stage II* under deterministic, cyclic, constant-amplitude load with mean value zero (see also section 2.3) is due to the plastic blunting process, i.e. the repetitive blunting during the tensile part of the load cycle and resharpening of the crack tip during the compressive part, see figure 2.4.

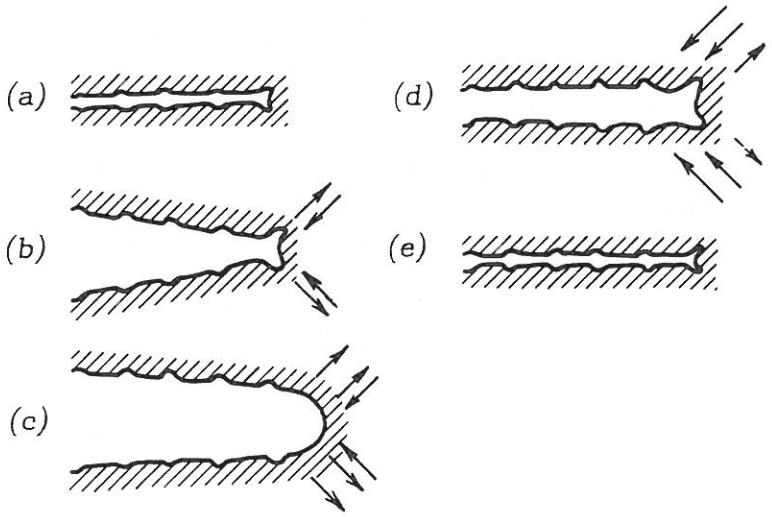

Figure 2.4: The plastic blunting process. (a) Unloaded crack, crack closed. (b) Small tensile load. (c) Maximum tensile load. Crack tip blunting. (d) Small compressive load. (e) Maximum compressive load. Crack tip sharpening of the increased crack.
From [Laird, C.; 1967].

The plastic blunting process begins with an unloaded crack where the crack is closed, figure 2.4(a). During the tensile part of the load cycle, large plastic strains at the crack tip cause localized slip, figure 2.4(b). When the tensile load obtains its maximum value, see figure 2.4(c), the plastic zone in front of the crack tip results in blunting of the crack tip. During unloading and the compressive part of the load cycle, the crack surfaces are forced together and parts of the crack are closed, figure 2.4(d). Finally, after completion of the compressive load, the increased crack is resharpened, see figure 2.4(e). The process (b)-(e) can start again.

Thus, *stage II* propagation is a result of irreversible plastic separation, in the form of slip, of the material at the crack tip.

If a micro crack is developed from a smooth (no defects) surface or from a surface with small defects (inclusions), 80-90% of the number of load cycles to cause failure is spent at *stage I* and thus, only 10-20% at *stage II*, [Laird, C.; 1967]. In case of larger defects, e.g. notches, about 90% of the number of load cycles to cause failure is spent at *stage II*, see [Schijve, J.; 1979].

After a crack has entered *stage II*, about 75% of the number of load cycles to cause

failure is spent on propagating the crack 25% of the failure crack length a_f, see also figure 2.14.

The last stage in the process of fatigue is the failure stage. As mentioned in chapter 1, fatigue failure can be defined as fracture or as the damage accumulation exceeding some limit.

Fracture is a failure mechanism in which unstable crack propagtion takes place in a structure. Thus, once the crack has started propagating, it enters into an accelerating growth ending with final rupture.

The final rupture takes place when $a = a_c$, i.e. when the crack length reaches the critical crack length. This fracture criterion corresponds to the energy release rate obtains the critical energy release rate, i.e. $\mathcal{G} = \mathcal{G}_c$. Griffith introduced $\mathcal{G}_c$, which is the loss of potential energy per unit of generated fracture surface, see e.g. [Hellan, K.; 1985, p.5].

The other definition of failure can be expressed by different criteria: A maximum permissible crack length can be prescribed, i.e. if $a \geq a_f$ failure is said to have occurred. Alternatively, failure can correspond to the maximum deformation exceeding a prescribed value.

For a given thickness, the state at the crack tip depends on the size of the volume - and thus the amount of energy - which is required before the state is developed. Thus, the volume which is in yielding in plane strain, is proportional to the square of the crack length, whereas the volume which is in yielding in plane stress is linearly dependent on the crack length. Since the proportional constant in the former case is most cases will be smaller than in the latter case, the state of the crack tip will initially be in plane strain. When the crack length increases, plane stress will take over.

This explains why the orientation of the fatigue surface to the loading direction changes through lifetime depending on the state of strain and stress.

Near the origin, the plastic zone in front of the micro crack is much smaller than the thickness of the specimen which results in plane strain condition. This corresponds to the maximum shear stress occurring at an angle of $\pm 45°$ to the first principal axis, as described earlier.

As long as the plain strain condition holds in the tensile mode propagation, the crack front is orientated perpendicular to the loading direction.

As the plastic zone in front of the crack tip becomes larger, plane stress occurs where the crack tip intersects the surfaces resulting in initial shear lip formation, see figure 2.5.

When the plastic zone obtains a dimension comparable to the thickness of the specimen, plane stress condition takes over. The fatigue surface is reorientated corresponding to an angle of 45° to the surfaces and to the loading direction. Either single or double shear lip(s) is formed.

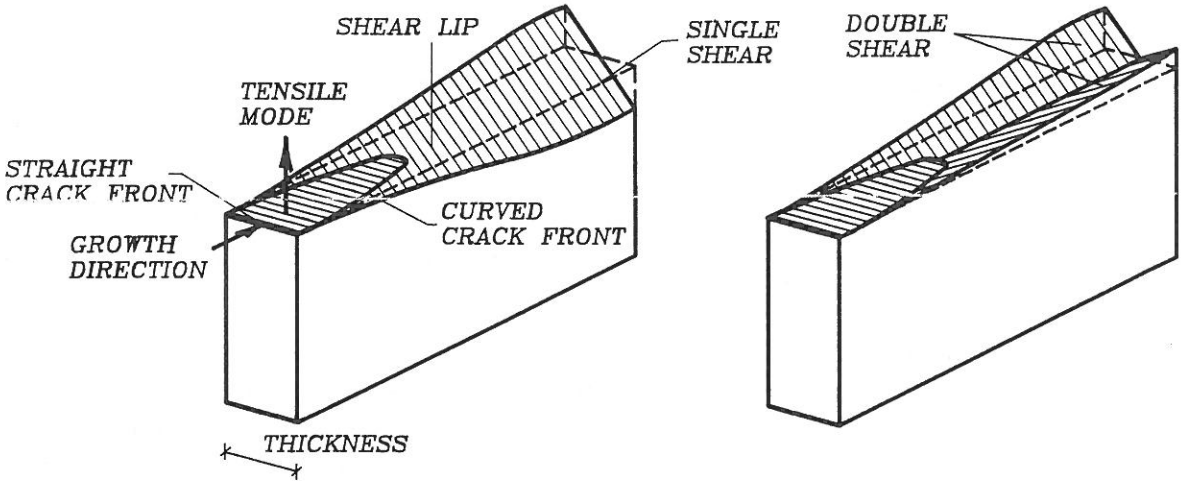

Figure 2.5: Orientation of fatigue surface.

The qualitative description of fatigue has contained micro as well as macro level. Further discussions are found in [Ewalds, H.L. and R.J.H. Wanhill; 1984, ch.3 and ch.12] and in [Laird, C.; 1967].

The quantitative description of fatigue, see section 2.2 and the following chapters, is restricted to the macro level, i.e. to the stages of crack growth and final fracture.

2.2 APPROACHES TO FATIGUE AT MACRO LEVEL

The object of this section is to explain the ideas of the existing approaches to quantitative description of fatigue at macro level, for the purpose of determining the life of a structure. This determination can be performed in two principally different ways.

In the first approach, the properties of fatigue of a structure are characterized solely by knowledge of the total number of cycles to cause fracture, N_c, which for a given harmonic load is used to develop fatigue fracture. This description is typically represented by the so-called SN-curves, see section 2.2.1.

In the other approach, the properties of fatigue of a structure are characterized by the progress of the fatigue fracture in the form of crack growth. In this description, both the propagation phase of the fatigue fracture and the final state are in focus. This description is represented by a crack propagation theory, see section 2.2.2 and chapter 3.

2.2.1 SN-Curves

Determination of the structural resistance to fatigue can be obtained from an SN-curve, established by a series of tests carried out at different stress ranges. In each test, which is performed with deterministic, constant-amplitude load, related values

of the number of cycles to cause fracture, N_c, and stress range $\Delta\sigma$ are registered. In this illustration it is traditional to denote the number of cycles to cause fracture N and the stress range S, see figure 2.6, 8-12 corresponding SN-values are required for drawing an SN-curve.

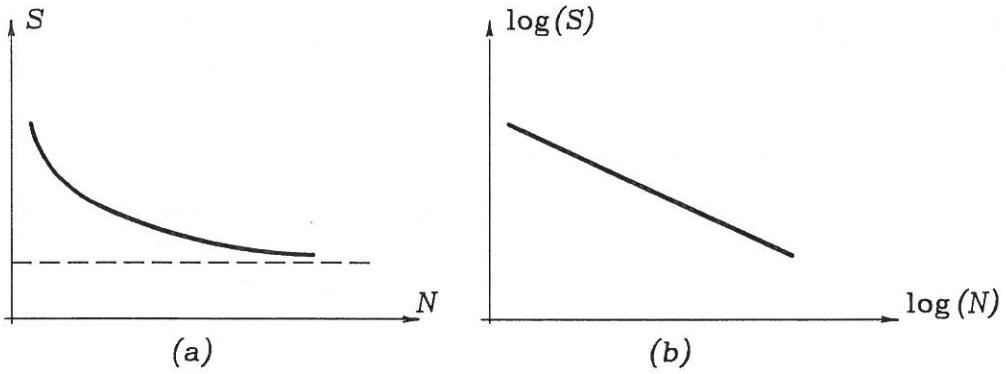

Figure 2.6: Typical SN-curve in arithmetic and logarithmic scale, respectively. N = number of cycles to cause fracture (= N_c). S = stress range (= $\Delta\sigma$).

It appears from figure 2.6(b) that a typical SN-curve forms a straight line in a double-logarithmic scale, i.e.

$$\log(S) = k_1 \log(N) + k_2 \tag{2.1}$$

where

k_1 = slope of line
k_2 = ordinate-intercept

If the number of stress cycles in a certain point of the structure is known, the maximum permissible stress range for that point, $\Delta\sigma_c$, can be obtained from the SN-curve. On the other hand, if the actual stress range is known then the maximum permissible number of cycles, N_c, can be found.

As illustrated in figure 2.6(a), a threshold value of the stress range appears so that stress ranges below this value do not cause fatigue. This corresponds to the loads applied to the structure being insufficient to create the necessary plastic deformation to advance the crack. Even though the threshold value is not well defined it can, as a general rule, be assumed that the value has not been reached if the stress range does not cause fracture after 2-5 million cycles or even more, [Gurney, T.R.; 1979, p.14]. The uncertainty of the threshold value is due to the extensive time consumption which is necessary for its determination.

Other types of representation of the SN-data exist, e.g. the Goodman diagram and the Smith diagram. In the former, half the stress range as a function of the mean stress is pictured, whereas in the latter, the maximum stress as a function of the mean stress is used. See also [Gurney, T.R.; 1979, p.20-21].

One of the drawbacks using the SN-approach is that if SN-data for a given geometry often do not exist, it is necessary to perform experimental tests.

Further, it is shown, [Fatigue Handbook; 1985, p.180], that different SN-curves are obtained depending on whether the mean stress, σ_m (see (2.6)), or the ratio between minimum stress and maximum stress, R (see (2.7)), is kept constant.

On the basis of the SN-curve, it is possible to estimate the damage accumulation introducing a damage indicator D. D has a non-decreasing progress with the initial value 0 and failure corresponding to $D = 1$.

The most common expression for D is the Palmgren-Miner rule in which it is assumed that the damage accumulation depends solely on the stress variation. The stress variation is measured in number of cycles with stress range $\Delta\sigma_i$ (i th cycle)

$$D = \sum_{i=1}^{k} \frac{n_i}{N_{c,i}} \tag{2.2}$$

where

k = number of different stress ranges
n_i = number of cycles with the i th stress range $\Delta\sigma_i$
$N_{c,i}$ = number of cycles to fracture for the i th constant-amplitude range

The Palmgren-Miner rule is based on the assumption that damage is a linear function of the number of cycles under constant amplitude. Thus, it is only necessary to have knowledge of $N_{c,i}$ and to divide the load into blocks of cycles with constant stress range. Notice that Palmgren-Miner's rule contains no information of the load sequence.

Palmgren-Miner's rule and other damage accumulation laws, which are variations of the Palmgren-Miner rule, are discussed in [Leve, H.L.; 1969]. Since, the SN-curves focus only on the failure state this approach will not be further discussed. It should be mentioned that the Palmgren-Miner rule is recommended because of its simplicity as an analytical criterion for comparison of different designs, see [Madsen, H.O., S. Krenk and N.C. Lind; 1986, p.254-255].

2.2.2 Crack Growth Theories

In order to evaluate the remaining lifetime of a structure, in which one or more cracks have been observed, it is appropriate to use the other approach mentioned to describe the resistance to fatigue, i.e. to use a crack growth theory.

As mentioned in section 2.1, the crack will result in development of a local stress field in front of the crack tip. The stress field can be modelled by fracture mechanical methods.

A basic idea in fracture mechanics is to use the stress intensity factor K defined by the elastic stress field near a crack tip, cf. [Hellan, K.; 1985, ch.2] and appendix A.

The stress intensity factor, which can be established from tables containing known solutions or from e.g. a finite element analysis, can in general be written as, see [Schijve, J.; 1979],

$$K = \sigma\sqrt{\pi a}F \tag{2.3}$$

where

σ = applied stress
a = crack length
F = factor which depends on geometry and load distribution

Introduction of K has as a result that the stress *distribution* in the vicinity of a crack being solely dependent on the position of the point considered in proportion to the crack tip, whereas the *magnitude* of the stresses, expressed by K, depends on the applied load and the geometry of the structure and the crack. Thus, an advantage using fracture mechanics is that in case of similar local conditions (stress intensity, environments) being applied, the same deformations in the crack tip area will be produced and thus cause similar consequences in the form of the same crack growth rate, cf. [Schijve, J.; 1979].

The stress singularity at the crack tip results in infinite stresses, see (A.1). Since, no material can support that large stresses, a plastic zone is formed in front of the crack tip.

In case of small-scale yielding, i.e. if the size of the plastic zone is small compared to the crack length or to the distance from the crack tip to the boundaries of the cracked body or points of loading, linear elastic fracture mechanics (LEFM) can be applied to describe the stress field. In spite of the restrictions LEFM is extensively used in fatigue crack growth problems, see also chapter 3. A short introduction to LEFM is given in appendix A. If the material behaves in a elastic-plastic manner large-scale yielding might occur, and elastic-plastic fracture mechanics (EPFM) or non-linear fracture mechanics (NLFM) must be introduced. EPFM and NLFM will not be further discussed, but is described in e.g. [Knott, J.F.; 1973, ch.6] and [Ewalds, H.L. and R.J.H. Wanhill; 1984, ch.6].

The most frequently used fracture mechanical crack growth theories are empirically based and express the resistance against crack propagation of a structure as

$$\frac{da}{dN} = f(\Delta K) \tag{2.4}$$

where

$f()$ = function
da = crack length increase [mm]
dN = increase in number of cycles

ΔK = stress intensity factor range [MPa$\sqrt{\text{m}}$]

Illustration of the crack growth rate, (da/dN), established from tests, as a function of the stress intensity factor range, (ΔK), in a double-logarithmic scale, typically forms a curve as shown in figure 2.7.

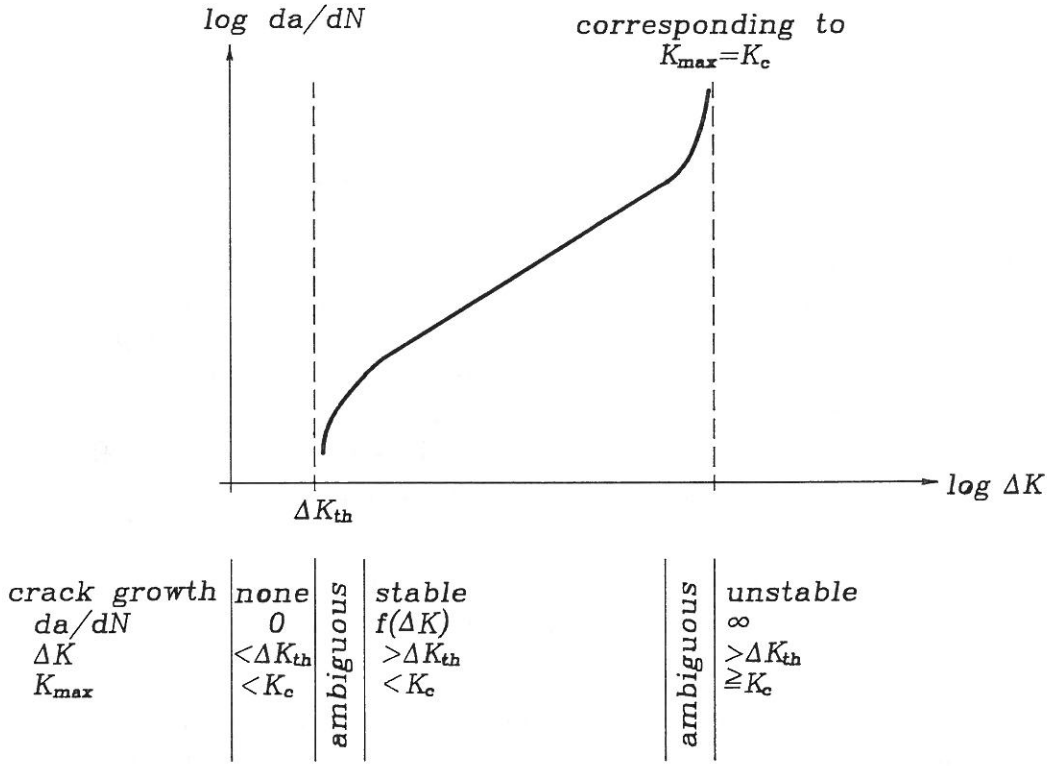

Figure 2.7: Typical $(da/dN) - (\Delta K)$ relationship in a double-logarithmic scale. ΔK_{th} = the threshold value of ΔK, K_c = the critical value of the stress intensity factor at which the final rupture occurs. The dashed line to the right corresponds to $K_{\max} = K_c$, where $K_{\max}$ is the maximum stress intensity factor in one load cycle.

It appears from figure 2.7, that the validity of (2.4) is restricted to the interval $(\Delta K > \Delta K_{th} \wedge K_{\max} < K_c)$, i.e. where the relationship is approximately described by a straight line. At low ΔK levels, the curve asymptotically approaches the threshold value ΔK_{th}, which must be exceeded before crack growth occurs. When the maximum stress intensity factor $K_{\max}$ approaches the critical value K_c, da/dN increases drastically, and when $K_{\max}$ equals K_c, the final rupture takes place.

Practically, [Priddle, E.K.; 1989] proposes that the threshold can be defined as the ΔK value at which less than 0.1 mm of growth is registered in 10^7 cycles, i.e. corresponding to a crack growth rate da/dN of 10^{-11} m per cycle.

For mild steel [Priddle, E.K.; 1989] found that $\Delta K_{th} \approx$ 5-10 MPa$\sqrt{\text{m}}$ depending on the stress ratio R (see (2.8)). The same result is stated in [Fuchs, H.O. and R.I. Stephens; 1980, p. 301] and [Pook, L.P. and R.A. Smith; 1979]. A general expression

for ΔK_{th} is derived in [Davenport, R.T. and R. Brook; 1979].

The critical value of the stress intensity factor, K_c, has been observed to be thickness dependent, cf. [Grandt, A.F., Jr.; 1984], which should be kept in mind if K_c is used as a fracture criterion (see section 2.1). In plane stress condition, i.e. for small thickness, K_c tends to increase in relation to K_c found in plane strain, i.e. for large thickness, see figure 2.8. Notice, when plane strain dominates, K_c approaches the so-called fracture toughness value K_{Ic}. This value is considered as a material constant, which can be determined experimentally, see e.g. [ASTM STP E399-83; 1985].

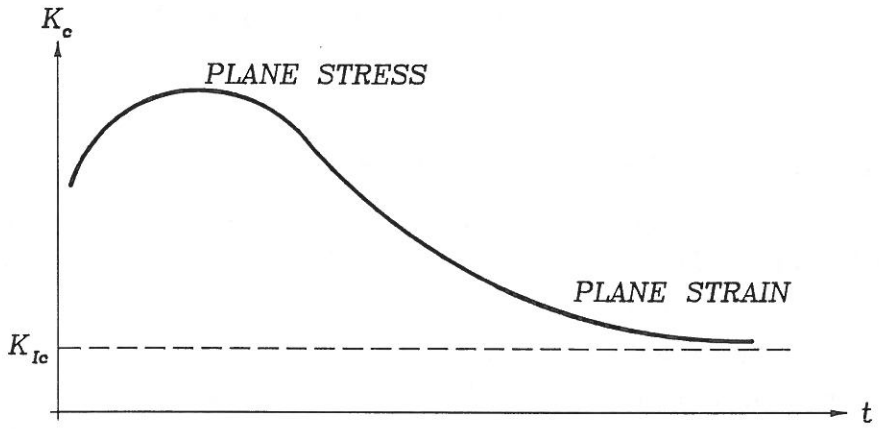

Figure 2.8: Variation of critical stress intensity factor K_c with respect to thickness t at a given temperature.
K_{Ic} = fracture toughness [MPa$\sqrt{\text{m}}$].

The value of K_c varies cf. [Fuchs, H.O. and R.I. Stephens; 1980, p. 301] between 50-150 MPa$\sqrt{\text{m}}$ depending on the performance of the mild steel.

The crack growth rate is very important for the determination of the service life of a structure. Thus, once a fracture mechanical crack growth theory has been chosen, and the parameters, which are included in the theory are established, the number of cycles to reach a given crack length, e.g. corresponding to failure, can be calculated.

Integration of (2.4) between pre-chosen limits of the size of the crack length gives

$$N_f = \int_{N_0}^{N_f} dN = \int_{a_0}^{a_f} \frac{da}{f(\Delta K)} \tag{2.5}$$

where

N_0 = initial number of cycles
N_f = number of cycles to cause failure
a_0 = initial crack length
a_f = failure crack length

Numerical integration of (2.5) is often necessary due to $f(\Delta K)$ which might be a complicated function of the crack length. The form of (2.5) indicates that the number

of cycles can be calculated for any crack length, so the possibility of calculation of the crack growth rate enables inspections and repairs to be made in time, which extend the lifetime.

Besides the stress intensity factor range ΔK, e.g. the plastic strain range $\Delta\epsilon_p$ can be used as a basic parameter. This parameter is advantageous in case of small cracks, see [Broek, D.; 1985], and thus in case of low-cycle fatigue - see also [Gurney, T.R.; 1979, p.282-287].

From (2.4) and (2.3) it is seen that the crack growth rate depends on the load. Determination of the load and its effects is described in section 2.3 and 2.4, respectively.

2.3 CHARACTERIZATION OF LOAD TYPES

The use of (2.5) demands knowledge of the number of load cycles, dN, applied to propagate the crack a length da. The magnitude of dN depends on the nature of the load applied to the structure and on the load of the crack tip.

Therefore, the intent of this section is to give a characterization of the load types mentioned in chapter 1. Once the type of load is established, it has to be decomposed into load cycles, which are then to be counted before entering a crack growth theory. Thus, the load cycles are defined and different counting methods are discussed. Finally, the crack tip load is defined.

The behaviour of fatigue crack growth under deterministic, cyclic, constant-amplitude load (CA-load) serves as a basis for description and prediction of fatigue crack growth under deterministic, variable-amplitude load (VA-load) and random load.

The CA-load is completely determined by the maximum stress, $\sigma_{\max}$, the minimum stress $\sigma_{\min}$, the frequency f and the shape of the alternating load, see figure 2.9.

The following quantities, shown in figure 2.9, are defined

$$\Delta\sigma = \sigma_{\max} - \sigma_{\min} \tag{2.6}$$

$$\sigma_m = \tfrac{1}{2}(\sigma_{\max} + \sigma_{\min}) \tag{2.7}$$

$$R = \frac{\sigma_{\min}}{\sigma_{\max}} \tag{2.8}$$

where

$\Delta\sigma$ = stress range [MPa]
σ_m = mean stress [MPa]

σ_{max} = maximum stress in a load cycle [MPa]
σ_{min} = minimum stress in a load cycle [MPa]
R = stress ratio

The number of load cycles applied can be counted directly.

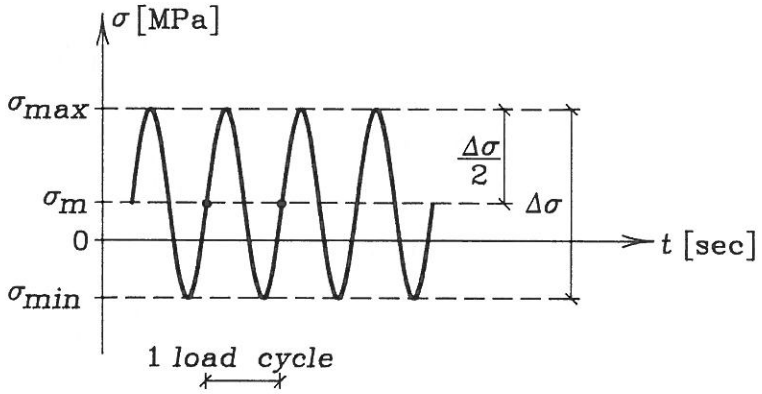

Figure 2.9: Definition of a load cycle in CA-load.
σ_{max}, σ_{min}, σ_m and $\Delta\sigma$ is the maximum stress, minimum stress, mean stress and stress range, respectively.

A possible grouping of deterministic, cyclic, variable-amplitude load sequences is shown in figure 2.10 in which the most important variables are also given.

VARIABLE-AMPLITUDE LOAD SEQUENCES		IMPORTANT VARIABLES	EXAMPLES
overload	single overload	magnitude of overload cycles sequence in overload cycles	
	repeated overloads		
	blocks of overload		
step load	sequences of steps (high-low)	magnitude and duration of steps	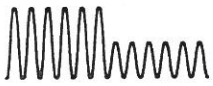
	sequences of steps (low-high)		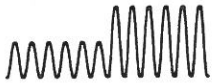
programmed block load	sequences of blocks sequences of groups of blocks	size of blocks distribution function of amplitudes	

Figure 2.10: Types of variable-amplitude load sequences and the most important variables.
Based on [Schijve, J.; 1976].

The variable-amplitude load sequences shown in figure 2.10 can all be described by the characteristics of the basic load, i.e. by (2.6)-(2.8) and figure 2.9, and by the characteristics of the overload, see figure 2.11. An overload is a load cycle whose numerical value and range exceeds the most common cycles (the basic load cycles). The differences in the sequences consist of the arrival time of the overload(s) and in the duration of the overload(s) (number of overloads).

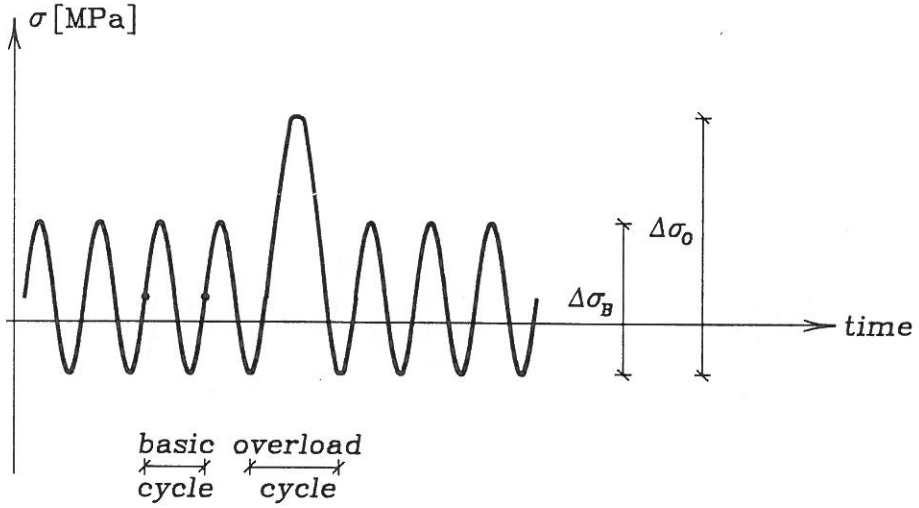

Figure 2.11: Definition of a basic load and an overload cycle in VA-load. The basic load cycle corresponds to figure 2.9, and are given with subscript B for basic case. $\sigma_{O,max}$, $\sigma_{O,min}$, $\sigma_{O,m}$ and $\Delta\sigma_O$ is the maximum stress, minimum stress, mean stress and stress range, respectively, of the overload. Subscript O refers to the overload.

The deterministic character gives a direct possibility to count the cycles, as for the CA-load.

As mentioned in chapter 1, far the most structures in civil engineering are influenced by dynamic loads, usually of random nature. Dealing with random load the distribution of the stress ranges and realizations of the stochastic process must be established. Further, the number of load cycles in the realizations must be determined.

The random load is often modelled as a Gaussian stochastic process characterized by the mean value and the variance, cf. [Madsen, H.O.; 1982, p. 2.2] and [Schijve, J.; 1979]. Further, it is often assumed that the process is stationary, i.e. the statistical properties are independent of time. Both Gaussian and stationary stochastic processes are further described in e.g. [Parzen, E.; 1962, ch.1].

Different realizations of the load history can be performed by simulation when the distribution and the other statistical moments of the stochastic process are known, see figure 2.12.

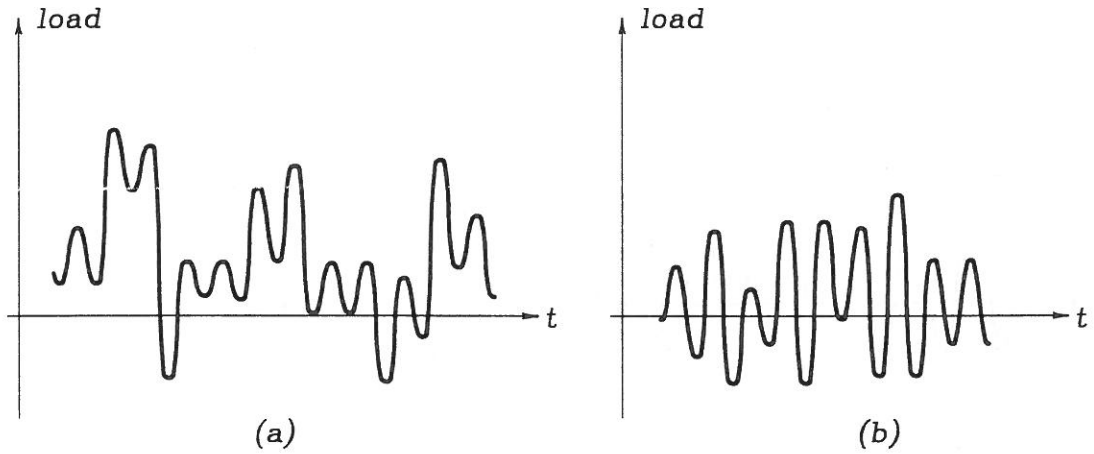

Figure 2.12: Realizations of stochastic processes. (a) Broad band. (b) Narrow band.

It is important to model the real dynamic, random load occurring from e.g. wind and waves as realistic as possible. The establishment of the random load (realizations) in relation to fatigue is a topic which has to be examined in more detailed, but which is beyond the scope of this thesis. The topic has been discussed in [Sørensen, J.D. and R. Brincker; 1989] and in [Brincker, R. and J.D. Sørensen; 1990].

The random load has to be decomposed into a collection of discrete load cycles, but unlike the deterministic load, a random load cycle cannot be defined explicitly. The definition of a load cycle in random load depends on the counting method.

Several counting methods exist, see e.g. [Fatigue Handbook; 1985, p.196-208], of which the Rainflow Counting Method and the Range Pair Counting Method are the two most common. An illustrative example of the use of the two counting methods is given in appendix B.

In the Rainflow Counting Method, an realization is converted into a process of peaks and troughs combined with straight lines. A range is formed by starting from a peak (or trough) and proceed until a opposite peak is more positive (opposite trough is more negative) than the starting point. This procedure is continued until the end of the realization and until all parts of the realization are used.

One of the drawbacks using the Rainflow Counting Method is that information of the stress ranges which have actually occurred is discarded and stress ranges of larger magnitude are introduced. The magnitude of the stress ranges is in section 2.4.1 shown to have a decisive influence of the fatigue crack growth and thus, this disregard can lead to miscalculations of the lifetime.

In the Range Pair Counting Method, a range is defined as the part of the realization between two adjacent points of reversal. Both the positive (ascending) and the negative (descending) ranges are counted. The cycles are formed by pairing positive and negative ranges of the same size. A simpler method is to count all the ranges, positive as well as negative, and then the total number of ranges of the same size is divided by two in order to get the number of cycles of the corresponding size.

In this method, information of the stress range which has actually occurred is retained, but information of the level at which they have occurred (mean stress and peak stress of each range) gets lost.

Using the Rainflow Counting Method or the Range Pair Counting Method the realizations can be statistically analysed with respect to load ranges, extreme loads etc., but information of the load sequences is lost in such a statistical analysis. The Rainflow Counting method seems to be superior to the Range Counting method since it is not disturbed by small cycles (noise) in an otherwise large cycle. In [Madsen, H.O.; 1982, p.4.4] it is concluded that the two counting methods result in minor differences between predicted and actual lifetime compared to other counting methods.

For the purpose of describing the stress field at the crack tip and thus establishing the stress intensity factor K, the load at the crack tip is divided into three modes, I, II and III designating the separation geometrically, see figure 2.13. Assuming linear elasticity the principle of superposition can be used to determine the total acting.

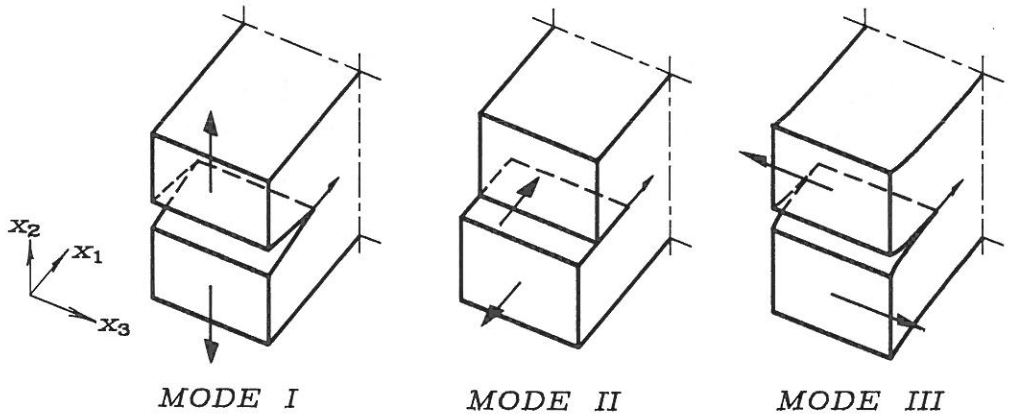

Figure 2.13: Illustration of mode I, mode II and mode III.

The mode I acting consists of a displacement which is symmetrical with regard to the x_1-x_3-plane and which is parallel with the x_2-direction. This mode is named the opening mode and is the dominant mode. The mode II acting, known as the shear mode, corresponds to a displacement which is asymmetrical with regard to the x_1-x_3-plane and where the displacement is in the x_1-direction. Finally, a displacement which is asymmetrical with regard to the x_1-x_3-plane and which goes in the x_3-direction, performs a mode III acting, the antiplane shear mode.

The stress and displacement fields for the three modes are shown in appendix A, (A.1)-(A.8).

Because of its dominance, only mode I will be considered in the following and for simplicity, $K_I = K$.

2.4 FATIGUE CRACK GROWTH DUE TO LOAD SEQUENCES

The final subject, which will be investigated in order to establish an improved fatigue model, is the effects which can be observed if a structure in mode I is influenced by the load types described in section 2.3. Further, the possible causes of the effects are discussed.

2.4.1 Effects of Load Sequences on Fatigue Crack Growth

No matter which type of load is applied to a structure, the crack growth in a load cycle is a function of: the geometry of the crack before the load cycle is applied, the state of the material at the crack tip, the damage already present and the magnitude of the load cycle, i.e. each load cycle affects the damage accumulation in subsequent cycles. These effects are called interaction effects.

As mentioned in section 2.3, fatigue crack growth due to CA-load serves as a basis for description and prediction of fatigue crack growth under VA-load and random load.

Several observations of crack growth under CA-load have been made, see e.g. [Paris, P.C.; 1962], [Walker, K.; 1970] (both on 2024-T3 and 7075-T6 aluminium alloy) and [Chand, S. and S.B.L. Garg; 1985] (different mild steels and aluminium alloys).

Figure 2.14 shows a typical progress of crack growth under CA-load.

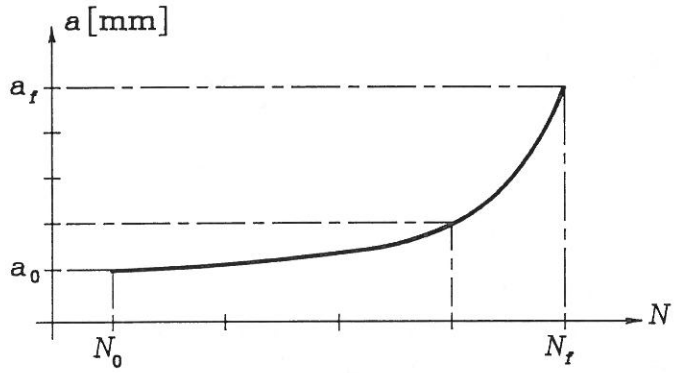

Figure 2.14: Crack growth curve ((N, a)-curve) for CA-load.
N = number of load cycles. a = crack length.

As illustrated, the (N, a)-curve has a smooth progress and approximately 75% of the cycles spent at macro level is used to propagate the crack only about 25% of its final length, see also section 2.1.

[Himmelein, M.K.; 1974] found that the crack growth rate (da/dN) depends on the R-value. The higher the value of R ($R \geq 0$), the higher the (da/dN) and thus the shorter the lifetime. Similar observations have been made by [Fuchs, H.O. and R.I. Stephens; 1980, p.82-91].

For $R \leq 0$, [Mukherjee, B. and D.J. Burns; 1972] found that the number of load

cycles required to propagate a crack to a given length increased for increasing values of R provided that the maximum load was kept constant. Similar observations have been made by [Führing, H. and T. Seeger; 1984]. This shows, that the negative (compressive) part of the load cycle has significant influence on the crack growth rate. Several authors have suggested that $\sigma_{\min} = 0$ should be used if $\sigma_{\min} < 0$, see e.g. [Elber, W.; 1971].

The rate of the progress shown in figure 2.14 will in a double-logarithmic scale give a curve as shown in figure 2.7.

Lots of metallic materials, e.g. steel and aluminium, exhibit transient changes in the crack growth rate as a result of perturbations in a CA-load, which is otherwise constant. Thus, when a structure is influenced by VA-load, the crack growth depends on the order in which the cycles are applied.

As shown in figure 2.10, the simplest case is a single overload. The single overload sequences shown in figure 2.15 are considered.

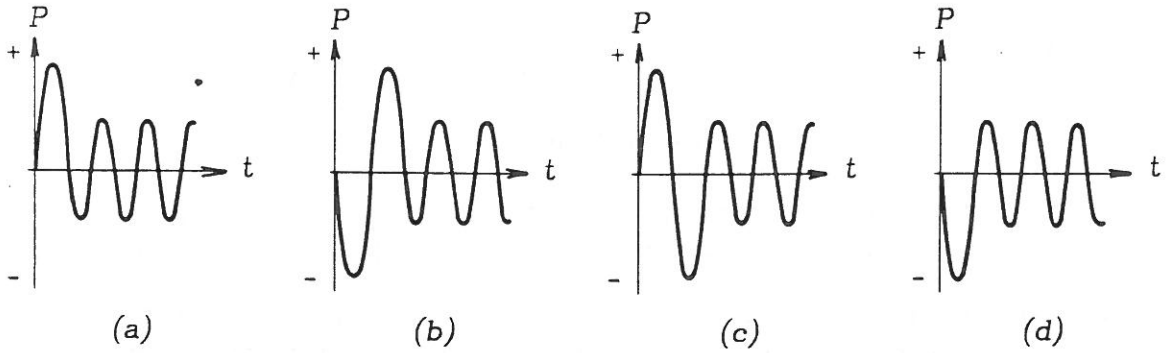

Figure 2.15: Overload sequences. (a) Tensile overload. (b) Compressive-tensile overload. (c) Tensile-compressive overload. (d) Compressive overload. Based on [Fuchs, H.O. and R.I. Stephens; 1980, p.194].

The load sequence shown in figure 2.15(a) causes a delay in the crack growth (retardation) while the situation in figure 2.15(d) results in an acceleration of the crack growth. The effect of acceleration is less pronounced than the effect of retardation, cf. [Schijve, J.; 1976]. The immediate cause for this deviation seems to be different material properties in tension and compression. Besides, it is considered more difficult to accumulate material within a given space in compression than to separate the material in tension. A more plausible explanation is that in the latter case the contact between the crack lips results in less changes in the stress distribution than in the former case. Further explanations are given in e.g. [McEvily, A.J. and K. Minakawa; 1988].

Likewise, if a compressive overload is followed by a corresponding tensile overload - figure 2.15(b) - a retardation of the crack growth is obtained. However, it is not as pronounced as the pure tensile overload, figure 2.15 (a). A small retardation is obtained if a compressive overload succeeds a tensile overload, figure 2.15(c), but reduced compared to the effect of a tensile overload. This has also been observed by

[Porter, T.R.; 1972] and [Alzos, W.X., A.C. Skat, Jr. and B.M. Hillberry; 1976].

The crack growth progress in the above-mentioned cases (a)-(d) is shown in figure 2.16.

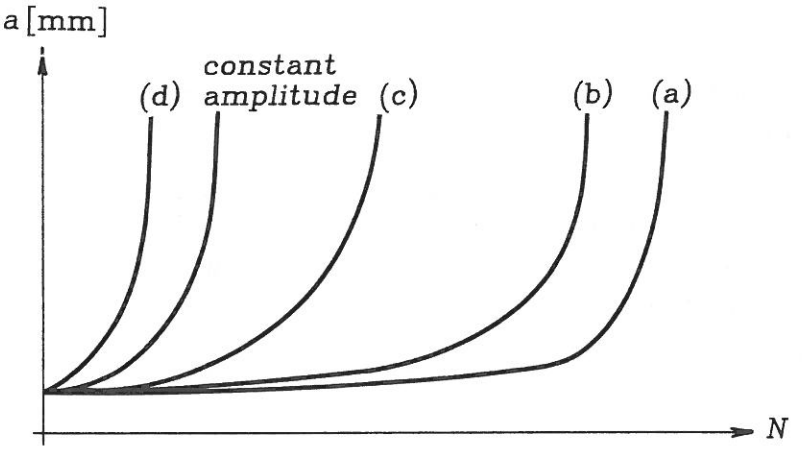

Figure 2.16: Crack growth curves for load as shown in figure 2.15 (a)-(d).
Based on [Fuchs, H.O. and R.I. Stephens; 1980].

In the following, only tensile overloads are considered because these are of greatest interest in increasing the fatigue life of a structure. The effects of compressive overloads are discussed in e.g. [Rice, R.C. and R.I. Stephens; 1973], [Stephens, R.I., D.K. Chen and B.W. Hom; 1976] and [Chu, W.-Y., C.-M. Hsiao and T.-H. Liu; 1984].

When a structure experiences a tensile overload, an immediate decrease in the crack growth rate to a minimum value occurs, whereas the return to the previous crack growth rate is gradual.

The duration of the retardation is highly affected by the minimum crack growth rate. This depends on several factors including the magnitude of the overload and the subsequent load cycles.

Several experiments show that for a given value of basic load, the higher the value of overload, the greater the delay in crack propagation. This has been observed by e.g. [Hudson, C.M. and K.N. Raju; 1970], [Porter, T.R.; 1972], [Corbly, D.M. and P.F. Packman 1973] (all on aluminium alloy 7075-T6), [Probst, E.P. and B.M. Hillberry; 1974] (aluminium alloy 2024-T3) and [Rice, R.C. and R.I. Stephens; 1973] (low strength steel).

[Druce, S.G., C.J. Beevers and E.F. Walker; 1979] observed that a reduction of the stress range where the maximum stress remains constant, hardly influenced the retardation effects. Similar results are found in [Grosskreutz, J.C.; 1971].

Occasionally it is possible to observe a delayed retardation of the crack growth as a consequence of a tensile overload. This form of retardation primarily appears when the overload is much greater than the maximum load in the other cycles in the load sequence. Thus, an acceleration is initially obtained before the retardation occurs,

see [Rice, R.C. and R.I. Stephens; 1973], [Schijve, J.; 1976] and [Robin, C., M. Louah and G. Pluvinage; 1983] and figure 2.17.

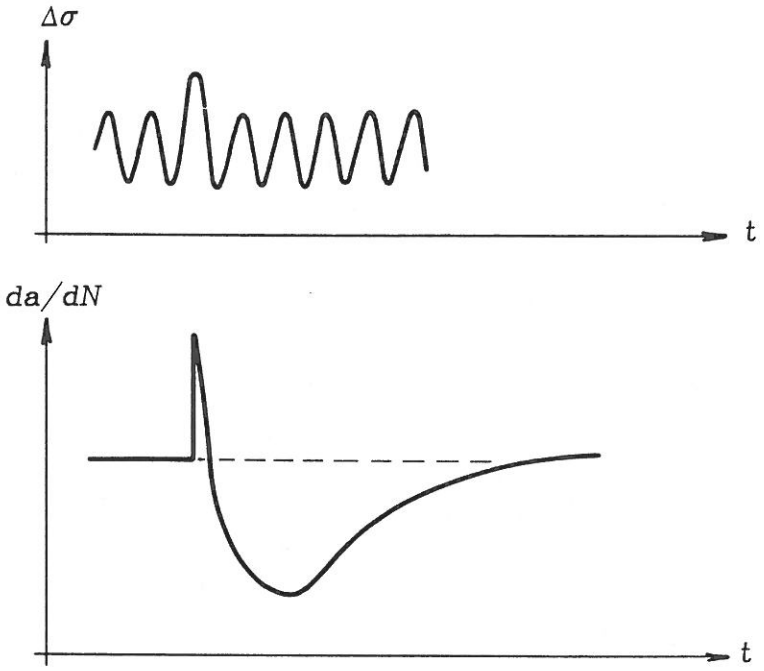

Figure 2.17: Illustration of the crack growth rates before and after a single tensile overload, which causes delayed retardation.
Based on [Corbly, D.M. and P.F. Packman; 1973].

From figure 2.17 it is seen that the crack growth behaviour following a single tensile overload consists of a delayed retardation period, i.e. momentary acceleration and then decrease of crack growth rate to a minimum value followed by an increasing crack growth rate until the original crack growth rate is obtained.

According to [Fleck, N.A.; 1988] the effects of an overload on the crack growth depends on the stress state at the crack tip. It was found - for a structural steel (BS4360 5013) - that in case of plane strain retardation occurs whereas in case of plane stress an overload causes delayed retardation.

Significant retardation generally occurs for overload which is 40-60% higher than the basic load, see [Bernard, P.J., T.C. Lindley and C.E. Richards; 1976]. Their observations of interaction effects due to a single overload can be illustrated as shown in figure 2.18.

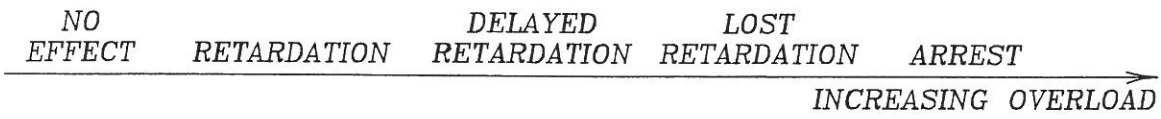

Figure 2.18: Effect of increased tensile overload on fatigue crack growth.

By repeated overloads or blocks of overloads, see figure 2.10, the same effects as

mentioned above are obtained but to a higher degree. [Porter, T.R.; 1972] found that the more cycles at small amplitude between the repeated overloads, the longer the retardation. This has also been observed by [Rice, R.C. and R.I. Stephens; 1973] and [Schijve, J.; 1979].

Furthermore, the retardation is increased with increasing number of overload cycles up to a limit. If only 1 overload is introduced 25% of the maximum retardation will be obtained whereas 10 overloads in one block will result in 50% of the maximum retardation, see [Himmelein, M.K.; 1974], [Corbly, D.M. and P.F. Packman; 1973] and [Hudson, C.M. and K.N. Raju; 1970].

Complete crack arrest at the small amplitude level for overload/small amplitude ratios greater than 2.0-3.0 has been observed when more than one overload are introduced, cf. [Robin, C., M. Louah and G. Pluvinage; 1983].

In case of step load, see figure 2.10, [Führing, H. and T. Seeger; 1984] observed that the acceleration effect of a low-high step load is much smaller than the retardation effect due to an equivalent high-low step load. This has also been observed by [Schijve, J.; 1973] and [Schijve, J.; 1976]. As shown before the number of high load cycles and the magnitude of these cycles have a decisive influence on the retardation effect in a high-low step load, as shown previously, see e.g. [Hudson, C.M. and K.N. Raju; 1970].

The latter type of VA-load mentioned in figure 2.10 is programmed block load. This is the type which is closest to the random load. The load sequence is composed of blocks of load cycles. Each block consists of a number of identical CA-load cycles which are characterized by figure 2.9. The blocks can be arranged in a random but known sequence or in a group of blocks which is repeated invariantly. An example of crack growth curve is given in figure 2.19.

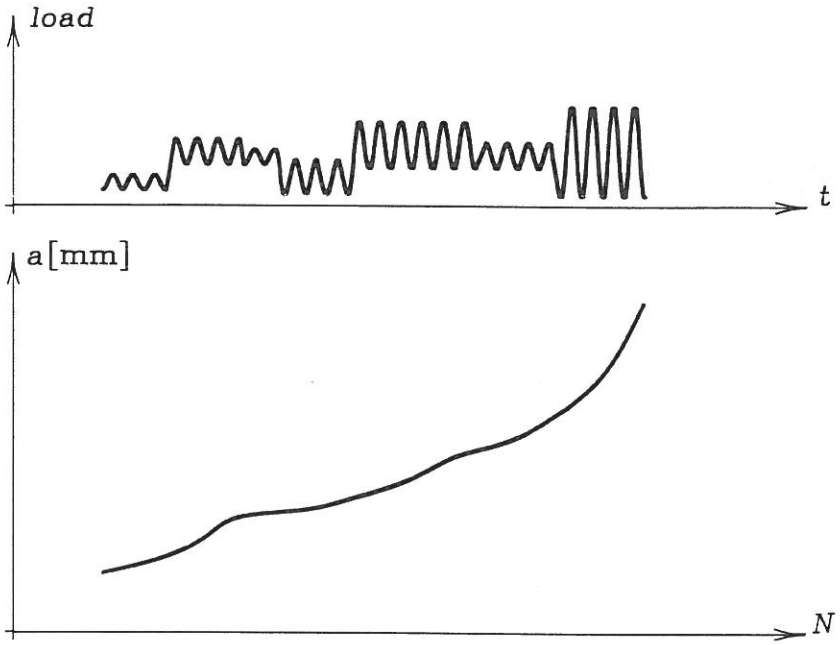

Figure 2.19: Example of crack growth curve under programmed block load.
N = number of load cycles. a = crack length.

It is seen that the crack growth rate da/dN changes every time a new load block is introduced.

Finally, fatigue crack growth under random load, see figure 2.12, will be discussed. Crack growth curves obtained from a realization of a random load have a less smooth progress than the curves obtained for CA-load and VA-load (figures 2.14, 2.16 and 2.19). An example is given in figure 2.20.

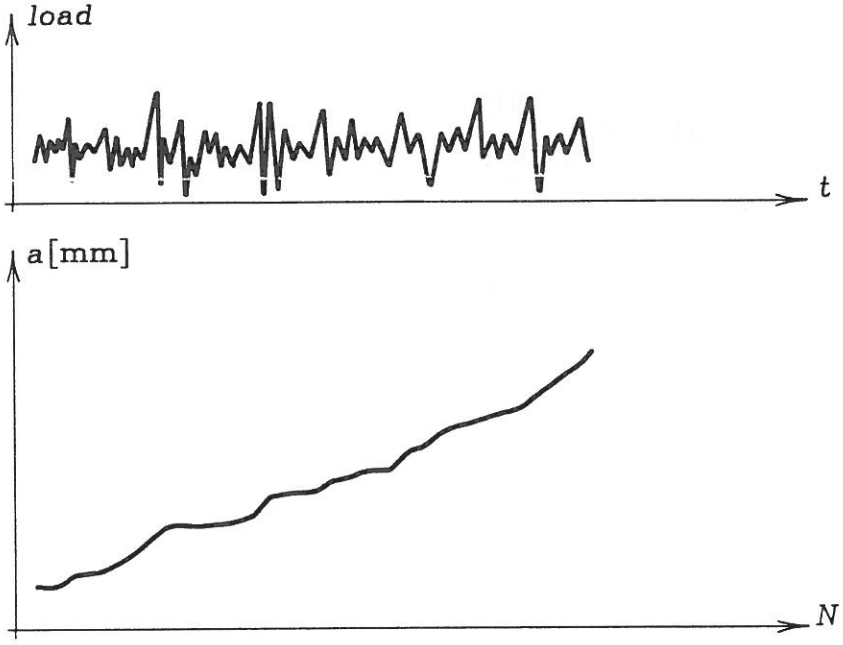

Figure 2.20: (N, a)-curve for a realization of a random load.
N = number of load cycles. a = crack length.

The (N, a)-curve shown in figure 2.20 is characterized by changes in the crack growth rate da/dN corresponding to the changes in the load, resulting in several acceleration and retardation parts.

Generally, very few observations of the crack growth progress under random load have been performed and typically, only SN-data are available.

The lack of information of fatigue crack growth under random load is due to several factors such as e.g. reproduction of random load - as mentioned in section 2.3 - is difficult. Further, lack of information may also be due to insufficient test equipment, especially reliable crack length measuring methods, and inadequate models to describe the fatigue crack growth. The latter factor is a result of the two first-mentioned factors.

Cf. [Iwasaki, T., A. Katoh and M. Kawahara; 1982] programmed block load sequences with the same load distribution as the random load can be used instead of the random load provided that the blocks are small. Otherwise, non-conservative results for number of load cycles to cause failure are obtained.

These conclusions are based on studies of the fatigue crack growth in high strength steel (SM50B) to which different types of VA-load and narrow band random load were applied.

Describing the random load by a distribution function, i.e. by a stochastic process, several advantages are obtained. Establishment of realizations of the stochastic process and calculation of the statistical properties are easily performed.

The main drawback is that the distribution function of counted load cycles does not give any information of the sequence in which the load cycles have occurred. This was previously found to have a decisive influence on the fatigue progress.

2.4.2 Causes of Load Sequence Effects

The possible causes of the interaction effects by variable-amplitude load are described in the following. The description is restricted to VA-load since, once the causes are understood, the results can be transferred to random load.

Three main explanations to the interaction effects are found in the literature:

- residual stresses,
- crack closure,
- crack tip blunting,

see e.g. [Probst, E.P. and B.M. Hillberry; 1974], [Bernard, P.J., T.C. Lindley and C.E. Richards; 1976] and [Schijve, J.; 1979].

When an overload succeeds a sequence of small-amplitude cycles (basic cycles) this overload gives rise to a plastic zone of larger extension than the plastic zone originating from one of the preceding small-amplitude cycles. At the moment the overload decreases from its maximum value to zero - i.e. when no external load is acting on the crack tip - residual stresses will arise in the plastic zone, see figure 2.21.

The sign of these residual stresses depends on the sign of the external load that caused the plastic zone, i.e. the sign of the overload. A tensile overload will lead to compressive residual stresses and vice versa.

When subsequently the amplitudes of the following cycles reassume their former value the effect from these on the crack growth is influenced by the residual stresses. Likewise, a great deal of the following small-amplitude cycles will be spent surmounting the zone of residual stresses. The crack growth rate will not assume its previous value until the residual stresses have been eliminated at the crack tip.

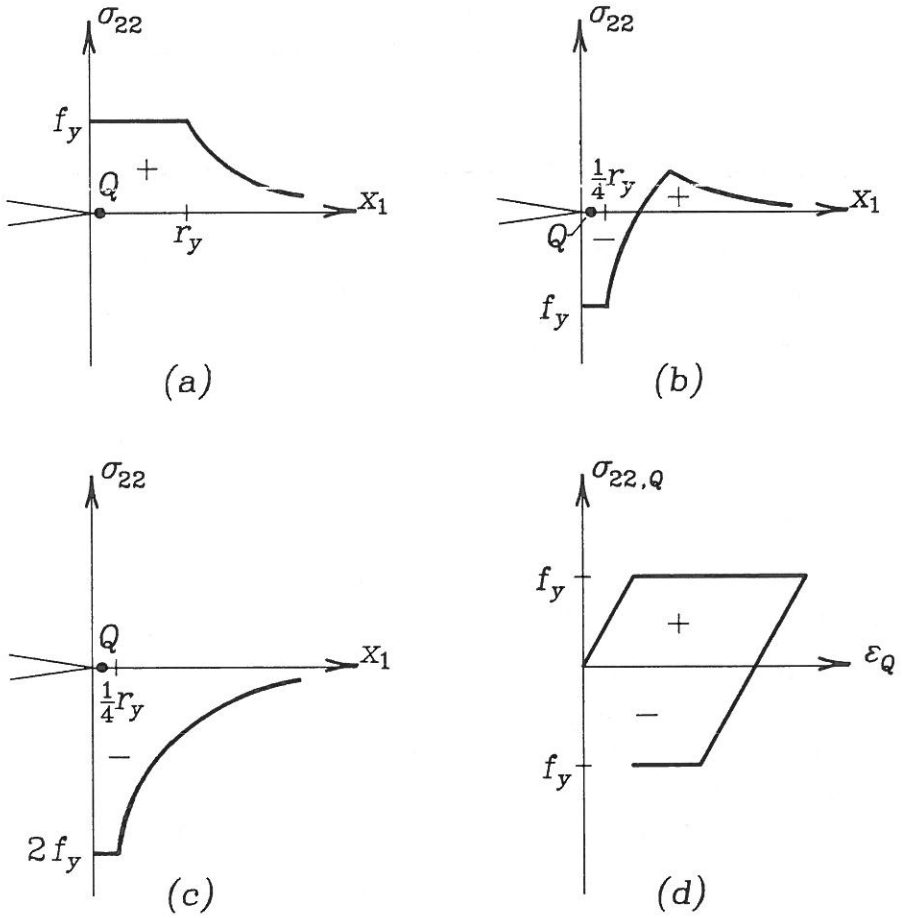

Figure 2.21: Stress distribution in front of the crack tip: (a) Tensile loading. (b) Residual stress field after elastic unloading. (c) Stresses added to (a) to obtain (b). (d) Stress-strain history at point Q. f_y = yield stress, r_y = plastic zone.
Based on [Hellan, K.; 1985, p.134].

The situation in figure 2.21(a) shows that during loading are the stresses at the crack tip achieving the tensile yield stress and a plastic zone is formed, see also appendix A.3.

In the elastic unloading phase the compressive yield stress at the crack tip is achieved and a reversed plastic zone appears, see figure 2.21(b) in which the stress distribution after complete unloading is also shown.

The residual stress distribution is obtained by adding the stresses shown in figure 2.21(c), i.e. twice the yield stress.

The stress-strain history of a point Q within the reversed plastic zone is given in figure 2.21(d). It may be pointed out that the stresses applied to the global structure are elastic.

As described in section 2.1, *stage II* crack propagation is a result of plastic separation

of the material at the crack tip. A direct consequence of this plastic deformation is that the two fracture surfaces become mismatching so they get in contact before complete unloading has taken place. Consequently, compressive residual stresses occur in the crack tip region when the load is still tensile. This phenomenon is known as crack closure and was first described by [Elber, W.; 1970] and [Elber, W.; 1971], see also [Schijve, J.; 1979].

The stress at which contact between the fracture surfaces is established during unloading is the crack closure stress, σ_{cl}, which exceeds the stress corresponding to complete unloading.

Due to the compressive residual stresses, the crack is partly closed during loading until the crack opening stress σ_{op} is reached. At the moment when the residual stresses are relieved and the crack is completely open, crack propagation can take place. Thus, the material around the crack tip only experiences a part of the actual stress range, and the fatigue process is now governed by the effective stress range $\Delta\sigma_{\text{eff}}$ (see also figure 2.22).

$$\Delta\sigma_{\text{eff}} = \sigma_{\max} - \sigma_{op} \tag{2.9}$$

where

$\sigma_{\max}$ = maximum stress in a load cycle [MPa]

The reduced effective stress gives rise to a smaller crack growth, i.e. retardation occurs. In case of tensile residual stresses an increased effective stress is obtained, whereby the crack growth is accelerated.

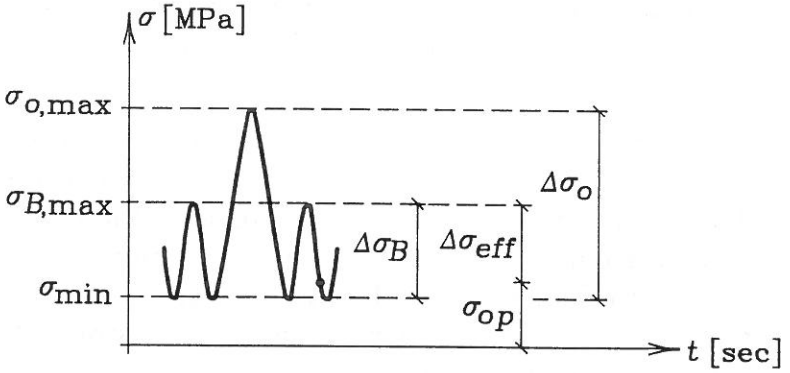

Figure 2.22: Definition of effective stress range, $\Delta\sigma_{\text{eff}}$ and crack opening stress σ_{op}.

Generally, $\sigma_{op} \neq \sigma_{cl}$, but often they are assumed equal. The variation of the crack opening stress σ_{op} (the crack closure stress σ_{cl}) in a VA-load sequence with a single tensile overload appears from figure 2.23.

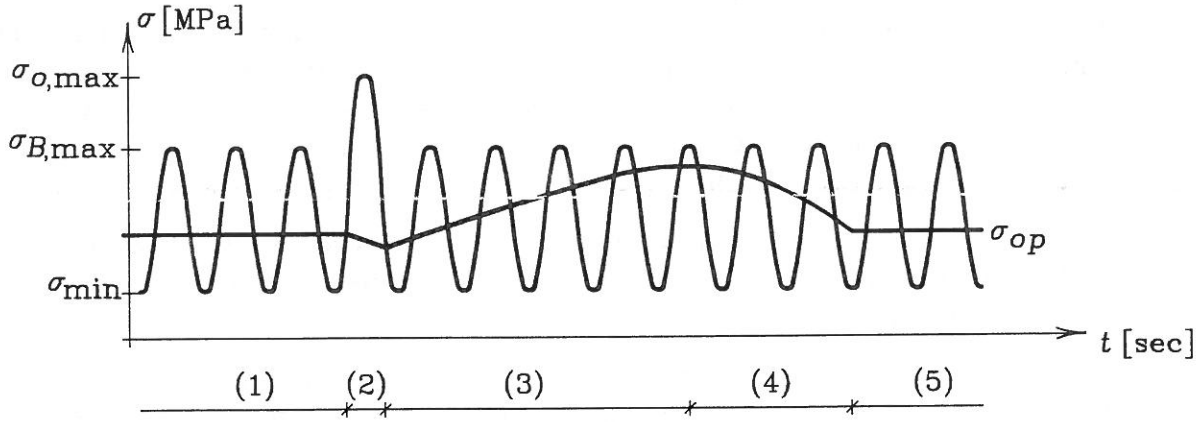

Figure 2.23: Variation in crack opening stress when one overload is introduced. (1) $\sigma_{op} \geq \sigma_{\min}$. (2) Decrease in σ_{op}. (3) $\sigma_{op} > \sigma_{\min}$, σ_{op} increasing. (4) $\sigma_{op} > \sigma_{\min}$, σ_{op} decreasing. (5) $\sigma_{op} \geq \sigma_{\min}$.

For CA-load $\sigma_{op} \geq \sigma_{\min}$. After introducing the tensile overload a decrease in σ_{op} appears which causes an accelerated crack growth. After this σ_{op} is increasing and when $\sigma_{op} > \sigma_{\min}$ the effective stress range $\Delta\sigma_{\text{eff}}$ is reduced, i.e. retardation occurs. At some moment another decrease in σ_{op} occurs and so $\Delta\sigma_{\text{eff}}$ is increased. When σ_{op} reassumes the value for CA-load the retardation is said to be ended.

This variation in σ_{op} is among others observed by [Schijve, J.; 1979] and [Fuchs, H.O. and R.I. Stephens; 1980].

In case of high-low step load the crack growth may arrest if the maximum stress in the low load cycles is smaller than the opening stress, cf. [Trebules, V.W., Jr., R. Roberts and R.W. Hertzberg; 1973].

Cf. [Schijve, J.; 1976], the opening stress decreases for increasing thickness due to a smaller plastic zone in plane strain (thick specimen) than in plane stress (thin specimen), see also section 3.3.1.

Further, crack tip blunting due to high tensile stresses causes a reduction of the stress concentration resulting in smaller crack growth, cf. [Druce, S.G., C.J. Beevers and E.F. Walker; 1979]. The duration of the retardation corresponds to the number of load cycles required to reinitiate the blunted crack tip. The plastic blunting process is described in figure 2.4. According to [Bernard, P.J., T.C. Lindley and C.E. Richards; 1976] crack tip blunting is more significant in plane strain than in plane stress. This is in good agreement with the phenomenon of retardation which occurs in plane strain and delayed retardation which occurs in plane stress as discussed in section 2.4.1.

Observations of the variation of crack closure during random load have not been found in the literature, but a less smooth progress than shown in figure 2.23 must be expected.

2.5 EVALUATION

The purpose of this chapter has been to give a basic knowledge and understanding of the concept "fatigue", which seems to be a necessity if an improved fatigue model is to be established.

Fatigue is in the present thesis defined as initiation and propagation of one or more cracks as a result of an alternating load, i.e. fatigue can only appear if one or more cracks are initiated in a structure. Thus, knowledge of the distribution of the location and size of the cracks is demanded. This subject will not be further discussed, but the problem has been investigated by [Berens, A.P. and P.W. Hovey; 1983] and [Trantia, G.G. and C.A. Johnson; 1983].

The fatigue process consists of a micro and a macro level corresponding to the initiation and micro crack stages and the macro crack stage, respectively. The main part of the chapter is concerned with the macro level of fatigue, which is probably the part best understood and investigated, but still not satisfactorily predictable.

As described, establishing the SN-curves and using a crack growth theory are two different ways of describing the properties of fatigue of a structure.

The establishment of the SN-curves is performed by registration of the stress range (see (2.6)) and the number of cycles to cause fracture. It is recommended to establish the SN-data either with constant stress ratio R or with constant mean stress σ_m. The approach based on the SN-curves will not be further discussed because no information of the crack propagation stages is given.

A crack growth theory is focused on the crack propagation during the alternating load and the failure state. Different types of crack growth theories exist, see e.g. [Grosskreutz, J.C.; 1971] and [Baïlon, J.-P. and S.D. Antolovich; 1983], two of which will be mentioned.

The dislocation based models describe the crack growth in terms of micro mechanism. A basic element in these models is the fracture criterion, which states that fatigue crack propagation takes place when the dislocation distribution and density in front of the crack tip attain a critical value. Further details are given in [Chakrabarti, A.K.; 1980], [Ellyin, F. and C.O.A. Fakindale; 1986] and [Ellyin, F. and C.O.A. Fakindale; 1987]. This type of model will not be further discussed in the present thesis.

The phenomenological models, which are primarily empirically based, are typically represented by a fracture mechanical fatigue crack growth theory. These models deal with macro level of fatigue as described in section 2.2.2. Some of the models are described in chapter 3.

The fatigue crack growth progress depends on several parameters including the character of the applied load, the crack tip load, the load frequency and the environments. As mentioned earlier, the effects of the last two parameters are not taken into account.

Three main types of applied load have been described in section 2.3: constant-amplitude load (CA-load), variable-amplitude load (VA-load) and random load. The

CA-load and VA-load are deterministic and therefore well-defined. The random load can e.g. be described by a distribution function.

The description of fatigue crack growth demands knowledge of the number of cycles applied to the structure. The transformation of the load history into individual load cycles and the counting of these cycles can be performed in several ways, see section 2.3. It is important to apply a cycle counting method which gives the physically most correct representation of the fatigue process. For the time being, the Rainflow Counting Method is considered to be the most appropriate method since, it is not disturbed by noise. A counting method in which account of the load sequence is taken is, however, still desirable.

Linear elastic fracture mechanics (LEFM) has been applied to describe the stress and displacement field around the crack tip after the crack tip load has been idealized in three modes, see figure 2.13. As described, mode I is the dominant mode which is the reason why only this mode is considered.

Depending on the type of load, different fatigue crack growth processes can be observed, see section 2.4.1. The most important load sequence effects are retardation, delayed retardation and acceleration of the crack growth.

Different explanations of these so-called interaction effects have been given in section 2.4.2. Recent studies by [Fleck, N.A.; 1988] show that crack closure dominates the retardation rather than residual, compressive stresses. Further, it was found that the formation of an irregular crack front in the form of crack tip branching reduced the crack growth rate. These explanations are also given by [Drew, M.W. and K.R.L. Thompson; 1988] and [Suresh, S.; 1983].

Once the geometry of the structure and of the crack is known and once the load history, the initial conditions and a fracture criterion are established, a proper fatigue model has to be selected. Only fatigue crack growth models are dealt with.

Ideally, a fatigue crack growth model takes into account the influence of all parameters which effect the fatigue crack propagation in a given material under given conditions.

Fulfilment of this will result in a large number of model parameters. Instead the model must be chosen so that the main question: "How long does it take for a crack to grow from a certain length to a given maximum permissible size at which failure is just avoided ?", can be answered in an acceptable way. Thus, the model must be able to predict the crack growth satisfactorily including the phenomena and effects described in this chapter and still have a simple mathematical relation.

Thus, so far the procedure in a fatigue analysis is:

- determine the geometry of the structure and crack,
- establish the initial state (distribution of number of cracks and crack size),
- describe the load history,

- choose a fatigue crack growth model.

The latter item is discussed in the following chapter.

3. STATE-OF-THE-ART ON FATIGUE CRACK GROWTH MODELS

As mentioned in chapter 2, the most appropriate approach to fatigue is the use of a fatigue crack growth theory, which is able to express the connection between the load process and the fatigue process.

The characterization of the load process depends on the load type. It is common to distinguish between constant-amplitude load (CA-load), variable-amplitude load (VA-load) and random load, see also section 2.3.

The fatigue crack growth is characterized by the crack growth rate da/dN and the total number of cycles to cause failure, N_f, see (2.4) and (2.5).

A large number of physically and/or empirically based fatigue crack growth theories expressing the connection between the load and fatigue process exist.

The purpose of this chapter is to obtain information of some of these fatigue models and their applications in relation to the demands in section 2.5.

3.1 DIMENSIONAL ANALYSIS

A general physically based fatigue crack growth model can be established using dimensional analysis. This method can be used when the analytical solution of a problem is unknown or inadequate.

Dimensional analysis requires knowledge of the physical parameters assumed to have significant influence on the problem considered. Applying the Buckingham π-theorem, the physical problem is described by a dimensionally homogeneous equation, reduced to an equation consisting of dimensionless products, cf. [Sabnis, G.M., H.G. Harris, R.N. White and M.S. Mirza; 1983, p.33].

In the paper by [Cherepanov, C.P. and H. Halmanov; 1972], on which the following is based, an evaluation of the parameters influencing the crack growth rate da/dN and thus on the fatigue process is made.

Assuming linear-elastic material behaviour, the crack growth rate will depend on the load process represented by the stress intensity factor K [MPa$\sqrt{\text{m}}$], varying between $K_{\min}$ and $K_{\max}$, see also section 2.2.2. $K_{\min}$ is the minimum stress intensity factor corresponding to the minimum stress $\sigma_{\min}$ in a load cycle, see section 2.3. Furthermore, the properties of the material in the form of Young's modulus E [N/mm^2], yield stress f_y [N/mm^2], Poisson's ratio ν and the surface energy γ [Nm/mm^2] have influence. The surface energy is the energy used for the formation of a unit area new crack surface. Thus

$$\frac{da}{dN} = f(K_{\max}, K_{\min}, E, f_y, \nu, \gamma) \tag{3.1}$$

Information about the function f in (3.1) is established by energy considerations. The crack energy calculated per unit thickness has to be equal to the total work per unit thickness performed by the crack propagation process corresponding to the crack length increase da, see also figure 3.1. Thus it is assumed that the energy does not vary in the direction of the thickness and the problem is thereby reduced to a two-dimensional problem. Due to the fact, that there are two crack surfaces, the factor 2 is introduced in the following. Thus, it is not a consequence of dimensional analysis.

$$2\gamma da = dW + dA_p \tag{3.2}$$

where

da = crack length increase [mm]
dW = crack work per unit thickness [Nm/mm]
dA_p = volume work per unit thickness [Nm/mm]

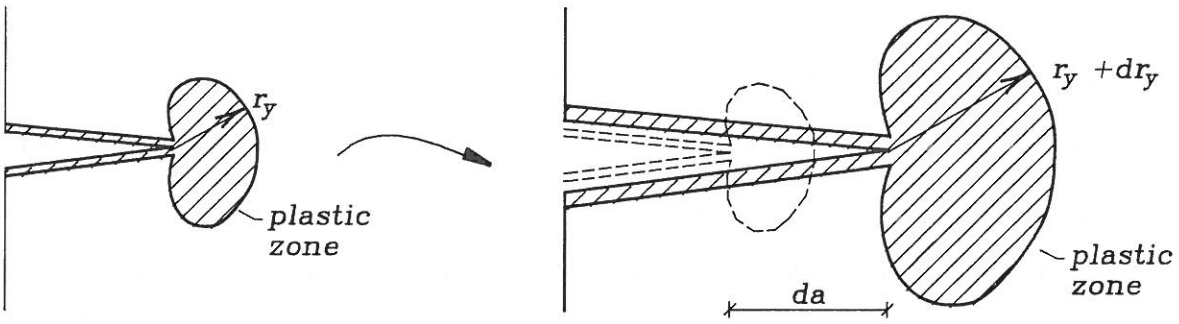

Figure 3.1: Schematic illustration of the crack and the plastic zone extension.

The crack work dW is the irreversible deformation work done by the plastic zone as it performs a "rigid-body" motion in the direction of the crack extension. dW depends on the load parameter K, varying between $K_{\min}$ and $K_{\max}$, σ_0 describing the pre-load history in form of initial stresses and the material parameters E, f_y and ν. Finally dW is dependent on the crack length increase da. Choosing K, E and da as independent variables, dimensional analysis leads to

$$dW = 2\frac{K^2}{E} da \; \alpha_1\left(\frac{f_y}{E}, \frac{\sigma_0}{E}, \nu\right) \tag{3.3}$$

where

α_1 = dimensionless function

The independent variable E in the dimensionless part containing dW is chosen because E is an implicit measure of the resistance against crack propagation.

The volume work dA_p is the irreversible deformation work due to the increase in the plastic zone size during load. dA_p depends on the same load and material parameters as dW. Further, dA_p is dependent on the change of load dK corresponding to the crack length increase da. Dimensional analysis leads to (K, dK and E as independent variables)

$$dA_p = 2\frac{K^3}{f_y^3} dK \; \alpha_2(\frac{f_y}{E}, \frac{\sigma_0}{E}, \nu) \tag{3.4}$$

where

α_2 = dimensionless function

The independent variable in the dimensionless part containing dA_p is chosen as f_y because the size of the plastic zone r_y depends on the yielding properties of the material, see (A.9).

Insertion of (3.3) and (3.4) into (3.2) results in

$$\gamma = \frac{K^2}{E}\alpha_1(\frac{f_y}{E}, \frac{\sigma_0}{E}, \nu) + \frac{K^3}{f_y^3}\alpha_2(\frac{f_y}{E}, \frac{\sigma_0}{E}, \nu)\frac{dK}{da}$$

which by reduction gives

$$\frac{\gamma E}{\alpha_1(\frac{f_y}{E}, \frac{\sigma_0}{E}, \nu)} = K^2 + \frac{\alpha_2(\frac{f_y}{E}, \frac{\sigma_0}{E}, \nu)}{\alpha_1(\frac{f_y}{E}, \frac{\sigma_0}{E}, \nu)} \frac{EK^3}{f_y^3} \frac{dK}{da}$$

$$\Downarrow$$

$$K_c^2 - K^2 = \alpha_3(\frac{f_y}{E}, \frac{\sigma_0}{E}, \nu) \frac{EK^3}{f_y^3} \frac{dK}{da}$$

$$\Downarrow$$

$$\frac{da}{dK} = \alpha_3(\frac{f_y}{E}, \frac{\sigma_0}{E}, \nu) \frac{EK^3}{f_y^3(K_c^2 - K^2)} \tag{3.5}$$

where

$$\alpha_3(\frac{f_y}{E}, \frac{\sigma_0}{E}, \nu) = \frac{\alpha_2(\frac{f_y}{E}, \frac{\sigma_0}{E}, \nu)}{\alpha_1(\frac{f_y}{E}, \frac{\sigma_0}{E}, \nu)}$$

$$K_c^2 = \frac{\gamma E}{\alpha_1(\frac{f_y}{E}, \frac{\sigma_0}{E}, \nu)}$$

K_c is known as the critical stress intensity factor, which is determined experimentally, see e.g. [Ewalds, H.L. and R.J.H. Wanhill; 1984, p.103-107]. This factor is conceptually introduced in section 2.2.2.

Assuming that the crack extension Δa in one load cycle does not change during unloading, i.e. from $K_{\max}$ to $K_{\min}$, Δa is found by integration of (3.5) over the load cycle between $K_{\min}$ and $K_{\max}$

$$\Delta a = \alpha_3(\frac{f_y}{E}, \frac{\sigma_0}{E}, \nu) \frac{E}{f_y^3} \int_{K_{\min}}^{K_{\max}} \frac{K^3}{K_c^2 - K^2} dK$$

$$\Downarrow$$

$$\Delta a = \alpha_3(\frac{f_y}{E}, \frac{\sigma_0}{E}, \nu) \frac{E}{f_y^3} (-\frac{1}{2}) [K_c^2 \ln \frac{K_c^2 - K_{\max}^2}{K_c^2 - K_{\min}^2} + (K_{\max}^2 - K_{\min}^2)]$$

$$\Downarrow$$

$$\Delta a = -\beta [\frac{K_{\max}^2 - K_{\min}^2}{K_c^2} + \ln \frac{K_c^2 - K_{\max}^2}{K_c^2 - K_{\min}^2}] \tag{3.6}$$

where

$$\beta = \alpha_3(\frac{f_y}{E}, \frac{\sigma_0}{E}, \nu) \frac{EK_c^2}{2f_y^3}$$

As continuous variables (3.6) becomes

$$\frac{da}{dN} = -\beta [\frac{K_{\max}^2 - K_{\min}^2}{K_c^2} + \ln \frac{K_c^2 - K_{\max}^2}{K_c^2 - K_{\min}^2}] \tag{3.7}$$

The size of the parameter β depends on the type of load expressed by σ_0 which, as mentioned earlier, stands for the pre-load history. The pre-load history can also be taken into account when calculating $K_{\max}$ and $K_{\min}$ whereby $\sigma_0 = 0$ and β becomes a constant.

In case of CA-load, only the number of load cycles influences the following crack propagation, whereas in case of VA-load or random load, the order in which the cycles are applied is decisive, see section 2.4.

The validity of (3.7) has been investigated by [Cherepanov, G.P. and H. Halmanov; 1972] in which a series of experiments forms the basis of the investigation. The experiments, which are carried out with specimens made of aluminium alloys (2024-T3 and 7075-T6), show very good agreement with (3.7) at two different values of β, $\beta = 0.10$ mm and $\beta = 0.15$ mm.

Expression (3.7) forms the basis of the evaluation of the empirically based crack growth theories, see sections 3.2.3 and 3.3.3.

3.2 FATIGUE UNDER CONSTANT-AMPLITUDE LOAD

In the past 25 years several crack propagation laws to describe crack growth under constant-amplitude load have been developed, see e.g. [Paris, P. and F. Erdogan; 1963] and [Chand, S. and S.B.L. Garg; 1985]. Common to the laws is that they express the crack growth rate da/dN as a function of for instance the stress intensity factor range ΔK, see section 2.2.2.

The purpose of this section is to describe some of the crack propagation laws and their applications. Considerations about the validity of the laws will be given in section 3.2.3.

3.2.1 Paris' Empirical Fatigue Crack Propagation Law

The purpose of this section is to present the fatigue crack growth model established by [Paris, P. and F. Erdogan; 1963] on the basis of the considerations in [Paris, P.C., M.P. Gomez and W.E. Anderson; 1961]. The model, which is known as Paris' law, is one of the most frequently used.

In order to establish a theory to describe the growth of an initial "crack-like" imperfection to failure size (final rupture), [Paris, P.C., M.P. Gomez and W.E. Anderson; 1961] assumed that the stress field and its variation around the crack tip controls the crack propagation rate in a given material. Thus, as described in section 2.2.2 and appendix A, the stress intensity factor K, (2.3), can be used to describe the magnitude of the stress singularity at the crack tip.

The stress intensity factor is linearly dependent on the applied load characterized by figure 2.9 and (2.6)-(2.8). Therefore, it follows that the stress field around the crack tip is completely determined by

$$K_{\max} = \sigma_{\max}\sqrt{\pi\, a}\, F \tag{3.8}$$

and

$$R = \frac{\sigma_{\min}}{\sigma_{\max}} = \frac{K_{\min}}{K_{\max}} \tag{3.9}$$

On the basis of the above-mentioned assumptions, [Paris, P.C., M.P. Gomez and W.E. Anderson; 1961] proposed that the crack extension per load cycle was given by

$$\frac{da}{dN} = f(K_{\max}, R) \tag{3.10}$$

where

da = increase in crack length [mm]
dN = increase in number of cycles

Generally, for a given structure of a given material, the maximum stress intensity factor $K_{\max}$ and the load ratio R during a load cycle depend on the arrival time of the load cycle in the load sequence, i.e. $K_{\max}$ and R vary with time (measured in number of load cycles N). On the other hand, R is a function of $K_{\max}$, which depends on the actual crack length a. Thus, (3.10) can be rewritten as

$$\frac{da}{dN} = f(K_{\max}(a), R(K_{\max}(a))) = f^*(a) \tag{3.11}$$

The fatigue crack growth progress can then be completely established by use of (2.4).

An expression for f^*, where the dependence of a is given through ΔK, is proposed in [Paris, P. and F. Erdogan; 1963] in case of CA-load.

$$\frac{da}{dN} = C\,(\Delta K)^m \tag{3.12}$$

where

C = material constant [mm/(MPa$\sqrt{\text{m}}$)^m]
m = material constant
ΔK = $K_{\max} - K_{\min}$ = stress intensity factor range [MPa$\sqrt{\text{m}}$]
$K_{\max}$ = maximum stress intensity factor in one load cycle [MPa$\sqrt{\text{m}}$]
$K_{\min}$ = minimum stress intensity factor in one load cycle [MPa$\sqrt{\text{m}}$]

The Paris law, (3.12), expresses explicitly the connection between the load process applied to a given structure and the process of fatigue at macro level in the structure as a power relation. The load process is described by the stress intensity factor range ΔK - see also section 2.2.2 - while the process of fatigue is characterized by the crack propagation rate da/dN and the number of cycles, N_c, to cause fracture.

The crack growth rate da/dN calculated from Paris' law will in a double-logarithmic illustration give a straight line as shown in figure 2.7.

Due to the power relation form of (3.12) it is seen that m has a larger influence on the crack growth rate than C, in the sense that a small change in m causes a large change in the predicted lifetime, whereas a small change in C only gives a small change. In [Madsen, H.O.; 1982, p.6.11] it is mentioned that C may depend on the stress-strain parameters and on the stress ratio R, whereas m is almost insensitive to these parameters.

The material constants C and m have to be determined by experiments. In [Paris, P. and F. Erdogan; 1963] $m = 4$ was assumed, whereas no value of C was specified for the 2024-T3 aluminium alloy used. [Tanaka, S., M. Ichikawa and S. Akito; 1981] found that C and m are correlated, but according to [Yao, J.T.P., F. Kozin, Y.-K. Wen, J.-N. Yang, G.I. Schuëller and O. Ditlevsen; 1986], the magnitude of the correlation coefficient depends on the physical units. [Chow, C.L., C.W. Woo and K.T. Chung; 1986] found for mild steel values of C in the interval $[8.772 \cdot 10^{-18}$; $3.304 \cdot 10^{-15}]$ mm/[(MPa$\sqrt{\text{mm}})^m$] and m varying between 3.625 and 4.434. The correlation between C and m was observed as an increase in m for decreasing C. Similar results are given in [Tanaka, S., M. Ichikawa and S. Akita; 1981], but with $m \in [2.5$; $3.5]$ and $C \in [2 \cdot 10^{-10}$; $1 \cdot 10^{-8}]$ mm/[(MPa$\sqrt{\text{m}})^m$].

3.2.2 Forman's Empirical Fatigue Crack Propagation Law

In section 2.4.1 it was found that in many cases, the crack growth rate depends on the stress ratio R. This dependence is not included in (3.12), which only takes account of the stress intensity factor range ΔK. Account of R, and thus the mean stress σ_m, has been proposed by Forman, see [Forman, R.G., V.E. Kearney and R.M. Engle; 1967] and [Schijve, J.; 1979]. This section gives a presentation of Forman's proposal.

[Forman, R.G., V.E. Kearney and R.M. Engle; 1967] noticed that the Paris law was unable to describe the singularity at the critical stress intensity factor, K_c, and included this effect besides the stress ratio effect.

As shown in figure 2.7, the crack growth rate da/dN will assume infinite values as the maximum stress intensity factor, $K_{\max}$, equals K_c, i.e.

$$\lim_{K_{\max} \to K_c} \frac{da}{dN} \to \infty \tag{3.13}$$

By inserting

$$K_{\max} = \frac{\Delta K}{1 - R} \tag{3.14}$$

where R is given by (3.9), (3.13) becomes

$$\lim_{\Delta K \to (1-R)K_c} \frac{da}{dN} \to \infty \tag{3.15}$$

It is assumed that the crack growth rate has a form given by (3.12) and further, that it has a singularity given by (3.15). Forman's suggestion was

$$\frac{da}{dN} = \frac{C\,(\Delta K)^m}{(1-R)K_c - \Delta K} = \frac{C\,(\Delta K)^m}{(1-R)(K_c - K_{\max})} \tag{3.16}$$

where K is given by (2.3).

It is observed that Forman's proposal contains two possible singularities. The first appears as $K_{\max}$ equals K_c and the second singularity is obtained if $R \to 1$, i.e. if $K_{\min}$ approaches $K_{\max}$ corresponding to the stress intensity factor approaching a constant value. This is primarily interesting for high stress levels.

3.2.3 Evaluation of the Empirical Fatigue Crack Propagation Laws

The purpose of this section is to evaluate the crack propagation laws, which are described in sections 3.2.1 and 3.2.2, with regard to their applicability. The evaluation is performed by comparison with the crack propagation expression in section 3.1 and the experiments which are mentioned by different authors.

The comparison of (3.7) and Paris' law (3.12) also shows good agreement. The reason is that (3.7) can be reduced to (3.12) with $m = 4$ for $K_{\min} = 0$, see [Cherepanov, C.P. and H. Halmanov; 1972] in which experiments give $m = 3.6$ for the aluminium alloys 2024-T3 and 7075-T6 with $\beta = 0.10$ mm and $\beta = 0.15$ mm, respectively.

As described, establishment of SN-curves and use of Paris' law are two different ways of describing the fatigue properties of a structure. In spite of the differences, a connection between the two approaches exists, which can be seen by integration of (3.12)

$$N_c = \frac{1}{C}\,(\Delta\sigma)^{-m} \int_{a_0}^{a_c} (\sqrt{\pi\, a}\, F)^{-m} da \tag{3.17}$$

where (2.3) is inserted in (3.12) and

a_0 = initial crack length
a_c = critical crack length

Assuming a_0 and a_c to be constants, (3.17) becomes

$$\log(\Delta\sigma) = -\frac{1}{m}\log(N_c) + k_3 \tag{3.18}$$

Comparison of (2.1) and (3.17) shows that the material parameter m is the negative reciprocal value of the slope of the SN-curve, i.e.

$$k_1 = -\frac{1}{m} \tag{3.19}$$

whereas the material parameter C is part of

$$k_2 = k_3 = \frac{1}{m} \log \left\{ \frac{1}{C} \int_{a_0}^{a_c} (\sqrt{\pi\, a}\, F)^{-m} da \right\} \tag{3.20}$$

This shows that the Paris law is approximately consistent with the SN-approach.

[Chow, C.L., C.W. Woo and K.T. Chang; 1986] have made experiments with mild steel and aluminium alloys (7076 and 2024) among other materials. Even at different stress ratios, R, experiments show that the crack propagation rate is satisfactorily described by (3.12). There is no complete agreement on the independence of the stress ratio. Thus, [Liaw, P.K., T.R. Leax, T.R. Fabis and J.K. Donald; 1987] has observed that an increase of R results in an increase of the crack growth rate.

Paris' law describes the majority of the crack growth adequately, but is unable to describe the threshold condition and instability condition, i.e.

$$\frac{da}{dN} \to 0 \quad \text{as} \quad \Delta K \to \Delta K_{th} \tag{3.21}$$

$$\frac{da}{dN} \to \infty \quad \text{as} \quad \Delta K \to (1-R)K_c \tag{3.22}$$

respectively. See also figure 2.7.

Different attempts to include these conditions have been made, e.g. [Yokobori, T.; 1979], [Zheng, X. and M.A. Hirt; 1983] and [Zheng, X.; 1987] have proposed a correction at ΔK_{th}.

As described in section 3.2.2 Forman's equation (3.16) takes account of the stress ratio. [Cherepanov, G.P. and H. Halmanov; 1972] have found that (3.16) gives a reasonable agreement with (3.7) for one set of the parameters (K_c, R, C and m). Other values of the parameters have not been used to compare (3.16) to (3.7).

Experiments carried out at different values of R with specimens made of 7075-T6 aluminium alloy show, according to [Chand, S. and S.B.L. Garg; 1985], that the crack growth is extremely well described by (3.16). Corresponding results appear from [Forman, R.G., V.E. Kearney and R.M. Engle; 1967] for 7075-T6 and 2024-T3 aluminium alloys. Finally, the applicability of (3.16) can be seen in [Chow, C.L., C.W. Woo and K.T. Chang; 1986], where for both aluminium alloys (7076-T6 and 2024-T3) and mild steel agreement between experiments and (3.16) has been observed.

It appears, that the specimens in far the most experiments are made of aluminium alloy. It is possible to transfer the conclusions to mild steel if a) a mathematical model for the phenomenon in consideration is known or b) the parameters influencing the phenomenon can be identified. In case of alternative a) model theory can be applied, whereas dimensional analysis applies in alternative b).

Due to the simplicity of the Paris law it cannot be expected to predict fatigue behaviour in all cases, but in spite of the shortcomings mentioned, it can be concluded

that Paris' law can describe the crack growth rate in mild steel in a satisfactory way. But after all, (3.16) is more exact.

Several other empirical crack growth laws exist, see e.g. [Kanazawa, T., S. Michida and K. Itoga; 1975] and [Chand, S. and S.B.L. Garg; 1985]. These will, however, not be discussed further because they are only variations of Paris' law.

Further, some energy-based crack growth laws exist, see [Kanazawa, T., S. Machida and K. Itoga; 1975] and [Chand, S. and S.B.L. Garg; 1985]. Since these crack growth laws, which are mutually very different, apparently do not give a better description than the so-far mentioned laws and since, they are not simple in their form, they will not be further described in the present thesis.

3.3 FATIGUE UNDER VARIABLE-AMPLITUDE LOAD

The effects of variable-amplitude load (VA-load) were investigated in section 2.4.1 in which it was found that the load sequence has a decisive influence on the fatigue crack propagation progress. Several attempts to take into account these interaction effects have been performed, two of which will be discussed in this section, the Wheeler and the Elber model. Both models are evaluated in section 3.3.3.

3.3.1 Wheeler's Model

One of the most well-known empirical crack propagation laws which takes into account the retardation effect of overloads is the Wheeler model, see [Wheeler, O.E.; 1972] and [Fuchs, H.O. and R.I. Stephens; 1980].

The model seeks to correlate fatigue crack propagation due to VA-load with fatigue crack propagation due to constant-amplitude load (CA-load) in order to describe the reduced crack propagation.

The Wheeler model takes its origin in the relation between the crack growth rate da/dN and the stress intensity factor range ΔK, given by (2.3). Thus, the crack length after N cycles is given by

$$a_N = a_0 + \sum_{i=1}^{N} f(\Delta K_i) \tag{3.23}$$

where

ΔK_i = stress intensity factor range in the i'th cycle [MPa$\sqrt{\text{m}}$]

Wheeler proposed (3.23) modified by introducing an empirical retardation parameter $C_{ret,i}$ for the i th load cycle after a tensile overload, given as

$$C_{ret,i} = \begin{cases} \left[\dfrac{r_{yi}}{a_{0L} + r_{0L} - a_i}\right]^d & \text{for } a_i + r_{yi} < a_{0L} + r_{0L} \\ 1 & \text{for } a_i + r_{yi} > a_{0L} + r_{0L} \end{cases} \tag{3.24}$$

where

r_{yi} = extension of the plastic zone at the crack tip in the i th load cycle [mm]
r_{0L} = extension of the plastic zone due to a previous overload [mm]
a_{0L} = crack length at the time when overload is introduced [mm]
a_i = crack length to an arbitrary time after introducing the overload [mm]
d = empirical coefficient

The meaning of the symbols is also shown in figure 3.2.

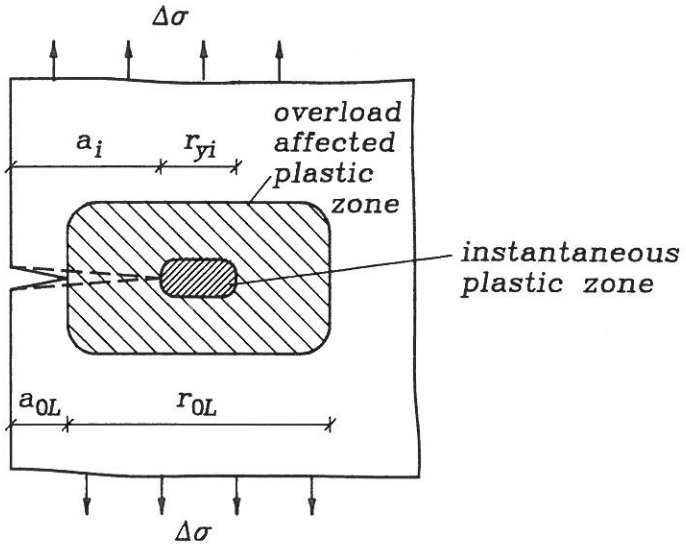

Figure 3.2: Schematic outline of plastic zones at the crack tip due to load cycles of large and small amplitude, respectively.

The size of the plastic zone in front of the crack tip can, cf. appendix A.1, be determined as

$$r_{y,i} = \begin{cases} \dfrac{1}{\pi}\left(\dfrac{K_i}{f_y}\right)^2 & \text{in plane stress} \\ \dfrac{1}{3\pi}\left(\dfrac{K_i}{f_y}\right)^2 & \text{in plane strain} \end{cases} \tag{3.25}$$

where

K = maximum stress intensity factor for the i th load cycle, i.e. for the overload and the basic load, respectively. [MPa$\sqrt{\text{m}}$]
f_y = yield stress of the material [MPa]

The crack growth in the i th load cycle is retarded if the plastic zone due to this cycle is situated inside the plastic zone due to the overload. When the actual cycle is causing a plastic zone which exceeds the extension of the plastic zone due to the large load cycle the effect of retardation is assumed to be ended. It is seen from (3.24) that the retardation parameter $C_{ret,i}$ varies between zero and one, corresponding to complete arrest of the crack growth and no retardation, respectively.

[Wheeler, O.E.; 1972] determined the empirical coefficient to $d = 1.3 - 1.75$ for a mild steel (D6ac steel).

By inserting (3.24) in (3.23) the Wheeler crack length is

$$a_N = a_0 + \sum_{i=1}^{N} C_{ret,i}\ f(\Delta K_i) \tag{3.26}$$

where f for e.g. is given by Paris' law (3.12) or Forman's equation (3.16).

The procedure for calculation of the crack length a_N is described in the following. Calculate for actual crack length a_i and actual load cycle:

a) Stress intensity factor ΔK_i

b) Size of plastic zone r_{yi}, e.g. by (3.25)

c) Retardation parameter $C_{ret,i}$ by (3.24)

d) Crack growth rate $da/dN = C_{ret,i}\, f(\Delta K_i)$

e) New crack length by (3.26)

f) New overload plastic zone if $a_i + r_{yi} \geq a_{0L} + r_{0L}$

Repeat a)-f) until $N > N_{\max}$.

3.3.2 Elber's Crack Closure Model

As explained in section 2.4.2, crack closure is one of the main causes for the interaction effects described in section 2.4.1. Elber's crack closure model, described in the present section, is one of the fatigue crack propagation laws which takes into account the phenomenon of crack closure.

Elber's crack closure model was originally derived to describe fatigue crack growth under CA-load in aluminium alloy (2024-T3), see [Elber, W.; 1971].

An effective stress range ratio, U, defined as

$$U = \frac{\sigma_{\max} - \sigma_{op}}{\sigma_{\max} - \sigma_{\min}} = \frac{\Delta\sigma_{\text{eff}}}{\Delta\sigma} \tag{3.27}$$

where the effective stress range $\Delta\sigma_{\text{eff}}$, given by (2.9), and the stress range $\Delta\sigma$, given by (2.6), are introduced in Paris' law (3.12), i.e.

$$\frac{da}{dN} = C\,(U\,\Delta K)^m = C\,(\Delta K_{\text{eff}})^m \tag{3.28}$$

The effective stress intensity factor range ΔK_{eff} defined by (3.28) can in case of linear elastic materials be written as

$$\Delta K_{\text{eff}} = K_{\max} - K_{op} \tag{3.29}$$

where $K_{\max}$ is given by (3.8) and where the opening stress intensity factor K_{op} according to (2.3) is given as

$$K_{op} = \sigma_{op}\sqrt{\pi\,a}\,F \tag{3.30}$$

This means that the crack growth rate under CA-load in (3.28) varies with the opening stress.

[Elber, W.; 1971] found that for constant ΔK, U increases for increasing stress ratio R, (3.9). I.e., K_{op} increases slower than $K_{\max}$.

It is seen, that if the variation of K_{op} - or σ_{op} - is known, Elber's crack closure model can explicitly be used in case of VA-load. [Robin, C., M. Louah and G. Pluvinage; 1983] found that for VA-load with a single overload the minimum crack growth rate decreased for increasing maximum value of the overload. At the minimum crack growth rate following an overload, K_{op} assumes its maximum value, see also figure 2.23. No information of other cases of VA-load has been found.

3.3.3 Evaluation of the Variable-Amplitude Fatigue Crack Propagation Models

The purpose of this section is to evaluate Wheeler's model (3.26) and Elber's crack closure model (3.28). The evaluation is primarily performed by comparison with the experiments which are mentioned by different authors.

The validity of (3.7) was proven in section 3.2. The parameter σ_0, which stands for the pre-load history, is changed and thus β is changed, when variable-amplitude load is introduced. A direct comparison between (3.26) and (3.7) has not been performed.

Wheeler's model gives a good description of the retardation due to deterministic, cyclic load in which one or more tensile overloads are introduced, cf. [Corbly, D.M. and P.F. Packman; 1973] and [Wheeler, O.E.; 1972]. But, if a great overload appears, Wheeler's model results in a poorer description of the crack growth rate. This is because the Wheeler model does not give any possibility for taking accelerated growth

in to consideration. Therefore, the model cannot describe delayed retardation (see section 2.4.1).

The effects of crack closure can be included in (3.7) by the parameter β, but Elber's crack closure model has not been directly compared to (3.7).

Determination of the progress, i.e. the variation and size of the opening stress σ_{op} is one of the main problems using the Elber model. The variation of σ_{op}, which was discussed in section 2.4.2, seems to be very well known, whereas disagreement on how to determine the size exists. Several attempts have been made.

[Shin, C.S. and N.A. Fleck; 1987] found that crack closure almost accounted for the interaction effects in BS4360 50B steel and in 2014-T4 aluminium alloy. According to [Robin, C., M. Louah and G. Pluvinage; 1983] the changes of the crack growth rate and of the U-ratio in a mild steel were not similar. This observation supports the statement that the interaction effects cannot solely be explained by the crack closure concept, but that other phenomena must have an influence.

Besides the Wheeler model and the Elber crack closure model, several other attempts have been made to describe fatigue crack growth under variable-amplitude load. But since most of them are more complicated than the two above-mentioned attempts without giving a better description of the fatigue progress they will not be further discussed.

3.4 FATIGUE UNDER RANDOM LOAD

As mentioned in chapter 1, the dynamic load on civil engineering structures is often of random character. The modelling of the random load was discussed in section 2.3.

The crack growth rate da/dN can, if the load history is of a relative simple random nature, be described directly as a random process determined by the load history, cf. [Arone, R.; 1986].

If the case is not as above, the crack growth rate has to be described by a different random process. [Jacoby, G.H. and H. Nowack; 1972] have by analysis of test data concluded that both the Weibull distribution and the Log-normal distribution are able to describe the crack growth rate.

The purpose of this section is to give some guidelines for estimating the fatigue crack growth rate in case of random load. Two different attempts will be discussed.

The first contains models based on the so-called characteristic K-value concept and in the other cycle-by-cycle prediction is used. The models, which are described in sections 3.4.1 and 3.4.2, are evaluated in section 3.4.3.

3.4.1 Characteristic K-Value Fatigue Crack Growth Models

Two models using the characteristic K-value concept are discussed in this section.

Both models are based on fatigue crack growth models used to describe fatigue crack growth under CA-load.

The basic idea in the characteristic K-value concept is to have a single (characteristic) stress intensity parameter that can be used to describe the fatigue crack growth under random load.

Several authors, e.g. [Barsom, J.M.; 1973] and [Alawi, H.; 1986], use the root mean square stress intensity factor range, ΔK_{rms}, in combination with Paris' law (3.12) to calculate the average fatigue crack growth rate

$$\frac{da}{dN} = C\ (\Delta K_{rms})^m \tag{3.31}$$

where

$$\begin{aligned} \Delta K_{rms} &= [\tfrac{1}{N}\textstyle\sum_{i=1}^{N}(\Delta K_i)^2]^{\frac{1}{2}}\ [\mathrm{MPa}\sqrt{\mathrm{m}}] \\ N &= \text{number of cycles} \\ \Delta K_i &= \text{stress intensity factor range in the } i\text{ th cycle } [\mathrm{MPa}\sqrt{\mathrm{m}}] \end{aligned}$$

To calculate ΔK_{rms} it is necessary to have realizations of the random load in order to identify the load cycles.

It seems reasonable to use the Paris law as a basis for a random fatigue model because this law gives an adequate description of fatigue crack growth under CA-load, see sections 3.2.1 and 3.2.3. But, it should be noted that the sequence effects discussed in section 2.4.1 are neglected. Further, e.g. stress ratio effects are disregarded.

The latter effects are taken into account in [Hudson, C.M.; 1981] in which the Forman equation (3.16) is used as a basis, i.e.

$$\frac{da}{dN} = \frac{C(\Delta K^*_{rms})^m}{(1-R_{rms})K_c - \Delta K_{rms}} \tag{3.32}$$

where

$$\begin{aligned} \Delta K^*_{rms} &= K_{\max,rms} - K_{\min,rms}\ [\mathrm{MPa}\sqrt{\mathrm{m}}] = \text{root mean square stress intensity factor} \\ R_{rms} &= K_{\min,rms}/K_{\max,rms} = \text{root mean square stress intensity factor ratio} \\ K_{\max,rms} &= [\tfrac{1}{N}\textstyle\sum_{i=1}^{N}(K_{\max})^2]^{\frac{1}{2}}\ [\ [\mathrm{MPa}\sqrt{\mathrm{m}}] \\ K_{\min,rms} &= [\tfrac{1}{N}\textstyle\sum_{i=1}^{N}(K_{\min})^2]^{\frac{1}{2}}\ [\mathrm{MPa}\sqrt{\mathrm{m}}] \end{aligned}$$

Notice, that the definition of ΔK^*_{rms} is different from the one used in (3.31). This new definition is simpler because it is not necessary to discuss how to define a cycle, but still relizations are demanded.

3.4.2 Cycle-by-Cycle Counting Fatigue Crack Growth Models

In this section a fatigue crack growth model based on the cycle-by-cycle counting concept are discussed.

Using cycle-by-cycle counting the fatigue crack growth rate is calculated after each load cycle applied.

The fatigue crack growth progress is discretized so the progress is described as a series of crack front extensions. It is assumed that the crack growth rate during the i th load cycle is constant and that the crack propagation in that load cycle is Δa_i. Thus, the crack length after N cycles is given as

$$a_N = a_0 + \sum_{i=1}^{N} \Delta a_i \tag{3.33}$$

From section 2.4.2 it is known that crack closure has a decisive influence on fatigue crack growth and in section 3.3 it was concluded that the effective stress intensity factor range can be used to take the crack closure effects into account.

Thus, it is convenient to use the effective stress intensity factor range, (3.29), to determine the crack growth rate in the i th load cycle,

$$\Delta a_i = f(\Delta K_{\text{eff},i}) \tag{3.34}$$

where f can be established by one of the methods previously discussed. This method was proposed in [Schijve, J.; 1980].

3.4.3 Evaluation of Fatigue Crack Growth Models under Random Load

Two types of model to describe fatigue crack growth under random load have been introduced.

The models based on characteristic K-values are less resource demanding compared to the cycle-by-cycle counting models, but the former models are also less accurate.

[Barsom, J.M.; 1973] used (3.31) to describe the fatigue crack growth in a high strength steel (ASTM A514-B steel) subjected to a pseudo narrow-banded random spectrum (repeated programmed block load - see figure 2.10) with tensile load. In this case, (3.31) was able to give a good description of the fatigue progress. It must be expected that the model fails if compressive loads or single overloads are introduced, but no further investigations have been found in the literature.

CCT-specimens (2219-T851 aluminium alloy) and simulated random flight-by-flight spectrum loads were used to test (3.32). For different R-ratios [Hudson, C.M.; 1981] found good agreement between (3.32) and the simulated data for small values of the crack growth rate da/dN. But, the model failed for increasing values of the stress intensity factor range where a large scatter of da/dN appeared.

Using the cycle-by-cycle counting concept together with an adequate fatigue crack growth model, i.e. one which takes into account the interaction effects, an appropriate description of the fatigue progress must be expected.

A disadvantage is that the cycle-by-cycle counting methods demand an enormous amount of calculation. In [Schijve, J.; 1980] several attempts to use the cycle-by-cycle counting concept have been performed, but in all cases the load spectrum has been simplified to some degree. Examples of the simplifications are assumption of constant crack opening stress intensity factor and omission of low-level amplitude cycles. Both conservative and non-conservative results were obtained.

Several other attempts have been made. [Arone, R.; 1986] established a model in which the fatigue crack growth was determined as a superposition of the constant-amplitude and the overload fatigue crack growth, respectively. Among others, [Chakrabarti, A.K.; 1980] used a dislocation model in which it was assumed that, the crack only grow when the dislocation distribution becomes critical. The critical dislocation distribution is difficult to determine. This model will not be further discussed in this paper.

All types of model demand knowledge of realizations of the random load. No attempts based solely on the statistical properties of the load have been found.

3.5 EVALUATION

The main purpose of this chapter was to describe and evaluate the existing fatigue crack growth models.

On the assumption that all parameters influencing the fatigue progress have been taken into account, dimensional analysis results in a general fatigue crack growth model. This will give a large number of parameters so in section 3.1 only those assumed to be the most important are used in the dimensional analysis to establish a fatigue crack growth model.

Only one parameter, β, depending on the load type and on the pre-load history is unknown, but also very difficult to determine.

In section 3.2 it was found that the empirical Paris law (3.12) gives a good description of fatigue crack growth in a structure subjected to constant-amplitude load even though the form of the law is simple. The two model parameters C and m, which must be determined experimentally, are assumed to be material constants, but especially C varies considerably. In spite of the difference in the description of the fatigue, a connection between SN-curves, (2.1), and the crack growth theory, (2.2), represented by Paris' law (3.12), exists, see section 3.2.3. It was also found that the Forman equation (3.16) is useful to describe fatigue crack growth under constant-amplitude load when different stress ratios are introduced. This model should be used if the fatigue properties of a material is sensitive to changes in the stress ratio.

If the structure is subjected to variable-amplitude load the fatigue crack growth model has to take into account the interaction effects due to overloads. The effects are retardation, acceleration and delayed acceleration. Two models were discussed in section 3.3. The Wheeler model (3.26) seems to give a reasonable description of the crack growth rate if the overloads are tensile. But, if the overloads are of compressive nature, the Wheeler model fails. Parts of the interaction effects can be taken into account using the Elber crack closure model. The concept of the model is good, but there is still some disagreement how to determine the size of the model parameter in the form of the crack opening stress intensity factor.

Fatigue crack growth under random load was dealt with in section 3.4. The characteristic K-value concept makes it possible to give a simple description of the fatigue crack growth under random load, but with the consequence that sequence effects are disregarded. This is not the case in the cycle-by-cycle counting models, but here two problems arise. Firstly, the method necessitates enormous amounts of calculation and secondly, the problem of the crack opening stress intensity factor appears.

Ideally, a fatigue crack growth model incorporates the influence of the load - including the stress range, the R-ratio and the load sequence effects - and of the material properties.

None of the above mentioned models fulfil these demands because all the models are deterministic and thus, they do not consider the inherent fluctuations characteristic of fatigue. The fluctuations are due to variations in

initial state, i.e. the distribution of the initial damage e.g. initial crack length,

magnitude and order of load cycles resulting in interaction effects in the form of retardation or acceleration of the fatigue crack growth rate,

material properties in the form of e.g. inhomogeneities and loss of isotropy,

all of which influence the fatigue crack growth.

Usually, distinction is made between two main groups of fatigue crack growth models: deterministic models and probabilistic models.

The deterministic models describe the expected value of the mean damage accumulation, whereas the probabilistic models in addition describe other statistical properties as e.g. variance of the crack growth rate. Thus, the probabilistic models take account of the fluctuations making the models more realistic.

The simplest way to establish a probabilistic model is to introduce random parameters in one of the deterministic models, e.g. in the Paris law.

This has been done in [Madsen, H.O.; 1982, p. 6.18-6.29] and in [Madsen, H.O., S. Krenk and N.C. Lind; 1986, p.272-276] by randomizing the Paris constant C. In case of CA-load this method gives satisfactory results, but the interaction effects are not taken into account. This approach will not be further discussed.

Several other probabilistic, fatigue crack growth models exist. In many cases, a direct

solution in the form of an analytical solution do not exist and thus, a numerical solution strategy is introduced.

This approach is found in the model described by [Ditlevsen, O. and R. Olesen; 1985] in which the crack increment da is measured for fixed values of the increment in number of load cycles, dN, i.e., da is random.

A more appropriate method is to use da as a fixed parameter and dN to cause da as a random variable so the distribution of number of cycles performed to reach a given crack length a, can be determined. Until now, no attempts to this approach have been made but, [Bogdanoff, J.L. and F. Kozin; 1985] have developed a numerical model based on Markov Chain theory and the state of damage. It looks like, this model might be useful and it will be further discussed in chapter 4, bearing in mind that the purpose of this thesis is to establish a simple, improved fatigue model which is based on the existing knowledge of fatigue crack growth. Further, it should be possible for a given material to transfer the results from one structure to another.

4. THE B-MODEL

As mentioned in chapter 3, it is often necessary to introduce a numerical model in order to describe the fatigue crack growth process.

For the purpose of establishing a numerical, probabilistic crack growth model based on the physical knowledge of fatigue, one of the most well-known models is presented in this chapter. The model, which in the present thesis is referred to as the B-model, is the cumulative damage model developed by Bogdanoff and Kozin, see e.g. [Bogdanoff, J.L. and F. Kozin; 1985], [Bogdanoff, J.L.; 1978a], [Bogdanoff, J.L. and W. Krieger; 1978], [Bogdanoff, J.L.; 1978b] and [Bogdanoff, J.L. and F. Kozin; 1980].

4.1 PRESENTATION OF THE B-MODEL

A short presentation of the B-model, focusing on the basic elements, is given in this section.

A basic element in the B-model is the division of the load into duty cycles, see figure 4.1. A duty cycle (DC) is defined as a repetitive period of operation in the life of a component during which damage may accumulate.

In figure 4.1(a) each DC is equal and consists of equal load cycles. The number of equal load cycles in the DCs can be e.g. 100 or 1000.

Likewise, the variable-amplitude load shown in figure 4.1(b) is divided into equal DCs, but each DC consists of different load cycles. It is also possible to have different but deterministic DCs, e.g. the sequence shown in figure 4.1(b) could be divided into 1th DC $= n_1$ cycles, 2nd DC $= n_2$ cycles and all the following DCs $= n_1$ cycles.

Dealing with random load a duty cycle is defined as half a load cycle, see figure 4.1(c). This gives a large number of DCs, so often the random load is modelled as a stochastic process, see also section 2.3. In the latter case, the information of the sequences of load cycles - and thus of the interaction effects (described in chapter 2) - will be lost, unless the state parameters in the model are chosen adequately.

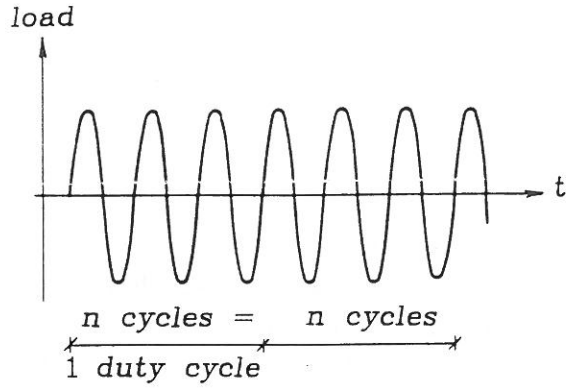

(a) Constant–amplitude load

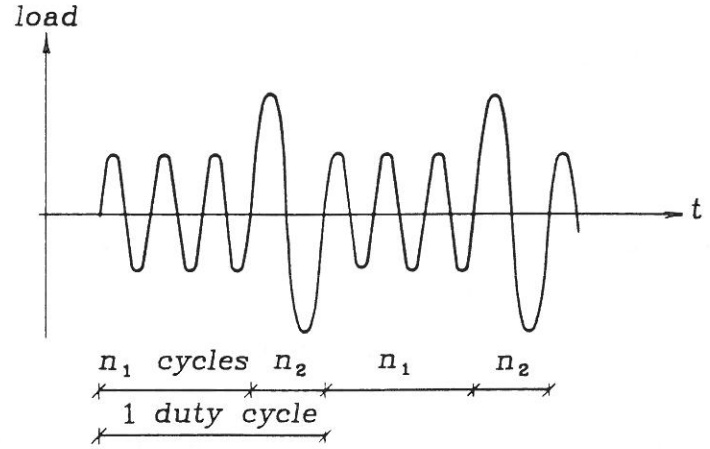

(b) Variable–amplitude load

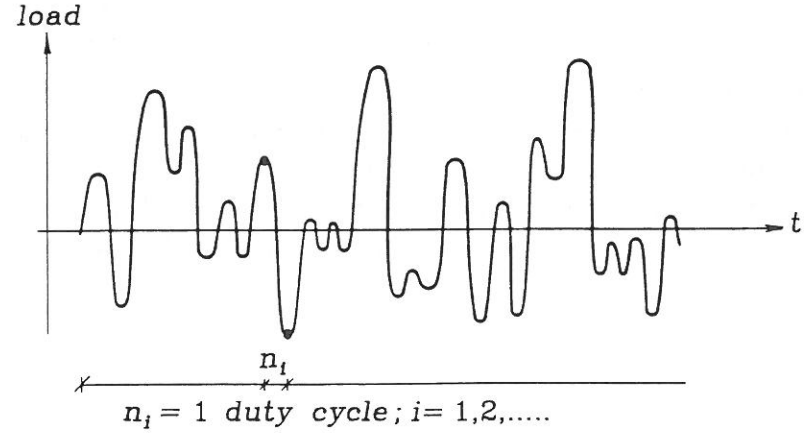

(c) Random load

Figure 4.1: Examples of duty cycles.

The discrete time, x, is measured in number of DCs, $x = 1, 2, \ldots$, number of DCs. The damage accumulation is considered to be a stochastic process in which the possibility of damage accumulation is present each time the structure has experienced a DC.

The damage d is assumed to be discrete with the states $d = 0, 1, 2, ..., b$, where b

corresponds to failure. Further, it is assumed that the increment of damage at the end of the DC only depends on the DC itself and the state of damage present at the start of the DC, i.e. the history of damage accumulation has no influence. The damage only increases by one unit at a time, see figure 4.2, and it is required that the damage measure describes a non-decreasing function.

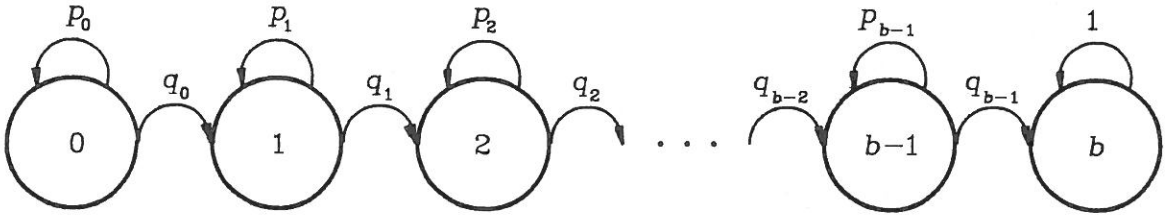

Figure 4.2: Illustration of the principle in the B-model. Each circle represents a damage state, $d = 0, 1, 2, ..., b$. The p_j and q_j values are defined in (4.3).

Hereby, the damage accumulation process can be regarded as a discrete-time, discrete-state Markov process, see e.g. [Bogdanoff, J.L. and Kozin, F; 1985, ch.2] and [Papoulis, A.; 1984, p.385].

Such a Markov process is completely described by its transition matrix (one transition matrix for each duty cycle) and by the initial conditions.

The initial probability distribution of the damage states is given by the vector

$$\overline{p}_0 = \{\pi_0, \pi_1, \pi_2, ..., \pi_{b-1}, \pi_b\} \quad ; \quad \pi_j \geq 0 \quad ; \quad \sum_{j=0}^{b} \pi_j = 1 \tag{4.1}$$

where

$$\begin{aligned} j &= 0, 1, 2, \ldots, b-1 \\ \pi_j &= \text{probability of damage initially being in state } j \\ \pi_b &= 0 \end{aligned}$$

As an example, mention can be made of the initial crack length distribution in a weld. It will be possible, from empirical knowledge of the initial crack lengths of the weld, to determine this distribution, e.g. by assuming that 10% of the initial cracks has a length of 1.3 mm, 5% has a length of 1.6 mm etc.

As mentioned earlier, the damage only increases by one unit at a time. Thus, it is possible to establish the $((b+1) \times (b+1))$ transition matrix $\overline{\overline{P}}_i$ for the i th duty cycle given by

$$\overline{\overline{P}}_i = \begin{bmatrix} p_0 & q_0 & 0 & 0 & \cdots & 0 & 0 & \cdots & 0 & 0 \\ 0 & p_1 & q_1 & 0 & \cdots & 0 & 0 & \cdots & 0 & 0 \\ 0 & 0 & p_2 & q_2 & \cdots & 0 & 0 & \cdots & 0 & 0 \\ \vdots & \vdots & \vdots & \vdots & \ddots & \vdots & \vdots & \ddots & \vdots & \vdots \\ 0 & 0 & 0 & 0 & \cdots & p_j & q_j & \cdots & 0 & 0 \\ \vdots & \vdots & \vdots & \vdots & \ddots & \vdots & \vdots & \ddots & \vdots & \vdots \\ 0 & 0 & 0 & 0 & \cdots & 0 & 0 & \cdots & p_{b-1} & q_{b-1} \\ 0 & 0 & 0 & 0 & \cdots & 0 & 0 & \cdots & 0 & 1 \end{bmatrix} \tag{4.2}$$

$i = 1, 2, \ldots,$ number of DCs

where the conditional probabilities

$$\begin{aligned} p_j &= \text{prob } \{\text{remain in state } j | \text{ previously in state } j\} \\ q_j &= \text{prob } \{\text{go to state } j+1 | \text{ previously in state } j\} \end{aligned} \tag{4.3}$$

and

$$\left.\begin{array}{l} 0 \le p_j \le 1 \\ 0 \le q_j \le 1 \\ p_j + q_j = 1 \end{array}\right\} \quad j = 0, 1, 2, \ldots, b-1$$

$$p_b = 1$$

The damage state at the time x is then given by the vector

$$\overline{p}_x = \overline{p}_0 \, \overline{\overline{P}}_1 \, \overline{\overline{P}}_2 \, \cdots \, \overline{\overline{P}}_x \tag{4.4}$$

where

$\overline{p}_0$ is given by (4.1)
$\overline{p}_x = \{p_x(j)\} = \{\text{prob } \{\text{damage is in state } j \text{ at time } x\}\}$

If $\overline{\overline{P}}_i$ is identical for all duty cycles, i.e. $\overline{\overline{P}}_i = \overline{\overline{P}}$, (4.4) is written as

$$\overline{p}_x = \overline{p}_0 \, \overline{\overline{P}}^{\,x} \tag{4.5}$$

The power notation refers to matrix multiplication, e.g. $\overline{\overline{P}}^{\,3} = \overline{\overline{P}}\,\overline{\overline{P}}\,\overline{\overline{P}}$.

Hereby, the basic ideas of the B-model are introduced.

4.2 EXAMPLE OF THE USE OF THE B-MODEL

As an illustration of the B-model, a very simple example is given in this section.

It is assumed that the number of damage states $b = 10$ and that the state of damage is considered after 5 duty cycles ($x = 5$). Further, the initial damage state vector, given by (4.1),

$$\overline{p}_0 = \{\, 0.10 \quad 0.18 \quad 0.13 \quad 0.12 \quad 0.12 \quad 0.09 \quad 0.08 \quad 0.08 \quad 0.07 \quad 0.03 \quad 0 \,\}$$

is assumed to be the same, no matter how the transition matrix $\overline{\overline{P}}$ is.

Firstly, the conditional probabilities (4.3) are $p_j = p = 0.80$ and $q_j = q = 0.20$ so $\overline{\overline{P}}_{\{1\},i} = \overline{\overline{P}}_{\{1\}}$,

$$\overline{\overline{P}}_{\{1\}} = \begin{bmatrix} 0.80 & 0.20 & 0 & 0 & 0 & 0 & 0 & 0 & 0 & 0 & 0 \\ 0 & 0.80 & 0.20 & 0 & 0 & 0 & 0 & 0 & 0 & 0 & 0 \\ 0 & 0 & 0.80 & 0.20 & 0 & 0 & 0 & 0 & 0 & 0 & 0 \\ 0 & 0 & 0 & 0.80 & 0.20 & 0 & 0 & 0 & 0 & 0 & 0 \\ 0 & 0 & 0 & 0 & 0.80 & 0.20 & 0 & 0 & 0 & 0 & 0 \\ 0 & 0 & 0 & 0 & 0 & 0.80 & 0.20 & 0 & 0 & 0 & 0 \\ 0 & 0 & 0 & 0 & 0 & 0 & 0.80 & 0.20 & 0 & 0 & 0 \\ 0 & 0 & 0 & 0 & 0 & 0 & 0 & 0.80 & 0.20 & 0 & 0 \\ 0 & 0 & 0 & 0 & 0 & 0 & 0 & 0 & 0.80 & 0.20 & 0 \\ 0 & 0 & 0 & 0 & 0 & 0 & 0 & 0 & 0 & 0.80 & 0.20 \\ 0 & 0 & 0 & 0 & 0 & 0 & 0 & 0 & 0 & 0 & 1 \end{bmatrix}$$

and (4.5) gives the damage state vector after 5 DCs,

$$\begin{aligned} \overline{p}_{\{1\},5} &= \overline{p}_0 \, \overline{\overline{P}}_{\{1\}}^{\,5} \\ &= \{\, 0.0328 \quad 0.0999 \quad 0.1368 \quad 0.1346 \quad 0.1250 \quad 0.1111 \quad 0.0947 \quad 0.0844 \\ &\qquad 0.0775 \quad 0.0596 \quad 0.0438 \,\} \end{aligned}$$

Secondly, the conditional probabilities are assumed to be equal, i.e. $p_j = p = q_j = q = 0.50$ so $\overline{\overline{P}}_{\{2\},i} = \overline{\overline{P}}_{\{2\}}$,

$$\overline{\overline{P}}_{\{2\}} = \begin{bmatrix} 0.50 & 0.50 & 0 & 0 & 0 & 0 & 0 & 0 & 0 & 0 & 0 \\ 0 & 0.50 & 0.50 & 0 & 0 & 0 & 0 & 0 & 0 & 0 & 0 \\ 0 & 0 & 0.50 & 0.50 & 0 & 0 & 0 & 0 & 0 & 0 & 0 \\ 0 & 0 & 0 & 0.50 & 0.50 & 0 & 0 & 0 & 0 & 0 & 0 \\ 0 & 0 & 0 & 0 & 0.50 & 0.50 & 0 & 0 & 0 & 0 & 0 \\ 0 & 0 & 0 & 0 & 0 & 0.50 & 0.50 & 0 & 0 & 0 & 0 \\ 0 & 0 & 0 & 0 & 0 & 0 & 0.50 & 0.50 & 0 & 0 & 0 \\ 0 & 0 & 0 & 0 & 0 & 0 & 0 & 0.50 & 0.50 & 0 & 0 \\ 0 & 0 & 0 & 0 & 0 & 0 & 0 & 0 & 0.50 & 0.50 & 0 \\ 0 & 0 & 0 & 0 & 0 & 0 & 0 & 0 & 0 & 0.50 & 0.50 \\ 0 & 0 & 0 & 0 & 0 & 0 & 0 & 0 & 0 & 0 & 1 \end{bmatrix}$$

and (4.5) gives

$$\begin{aligned} \overline{p}_{\{2\},5} &= \overline{p}_0 \, \overline{\overline{P}}_{\{2\}}^{\,5} \\ &= \{\, 0.0031 \quad 0.0213 \quad 0.0634 \quad 0.1116 \quad 0.1350 \quad 0.1309 \quad 0.1175 \quad 0.1034 \\ &\qquad 0.0903 \quad 0.0797 \quad 0.1438 \,\} \end{aligned}$$

Finally, $p_j = p = 0.20$ and $q_j = q = 0.80$ so $\overline{\overline{P}}_{\{3\},i} = \overline{\overline{P}}_{\{3\}}$,

$$\overline{\overline{P}}_{\{3\}} = \begin{bmatrix} 0.20 & 0.80 & 0 & 0 & 0 & 0 & 0 & 0 & 0 & 0 & 0 \\ 0 & 0.20 & 0.80 & 0 & 0 & 0 & 0 & 0 & 0 & 0 & 0 \\ 0 & 0 & 0.20 & 0.80 & 0 & 0 & 0 & 0 & 0 & 0 & 0 \\ 0 & 0 & 0 & 0.20 & 0.80 & 0 & 0 & 0 & 0 & 0 & 0 \\ 0 & 0 & 0 & 0 & 0.20 & 0.80 & 0 & 0 & 0 & 0 & 0 \\ 0 & 0 & 0 & 0 & 0 & 0.20 & 0.80 & 0 & 0 & 0 & 0 \\ 0 & 0 & 0 & 0 & 0 & 0 & 0.20 & 0.80 & 0 & 0 & 0 \\ 0 & 0 & 0 & 0 & 0 & 0 & 0 & 0.20 & 0.80 & 0 & 0 \\ 0 & 0 & 0 & 0 & 0 & 0 & 0 & 0 & 0.20 & 0.80 & 0 \\ 0 & 0 & 0 & 0 & 0 & 0 & 0 & 0 & 0 & 0.20 & 0.80 \\ 0 & 0 & 0 & 0 & 0 & 0 & 0 & 0 & 0 & 0 & 1 \end{bmatrix}$$

and (4.5) gives

$$\begin{aligned} \overline{p}_{\{3\},5} &= \overline{p}_0 \, \overline{\overline{P}}_{\{3\}}^{\,5} \\ &= \{\, 0.0000 \quad 0.0007 \quad 0.0063 \quad 0.0306 \quad 0.0853 \quad 0.1401 \quad 0.1436 \quad 0.1215 \\ &\qquad 0.1115 \quad 0.0971 \quad 0.2634 \,\} \end{aligned}$$

A comparison between the state vectors $\overline{p}_{\{1\},5}$, $\overline{p}_{\{2\},5}$ and $\overline{p}_{\{3\},5}$ is possible because the initial state vector is the same in all 3 cases. It shows that the probability of being in a state, e.g. state 2, after 5 DCs is highly dependent on the transition probability.

Thus, the probability of being in state 2 is changing from the initial value 0.13 to 0.1368, 0.0634 and 0.0063, respectively.

4.3 EVALUATION OF THE B-MODEL

The advantage of the B-model is, that once the model parameters π_j, p_j, q_j; $j = 0, 1, 2, \ldots, b$ are determined, the state of damage in the given structure is available at any time using (4.4). This means that all statistical information about the damage process can be represented by the model.

One of the drawbacks of the model is that a great number of parameters are involved and that it is not clear how to determine these parameters. Further, the physical knowledge of the structure is not directly used, but is contained in the model parameters p_j and q_j; $j = 0, 1, 2, \ldots, b$, which are only valid for the given problem. Thus, the damage states are not uniquely related to measurable physical quantities.

The B-model has been tested on data originating from several experiments. The most well-known set of data is the Virkler data, cf. [Bogdanoff, J.L and F. Kozin; 1985, ch.4] and [Virkler, D.A., B.M. Hillberry and P.K. Goel; 1979]. The Virkler data, shown in figure 6.1, are further discussed in section 6.1.

The Virkler data were obtained in 68 tests using 2024-T3 aluminium alloy CCT-specimens (Center Cracked Tension). The CCT-specimens were influenced by constant-amplitude loading and in each test 164 values of the number of cycles and the crack length (N, a) were recorded for fixed values of δa. The initial crack length a_0 = 9.0 mm and the failure crack length a_f = 49.8 mm.

The estimated mean (N, a)-curve, obtained by using the B-model, has a remarkably smooth progress. In accordance with [Bogdanoff, J.L. and F. Kozin; 1980] the model parameters have the values as follows. The number of damage states are $b = 225$. The ratio $r_j = p_j/q_j$ varies from about 10-15 for the states $d = 1, \ldots, 214$ to 30.4 at states $d = 215, \ldots, 221$ and finally 42.5 at states $d = 222, \ldots, 224$. A damage state corresponds to a crack length. However, no systematic method for parameter estimation exists, and it is not clear how they are determined. Additionally, it seems strange that the r_j-ratios are increasing for increasing d. It should be expected, that r_j decreases because the probability of going to the next damage state after a DC increases during lifetime.

Further, the cumulative distribution function obtained from the model to reach the crack length a = 20 mm is compared with the corresponding empirical distribution function, see figure 4.3.

The distributions are obtained as follows: For a given number of cycles the fraction of the total number of observations having the crack length a = 20 mm is determined.

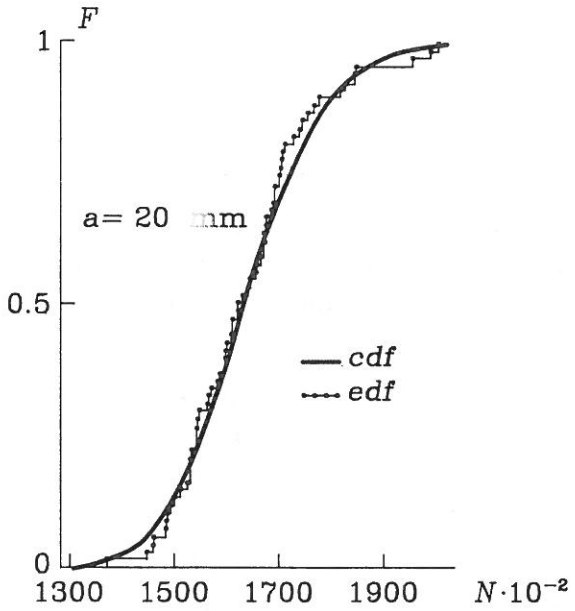

Figure 4.3: Cumulative distribution function (cdf) obtained from the B-model to reach the crack length $a = 20$ mm and the corresponding empirical distribution function (edf). Based on [Bogdanoff, J.L. and F. Kozin; 1985, p.249].

As illustrated, minimum 130000 cycles must be applied to reach the crack length $a = 20$ mm. Half of the specimens will have reached $a = 20$ mm applying ≈ 163000 cycles, whereas ≈ 203000 cycles must be applied before all specimens have reached $a = 20$ mm.

Thus, when the model parameters are determined from a set of empirical data (and it is still not clear how to do that), the model describes these data extremely well.

Similar results are found applying the B-model to other data, cf. [Bogdanoff, J.L. and F. Kozin; 1985, ch.4] and [Tanaka, S., M. Ichikawa and S. Akita; 1984]. The good agreement between observed and estimated (N, a)-curves indicates that the Markov assumption used in the B-model is reasonable. Taking account of the load history in the state parameters, the Markov assumption can be used since, steel it-self has no memory.

This result is used in chapter 5 where existing knowledge of crack propagation is incorporated into the B-model.

5. THE FRACTURE MECHANICAL MARKOV CHAIN FATIGUE MODEL

The purpose of this chapter is to develop a fatigue crack growth model, which is based on the ideas of the B-model - described in chapter 4 - and on the existing knowledge of fatigue crack growth, see chapters 2 and 3. Further, it should be possible for a given material to transfer the results from one structure to another. The model, which is developed in section 5.1-5.4, is named the Fracture Mechanical Markov Chain Fatigue Model (FMF-model). The model is stochastic in the manner that the material properties are assumed stochastic. Thus, it is assumed that under the same external conditions such as material, geometry and load, the damage state will be different due to the inherent variability of the material. The load can be deterministic as well as random.

5.1 THE BASIC IDEAS OF THE FMF-MODEL

As mentioned in chapter 3, the crack length, a, can be used as a damage measure which is an advantage since a is a quantity that can easily be observed. Further, a reliable connection between the load process and the process of fatigue, in the form of crack growth, has been established and verified by experiments. The connection is represented by a crack propagation law, which in most cases expresses the crack propagation as a function of the so-called stress intensity factor range ΔK, see also section 2.2.2.

In the FMF-model, the damage is assumed to progress in steps of the length δa. Under given conditions, see section 5.2, δa can be determined from (5.30). Thus, the j th state of damage can be defined as

$$a_j = a_0 + j\ \delta a \quad ; \quad a_j \leq a_b \quad ; \quad j = 0, 1, 2, \ldots, b \tag{5.1}$$

where

a_j = crack length at damage state j [mm]
a_0 = initial crack length [mm]
a_b = failure crack length [mm]

The above has the effect that both the damage process and the crack growth process are stepwise even though a continuous process for the latter would be more realistic from a continuum point of view.

In agreement with the Markov assumption used in the B-model (see chapter 4), damage is only accumulated when the crack propagates. As long as the crack remains in a given state, the same test is repeated each time a DC is applied. This means, that at a given crack state, $a = a_j$, the propagation of the crack can be modelled

by a Bernoulli random variable Z, see e.g. [Benjamin, J.R. and C.A. Cornell; 1970, p.222].

$$z = \begin{cases} 0 & \text{the crack remains in the given state} \\ 1 & \text{the crack propagates } \delta a \end{cases} \tag{5.2}$$

The probability density function of Z then is

$$\mathrm{f}_Z(z) = \begin{cases} p_j = 1 - q_j & \text{for } z = 0 \\ q_j & \text{for } z = 1 \end{cases} \qquad j = 0, 1, 2, \ldots, b \tag{5.3}$$

The quantity q_j is known as the transition probability, see also (4.3). The crack growth problem is then reduced to the determination of the transition probability which is a function of the stress intensity factor range, which is a function of the crack state, i.e. $q_j = q(\Delta K_j) = q(\Delta K(a_j))$.

The most simple situation occurs if ΔK is constant, i.e. the crack tip load is constant - thus the applied stress range $\Delta\sigma$ is decreasing - no matter how long the crack is. If so, $\Delta K_j = \Delta K$ and hence, $q_j = q$. This situation is dealt with in the rest of this section and is taken into account as an illustrative introduction to the FMF-model.

On the basis of the empirical Paris' law, which is one of the most frequently used crack propagation laws, see chapter 3, and the geometric distribution, see (5.6), the estimation of q is possible.

Paris' law, see [Paris, P. and F. Erdogan; 1963], is given as (see also (3.12))

$$\frac{da}{dN} = C\,(\Delta K)^m \tag{5.4}$$

where

$$\begin{array}{lcl} da/dN & = & \text{crack growth rate [mm/cycle]} \\ C & = & \text{material constant [mm/(MPa}\sqrt{\text{m}})^m] \\ m & = & \text{material constant} \\ \Delta K & = & \text{stress intensity factor range [MPa}\sqrt{\text{m}}] \end{array}$$

Empirically, a set of sample curves - (N, a)-curves - is measured. The number of duty cycles N are assumed to be observed for fixed values of the crack length a. Further, the duty cycles are assumed to be equal.

The crack growth rate can be estimated in different ways depending on the definition of the slope of the sample curves. In the FMF-model, the crack growth rate is defined as the crack step length, δa, divided by the mean value of number of duty cycles, $\mathrm{E}[\delta N]$ applied at a crack state, i.e.,

$$\frac{\delta a}{\mathrm{E}[\delta N]} = \lambda\, C\,(\Delta K)^m \tag{5.5}$$

where

$\mathrm{E}[\delta N]$ = the expected value of the random variable δN corresponding to the expected number of duty cycles which is used to propagate the crack one step δa

λ = number of load cycles in one duty cycle

Notice that the Paris law has not become stochastic, all quantities in (5.5) are deterministic. (δN is a stochastic variable, but it is $\mathrm{E}[\delta N]$ which is used in (5.5)).

Every time the crack tip is exposed to one duty cycle, the same test is repeated. The expected value and variance of the number of duty cycles performed to propagate the crack δa is to be determined.

It is assumed that for a realization δn of δN the first $(\delta n - 1)$ duty cycles do not lead to crack propagation, i.e. $Z = 0$ in (5.2), and that $Z = 1$ in the δn th duty cycle, i.e. the δn th duty cycle results in crack propagation. The probability of the two events is $p^{(\delta n - 1)}$ and q, respectively. Thus, the probability distribution of δN is a geometric distribution given as:

$$\mathrm{P}[\delta N = \delta n] = \mathrm{f}_{\delta N}(\delta n) = q\, p^{\delta n - 1} \tag{5.6}$$

The expected value and the variance of the number of duty cycles are given as the first and second moment of the geometric distribution, respectively. Cf. [Benjamin, J.R. and C.A. Cornell; 1970, p.229-230],

$$\mathrm{E}[\delta N] = \sum_{\delta n=0}^{\infty} \delta n\, \mathrm{f}_{\delta N} = \sum_{\delta n=0}^{\infty} \delta n\, q\, (1-q)^{\delta n - 1} = \frac{1}{q} \tag{5.7}$$

$$\mathrm{Var}[\delta N] = \mathrm{E}[\delta N^2] - (\mathrm{E}[\delta N])^2 = \frac{1-q}{q^2} \tag{5.8}$$

Insertion of (5.7) into (5.5) leads to

$$q = \frac{\lambda C}{\delta a} (\Delta K)^m \tag{5.9}$$

This means, that for a given material the transition matrix (4.2) is determined. The damage states in structures, made of the given material, are then calculated using (4.5). Account of the geometry of the structure is taken through the stress intensity factor range ΔK.

Generally, ΔK is variable due to the load. Two cases are considered: constant-amplitude load resulting in slowly varying ΔK, section 5.2 and random load resulting in random ΔK, section 5.3.

5.2 THE FMF-MODEL FOR CONSTANT-AMPLITUDE LOAD

In this section, the FMF-model for constant-amplitude load is considered, i.e. the stress range $\Delta\sigma$ applied to the structure in consideration is constant. Hence, Paris' law (5.5) can be used as crack propagation law. Since $\Delta\sigma$ is constant, the stress intensity factor range ΔK varies slowly, and therefore, ΔK can be assumed constant in the vicinity of the given crack position.

At each crack position, given by (5.1), the random variable δN_j, which is the number of duty cycles applied to propagate the crack one step from a_j to $a_j + \delta a$, is considered, see also figure 5.1. It is assumed that a_0 is constant so that the δN_j-values express the properties of the material.

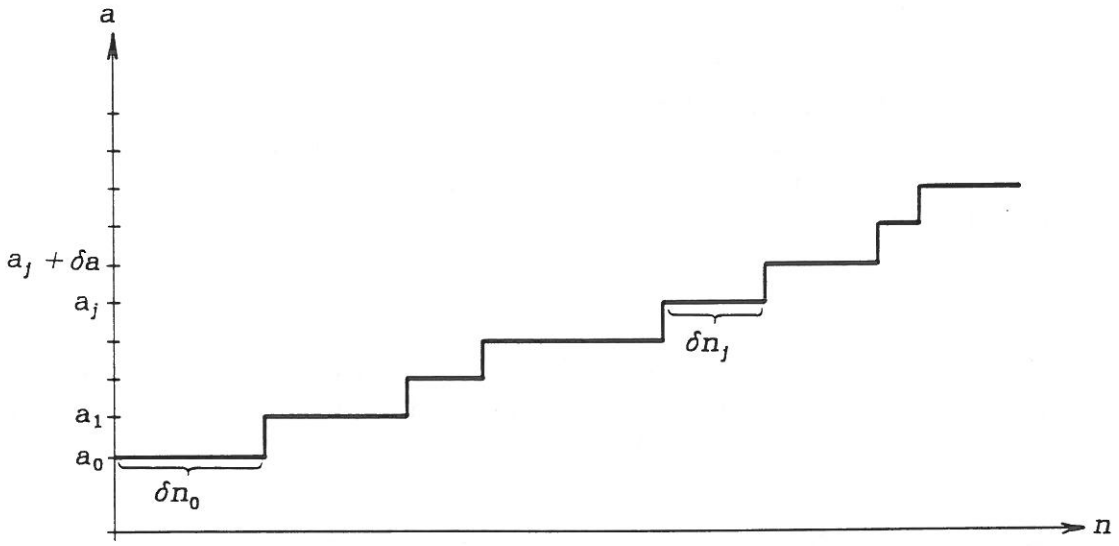

Figure 5.1: Crack propagation in the FMF-model.
a = crack length, n = realization of number of duty cycles.

Similar to the results in section 5.1, the first $(\delta n_j - 1)$ duty cycles with the probability $p_j^{(\delta n_j - 1)}$ do not lead to crack propagation, whereas the δn_j th duty cycle with probability q_j results in crack propagation. Thus, the probability distribution of δN_j is a geometric distribution given as:

$$\mathrm{P}[\delta N_j = \delta n_j] = \mathrm{f}_{\delta N_j}(\delta n_j) = q_j\, p_j^{\delta n_j - 1} \qquad j = 0, 1, 2, \ldots, b-1 \tag{5.10}$$

where the expected value and the variance of δN_j are given by (5.7) and (5.8) replacing δN and q by δN_j and q_j, i.e.

$$\mathrm{E}[\delta N_j] = \frac{1}{q_j} \tag{5.11}$$

$$\mathrm{Var}[\delta N_j] = \frac{1 - q_j}{q_j^2} \tag{5.12}$$

where

$$q_j = \frac{\lambda C}{\delta a} \left(\Delta K(a_0 + j\delta a)\right)^m = \frac{\lambda C}{\delta a} \left(\Delta K(a_j)\right)^m \tag{5.13}$$

$$p_j = 1 - q_j$$

The probability density function of δN_j is illustrated in figure 5.2.

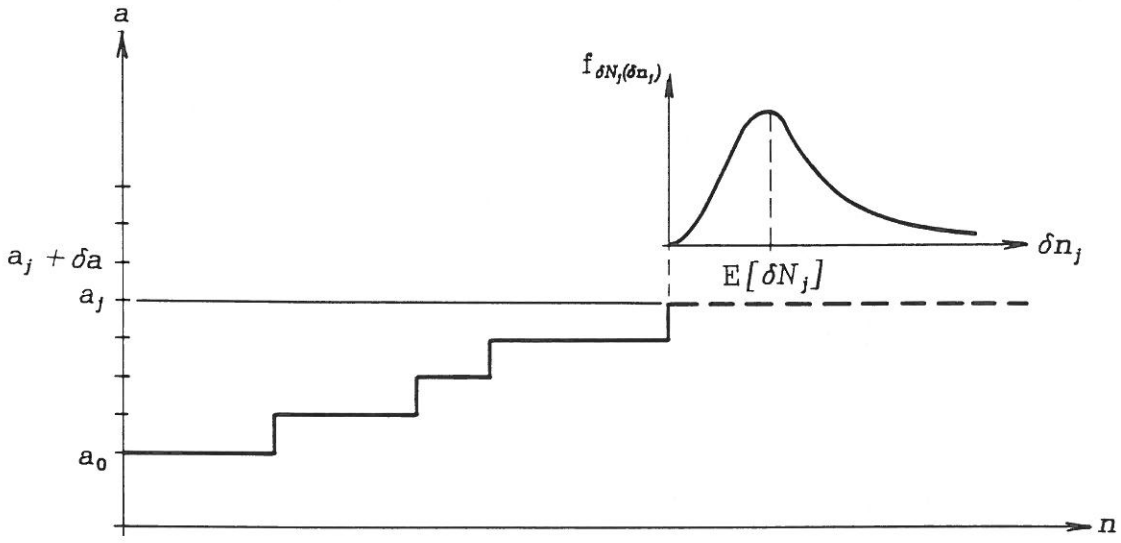

Figure 5.2: The probability density function of the number of duty cycles δN_j performed at state a_j to go to state $a_j + \delta a$.

The total number of duty cycles applied to a structure to propagate the crack to the crack length a_j is

$$N_j = \sum_{k=0}^{j-1} \delta N_k \tag{5.14}$$

Since the random variable is a sum of independent random variables, the expected value of the number of duty cycles is

$$\mathrm{E}[N_j] = \mathrm{E}\left[\sum_{k=0}^{j-1} \delta N_k\right] = \sum_{k=0}^{j-1} \mathrm{E}[\delta N_k] = \sum_{k=0}^{j-1} \frac{1}{q_k} \tag{5.15}$$

Inserting (5.13) and approximating the sum with an integral lead to

$$\mathrm{E}[N_j] = \frac{\delta a}{\lambda C} \sum_{k=0}^{j-1} (\Delta K_k)^{-m} \simeq \frac{1}{\lambda C} \int_{a_0}^{a_j} (\Delta K(a))^{-m}\, da \tag{5.16}$$

which for $\lambda = 1$ corresponds to the integrated Paris law. Thus, it is possible to return to the basic point (Paris' law) which means that the model is consistent so far.

The variance of a sum of independent variables is given as, see e.g. [Benjamin, J.R. and C.A. Cornell; 1970, p.227], using (5.12)

$$\mathrm{Var}[N_j] = \sum_{k=0}^{j-1} \mathrm{Var}[\delta N_k] = \sum_{k=0}^{j-1} \frac{1-q_k}{q_k^2} \tag{5.17}$$

Inserting (5.13) and approximating the sum with an integral lead to

$$\begin{aligned}
\mathrm{Var}[N_j] &= \frac{\delta a}{\lambda^2 C^2} \sum_{k=0}^{j-1} \delta a \left[(\Delta K(a_k))^{-2m} - \frac{\lambda C}{\delta a} (\Delta K(a_k))^{-m} \right] \\
&\simeq \frac{\delta a}{\lambda^2 C^2} \int_{a_0}^{a_j} \left[(\Delta K(a))^{-2m} - \frac{\lambda C}{\delta a} (\Delta K(a))^{-m} \right] da \\
&= \frac{\delta a}{\lambda^2 C^2} \left[f(a) - g(a) \right]
\end{aligned} \tag{5.18}$$

where

$$f(a) = \int_{a_0}^{a_j} (\Delta K(a))^{-2m} \, da \tag{5.19}$$

$$g(a) = \frac{\lambda C}{\delta a} \int_{a_0}^{a_j} (\Delta K(a))^{-m} \, da \tag{5.20}$$

The probability density function of N_j is illustrated in figure 5.3.

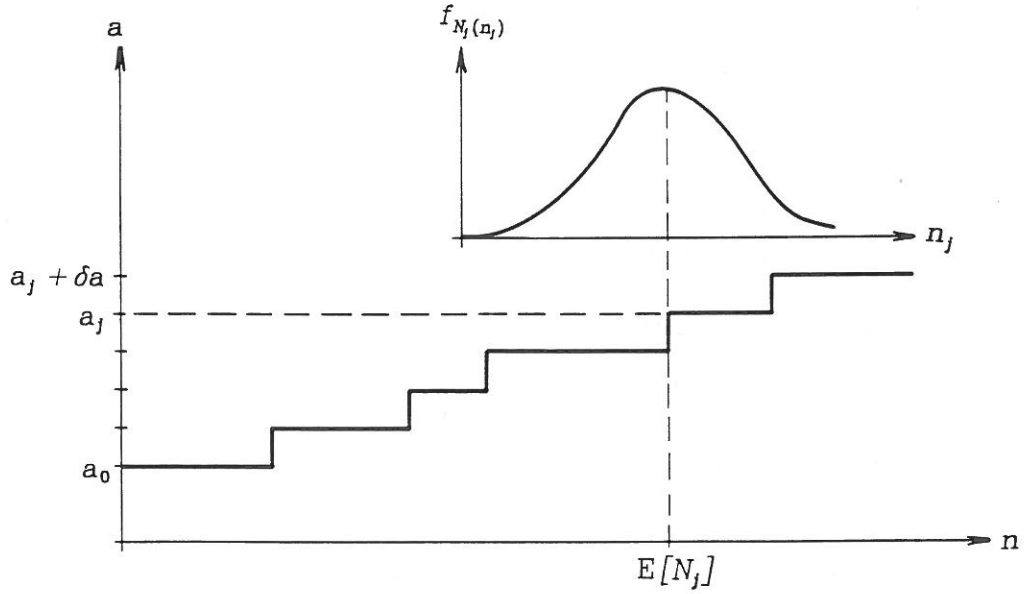

Figure 5.3: The probability density function of the number of duty cycles N_j performed to go to state a_j.

Having a set of realizations, one of which is shown in figure 5.3, it can be noticed that the mean curve corresponds to the values of the material constants C and m.

As an example, consider an infinite plate with a central crack influenced by a constant-amplitude load, $\Delta\sigma$ is considered, see figure 5.4.

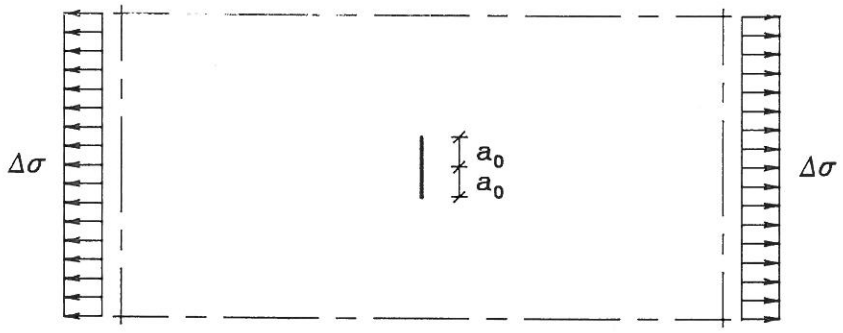

Figure 5.4: An infinite plate with a central crack, with initial crack length $2a_0$, influenced by the stress range $\Delta\sigma$.

In this case, the stress intensity factor range is given by

$$\Delta K = \Delta\sigma\sqrt{\pi a} \tag{5.21}$$

where

$\Delta\sigma$ = stress range [MPa]
a = crack length [mm]

Further, it is assumed that for small values of q_k, $1 - q_k \approx 1$ so (5.17) reduces to

$$\mathrm{Var}[N_j] = \sum_{k=0}^{j-1} \frac{1}{q_k^2} \tag{5.22}$$

and thus, (5.18) reduces to

$$\mathrm{Var}[N_j] = \frac{\delta a}{\lambda^2 C^2} f(a) \tag{5.23}$$

where $f(a)$ is given by (5.19).

Inserting (5.21) into (5.19) leads to

$$f(a) = \frac{1}{\pi} \frac{(\Delta\sigma)^{-2m}}{(m-1)} \left[\frac{1}{(\pi a_0)^{m-1}} - \frac{1}{(\pi a_j)^{m-1}} \right] \tag{5.24}$$

which for a_j (corresponding to $a_{cr} \gg a_0$ where a_{cr} is the critical crack length and a_0 is the initial crack length) approximates

$$f(a) = \frac{1}{\pi} \frac{(\Delta\sigma)^{-2m}}{(m-1)} \frac{1}{(\pi a_0)^{m-1}} \tag{5.25}$$

Introducing

$$\gamma_0 = \left.\frac{da}{dN}\right|_{a=a_0} = \lambda C \, (\Delta\sigma\sqrt{\pi a_0})^m \tag{5.26}$$

into (5.23) together with (5.25) results in

$$\begin{aligned} \mathrm{Var}[N_j] &= \frac{\delta a}{\lambda^2 C^2} \frac{(\Delta\sigma)^{-2m}}{(m-1)} \frac{a_0}{(\pi\, a_0)^m} \\ &= \frac{a_0}{\gamma_0^2} \frac{\delta a}{(m-1)} \end{aligned} \tag{5.27}$$

For steel, $m \approx 3$, [Gurney, T.R.; 1979, p.62], (5.27) thus is

$$\mathrm{Var}[N_j] \approx 0.5 \frac{a_0}{\gamma_0^2} \delta a \tag{5.28}$$

From (5.28) it is seen that for constant initial crack growth rate γ_0 and for constant crack step length δa, the variance of N_j is constant. Further, it is seen that the variance is increasing for increasing δa.

Notice, that N_j is the number of DCs. The variance of the number of load cycles is found by multiplying (5.17) and thus (5.27) by λ^2, i.e.

$$\mathrm{Var}[\lambda^2 N_j] = \lambda^2 \frac{a_0}{\gamma_0^2} \frac{\delta a}{(m-1)} = \frac{a_0}{C^2 \, (\Delta\sigma\sqrt{\pi\, a_0})^{2m} \, (m-1)} (\delta a) \tag{5.29}$$

The only unknown quantity in (5.28) is the step length δa. The value of δa can be estimated if the variance of N_j (or the variance of $\lambda^2 N_j$, i.e. of the number of load cycles) is known from experiments. Rewriting (5.29) results in

$$\delta a = \frac{C^2 \, (\Delta\sigma\sqrt{\pi\, a_0})^{2m} \, (m-1)}{a_0} \mathrm{Var}[\lambda^2 N_j] \tag{5.30}$$

In case the plate is not infinite, which of course is the normal case, (5.21) - and thus (5.28)-(5.30) - has to be corrected introducing the geometry function, see also (2.3).

5.3 THE FMF-MODEL FOR RANDOM LOAD

The load on many structures in civil engineering is of random character, which is more difficult to handle than deterministic load.

Due to the randomly varying load, the stress intensity factor will also vary randomly. The value of the stress intensity factor range, ΔK, depends on the definition of a load cycle.

A realization of a stochastic stress process is shown in figure 5.5. The stress range of half of a stress cycle is defined as the part of the realization between two adjacent points of reversal, i.e.

$$\Delta\sigma = \sigma_1 - \sigma_2 \tag{5.31}$$

where

$\Delta\sigma$ = stress range [MPa]
σ_1 = maximum stress [MPa]
σ_2 = minimum stress [MPa]

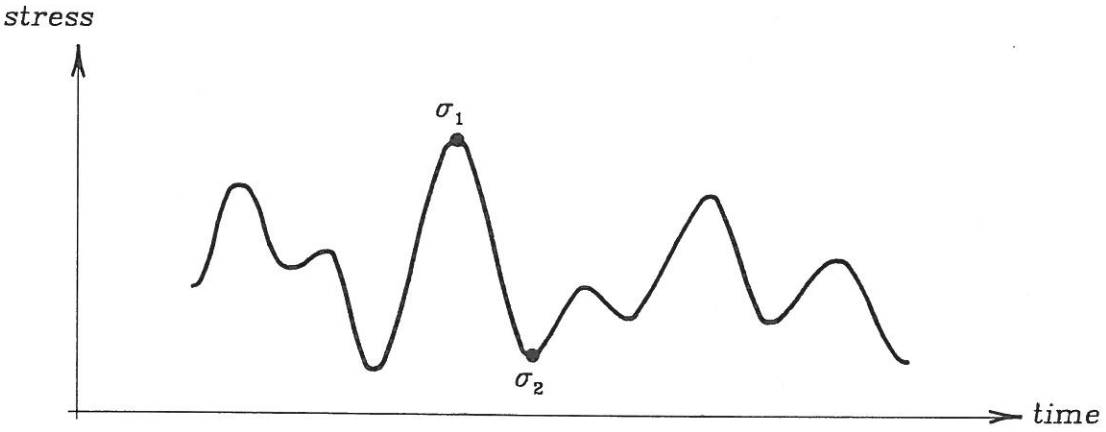

Figure 5.5: Realization of a stochastic stress process. σ_1 and σ_2 correspond to the maximum stress and the minimum stress, respectively, in the forthcoming half load cycle.

The FMF-model itself does not take into account the well-known effects of acceleration and retardation, described in chapter 2. This can be done using a crack closure model when ΔK is calculated, see e.g. [Schijve, J.; 1979] and [Corbly, D.M. and P.F. Packman; 1973] and section 3.3.2.

Considering the realization in figure 5.5, the damage increment in the next half cycle will depend on the load history, the geometry of the structure and the extreme values σ_1 and σ_2. The load history is contained in the parameter describing the damage state at the start of the duty cycle, see also chapter 4.

Since crack closure occurs before the stress reaches the value σ_2, the effective stress intensity factor is not following the same progress as the load progress, but has cut-

offs at values corresponding to the crack closure stress. The crack closure stress is the stress at which the crack during unloading will close. Crack closure is due to plastic deformations in the crack tip region, see also [Schijve, J.; 1979], [Corbly, D.M. and P.F. Packman; 1973] and section 2.4.2.

The progress of the effective stress intensity factor, corresponding to the realization in figure 5.5, is shown in figure 5.6.

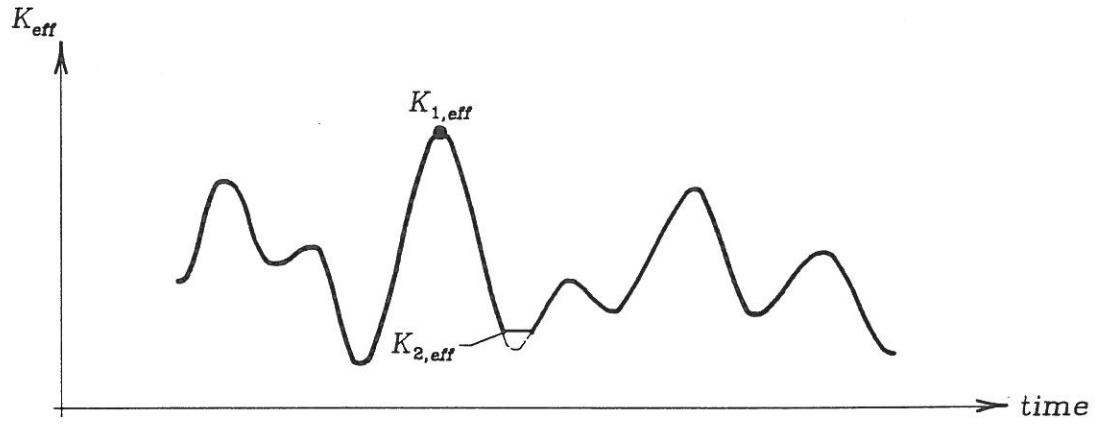

Figure 5.6: Progress of effective stress intensity factor, K_{eff}, corresponding to the realization in figure 5.5. $K_{1,\text{eff}}$ and $K_{2,\text{eff}}$ correspond to the maximum and the minimum effective stress intensity factor, respectively, in the forthcoming half cycle.

The idea is to use the results of section 5.2, replacing ΔK with the effective stress intensity factor range,

$$\Delta K_{\text{eff}} = K_{1,\text{eff}} - K_{2,\text{eff}} = \Delta\sigma_{\text{eff}} F \sqrt{\pi a} = (\sigma_1 - \sigma_{op}) F \sqrt{\pi a} \tag{5.32}$$

where

$\Delta\sigma_{\text{eff}}$	=	effective stress range [MPa]
σ_{op}	=	crack opening stress [MPa]
F	=	geometry function
a	=	crack length

Paris' law (5.4) becomes

$$\frac{da}{dN} = C\,(\Delta K_{\text{eff}})^m \tag{5.33}$$

The transition probability (5.13) changes to

$$q_j = \frac{\lambda C}{\delta a}\,(\Delta K_{\text{eff}}(a_j))^m \tag{5.34}$$

whereas the expected value and variance of the number of duty cycles to propagate the crack one step from a_j to $a_j + \delta a$, (5.11) and (5.12) remain the same.

The total number of duty cycles applied to the structure to propagate the crack to the crack length a_j, (5.14), and the expected value (5.15) are also unchanged.

The approximate value of (5.16) becomes

$$\mathrm{E}[N_j] \simeq \frac{1}{\lambda C} \int_{a_0}^{a} (\Delta K_{\mathrm{eff}}(a))^{-m} \, da \tag{5.35}$$

The variance is still given as (5.17) but, with the approximate value,

$$\mathrm{Var}[N_j] \simeq \frac{\delta a}{\lambda^2 C^2} \left[f_{\mathrm{eff}}(a) - g_{\mathrm{eff}}(a) \right] \tag{5.36}$$

where

$$f_{\mathrm{eff}}(a) = \int_{a_0}^{a_j} (\Delta K_{\mathrm{eff}}(a))^{-2m} \, da \tag{5.37}$$

$$g_{\mathrm{eff}}(a) = \frac{\lambda C}{\delta a} \int_{a_0}^{a_j} (\Delta K_{\mathrm{eff}}(a))^{-m} \, da \tag{5.38}$$

Thus, the FMF-model is also available if the load is random.

5.4 EVALUATION OF THE FMF-MODEL

On the basis of the well-known B-model, see chapter 4, a new numerical, cumulative damage model based on fracture mechanics is introduced. This model, the FMF-model described in this chapter, incorporates existing physical knowledge of crack propagation.

The cumulative damage is described by a discrete-time, discrete-state Markov process. The time is measured in number of duty cycles, whereas the state of damage is given as a crack length. The crack is assumed to propagate in steps of the length δa characteristic of the material

One of the main results is that the stochastic properties of the material can be modelled using the crack step length δa. Thus, once the material constants in Paris' law, C and m, as well as δa are determined, the state of damage in any structure of the given material can be calculated numerically.

The FMF-model is to be tested. This is done in two ways: a numerical and an experimental test. The numerical test is described in chapter 6 and contains simulations of crack growth data which are compared with existing data obtained for an aluminium alloy. Performance of the experimental test in chapter 7 using a mild steel, makes it possible to determine the material parameters included in the FMF-model and to compare the observed crack growth data with the numerically obtained data.

6. NUMERICAL TESTS OF THE FRACTURE MECHANICAL MARKOV CHAIN FATIGUE MODEL

In this chapter it is described how the FMF-model introduced in chapter 5 is tested numerically for the purpose of evaluating its applicability and to test if δa can be regarded as a characteristic value of the material.

This evaluation is based on the following criteria concerning the properties of the model.

Firstly, the model should be able to give a good qualitative description of empirical crack growth curves, i.e. the model can replicate the empirical curves. Secondly, the crack growth data obtained from the model must have the same statistical properties as the empirical data in the form of mean values, standard deviations and probability density functions.

The qualitative demand is tested by plotting the crack growth curves obtained from the model and from the empirical data, respectively. The form and progress of the curves must be similar.

The quantitative tests are performed by using several C-programs developed in connection with the FMF-model, see also appendix C. Further, the most well-known set of data originating from several experiments, i.e. the Virkler data, has been used in the tests as reference. The Virkler data, which in their original form have been available to the author, are described in [Bogdanoff, J.L and F. Kozin; 1985, ch.4] and [Virkler, D.A., B.M. Hillberry and P.K. Goel; 1979], see also section 4.3.

6.1 THE VIRKLER DATA

The purpose of this section is to give a description including the statistical properties of the fatigue crack growth data used as references in the numerical test of the FMF-model.

The Virkler data - shown in figure 6.1 - were obtained in 68 tests using 2024-T3 aluminium alloy CCT-specimens (Center Cracked Tension). The size of the CCT-specimens were $152.4 \cdot 558.8$ mm^2 ($6 \cdot 22$ in^2) with a thickness of 2.54 mm (0.10 in). No specifications of the material properties have been found. The CCT-specimens were influenced by constant-amplitude load with stress range (see (2.6)) $\Delta\sigma = 48.28$ MPa, maximum stress $\sigma_{\mathbf{max}} = 60.35$ MPa and minimum stress $\sigma_{\mathbf{min}} = 12.07$ MPa.

In each test, 164 values of the number of cycles and the crack length, (N, a), were recorded for fixed values of the increase of the crack length, da. For $a \in [9.0\ ;\ 36.2]$mm, $da = 0.20$ mm where $a_0 = 9.0$ mm is the initial crack length. For $a \in [36.2\ ;\ 44.2]$mm, $da = 0.40$ mm and finally, $da = 0.80$ mm for $a \in [44.2\ ;\ 49.8]$mm where

$a_f = 49.8$ mm is the failure crack length.

The crack lengths were measured with a zoom stereo microscope operated at a magnification of 150×. The microscope was mounted on a digital traversing system with a resolution of 0.001 mm. Illuminating the crack with a strobe light, measuring of the crack length was possible without interrupting the loading.

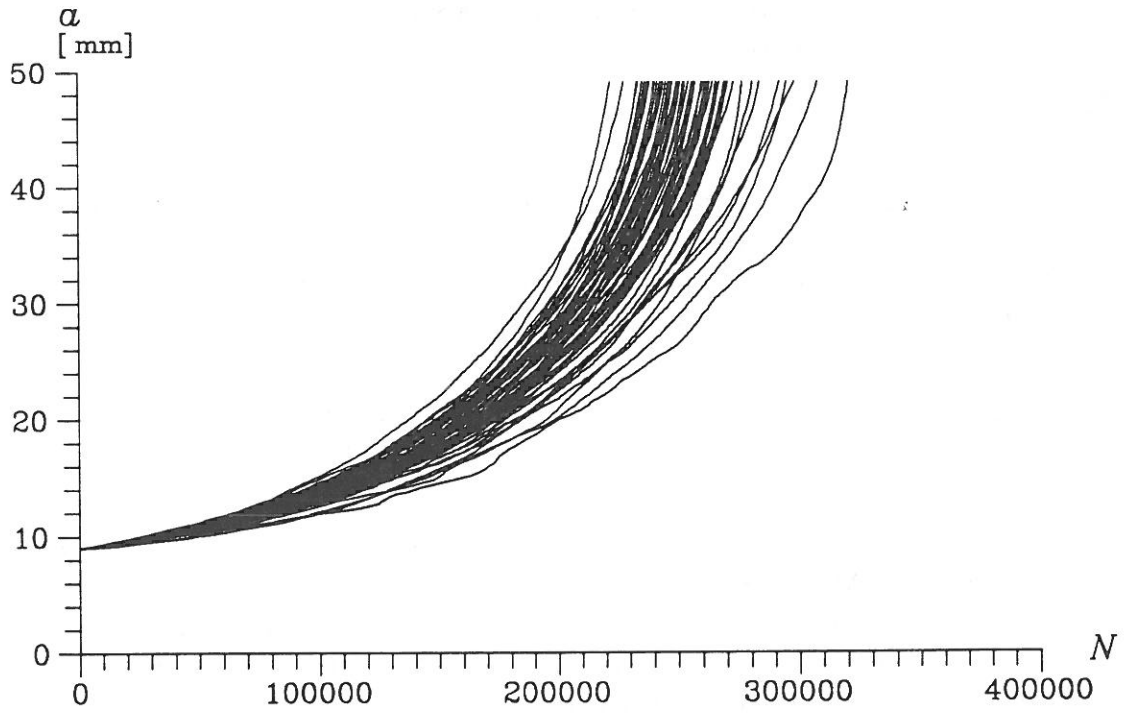

Figure 6.1: The 68 (N, a)-curves obtained from the Virkler data.
N = number of load cycles, a = crack length. Based on [Bogdanoff, J.L. and F. Kozin; 1985, p.241].

The form of the curves in figure 6.1 shows great similarity. Thus, all the curves have a smooth progress with only a few sudden changes in the crack growth rate. Further, the curves approach a vertical line for large a-values corresponding to only a few number of cycles being applied in the last part of the fatigue failure - see also section 2.1 and figure 2.14. This approach would have been even more significant if the measurements were continued until final rupture was obtained.

It is seen that a large initial crack growth rate results in a small number of cycles to cause failure and vice versa. Further, the main part of the curves is concentrated within a small band where $N_f \in [230000 ; 270000]$ cycles.

The statistical properties, i.e. the mean value, the standard deviation and the probability density of the number of cycles applied in each crack state to reach the successive state and of the number of cycles applied totally to reach a given crack state (the values of (5.11), (5.12), (5.15) and (5.17)), of the Virkler data are determined using the program **VSTAT** from **STAT-PACK**. All the programs have been developed by the author. The programs are briefly described in appendix C.

The results from **VSTAT** are illustrated in figure 6.2 to 6.7.

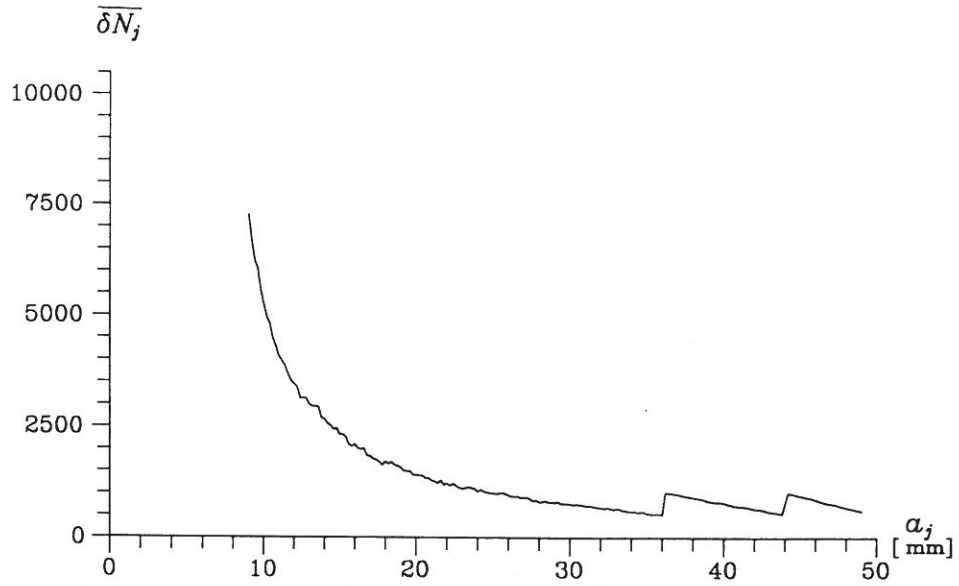

Figure 6.2: Mean value of the number of load cycles ($\overline{\delta N_j}$) applied at each crack state (a_j) to reach the successive crack state, for the Virkler data. $j = 0, 1, 2, \ldots, 162$, $a_0 = 9.0$ mm and $a_{162} = 49.0$ mm.

From figure 6.2 it is seen that the mean value of the number of load cycles $\overline{\delta N_j}$ applied at a crack state a_j is decreasing for increasing crack length. This progress was to be expected because the probability of crack propagation increases during lifetime; cf. (5.11) and (5.13). The discontinuities at $a_{136} = 36.2$ mm and $a_{156} = 44.2$ mm are due to the changes in the intervals of crack length measurements, i.e. da changes from 0.2 mm to 0.4 mm ending with 0.8 mm. Otherwise, the progress is very smooth.

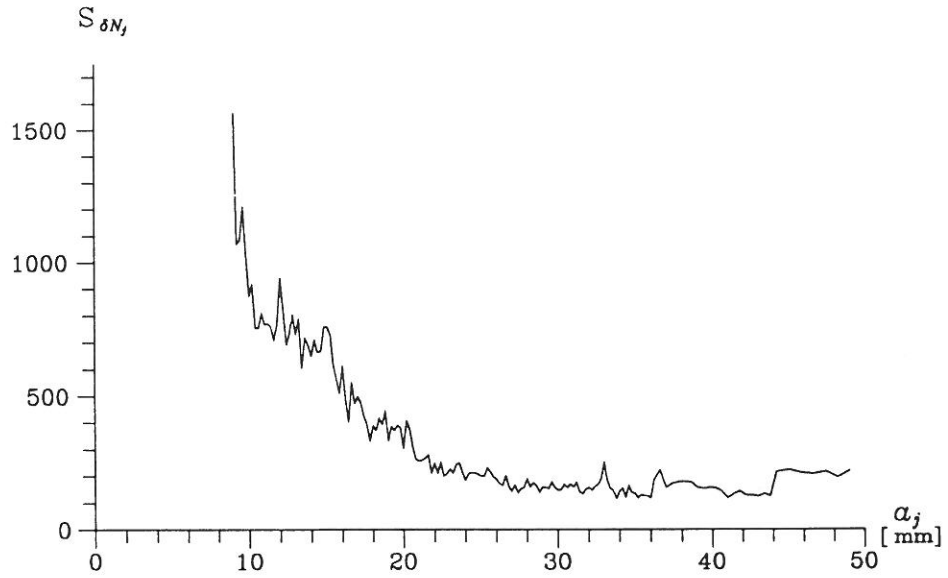

Figure 6.3: Standard deviation of the number of load cycles ($S_{\delta N_j}$) applied at each crack state (a_j) to reach the successive crack state, for the Virkler data. $j = 0, 1, 2, \ldots, 162$, $a_0 = 9.0$ mm and $a_{162} = 49.0$ mm.

Figure 6.3 shows that the standard deviation of the number of load cycles $S_{\delta N_j}$ applied at a crack state a_j is decreasing for increasing crack length which is in good agreement with the asymptotic approach to a vertical line of the (N, a)-curves in figure 6.1. Further, it shows that even though the variations are large for small crack lengths ($a < 20$ mm), the relative deviation is almost constant 20%. Smaller variations are obtained for large crack lengths, where the relative deviation is almost constant 10% (cf. figure 6.2).

The histograms in figure 6.4 and figures 6.13-6.15 are shown for the crack lengths $a_0 = 9.0$ mm, $a_{81} = 25.2$ mm and $a_{162} = 49.0$ mm, corresponding to the first, middle and final crack lengths for which the number of load cycles applied at a crack state is measured. The corresponding crack lengths for which the total number of cycles is measured are $a_1 = 9.2$ mm, $a_{82} = 25.4$ mm and $a_{163} = 49.8$ mm. The histograms for these crack lengths are illustrated in figures 6.7 and 6.18-6.20.

Each interval I_k in the histograms consists of a number of load cycles - 250 for δN_j and 1000 for N_j - distributed as $I_k =]k{\cdot}250\ ;\ (k+1){\cdot}250]$ cycles and $I_k =]k{\cdot}1000\ ;\ (k+1){\cdot}1000]$ cycles, respectively. $k = 0, 1, 2, \ldots, 39$.

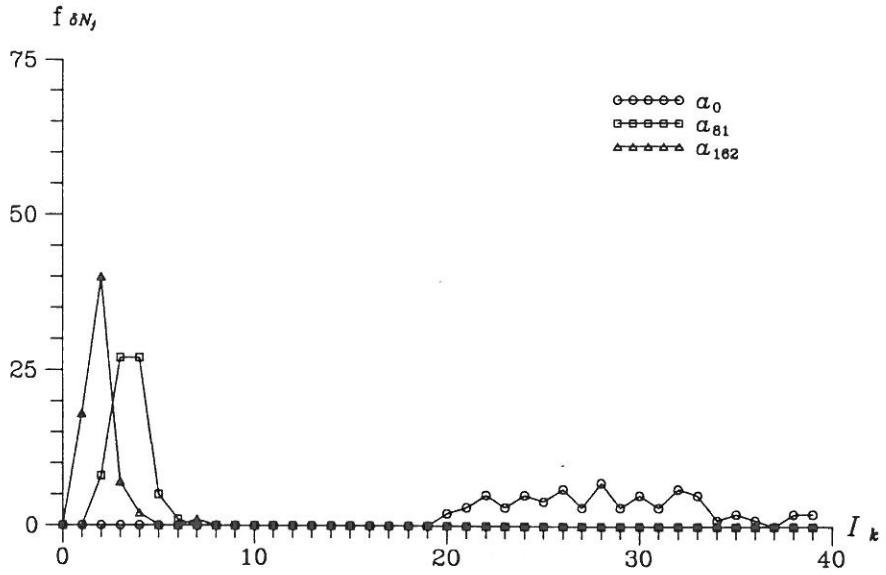

Figure 6.4: Histogram of the number of load cycles ($f_{\delta N_j}$) applied at the crack state $a_0 = 9.0$ mm, $a_{81} = 25.2$ mm and $a_{162} = 49.0$ mm, respectively, for the Virkler data.
$I_k =]k{\cdot}250\ ;\ (k+1){\cdot}250]$ cycles, $k = 0, 1, 2, \ldots, 39$.

Comparison of the three histograms $f_{\delta N_0}$, $f_{\delta N_{81}}$ and $f_{\delta N_{162}}$ in figure 6.4 shows that $f_{\delta N_0}$ is distributed over several intervals while $f_{\delta N_{81}}$ and $f_{\delta N_{162}}$ are concentrated within a few intervals.

Thus, δN_0 (the number of cycles applied in crack state a_0 to reach crack state a_1) is given in I_{20} to I_{39}, i.e. $\delta N_0 \in]5000\ ;\ 10000]$ cycles. The distribution over 20 intervals is in agreement with the large standard deviation found in figure 6.3 for small crack lengths.

The more concentrated distribution for $f_{\delta N_{81}}$ is limited to I_2 to I_7, i.e. $\delta N_{81} \in]500\ ;\ 2000]$ cycles, which corresponds to the decrease in the standard deviation in figure 6.3.

Finally, $f_{\delta N_{162}}$ has the most concentrated distribution including only five intervals, I_1 to I_4 and I_7, i.e. $\delta N_{162} \in]250\ ;\ 1250]$ cycles and $]1750\ ;\ 2000]$ cycles. Thus, for large crack lengths the same number of cycles are required to propagate the crack from one state to the next state no matter how the previous progress has been.

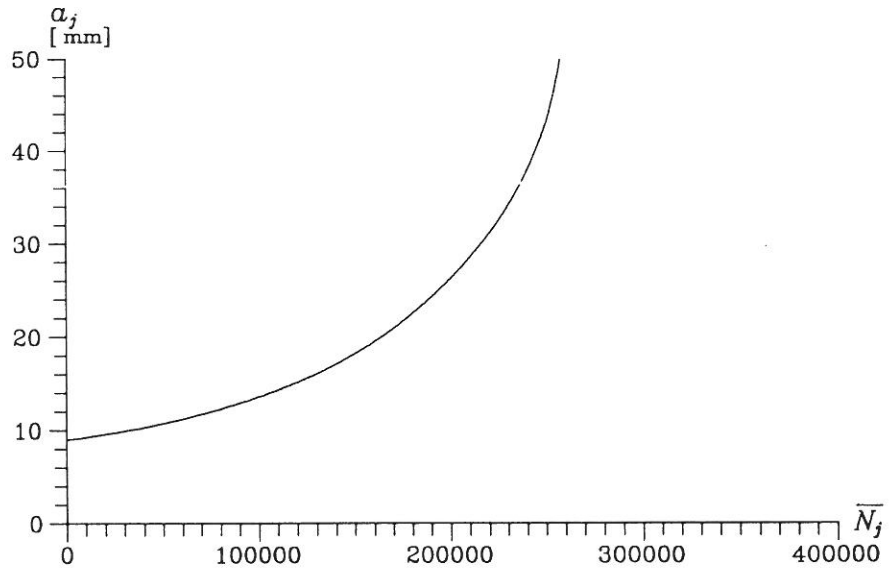

Figure 6.5: Mean value of the number of load cycles ($\overline{N_j}$) applied to reach the crack state (a_j), for the Virkler data.
$j = 0, 1, 2, \ldots, 163$, $a_0 = 9.0$ mm and $a_{163} = 49.8$ mm.

The mean value of the number of load cycles describes a non-decreasing function which has a remarkably smooth progress, see figure 6.5. Thus, the irregularities of the curves in figure 6.1 are equalized in the mean curve. The mean number of load cycles to cause failure $\overline{N_{163}} \approx 260000$ which is within the interval for the number of cycles to cause failure N_f found in figure 6.1.

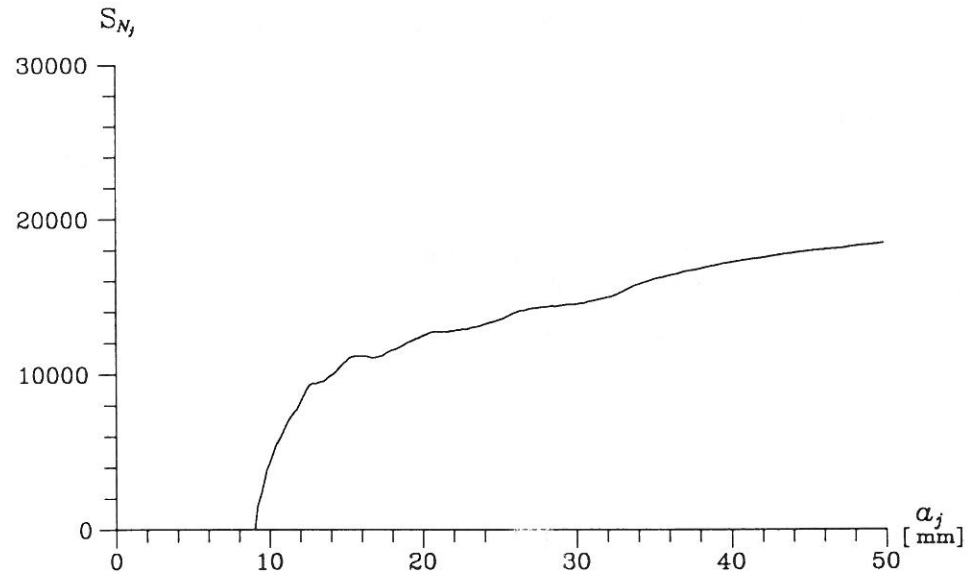

Figure 6.6: Standard deviation of the number of load cycles (S_{N_j}) applied to reach the crack state (a_j), for the Virkler data.
$j = 0, 1, 2, \ldots, 163$, $a_0 = 9.0$ mm and $a_{163} = 49.8$ mm.

Contrary to figure 6.3, the standard deviation of the number of load cycles S_{N_j} applied to reach the crack state a_j is increasing for increasing crack length, see figure 6.6. The increase is largest for small crack lengths ($a < 12$ mm) after which the standard deviation slowly increases towards a constant value of ≈ 20000. The relative deviation varies from $\approx 10\%$ for small crack lengths to $\approx 7\%$ for large crack lengths.

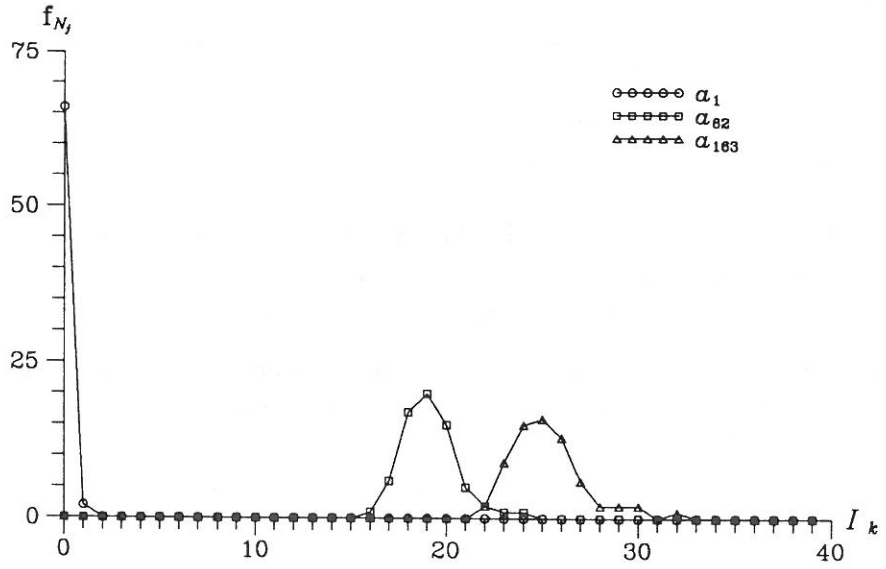

Figure 6.7: Histogram of the number of load cycles (f_{N_j}) applied to reach the crack state, $a_1 = 9.2$ mm, $a_{82} = 25.4$ mm and $a_{163} = 49.8$ mm, respectively, for the Virkler data.
$I_k =]k{\cdot}10000\ ;\ (k+1){\cdot}10000]$ cycles, $k = 0, 1, 2, \ldots, 39$.

The histograms in figure 6.7 show that f_{N_1} is concentrated to only two intervals, I_0 and I_1, i.e. $N_1 \in]0\ ;\ 20000]$ cycles with the main part in $]0\ ;\ 10000]$ cycles, which also is seen from figure 6.1.

The larger scatter of the curves in figure 6.1 at $a_{82} = 25.4$ mm and at $a_{163} = 49.8$ mm is reflected in the histograms in which 9 and 11 intervals, respectively, have values different from zero. Thus, $f_{N_{82}}$ is distributed over I_{16} to I_{24}, i.e. $N_{82} \in]160000\ ;\ 250000]$ cycles and $f_{N_{163}}$ over I_{22} to I_{32}, i.e. $N_{163} \in]220000\ ;\ 330000]$ cycles. The overlap of intervals corresponds to N_f for some tests being smaller than N_{82} for others.

The curves shown in figures 6.2-6.7 form the basis of the simulations in section 6.2 and for the evaluation of the applicability of the FMF-model, see section 6.3.

6.2 SIMULATION OF FMF-DATA WITH VIRKLER PARAMETERS

For the purpose of testing the FMF-model (N, a)-data (N = number of cycles, a = crack length) are simulated on the basis of the FMF-model. The simulations are performed by the program **SIMULA** (see appendix C). The number of data set in

each simulation series is 500.

The input parameters shown in table 6.8 are kept constant corresponding to the Virkler data. The initial crack length a_0, the failure crack length a_f and the stress range $\Delta\sigma$ are explicitly known from [Virkler, D.A., B.M. Hillberry and P.K. Goel; 1979], whereas C and m are determined on the basis of the original Virkler data using program **PARIS** in appendix C.

a_0 [mm]	a_f [mm]	$\Delta\sigma$ [MPa]	C [mm/(MPa$\sqrt{\text{m}}$)$^{3.73}$]	m
9.0	49.8	48.28	$1.26 \cdot 10^{-8}$	3.73

Table 6.8: Input parameters to program **SIMULA** for simulation series VSIM 1-8. a_0 = initial crack length, a_f = failure crack length, $\Delta\sigma$ = stress range, C = material constant and m = material constant.

The two remaining parameters λ (number of load cycles in each duty cycle) and δa (crack step length) are varied. The combinations of λ and δa used in the performance of the simulations of FMF-data are shown in table 6.9.

δa \ λ	1000	100	10	1
0.2 mm	VSIM 1	VSIM 2	VSIM 3	VSIM 4
0.1 mm	VSIM 5	VSIM 6	VSIM 7	VSIM 8

Table 6.9: Combinations of λ and δa used in the simulation series VSIM 1-8.

The results of the simulations are shown in appendix D. To keep the overlook, only 100 of the 500 simulated (N, a)-curves are shown in each plot. The curves have been plotted successively, i.e. the first plot contains the first 100 curves and so on. Further, only one typical plot from each simulation series is shown, see figures D1-D.8.

It is worth mentioning that, VSIM 1 and VSIM 5 will not be used in the test due to the form of the (N, a)-curves - see the following. An example of (N, a)-curves from the simulation series are shown in figure 6.10.

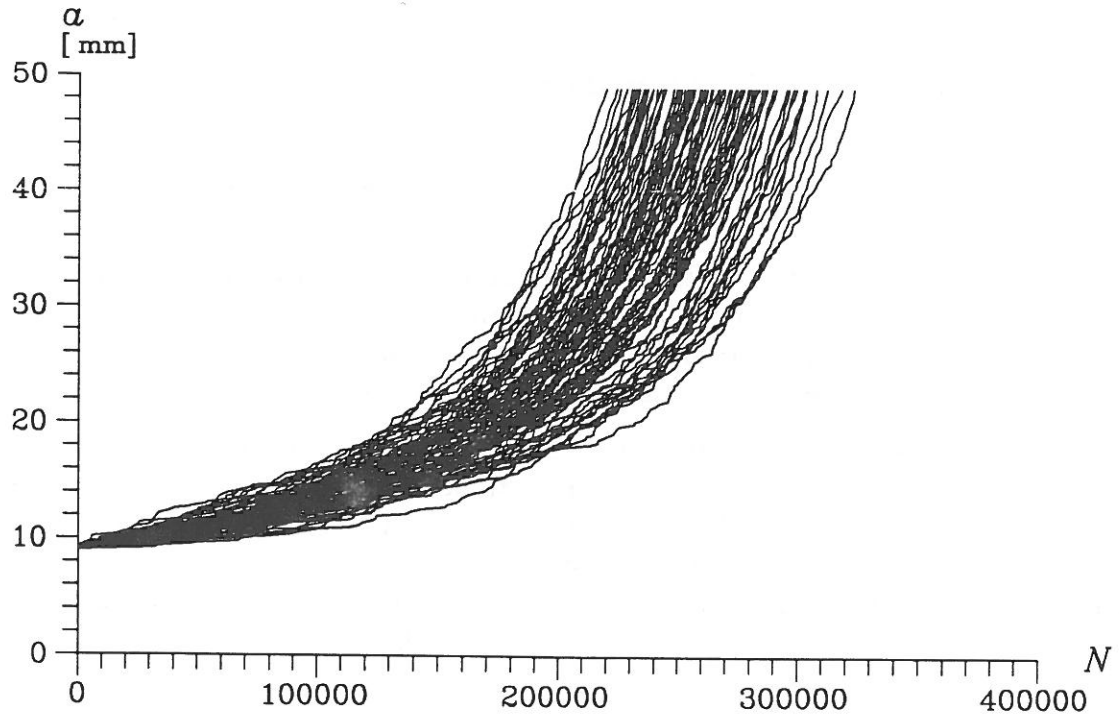

Figure 6.10: Typical plot of (N, a)-curves from simulation series VSIM 2.
N = number of load cycles, a = crack length.

A qualitative evaluation of figure 6.10, figures D.2-D.4 and D.6-D.8 shows that the (N, a)-curves have almost the same characteristics as the curves in figure 6.1 for the Virkler data.

The smoothness of the curves increases as λ decreases. Thus, for simulation series VSIM 2, $\lambda = 100$ (figure D.2), the curves have a less smooth progress compared to e.g. simulation series VSIM 4, $\lambda = 1$ (figure D.4).

This is caused by the fact that in simulation series VSIM 2, the crack is forced to propagate 0.2 mm using a multiple of 100 cycles. If, it e.g. requires 3207 cycles to propagate the crack from 12.2 mm to 12.4 mm in the Virkler data, the FMF-model would give the result 3300 cycles due to λ and thus a flatter curve. This phenomenon is more pronounced for large a-values, where fewer cycles are required in each crack step.

The consequences of the choice of λ for a given δa are clearly seen in figures D.1 and D.5, where the progress becomes linear for large a-values. It can immediately be concluded that the two simulation series VSIM 1 and VSIM 5 do not describe the Virkler data adequately. Since the qualitative test obviously is not fulfilled, these two simulation series are not included in the following analyses.

As for the Virkler data it is seen that a large initial crack growth results in a small number of cycles to cause failure and vice versa. The main part of the curves has the failure number of cycles concentrated within the interval $N_f \in [200000\ ;\ 300000]$.

A quantitative evaluation of the simulation results is given in sections 6.2.1 and 6.2.2.

6.2.1 Statistical Analysis of Simulated FMF-Data

The statistical properties of the simulated FMF-data, which form the basis of the quantitative test of the FMF-model in section 6.2.2, are determined in the present section.

The results from **SIMULA**, in the form of connected (N, a)-values (see figures 6.10, D.2-D.4 and D.6-D.8), are used as input parameters in the program **SORT** (see appendix C). This program sorts the (N, a)-data so that only the data corresponding to the crack lengths used in the Virkler data, see section 6.1, are selected.

The sorted data are input parameters to program **STAT** from the **STAT-PACK** in appendix C. This program calculates the statistical properties, i.e. the mean value, the standard deviation and the probability density of the number of cycles applied in each crack state to reach the successive state and of the total number of cycles applied to reach a given crack state, i.e. the values of (5.11), (5.12), (5.15) and (5.17), of the FMF-data. The results are shown in figures 6.11-6.20.

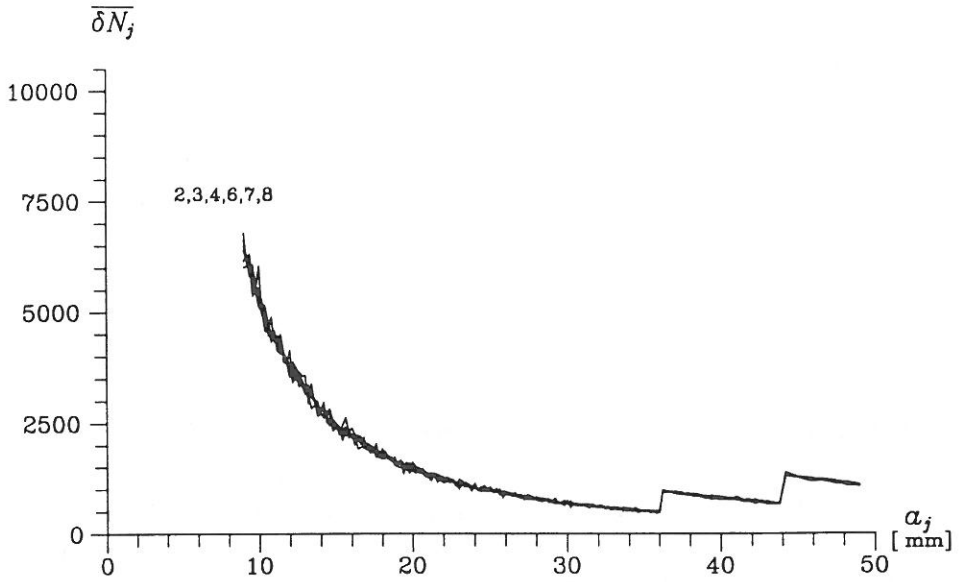

Figure 6.11: Mean value of the number of load cycles $(\overline{\delta N_j})$ applied at each crack state (a_j) to reach the successive crack state for VSIM 2-4 and VSIM 6-8.
$j = 0, 1, 2, \ldots, 162$, $a_0 = 9.0$ mm and $a_{162} = 49.0$ mm.

The mean number of load cycles $\overline{\delta N_j}$ applied at crack state a_j is in figure 6.11 seen to decrease for increasing crack length for simulation series VSIM 2-4 and VSIM 6-8. The progress, which coincide show the same characteristics as the curve in figure 6.2. Notice, that a larger scatter occurs at small crack lengths.

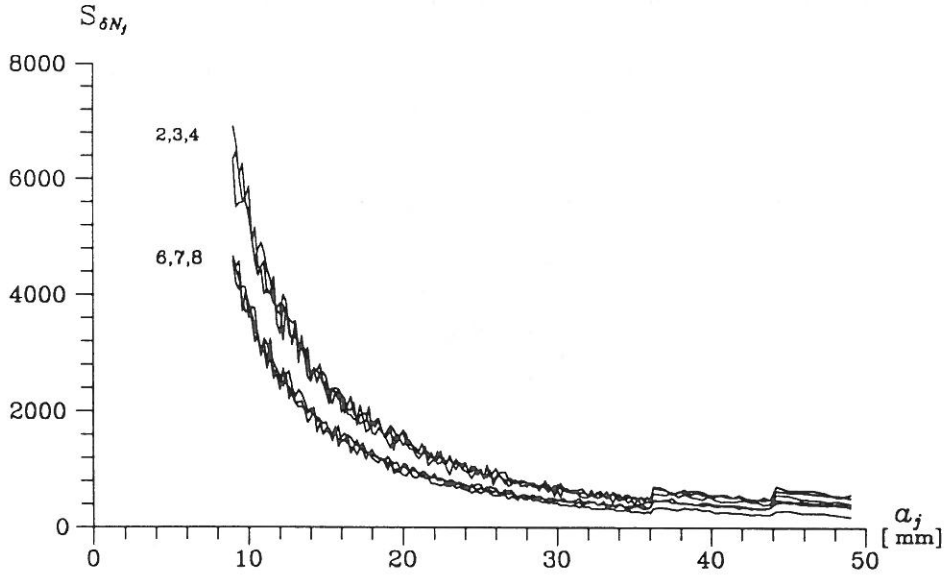

Figure 6.12: Standard deviation of the number of load cycles ($S_{\delta N_j}$) applied at each crack state (a_j) to reach the successive crack state for VSIM 2-4 and VSIM 6-8.
$j = 0, 1, 2, \ldots, 162$, $a_0 = 9.0$ mm and $a_{162} = 49.0$ mm.

The standard deviation of the number of load cycles $S_{\delta N_j}$ applied at a crack state a_j is in figure 6.12 seen to decrease for increasing crack length. As in figure 6.3 large variations occur for small crack lengths ($a < 15$ mm) and vice versa. Notice that generally $S_{\delta N_j}$ is larger for VSIM 2-4 than for VSIM 6-8. This is probably caused by the δa-value being larger in the former series, see also the comments on figure 6.10.

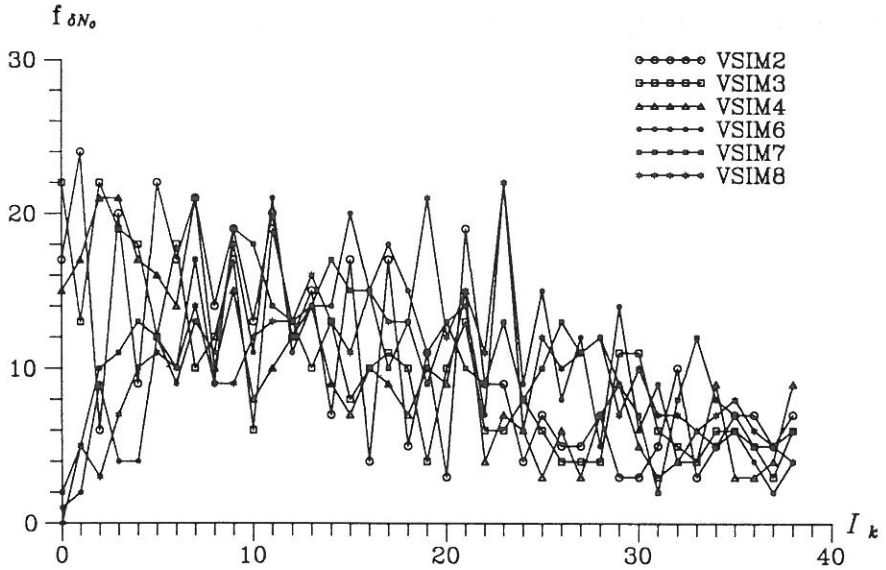

Figure 6.13: Histogram of the number of load cycles ($f_{\delta N_0}$) applied at the crack state $a_0 = 9.0$ mm for VSIM 2-4 and VSIM 6-8.
$I_k =]k{\cdot}250\ ;\ (k+1){\cdot}250]$ cycles, $k = 0, 1, 2, \ldots, 39$.

In figure 6.13 it is seen that the histogram $f_{\delta N_0}$ is almost equally distributed over all intervals. The only exception is the interval I_{39}, i.e. $\delta N_0 > 9750$ cycles, where $f_{\delta N_0} \approx$ 100-120 (not shown). This indicates that δN_0 for the simulated FMF-data generally are larger than the Virkler data. This is also seen from figure 6.12 compared to figure 6.3.

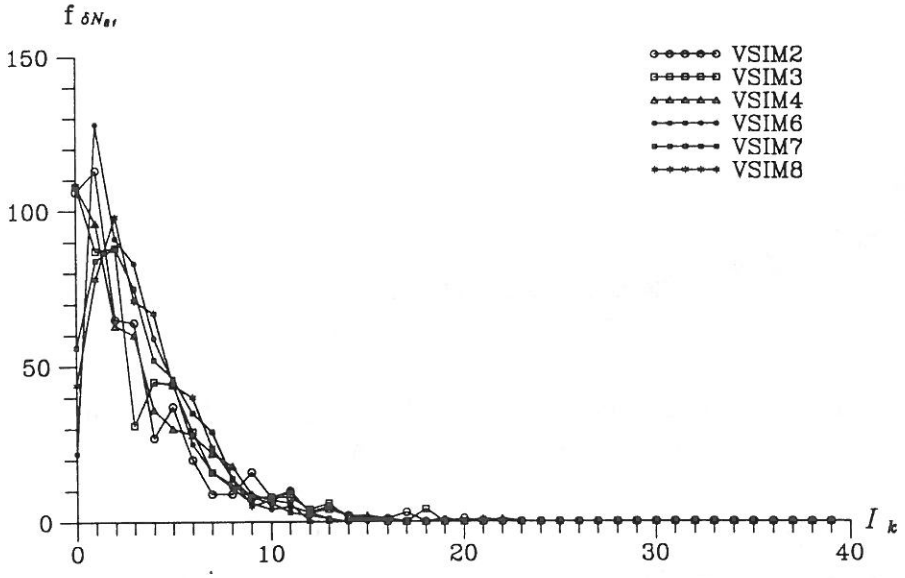

Figure 6.14: Histogram of the number of load cycles ($f_{\delta N_{81}}$) applied at the crack state $a_{81} = 25.2$ mm for VSIM 2-4 and VSIM 6-8.
$I_k =]k{\cdot}250\ ;\ (k+1){\cdot}250]$ cycles, $k = 0, 1, 2, \ldots, 39$.

The histogram $f_{\delta N_{81}}$, see figure 6.14, shows the same characteristics as in figure 6.4, i.e. the distributions are concentrated in a few intervals. This reflects the small scatter and small standard deviation at $a_{81} = 25.2$ mm in figure 6.12.

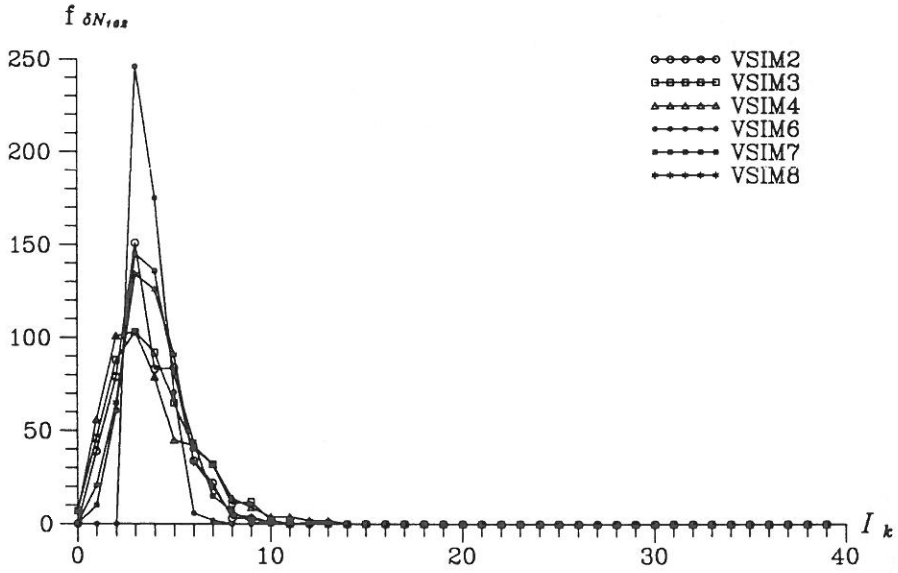

Figure 6.15: Histogram of the number of load cycles ($f_{\delta N_{162}}$) applied at the crack state $a_{162} = 49.0$ mm for VSIM 2-4 and VSIM 6-8.
$I_k =]k{\cdot}250\ ;\ (k+1){\cdot}250]$ cycles, $k = 0, 1, 2, \ldots, 39$.

The histogram $f_{\delta N_{162}}$ shown in figure 6.15 is concentrated within a few intervals (I_0 to I_{13}), i.e. $\delta N_{162} \in]0\ ;\ 3500]$ cycles. Generally, the distribution of VSIM 6-8 is more concentrated than the distribution of VSIM 2-4, which once again indicates that the value of δa influences the results. Notice, that almost 50% of the δN_j-values in VSIM 6 is placed in one interval and that only five intervals are included.

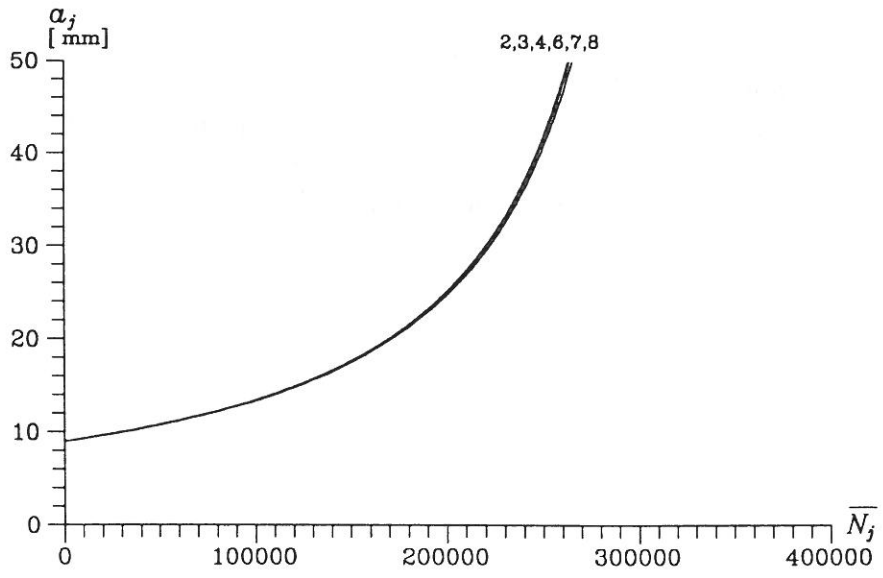

Figure 6.16: Mean value of the number of load cycles ($\overline{N_j}$) applied to reach the crack state (a_j) for VSIM 2-4 and VSIM 6-8.
$j = 0, 1, 2, \ldots, 163$, $a_0 = 9.0$ mm and $a_{163} = 49.8$ mm.

Even though the (N, a)-curves in figure 6.10, D.2-D.4 and D.6-D.8 have some variations in their progress, the mean value of the number of load cycles $\overline{N_j}$ applied to reach a crack state a_j describes a very smooth non-decreasing function, see figure 6.16. The mean number of cycles to cause failure $\overline{N_{163}} \approx 260000$ cycles which is exactly the same as found for the Virkler data in figure 6.5.

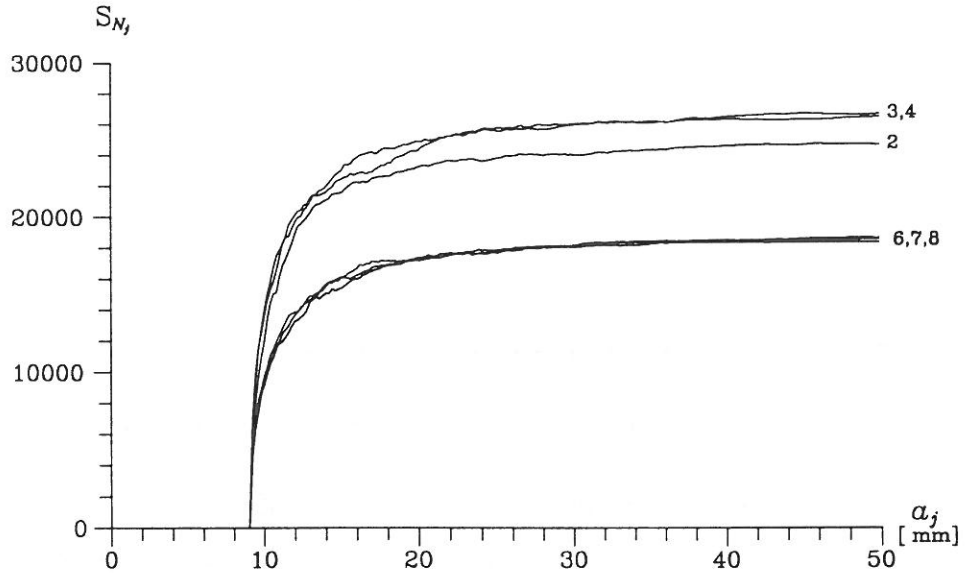

Figure 6.17: Standard deviation of the number of load cycles (S_{N_j}) applied to reach the crack state (a_j) for VSIM 2-4 and VSIM 6-8.
$j = 0, 1, 2, \ldots, 163$, $a_0 = 9.0$ mm and $a_{163} = 49.8$ mm.

The standard deviation of the number of load cycles S_{N_j} applied to reach the crack state a_j is increasing for increasing crack length, see figure 6.17. The increase is largest for small crack lengths ($a < 12$ mm) after which the standard deviation slowly increases towards a constant value. The constant value is seen to be influenced by δa. Thus, for $\delta a = 0.2$ mm (VSIM 2-4) $S_{N_j} \approx 28000$ cycles and for $\delta a = 0.1$ mm (VSIM 6-8) $S_{N_j} \approx 18000$ cycles. The relative deviation varies from $\approx 20\%$ for small crack lengths to $\approx 8\%$ for large crack lengths for all simulation series.

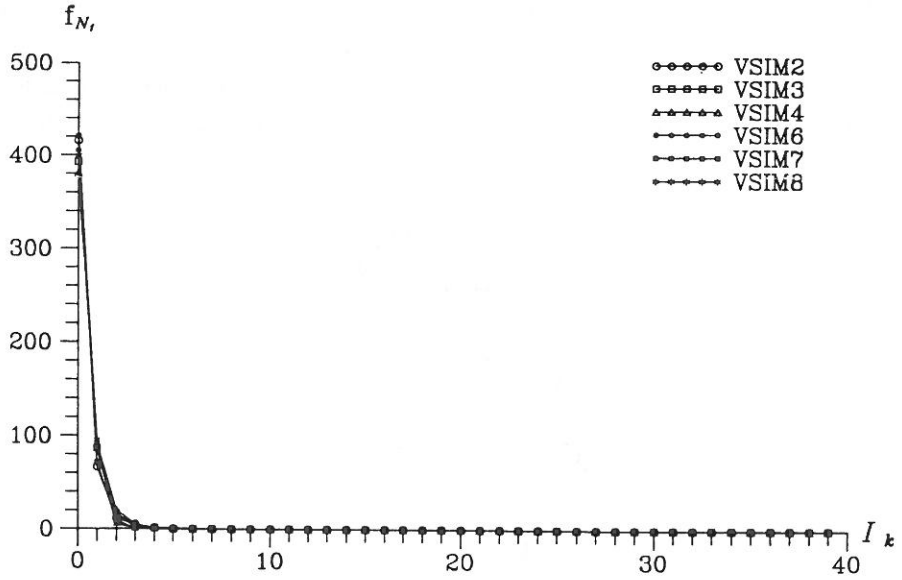

Figure 6.18: Histogram of the number of load cycles (f_{N_1}) applied to reach the crack state $a_1 = 9.2$ mm for VSIM 2-4 and VSIM 6-8.
$I_k =]k{\cdot}10000\ ;\ (k+1){\cdot}10000]$ cycles, $k = 0, 1, 2, \ldots, 39$.

Only four intervals are included in figure 6.18, i.e. $N_1 \in]0\ ;\ 40000]$ cycles with the main part in the first interval, $]0\ ;\ 10000]$. The small scatter in the total number of cycles to reach the first crack state was also seen in figures 6.17 and 6.7.

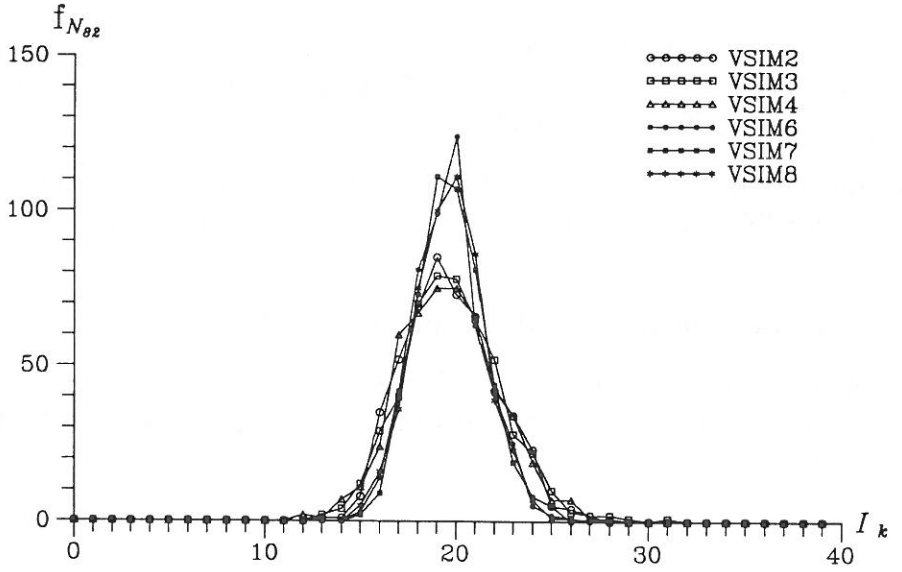

Figure 6.19: Histogram of the number of load cycles ($f_{N_{82}}$) applied to reach the crack state $a_{82} = 25.4$ mm for VSIM 2-4 and VSIM 6-8.
$I_k =]k{\cdot}10000\ ;\ (k+1){\cdot}10000]$ cycles, $k = 0, 1, 2, \ldots, 39$.

The importance of the value of the crack step length δa is, as in figure 6.12, seen in figure 6.19 in which a smaller δa-value results in a fewer number of intervals included

in the distribution of the total number of cycles applied to reach the crack state $a_{82} = 25.4$ mm. Thus, for VSIM 2-4 the intervals I_{12} to I_{31} are included whereas the intervals I_{14} to I_{26} are included for VSIM 6-8 corresponding to]120000 ; 320000] cycles and]140000 ; 270000] cycles, respectively. The value of λ seems not to influence the distribution since, the curves with same δa-value but different λ-value coincide.

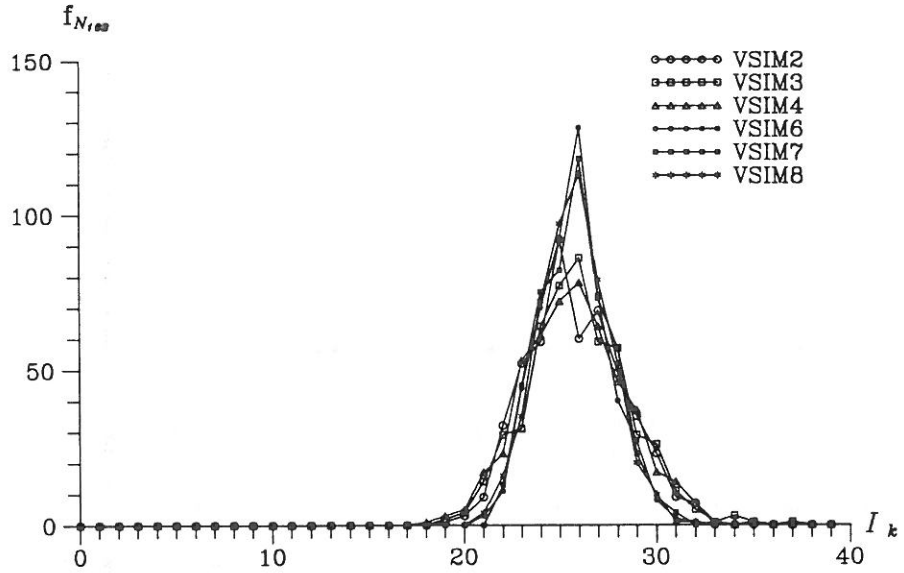

Figure 6.20: Histogram of the number of load cycles ($f_{N_{163}}$) applied to the reach crack state $a_{163} = 49.8$ mm for VSIM 2-4 and VSIM 6-8.
$I_k =]k{\cdot}10000 ; (k+1){\cdot}10000]$ cycles, $k = 0, 1, 2, \ldots, 39$.

The same tendency as in figure 6.19 is found in figure 6.20, but with the intervals I_{18} to I_{37} for VSIM 2-4 and I_{20} to I_{33} for VSIM 6-8 included. This corresponds to]180000 ; 380000] cycles and]200000 ; 340000] cycles, respectively.

These statistical results are in sections 6.2.2 and 6.3 compared with the corresponding results obtained from **VSTAT** on the basis of the Virkler data (see section 6.1).

6.2.2 Comparison of Virkler Data and Simulated FMF-Data

For the purpose of evaluating how well the FMF-model is able to describe fatigue crack growth, the statistical properties from section 6.2.1 are compared with the similar values of the Virkler data.

The comparison is based on the following norm, which is applied to each of the statistical properties.

$$q_X = \left[\sum_{j=0}^{n} (x_{\text{VSIM}} - x_{\text{VIRKLER}})^2 \right]^{\frac{1}{2}} \tag{6.1}$$

where

X = the statistical property in consideration
n = 162 for δN_j and 163 for N_j
x_{VSIM} = statistical value of VSIM 2-4 and VSIM 6-8
x_{VIRKLER} = statistical value of the Virkler data

The calculations of the q-values based on the statistical results from **VSTAT** (section 6.1) and **STAT** (section 6.2.1) are performed by program **VNORM** (appendix C). The results are given in table 6.21.

	$q_{\overline{\delta N_j}}$ (10^6)	$q_{S_{\delta N_j}}$ (10^6)	$q_{f_{\delta N_j}}$ (10^6)	$q_{\overline{N_j}}$ (10^6)	$q_{S_{N_j}}$ (10^6)	$q_{f_{N_j}}$ (10^6)
VSIM 2	6.8	414.6	4.6	3128.0	15038.0	4.0
VSIM 3	6.2	443.5	4.2	5103.9	20483.2	3.8
VSIM 4	5.1	453.6	4.2	2589.4	20088.6	3.8
VSIM 6	4.4	158.0	5.2	2554.8	2745.9	5.4
VSIM 7	5.8	178.0	4.0	3580.2	2807.8	5.3
VSIM 8	4.3	173.6	4.0	2459.3	2537.1	5.4

Table 6.21: Norm values q for: mean value ($\overline{\delta N_j}$), standard deviation ($S_{\delta N_j}$) and probability density ($f_{\delta N_j}$) of the number of load cycles applied at each crack state (a_j); mean value ($\overline{N_j}$), standard deviation (S_{N_j}) and probability density (f_{N_j}) of the number of load cycles applied to reach a crack state (a_j). The norm values are calculated for simulation series VSIM 2-4 and VSIM 6-8 (see table 6.9).

The purpose is that the parameters λ and δa in the FMF-model have such values that the statistical properties of the simulated FMF-data correspond to the similar properties of the Virkler data, i.e. the q-values should be as small as possible.

Besides the total number of cycles to reach the failure state N_f - see comments on figure 6.16 - the standard deviation of the total number of cycles to reach a given crack state $S_{N_j} = (\text{Var}[N_j])^{1/2}$ is considered to be the most important statistical property.

This considering that, by observation of a given crack length the primary requirement is to be able to predict the number of load cycles, which can be further applied before the failure state (or any other state) is reached.

In table 6.21 it is seen that a significant difference between the q-values for S_{N_j} for VSIM 2-4 and VSIM 6-8, respectively, occurs. The values for VSIM 2-4 are 5-8 times the values for VSIM 6-8, i.e. the value of δa has a decisive influence on how well the crack growth data are described by the FMF-model. Further, it is seen, as expected, that the value of λ only has minor influence, as long as the value is kept small.

The difference between VSIM 2-4 on one side and VSIM 6-8 and the Virkler data

on the other side, is also seen by comparison of figures 6.6 and 6.17. The curves for VSIM 2-4 generally assume larger values than the curve for the Virkler data and thus they are responsible for the high q-value for S_{N_j} in table 6.21.

The lower q-values for S_{N_j} for VSIM 6-8 are due to the fact that the S_{N_j}-curves for VSIM 6-8 are placed at the same level as the curve for the Virkler data. The difference between the curves is seen to occur especially for small a-values, whereas the same final value is approached asymptotically.

Comparison of the q-values for VSIM 6-8 shows that generally VSIM 8 has the lowest values. Thus, the Virkler data are best described by the FMF-model using $\lambda = 1$ and $\delta a = 0.1$ mm, but almost the same results can be obtained using $\lambda = 10$ or $\lambda = 100$ (VSIM 7 and VSIM 6, respectively).

Using (5.29) - and bearing in mind that N_j is the number of DCs - the standard deviation of the number of load cycles to cause failure, S_{N_f}, can be found as

$$S_{N_f} = \frac{a_0^{1/2}\,(10^3)^{m/2}}{C\,(\Delta\sigma\,\sqrt{\pi\,a_0})^m\,(m-1)^{1/2}}\,(\delta a)^{1/2} \tag{6.2}$$

where the initial crack length a_0 and the crack step length δa are measured in [mm], the material parameter C in [mm/(MPa$\sqrt{\text{m}}$)^m] and the stress range $\Delta\sigma$ in [MPa]. The factor $(10^3)^{m/2}$ is necessary to obtain consistentcy in dimensions.

Using the values from table 6.8 in (6.2), the standard deviation of N_f can be calculated as a function of δa. This is illustrated in figure 6.22.

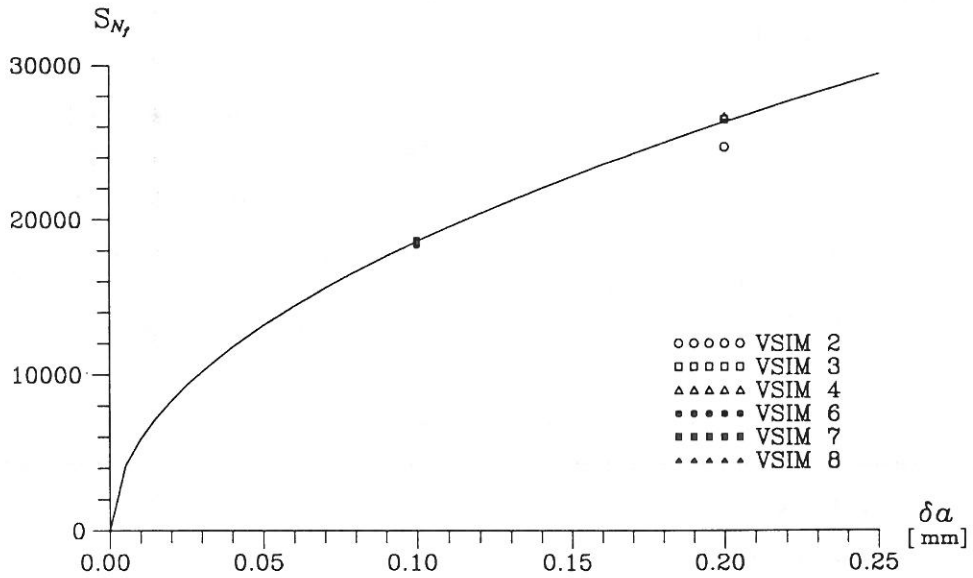

Figure 6.22: Standard deviation of the number of load cycles to cause failure as a function of the crack step length. The S_{N_f}-values for VSIM 2-4 and VSIM 6-8 are also seen in figure 6.17.

Figure 6.22 shows good agreement between (6.2) and the simulations VSIM 3-4 and VSIM 6-8. Only VSIM 2 deviates visibly from the curve given by (6.2) which is either

due to the combination of δa and the high λ-value ($\lambda = 100$) or more probably is an expression of coincidence.

As a consequence of the agreement between the analytical expression (6.2) and the numerical results, the most appropriate estimate of δa can be found from (5.30) or (6.2) on the basis of the S_{N_f}-value for the Virkler data, i.e.

$$\delta a = \frac{C^2 \left(\Delta\sigma \sqrt{\pi\, a_0}\right)^{2m} (m-1)}{a_0 \,(10^3)^m} \, S_{N_f}^2 \tag{6.3}$$

Inserting the values from table 6.8 and $S_{N_f} = 18446.80$ cycles (see figure 6.6) results in $\delta a = 0.0983$ mm as an estimate of the δa-value giving the best description of the Virkler data. The value used in the simulations VSIM 6-8 ($\delta a = 0.1$ mm) roughly corresponds to the estimated value ($\delta a = 0.0983$ mm) so no further calculations will be made.

It should be noted that δa is strongly dependent on which S_{N_f}-value - and thus which failure crack length a_f - is used. This can be seen in figure 6.23 in which S_{N_j} as a function of a_j is illustrated for the Virkler data and VSIM 8, respectively.

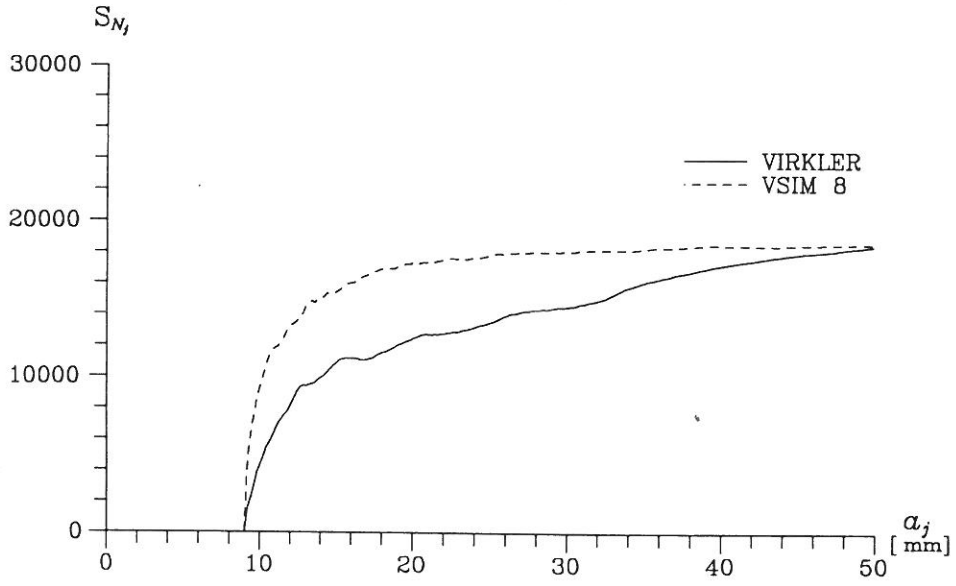

Figure 6.23: Standard deviation of the number of load cycles (S_{N_j}) applied to reach the crack state (a_j) for the Virkler data and VSIM 8.
$j = 0, 1, 2, \ldots, 163$, $a_0 = 9.0$ mm and $a_{163} = 49.8$ mm.

Figure 6.23 shows that for $a_j < a_f$, S_{N_j} for the simulated data deviates from S_{N_j} for the Virkler data. In this case, the δa-value determined by (6.3) where S_{N_j} is inserted will not give an adequate description of the Virkler data. It should be remembered that (5.30) and thus (6.3) are established under the assumption that $a_f \gg a_0$.

The evaluation of the FMF-model on the basis of the numerical results is performed in section 6.3.

6.3 EVALUATION

The applicability of the FMF-model is in this section evaluated on the basis of the results in sections 6.1 and 6.2. Further, it is discussed if the crack step length can be regarded as a characteristic value of the material as assumed in chapter 5.

The properties of the FMF-model are evaluated on the basis of a qualitative demand and a quantitative demand.

The first demand concerning similarity in the form and the progress of the fatigue crack growth curves can be fulfilled if λ - the number of load cycles in a duty cycle - is small, e.g. $\lambda \leq 100$. Further, the material parameters C and m in Paris' law (5.4) must be determined from tests with specimens made of material from the same casting as the structure.

The statistical properties of fatigue crack growth data established by simulation correspond to the statistical properties of experimental fatigue data if adequate choices of the model parameters used in the FMF-model are made. In fact, the analyses in section 6.2.2 show that if λ is small, e.g. $\lambda \leq 100$, the crack step length δa can be regarded as a characteristic value of the material determined by (6.2).

Thus, the FMF-model can fulfil both the qualitative and quantitative demand by a careful establishment of the model parameters.

7. EXPERIMENTAL FATIGUE TESTS OF STEEL

The purpose of the experimental tests described in the present chapter is to determine the material parameters included in the Fracture Mechanical Markov Chain Fatigue Model (FMF-model), introduced in chapter 5 and 6, for a mild steel, see section 7.1.

Further, the experimental test data serve as reference data for the evaluation of the applicability of the FMF-model. Thus, the numerical results (see section 7.2) obtained by application of the FMF-model - using the experimentally determined model parameters as input parameters - can be compared with the results from the experimental tests, section 7.3.

The material used in all the tests has the chemical composition as shown in table 7.1.

Fe	Ec	C	Si	Mn	P	S	N	Cr	Ni	Cu	Al
63	14	7	1	0.33	1.2	0.9	0.4	4	3	1	3.8

Table 7.1: Chemical composition of the STW22 DIN 1614 steel used in experimental tests. In percentage by weight.

The modulus of elasticity E, the Poisson ratio ν, the yield stress f_y and the ultimate stress f_u are determined in a simple static tension test. Two test specimens are carved from the same steel cast as used in the dynamic tests, described in section 7.1. The material parameters, determined as the mean value of the two tests, are

Modulus of elasticity E	$1.9 \cdot 10^5$ MPa
Poisson ratio ν	0.3
Yield stress f_y	266 MPa
Ultimate stress f_u	330 MPa
Ultimate strain ϵ_u	0.28

Table 7.2: Material properties for the mild steel used in the constant-amplitude load fatigue tests described in section 7.1.

Further description of the static tests is given in [Gansted, L.; 1991].

7.1 FATIGUE TESTS

Two series of dynamic tests have been performed in order to establish the fatigue properties of the mild steel in tables 7.1 and 7.2. Both series are performed with CA-load, but the first series - described in section 7.1.1 - includes different stress ranges, whereas the second series - described in section 7.1.2 - is performed under "identical" conditions.

The specimens, which were carved from the same steel plate, were arbitrary chosen to the two series of tests. In all the fatigue tests, CCT-specimens (Center Cracked Tension Specimen) have been used, see figure 7.3.

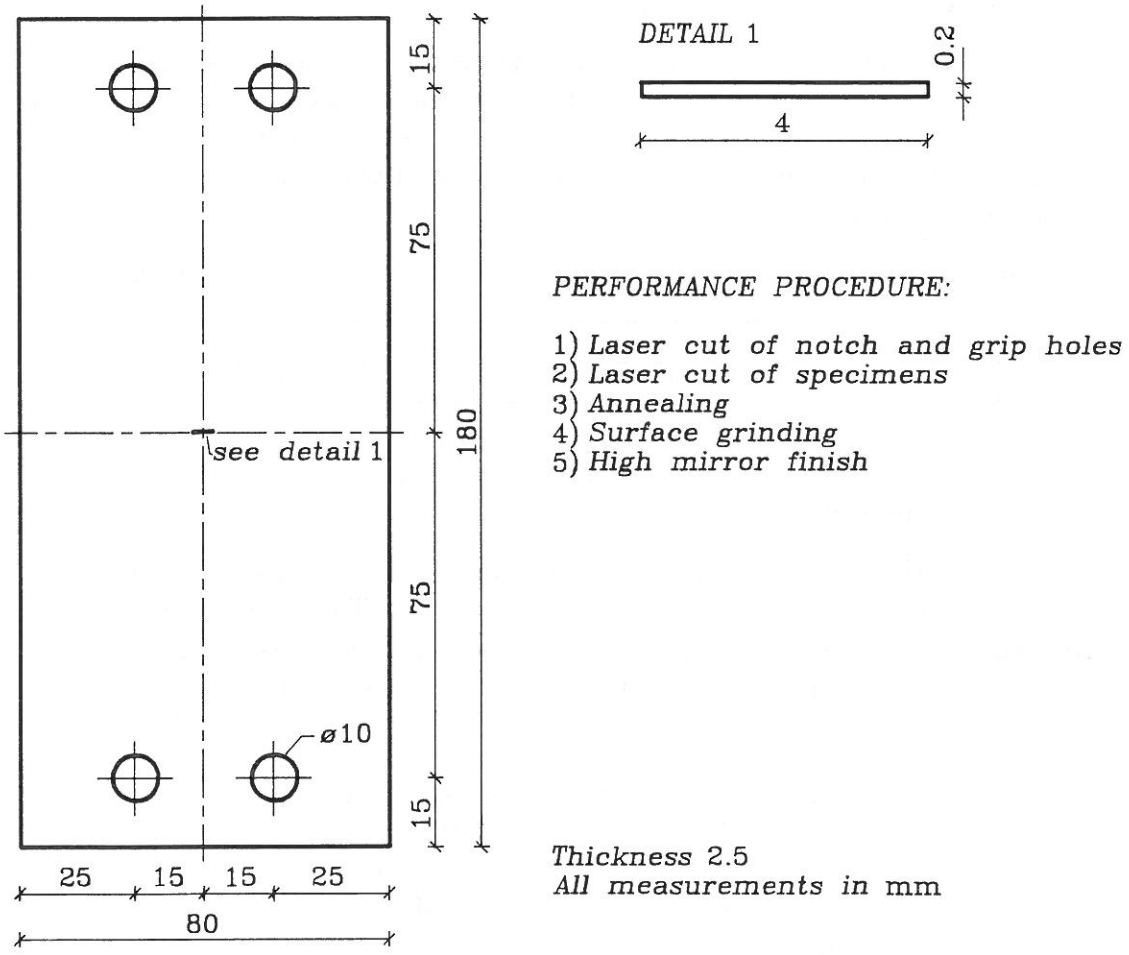

Figure 7.3: CCT-specimen used in fatigue testing.

The test equipment shown in figure 7.4 consists of a servo-hydraulic fatigue testing machine (± 40 kN), a camera including a monitor and a PC used as controller. The PC is equipped with image analysing hardware (cards) used in Digital Image Processing (DIP). The software control program consists of two parts, one used to control the fatigue testing machine, developed by [Brincker, R. and J.D. Sørensen; 1990], and one used to control the DIP, see [Lyngbye, J. and R. Brincker; 1990].

The main advantages of DIP are: A more precise measuring of the crack length; short interruptions of the loading (5-10 seconds) during measuring and less resource demanding since, nobody has to survey the test.

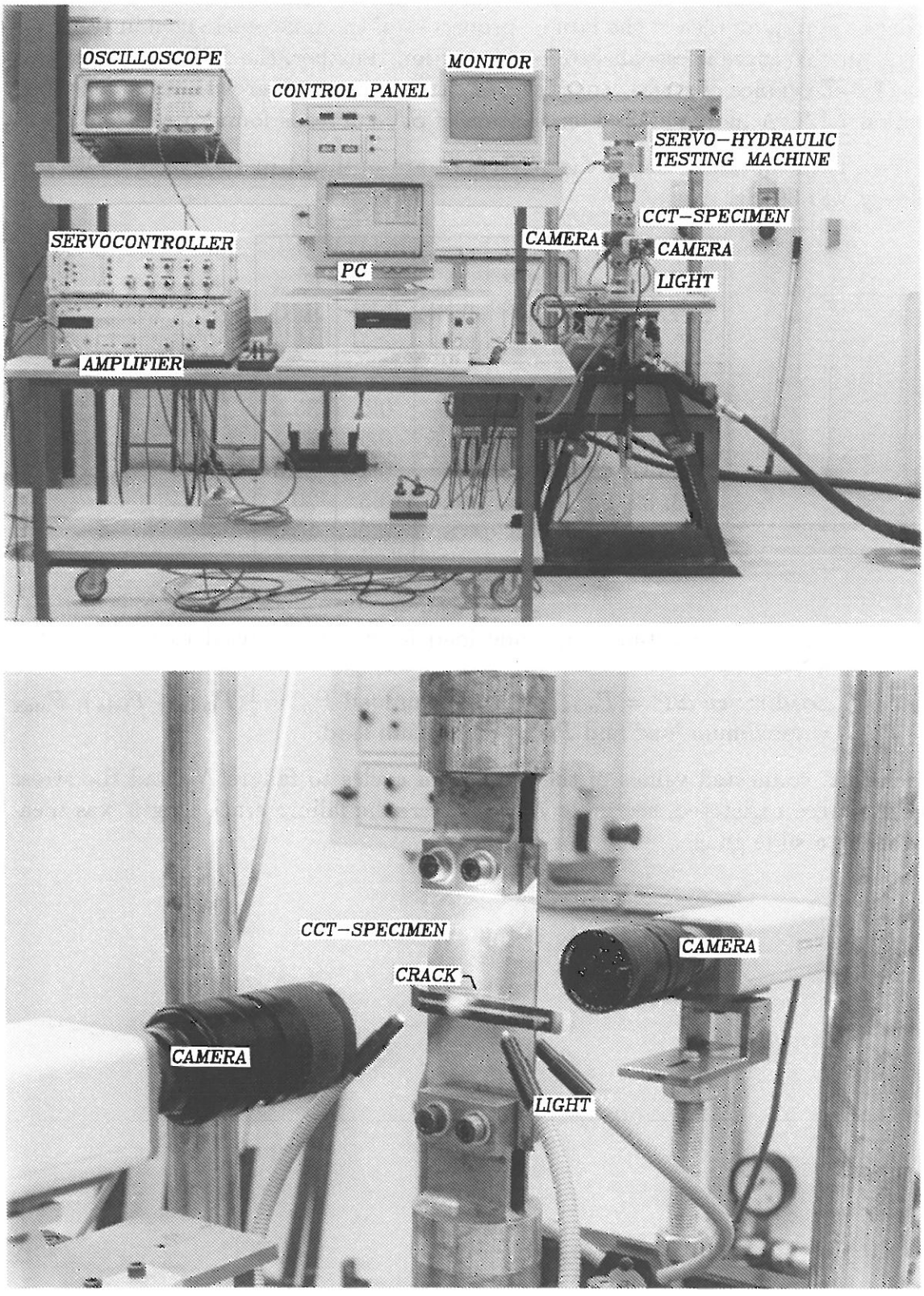

Figure 7.4: Test equipment for fatigue testing.

7.1.1 SN-Curve

In order to obtain an idea of the fatigue properties of the mild steel given in table 7.1 and 7.2, an SN-curve is established in this section. Further, the SN-curve serves as a basis for the choice of stress range level in the fatigue crack growth tests described in section 7.1.2. A more detailed description of SN-curves is found in section 2.2.1.

The tests used for establishing the SN-curve are outlined in table 7.5. The test frequency was 30 Hz.

TEST SPECIMEN	ΔP [kN]	P_m [kN]	$P_{\min}$ [kN]	$P_{\max}$ [kN]
36, 64, 99	35	18	0.5	35.5
2, 26, 61	30	15.5	0.5	30.5
19, 31, 49	25	13	0.5	25.5
13, 82, 93	20	10.5	0.5	20.5
7, 43, 75	15	8	0.5	15.5

Table 7.5: Review of constant-amplitude load fatigue tests, used to establish the SN-curve.
Load range $\Delta P = P_{\max} - P_{\min}$, mean load $P_m = \frac{1}{2}(P_{\max} + P_{\min})$, $P_{\max}$ = maximum load and $P_{\min}$ = minimum load.

In each test, connected values of the number of cycles to failure N_f and the stress range $\Delta\sigma$ were registered, see table 7.6. Further, the failure crack length was measured using a slide gauge.

TEST SPECIMEN	$\Delta\sigma$ [MPa]	N_f	a_f [mm]
36	175	85004	12.35
64	175	87133	13.15
99	175	95493	11.85
2	150	165869	16.35
61	150	169409	17.40
26	150	173926	16.75
31	125	341537	21.40
19	125	365854	20.95
49	125	366508	20.70
13	100	745761	24.85
82	100	785261	24.75
93	100	787116	24.65
43	75	2329197	29.10
75	75	4756346	29.20
7	75	5325000	28.70

Table 7.6: Results of the fatigue tests in table 7.5.
$\Delta\sigma$ = stress range. N_f = number of cycles to failure. a_f = failure crack length.

On the basis of these values the SN-curve shown in figure 7.7 is drawn.

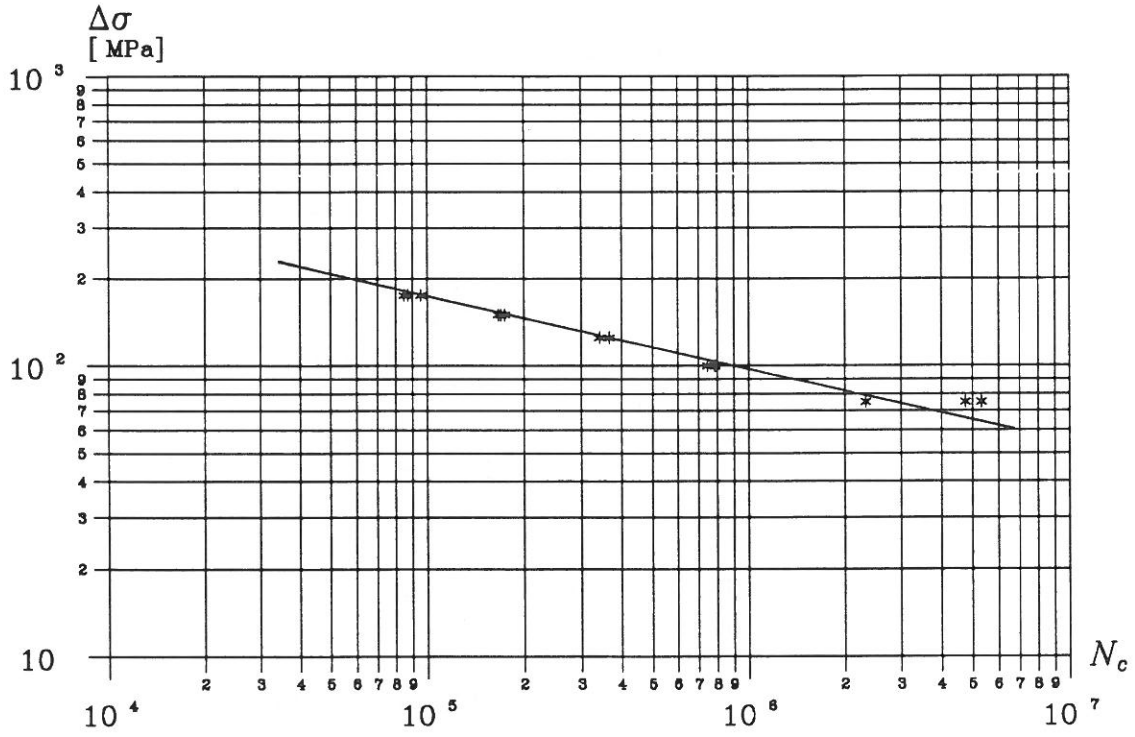

Figure 7.7: SN-curve for CCT-specimens of mild steel.
N_c = number of load cycles to cause fracture. $\Delta\sigma$ = stress range.

From table 7.6 and figure 7.7 it is seen that a small stress range results in a large critical crack length, which leaves the possibility of a large number of measurements, but on the other hand a long time of testing. In contrast, a large stress range gives a smaller critical crack length and thus the possibility of a fewer number of measurements, but a short time of testing.

The stress range used in the fatigue crack growth tests is chosen as $\Delta\sigma = 125$ MPa at the mean stress level $\sigma_m = 65$ MPa ($\Delta P = 25$ kN and $P_m = 13$ kN). This stress range allows a reasonable number of crack length measurements and a reasonable time of testing ($\approx$ 4 hours at a frequency of 30 Hz). The fatigue crack growth tests are described in section 7.1.2.

7.1.2 Fatigue Crack Growth Curves

In order to describe the fatigue crack growth process by the FMF-model for structures made of the mild steel in table 7.1 and 7.2, the model parameters included in the FMF-model, are determined.

The constant-amplitude load (CA-load) tests were performed with maximum load $P_{\max} = 25.5$ kN, minimum load $P_{\min} = 0.5$ kN corresponding to the load range $\Delta P = 25$ kN.

In each test, the number of load cycles and the crack length (N, a) was recorded for fixed values of δN by use of the DIP technique (Digital Image Processing).

The FMF-model requires that δa and not δN is a fixed parameter, but so far this is not possible with the DIP technique and thus, measurements with fixed δa values would have required manual performance of the tests. The latter solution includes several disadvantages e.g. less accuracy and larger resources in the form of working hours. The problem was solved by interpolating the (N, a)-values corresponding to fixed values of δa.

The (N, a)-curves are shown in figure 7.8 where $(N_0, a_0) = (0, 3.0 \text{ mm})$ for all curves.

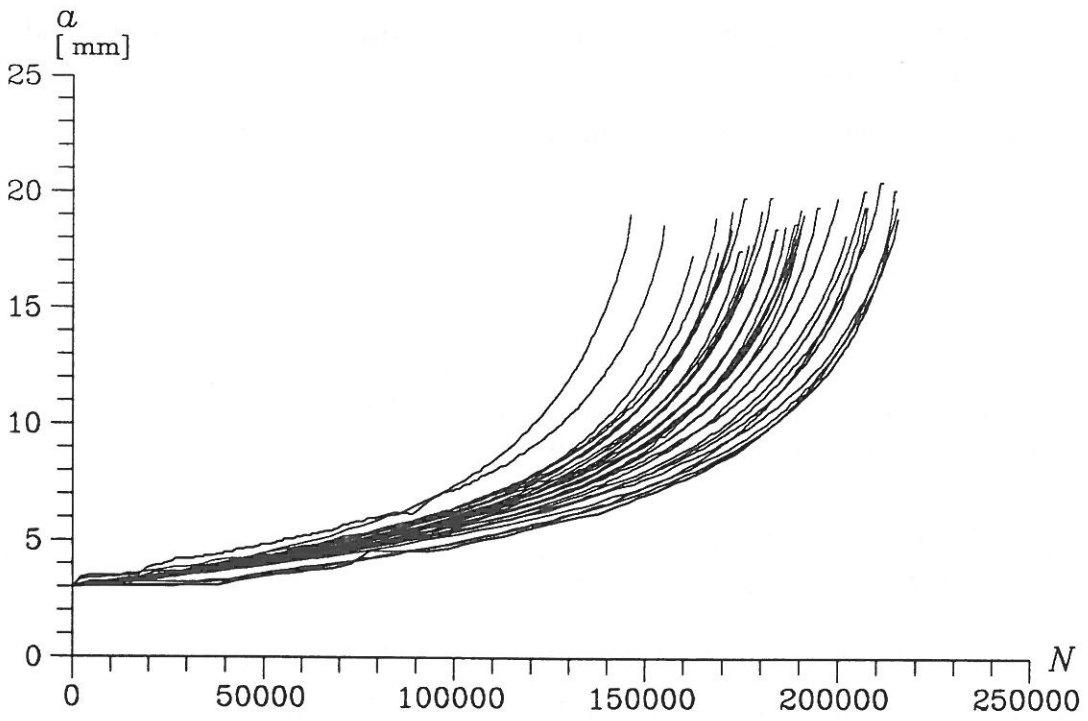

Figure 7.8: (N, a)-curves for CA-load tests performed in the spring of 1990. All 34 tests were performed with $\Delta P = 25$ kN. Material parameters are given in tables 7.1 and 7.2.
N = number of load cycles, a = crack length.

From figure 7.8 it is seen that the curves have the same form and that they are characterized by a smooth progress. The approach to a vertical line for large a-values is less pronounced than for the Virkler data shown in figure 6.1. This is due to two factors: Firstly, the failure crack length a_f is obtained for $a = 0.5\, a_{\max}$, where $a_{\max} = 0.5\, b = 40$ mm (see figure 7.3), whereas $a_f = 0.65\, a_{\max}$ for the Virkler data. Secondly, the measuring method is very sensitive to changes in the surface of the specimen which makes its impossible to measure when the plastic deformations become too large.

Further, it is seen that a large initial crack growth rate results in a small value of N_f and vice versa, and that there is a small tendency towards getting larger values of a_f

for increasing N_f. This was also found in table 7.6.

The material parameters C and m are determined on the basis of the (N, a)-data by calculating the crack growth rate (da/dN) and the stress intensity factor range (ΔK) using a developed C-program, **PARIS** (see appendix C).

The stress intensity factor range for a finite CCT-specimen is given as, [ASTM E647-83].

$$\Delta K = \Delta\sigma\sqrt{\pi\, a \sec\left(\frac{\pi\, a}{b}\right)} \tag{7.1}$$

where the applied stress range $\Delta\sigma = 125$ MPa, the width of the specimen $b = 80$ mm and $a =$ the crack length.

The crack growth rate (da/dN) is found as the secant between two adjacent (N, a)-values, i.e.

$$\left(\frac{da}{dN}\right)_{a=\frac{1}{2}(a_i+a_{i+1})} = \frac{a_{i+1} - a_i}{N_{i+1} - N_i} \tag{7.2}$$

The CCT-specimen shown in figure 7.3 is designed so plane stress state occurs during the entire experiment. Evaluation of the extent of the plastic zone (r_y) in front of the crack tip is based on appendix A (A.9),

$$r_y = \frac{1}{\pi}\left(\frac{K_I}{f_y}\right)^2 = \left(\frac{\sigma_{\max}}{f_y}\right)^2 a \sec\left(\frac{\pi a}{b}\right) \tag{7.3}$$

where (7.1) is used for the maximum stress intensity factor for K_I.

Insertion of $f_y = 266$ MPa (see table 7.2), $\sigma_{\max} = 127.5$ MPa, $b = 80$ mm and the initial crack length $a_0 = 3.0$ mm and the failure length $a_f = 17.5$ mm results in

$$r_y = \begin{cases} 0.69\,\text{mm} & \text{for } a_0 = 3.0 \text{ mm} \\ 4.02\,\text{mm} & \text{for } a_f = 17.5 \text{ mm} \end{cases}$$

Since the extent of the plastic zone is $\approx 20\%$ of the crack length it is found necessary to replace the crack length a by an effective crack length given as

$$a_{\text{eff}} = a + \tfrac{1}{2} r_y \tag{7.4}$$

Introducing (7.4) in (7.1), the stress intensity factor range becomes

$$\Delta K = \Delta\sigma\sqrt{\pi\, a_{\text{eff}} \sec\left(\frac{\pi\, a_{\text{eff}}}{b}\right)} \tag{7.5}$$

and in (7.2), the crack growth rate is

$$\left(\frac{da}{dN}\right)_{a=\frac{1}{2}(a_{\text{eff},i}+a_{\text{eff},i+1})} = \frac{a_{\text{eff},i+1} - a_{\text{eff},i}}{N_{i+1} - N_i} \tag{7.6}$$

On the basis of (7.1)-(7.2) or (7.5)-(7.6), the material parameters C and m can be found by linear regression analysis bearing in mind that if $(\Delta K, da/dN)$ is represented in a double logarithmic scale, see figure 2.7 and section 3.2.3, C and m can be found as the intersection with the ordinate axis and as the slope of the straight line, respectively. Thus,

$$\log(\frac{da}{dN}) = \log C + m \log(\Delta K) \tag{7.7}$$

Both the results from (7.1)-(7.2) and (7.5)-(7.6) are used.

The linear regression analysis performed in **PARIS** gives the results in table 7.9.

		(7.1)-(7-2)	(7.5)-(7.6)
$\log C$	$[\text{mm}/(\text{MPa}\sqrt{\text{m}})^m]$	-8.60076	-8.53291
C	$[\text{mm}/(\text{MPa}\sqrt{\text{m}})^m]$	$2.5075 \cdot 10^{-9}$	$2.9315 \cdot 10^{-9}$
$S_{\log C}$	$[\text{mm}/(\text{MPa}\sqrt{\text{m}})^m]$	0.019	0.018
m		3.486	3.400
S_m		0.014	0.013

Table 7.9: Values of the material parameters C and m found from experimental data by the linear regression analysis performed in **PARIS**. Further, the standard deviations of $\log C$ and m are given.

It is seen that almost the same results for C and m are obtained no matter which of a or a_{eff} is used. Further, only small deviations are found, which means that (7.7) gives a good description of the data. The following calculations are therefore based on the crack length a, which is simpler than using the effective crack length.

In order to calculate the statistical properties of the (N, a)-curves, the data are transformed into (N, a)-data for fixed values of a, $a = a_0 + \delta a$, where $a_0 = 3.0$ mm, $\delta a = 0.1$ mm and $a \in [3.0\ ;\ 17.5]$mm. The transformation is performed by linear interpolation between the two adjacent values of a, one smaller and one greater than the desired a value. The corresponding N value is found in a similar fashion.

All the following analyses are based on these (N, a)-data.

The above-mentioned transformation is performed in the program **CASTAT** (see appendix C) before the statistical properties, (which are likewise those in sections 6.1 and 6.2.1), of the experimental data are calculated. The results from **CASTAT** are shown in figures 7.12-7.21 in section 7.3.

7.2 SIMULATION OF FMF-DATA WITH EXPERIMENTAL PARAMETERS

For the purpose of testing the FMF-model on steel by the experimentally established fatigue crack growth data in section 7.1.2, (N, a)-data (N = number of cycles, a = crack length) are simulated on the basis of the FMF-model. The simulations are performed by the program **SIMULA** - see appendix C. The number of data set in the simulation series is 500.

The input parameters to **SIMULA**, shown in table 7.10, are found in section 7.1. The values are kept constant.

a_0 [mm]	a_f [mm]	$\Delta\sigma$ [MPa]	C [mm/(MPa$\sqrt{\text{m}}$)$^{3.49}$]	m
3.0	17.5	125	$2.51 \cdot 10^{-9}$	3.49

Table 7.10: Input parameters to program **SIMULA** for simulation series ESIM. a_0 = initial crack length, a_f = failure crack length, $\Delta\sigma$ = stress range, C = material constant and m = material constant.

The parameter λ (number of load cycles in each duty cycle) is chosen as 1 because the time factor in the simulations in this case is not of decisive importance. If so, $\lambda = 10$ or $\lambda = 100$ could be chosen.

The remaining parameter δa (crack step length) is established using (6.3). This is done due to the good results obtained in section 6.2.2 (figure 6.22).

Insertion of a_0, $\Delta\sigma$, C and m from table 7.10, $\lambda = 1$ and $S_{N_f} = 17115$ (see figure 7.18) gives $\delta a = 0.0552$ mm.

Thus, all the input parameters to **SIMULA** are established. The results, in the form of (N, a)-curves, are shown in appendix E, figures E.1-E.5. To keep the overlook only 100 (N, a)-curves are shown in each plot. A typical plot from appendix E is shown in figure 7.11.

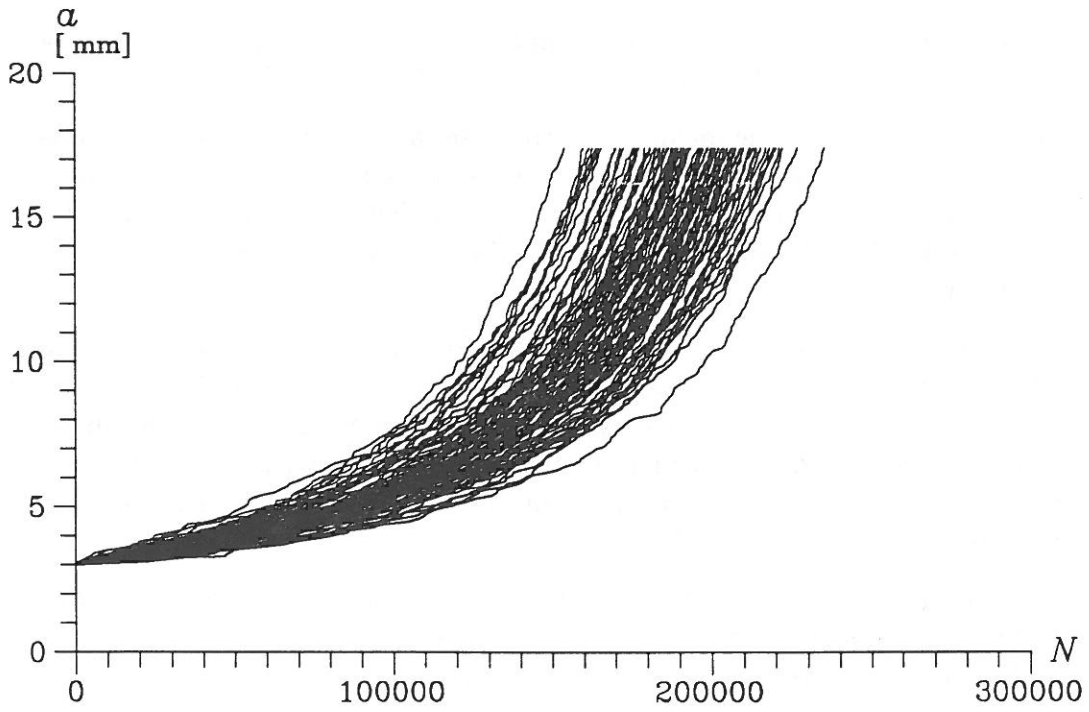

Figure 7.11: Typical plot of (N, a)-curves from simulation series ESIM.
N = number of load cycles, a = crack length.

Qualitatively, the (N, a)-curves in figure 7.11 are almost similar to those in figure 7.8. Thus, the curves are characterized by having the same form and by having a smooth progress.

As earlier described (see sections 6.1 and 6.2) a large initial crack growth rate results in a small number of cycles to cause failure and vice versa. The main part of the curves has the failure number of cycles concentrated within the interval $N_f \in$ [150000 ; 220000] cycles whereas the experimental curves in figure 7.8 cover the interval, $N_f \in$ [140000 ; 215000] cycles.

The quantitative evaluation of the experimental data and the simulated data is performed in section 7.3.

7.3 QUANTITATIVE PROPERTIES OF THE EXPERIMENTAL DATA AND THE FMF-DATA

In this section, the quantitative properties of the FMF-model is discussed on the basis of the statistical properties of the experimental data and the simulated FMF-data, respectively.

The statistical properties are given in section 7.3.1, whereas the comparison is performed in section 7.3.2.

7.3.1 Statistical Analysis of Experimental Data and FMF-Data

The statistical properties of the experimental data from the CA-load tests in section 7.1.2 and of the FMF-data from ESIM in section 7.2 are given in the present section.

The statistical values, i.e. the mean value, the standard deviation and the probability density of the number of cycles applied in each crack state to reach the successive crack state and of the total number of cycles applied to reach a crack state, are determined by **CASTAT** and **STAT** form **STAT-PACK** (see appendix C) and are shown in figures 7.12-7.21.

The histograms in figures 7.14-7.16 are shown for the crack lengths $a_0 = 3.0$ mm, $a_{72} = 10.2$ mm and $a_{144} = 17.4$ mm, corresponding to the first, middle and final crack lengths for which the number of load cycles applied at a crack state is measured. The corresponding crack lengths for which the total number of cycles is measured are $a_1 = 3.1$ mm, $a_{73} = 10.3$ mm and $a_{145} = 17.5$ mm. The histograms for these crack lengths are illustrated in figures 7.19-7.21.

Each interval I_k in the histograms consists of a number of load cycles - 250 for δN_j and 1000 for N_j - distributed as $I_k =]k{\cdot}250\ ;\ (k+1){\cdot}250]$ cycles and $I_k =]k{\cdot}1000\ ;\ (k+1){\cdot}1000]$ cycles, respectively. $k = 0, 1, 2, \ldots, 39$.

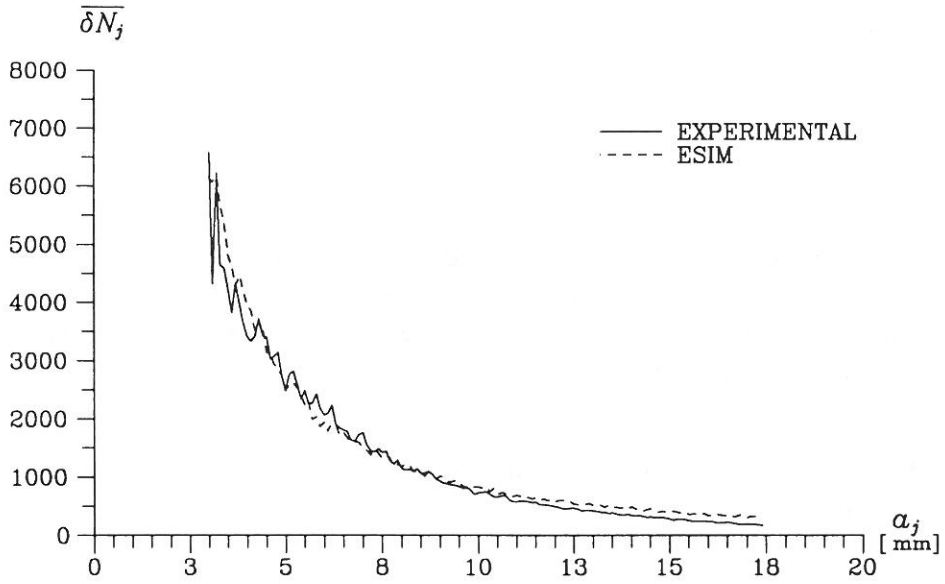

Figure 7.12: Mean value of the number of load cycles ($\overline{\delta N_j}$) applied at each crack state (a_j), for CA-load tests and for ESIM.
$j = 0, 1, 2, \ldots, 144$, $a_0 = 3.0$ mm and $a_{144} = 17.4$ mm.

Figure 7.12 shows that the mean number of load cycles $\overline{\delta N_j}$ applied at the crack state a_j is decreasing for increasing crack length, which could be expected because the crack growth rate increases during lifetime. Notice, that the progresses for the CA-load tests and for ESIM almost coincide, but that the largest scatter occurs for the CA-load tests at small crack lengths ($a \leq 5$ mm).

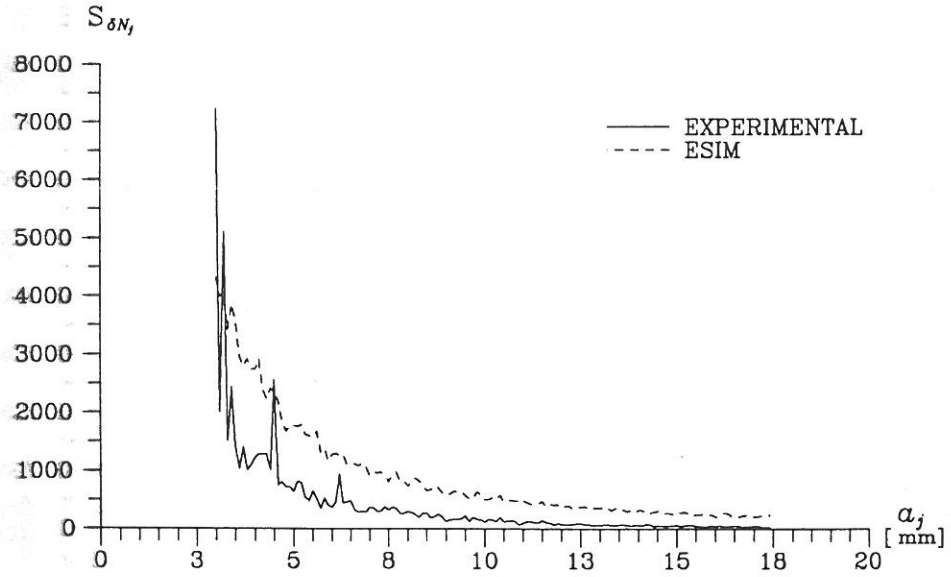

Figure 7.13: Standard deviation of the number of load cycles ($S_{\delta N_j}$) applied at each crack state (a_j), for CA-load tests and for ESIM.
$j = 0, 1, 2, \ldots, 144$, $a_0 = 3.0$ mm and $a_{144} = 17.4$ mm.

The standard deviation of the number of load cycles $S_{\delta N_j}$ applied at a crack state a_j is decreasing for increasing crack length, see figure 7.13. The scatter in the standard deviation is seen to be large for small crack lengths ($a \leq 5$ mm), whereas it is small for large crack lengths. Generally, $S_{\delta N_j}$ for ESIM is larger than for the experimental data, which might be due to a larger number of curves (500) included. The CA-load tests only includes 34 curves.

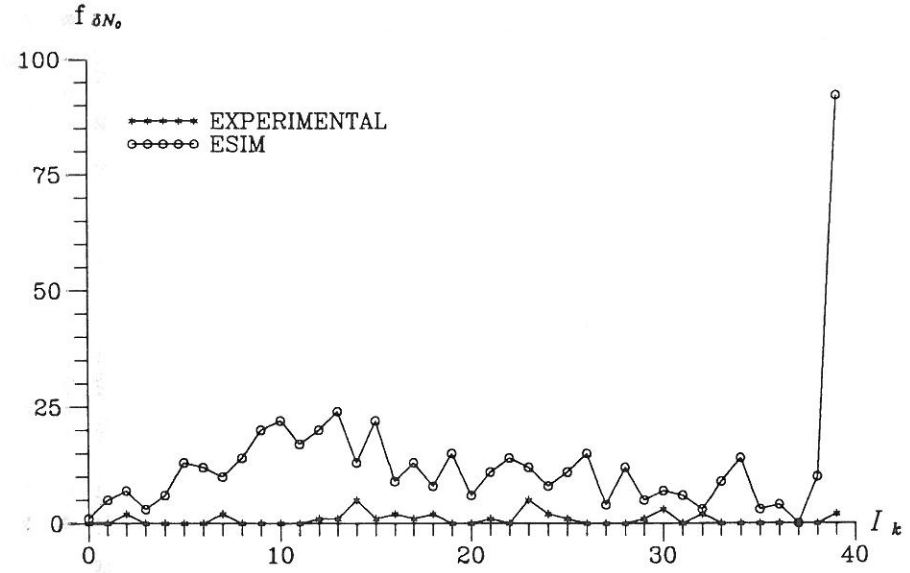

Figure 7.14: Histogram of the number of load cycles ($f_{\delta N_0}$) applied at the crack state $a_0 = 3.0$ mm for CA-load tests and for ESIM.
$I_k =]k{\cdot}250\ ;\ (k+1){\cdot}250]$ cycles, $k = 0, 1, 2, \ldots, 39$.

From figure 7.14 it is seen that, the probability density $f_{\delta N_0}$ for both the CA-load tests and for ESIM is uniformly distributed over all intervals. Excepted from this is the interval I_{39} ($\delta N_0 > 9750$ cycles) for ESIM. In this interval approximately $\frac{1}{6}$ of the δN_0 values are found.

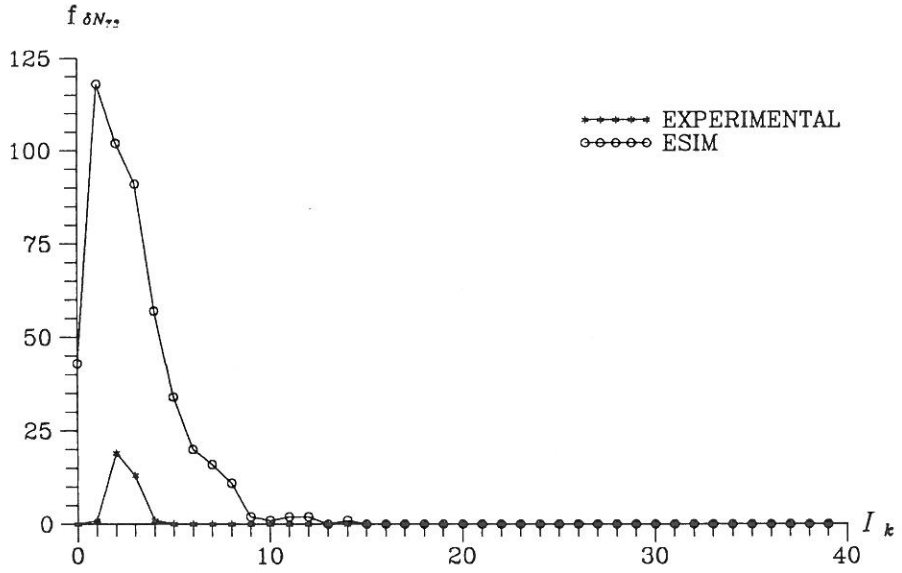

Figure 7.15: Histogram of the number of load cycles ($f_{\delta N_{72}}$) applied at the crack state $a_{72} = 10.2$ mm for CA-load tests and for ESIM.
$I_k =]k{\cdot}250\ ;\ (k+1){\cdot}250]$ cycles, $k = 0, 1, 2, \ldots, 39$.

The decrease in the standard deviation of δN_j is reflected in the probability density $f_{\delta N_{72}}$. Thus, only 4 intervals (I_1 to I_4, i.e. $\delta N_{72} \in]250\ ;\ 1250]$ cycles) for the CA-load tests and 15 intervals (I_0 to I_{14}, i.e. $\delta N_{72} \in]0\ ;\ 3750]$ cycles) for ESIM are included. Notice, that the main part of are concentrated in a fewer intervals.

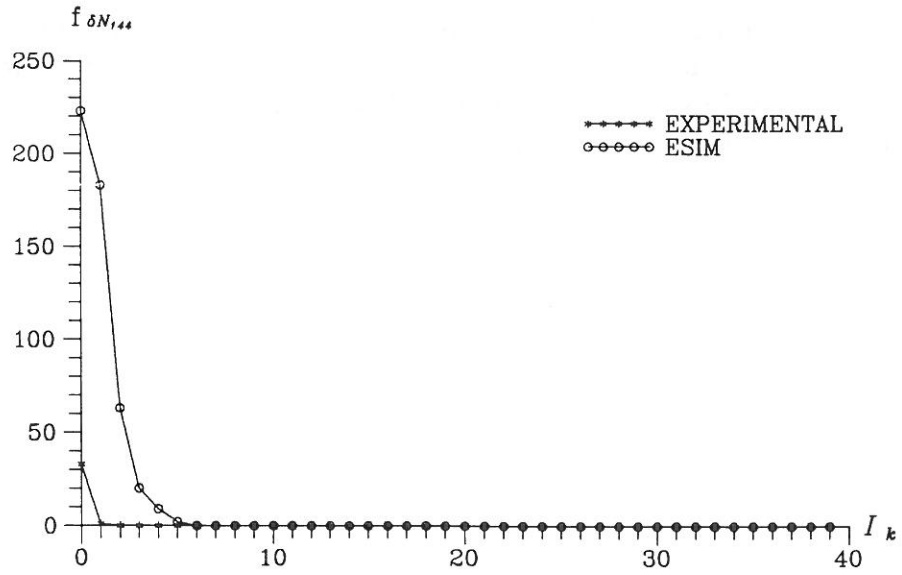

Figure 7.16: Histogram of the number of load cycles ($f_{\delta N_{144}}$) applied at the crack state $a_{144} = 17.4$ mm for CA-load tests and for ESIM.
$I_k =]k{\cdot}250\ ;\ (k+1){\cdot}250]$ cycles, $k = 0, 1, 2, \ldots, 39$.

No matter how many cycles have been applied to reach crack state $a_{144} = 17.4$ mm, almost the same number of cycles are required to reach the failure state. This is seen in figure 7.16 in which $f_{\delta N_{144}}$ is concentrated in 2, respectively 6 intervals for the CA-load tests and ESIM. Thus, $\delta N_{144} \in]0\ ;\ 500]$ cycles for the experimental data and $\delta N_{144} \in]0\ ;\ 1500]$ cycles for the simulated data.

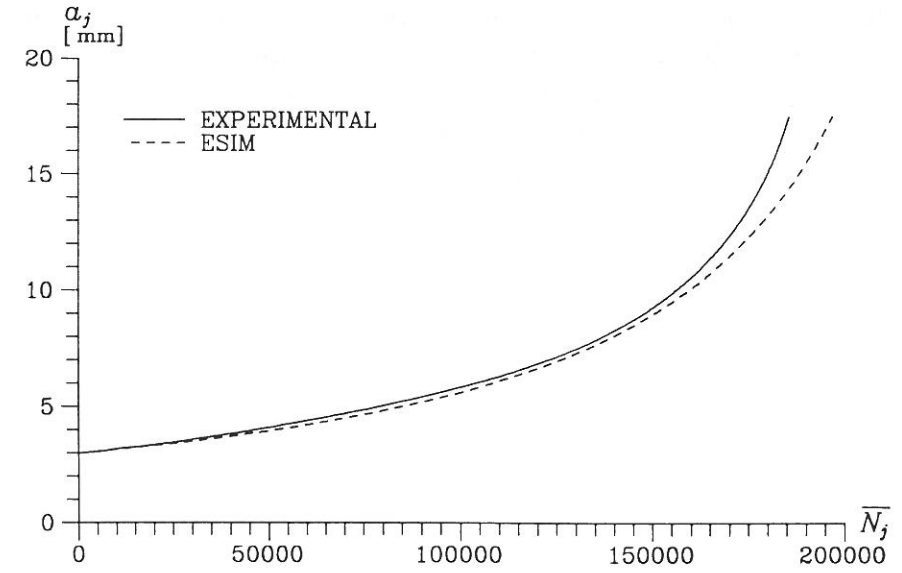

Figure 7.17: Mean value of the number of load cycles ($\overline{N_j}$) applied to reach the crack state (a_j), for CA-load tests and for ESIM.
$j = 0, 1, 2, \ldots, 145$, $a_0 = 3.0$ mm and $a_{145} = 17.5$ mm.

The mean number of load cycles $\overline{N_j}$ applied to reach a crack state a_j has a smooth, non-decreasing progress, see figure 7.17. The experimental data have a larger crack growth rate and thus, the number of cycles to cause failure N_f is smaller than for the simulated data. N_f are 185353 cycles and 196704 cycles, respectively, and thus ESIM overestimates the lifetime by approximately 6 %.

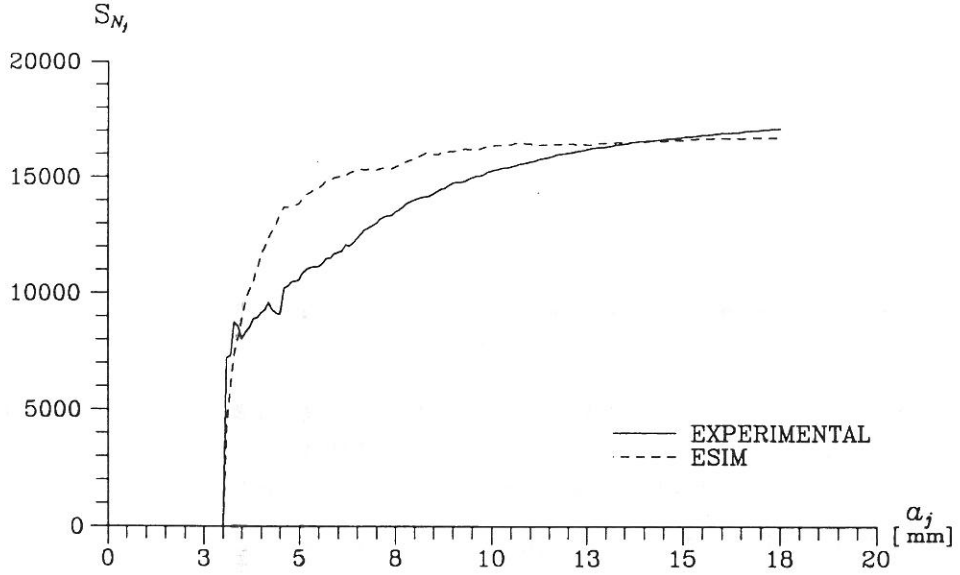

Figure 7.18: Standard deviation of the number of load cycles (S_{N_j}) applied to reach the crack state (a_j), for CA-load tests and for ESIM.
$j = 0, 1, 2, \ldots, 145$, $a_0 = 3.0$ mm and $a_{145} = 17.5$ mm.

It is seen in figure 7.18 that the standard deviation of the number of load cycles S_{N_j} applied to reach the crack state a_j is increasing for increasing crack length. The rate of increase is largest for small crack lengths ($a < 7$ mm) after which the standard deviation slowly increases towards a constant value of ≈ 17000. The relative deviation is $\approx 9\%$. Notice, that the difference between the curves primarily occurs for small a-values, whereas the same final value is approached.

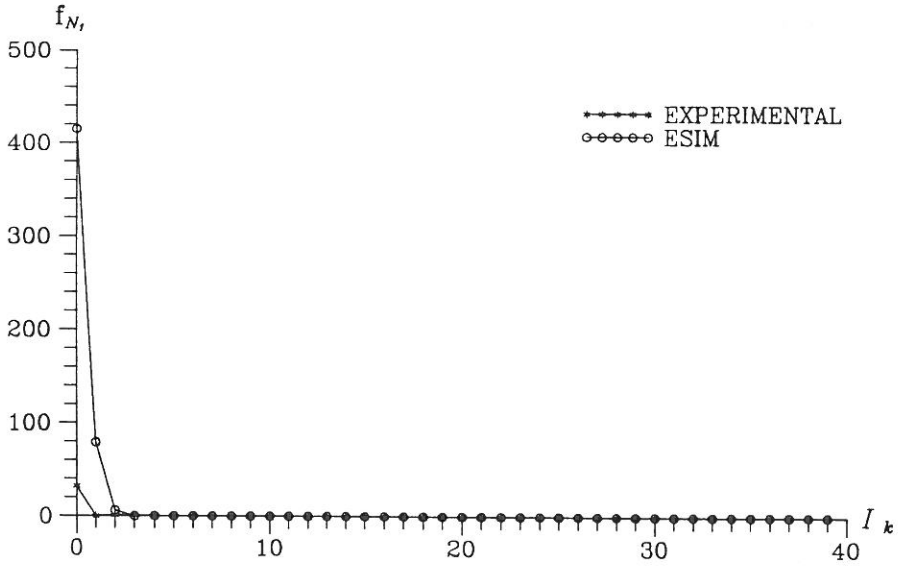

Figure 7.19: Histogram of the number of load cycles (f_{N_1}) applied to reach the crack state $a_1 = 3.1$ mm for CA-load tests and for ESIM.
$I_k =]k{\cdot}10000\ ;\ (k+1){\cdot}10000]$ cycles, $k = 0, 1, 2, \ldots, 39$.

The distribution of the histogram f_{N_1} in figure 7.19 shows that only one interval is included for the CA-load tests, i.e. $N_1 \in]0\ ;\ 10000]$ cycles and that ESIM only includes 3 intervals, i.e. $N_1 \in]0\ ;\ 30000]$ cycles. The main part is in the latter case within the first interval $]0\ ;\ 10000]$ cycles. This can also be seen in figures 7.8 and 7.11.

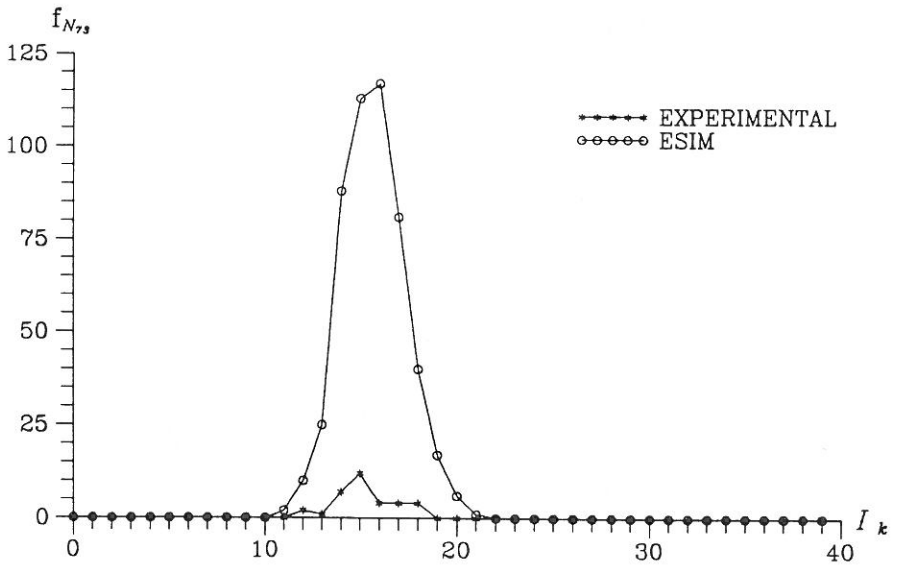

Figure 7.20: Histogram of the number of load cycles ($f_{N_{73}}$) applied to reach the crack state $a_{73} = 10.3$ mm for CA-load tests and for ESIM.
$I_k =]k{\cdot}10000\ ;\ (k+1){\cdot}10000]$ cycles, $k = 0, 1, 2, \ldots, 39$.

Due to the larger scatter at crack state $a_{73} = 10.3$ mm more intervals are included, but the distributions for both the experimental data and the simulated data have the same form. The CA-load tests are distributed over I_{12} to I_{18}, i.e. $N_{73} \in]120000 ; 190000]$ cycles, whereas ESIM are distributed over I_{11} to I_{21}, i.e. $N_{73} \in]110000 ; 220000]$ cycles.

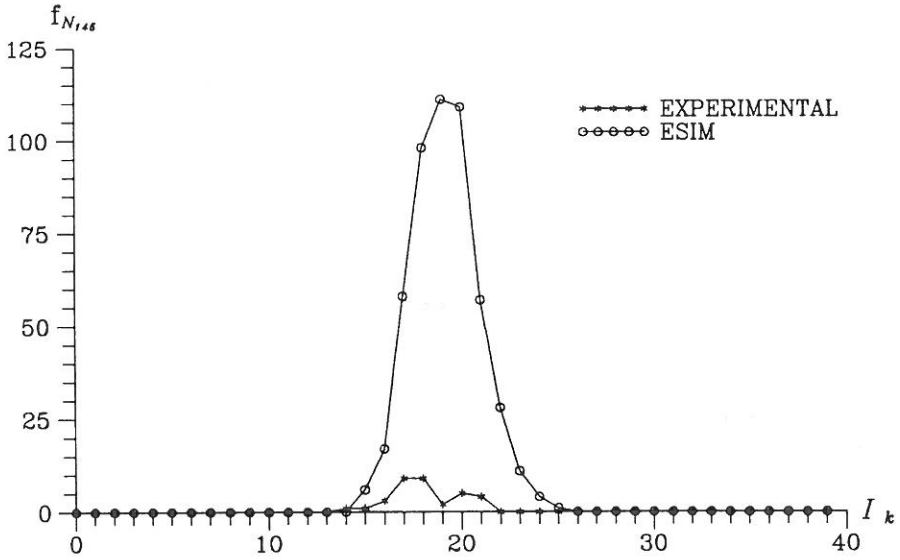

Figure 7.21: Histogram of the number of load cycles ($f_{N_{145}}$) applied to reach the crack state $a_{145} = 17.5$ mm for CA-load tests and for ESIM.
$I_k =]k{\cdot}10000 ; (k+1){\cdot}10000]$ cycles, $k = 0, 1, 2, \ldots, 39$.

The same tendency as in figure 7.20 is found in figure 7.21, but with the intervals I_{14} to I_{22}, i.e. $N_{145} \in]140000 ; 230000]$ cycles for CA-load tests and I_{14} to I_{25}, i.e. $N_{145} \in]140000 ; 260000]$ cycles for ESIM. The overlap of intervals for N_{73} and $N_f = N_{145}$ corresponds to N_{73} being larger than N_f for some tests.

The curves shown in figures 7.12-7.21 form the basis of comparison of the CA-load tests (section 7.1) and the simulations (section 7.2), see section 7.3.2.

7.3.2 Comparison of Experimental Data and FMF-Data

For the purpose of evaluating how well the FMF-model - in the form of the simulated data - describes the experimental data from the CA-load tests (see section 7.1.2) a further discussion of the statistical values from section 7.3.1 is performed in this section.

The total number of cycles to reach the failure state N_f and the standard deviation of the total number of cycles to reach a crack state $S_{N_j} = (\mathrm{Var}[N_j])^{1/2}$ are considered to be the most important statistical properties, see also section 6.2.2.

The former property was discussed in relation to figures 7.11 and 7.17. The main

result was that there is a very good agreeement between the experimental data and the simulated data.

A larger disagreement is seen for the progress of S_{N_j} for small crack lengths. Only in case of $a_f \gg a_0$ a satisfactory coincidence is obtained. Besides, this demand is in agreement with the assumptions in chapter 5 in which it is assumed that $a_{cr} \gg a_0$, see section 5.2.

The evaluation of the possibility of using (6.3) to estimate the crack step length δa for $a_f \gg a_0$ is based on figure 7.22. The standard deviation of the failure number of load cycles S_{N_f} is calculated using (6.3) with the model parameters in table 7.10 inserted.

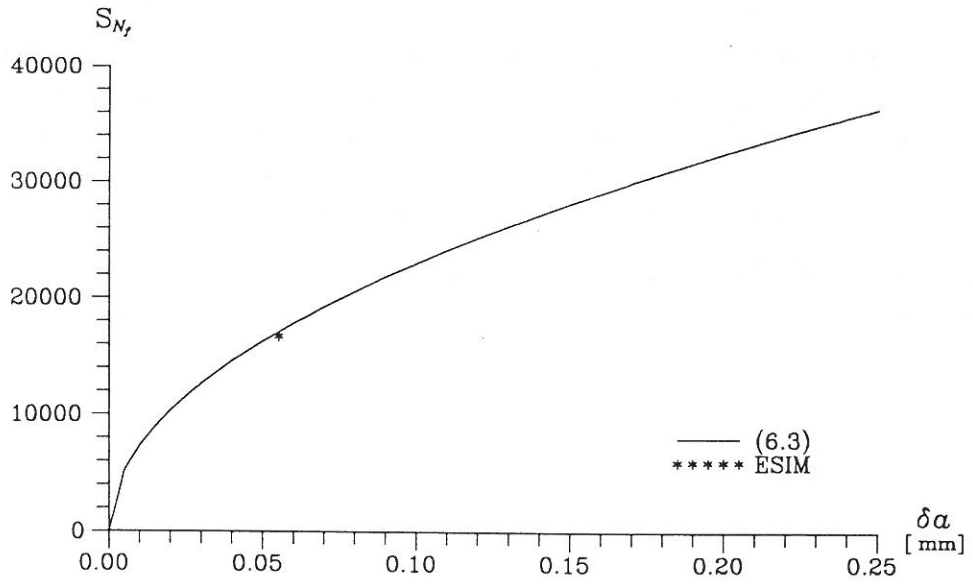

Figure 7.22: Standard deviation of the number of load cycles to cause failure as a function of the crack step length. The S_{N_f}-values for ESIM is also seen in the figure.

From figure 7.22 it is seen that the S_{N_f}-value for the simulated data almost coincides with the corresponding value for the experimental data. Thus, it is possible to estimate an appropriate value of δa using (6.3).

The main results of the fatigue tests are summarized in section 7.4.

7.4 EVALUATION

The results of the experimental fatigue tests of steel are evaluated in this section.

A series of fatigue crack growth curves for a mild steel has been experimentally established, see section 7.1.2. The curves show great similarity and serve as a basis for the determination of the model parameters used in the FMF-model. The main problem is to determine if it is necessary to use an effective crack length in the

calculation of the material parameters C and m. This might be necessary in case of a large extent of the plastic zone in front of the crack tip.

On the basis of the model parameters, simulation of fatigue crack growth data have been performed in section 7.2. It is assumed that the crack step length δa can be regarded as a material constant, which explicitly can be calculated from the statistical properties of the fatigue crack growth data.

The evaluation of the FMF-model is based on a comparison of the experimental data and the simulated data. Both qualitative and quantitative criteria have been used.

The qualitative demands concerning similarity in the form and progress of the fatigue crack growth curves are fulfilled. Thus, the simulated curves reflect the experimental curves including the interval for number of cycles to cause failure (N_f).

The comparison of the statistical analyses of the experimental data and the FMF-data, respectively, show that almost the same properties and characteristics apply. For the given choice of model parameters, the FMF-model overestimates the lifetime by approximately 6% and the standard deviation S_{N_f} is only coinciding for large a-values. Otherwise, satisfactory results have been obtained.

A better agreement might be obtained by making it possible to the crack to progress in steps which are a multiply of the crack step length δa. This possibility will be left to further research.

8. CONCLUSIONS

The results of the analyses and descriptions performed in chapters 2-7 are in this chapter discussed in relation to chapter 1. Objects for further research are also mentioned.

The main purpose of this thesis was to establish a simple, improved, numerical fatigue based on existing knowledge of fatigue due to dynamic load in mild steel in order to predict the fatigue crack growth progress.

Fatigue is defined as initiation and propagation of one or more cracks, resulting in failure, as a result of an alternating stress (chapter 1).

The fatigue process consists of a micro level state where crack initiation and micro cracking take place, and a macro level state at which macro cracking including failure takes place (section 2.1). The macro level can be described by two different approaches: SN-curves and crack growth theories. The latter approach was in section 2.2 found to be the most appropriate.

The type of load, which must be known when using a crack growth theory, can be divided into three categories: deterministic, constant-amplitude load (CA-load); deterministic, variable-amplitude load (VA-load) and random load. The characteristics of the load types are described in section 2.3.

Depending on the sequences of load cycles different effects on the fatigue crack growth can be registered. The most important interaction effects are retardation, delayed retardation and acceleration of the fatigue crack growth, see section 2.4.1. Two main explanations of the interaction effects are given in section 2.4.2, i.e. crack closure and residual stresses. The former seems to be the dominating factor.

A large number of fatigue crack growth models describing the fatigue progress as a function of the load process and/or the material properties exists some of which are described in chapters 3 and 4:

In section 3.1 a general fatigue model based on the physical knowledge of fatigue is sought established by use of dimensional analysis. The major problem, which is unsolved, is to determine the factor denoting the pre-load history.

The most important empirically based model is the Paris law developed for CA-load, see section 3.2.1. This law describes the fatigue crack growth rate as a function of some material parameters and a load parameter in the form of the stress intensity factor. It is a very simple and often satisfactory model, see also section 3.2.3. A modification is found in the proposal by Forman in which the stress ratio effect is taken into account (section 3.2.2).

Account of the previously-mentioned interaction effects are taken in the Wheeler model (section 3.3.1) and in the Elber crack closure model (section 3.3.2). The former is able to describe the retardation phenomenon and thus it is adequate if small tensile overloads are introduced. The latter is more general and can be used for all types of VA-load, but there are difficulties with the determination of model parameters. Further, only crack closure effects are included.

Dealing with random load the basic problems are how to define a load cycle and how to count the cycles. Using a characteristic stress intensity factor value to describe the load process, Paris' law can be used to describe the fatigue process, see section 3.4.1. It gives a simple expression, but the sequence effects are disregarded. This is not the case if the fatigue progress is updated after each cycle applied, but the use of this so-called cycle-by-cycle counting concept demands an enormous amount of calculations. In all cases, realizations of the stochastic process is required.

None of the above-mentioned fatigue models can describe the fatigue progress satisfactory for any type of load. One of the reasons is that all the models are deterministic and thus, they do not consider the inherent variability characteristic of fatigue. Instead, damage accumulation should be regarded as a stochastic process even under deterministic loads due to the statistical nature of fatigue and thus the fatigue model has to be probabilistic. This often requires a numerical solution strategy including estimation of model parameters, simulations of sample functions and estimates of statistical moments (section 3.5).

In the probabilistic fatigue model discussed in chapter 4 (the B-model), it is assumed that the fatigue progress can be described as a discrete-time, discrete-state Markov process. The time is measured in numbers of duty cycles each consisting of a number of load cycles, whereas the damage state is given as a crack length. The model is able to describe existing fatigue crack growth data (the Virkler data) extremely well. But, it is unknown how the model parameters are estimated.

On the basis of the existing knowledge of fatigue and fatigue crack growth models, an improved fatigue model is developed in chapter 5, requiring that the model also possesses such properties that the model parameters can be regarded as a characteristic values of the material, so no restrictions of the geometry of the structure are necessary. The model, named the Fracture Mechanical Markov Chain Fatigue Model, is stochastic in the manner that, the material properties are considered stochastic. Further, deterministic as well as random load apply.

The FMF-model is based on the same assumptions as the B-model, i.e. it is assumed that the fatigue crack growth process can be described as a discrete space Markov process. As in the B-model, the time is measured in duty cycles and the damage state in crack lengths.

The discrete-time, discrete-state Markov process is completely described by its transition matrix (one for each duty cycle) and by the initial conditions. The transition

probability, which among other parameters is a function of the stress intensity factor range, is determined on the basis of Paris' law and the geometric distribution of a Bernoulli random variable, see section 5.1.

The different types of load and geometries are taken into account by the stress intensity factor range. Thus, in case of CA-load the stress intensity factor range is a function of the stress range, whereas VA-load and random load requires use of an effective stress range due to the previously-mentioned interaction effects.

The FMF-model introduces two new model parameters: the number of load cycles in a duty cycle, λ, and the crack step length, i.e. the step by which the crack is assumed to progress to reach the successive damage state, δa. The crack step length is assumed to be a characteristic value of the material.

The applicability of the FMF-model is tested on the basis of two criteria concerning the properties of the model:

The model must be able to replicate empirical curves, i.e. the form and progress of the curves must be similar. This qualitative demand is tested by plotting the crack growth curves from the model and from the empirical data, respectively.

Quantitatively, the fatigue crack growth data obtained from the model must have the same statistical properties - in the form of mean values, deviations and probability density functions - as the empirical data. Comparison of the statistical values is performed both graphically and numerically, the latter being based on a norm.

Two sets of empirical data have been used in the test of the FMF-model, i.e. the Virkler data (section 6.1) and the CA-data established in connection to the thesis (section 7.1).

The Virkler data are used to determine the model parameters included in FMF-model letting two of the parameters vary. Thus, different combinations of the number of load cycles in a duty cycle and the crack step length have been used in the simulations of FMF-data (section 6.2). Using the Virkler data as reference for the FMF-data, the most adequate combination of the two parameters is determined on the basis of the above-mentioned criteria (sections 6.2.1 and 6.2.2). For small values of the two parameters and for failure crack lengths much larger than the initial crack length, the FMF-model gives a good description of the Virkler data. In fact, it seems reasonable to regard the crack step length as a characteristic value of the material.

For the purpose of simulating FMF-data corresponding to the CA-data, establishment of the model parameters for the FMF-data is simpler than for the Virkler data. This is because of the assumption that the crack step length can be regarded as a characteristic value of the material and thus only one combination of the number of

load cycles in a duty cycle and the crack step length is used in section 7.2.

Comparison of the CA-data and the FMF-data, where the former set of data are reference data, shows good agreement. Both the qualitative and the quantitative demand are reasonable satisfied.

The main result of the thesis is that it has been possible to establish a simple, improved, numerical fatigue model, which is based on existing knowledge of fatigue.

Thus, the tests of the FMF-model show that the model is able to describe fatigue crack growth in a simple geometry subjected to CA-load and that for adequate small values of the number of load cycles in a duty cycle ($\lambda < 100$), the crack step length can be regraded as a characteristic value of the material.

The following related subjects remain unsolved in the present thesis:

- Establishment of random load processes.
- Choice of an adequate counting method in case of random load.
- Determination of geometry functions for other geometries, i.e. determination of the stress intensity factor. This can be done by Finite Element Method analysis.
- Relation to e.g. reliability analysis.

The following items can be included in forthcoming research:

- Improvement of the FMF-model so it applies crack lengths close to the initial crack length.
- Optimization of the crack step length so the norm values are minimized.
- Incorporation of crack closure in the FMF-model.
- Application of the FMF-model to other geometries e.g. structural connections.
- Experimental establishment of fatigue crack growth data for different materials and geometries.
- Practical use, i.e. an estimate of the lifetime of a real structure.

REFERENCES

[Alawi, H.; 1986]
"A Probabilistic Model for Fatigue Crack Growth Under Random Loading"
Engineering Fracture Mechanics, Vol.23, No.3, p.479-487
Pergamon Press Ltd.

[Alzos, W.X., A.C. Skat, Jr. and B.M. Hillberry; 1976]
"Effect of Single Overload/Underload Cycles on Fatigue Crack Propagation"
Fatigue Crack Growth Under Spectrum Loads, ASTM STP 595, p.41-60
American Society for Testing and Materials

[Arone, R.; 1986]
"Fatigue Crack Growth Under Random Overloads Superimposed on Constant-Amplitude Cyclic Loading"
Engineering Fracture Mechanics, Vol.24, No.2, p.223-232
Pergamon Journals Ltd.

[ASTM STP E399-83; 1985]
"Standard Test Method for Plane-Strain Fracture Toughness of Metallic Materials"
1985 Annual Book of ASTM Standards Volume 03.01, p.547-582
American Society for Testing and Materials

[Baïlon, J.-P. and S.D. Antolovich; 1983]
"Effect of Microstructure on Fatigue Crack Propagation: A Review of Existing Models and Suggestions for Further Research"
Fatigue Mechanisms: Advances in Quantitative Measurement of Physical Damage, ASTM STP 811, p.313-349
American Society for Testing and Materials

[Barsom, J.M.; 1973]
"Fatigue-Crack Growth Under Variable-Amplitude Loading in ASTM A514-B Steel"
Progress in Flaw Growth and Fracture Toughness Testing, ASTM STP 536, p.147-167
American Society for Testing and Materials

[Benjamin, J.R. and C.A. Cornell; 1970]
"Probability, Statistics, and Decision for Civil Engineers"
McGraw-Hill, Inc.

[Berens, A.P. and P.W. Hovey; 1983]
"Statistical Methods for Estimating Crack Detection Probabilities"
Probabilistic Fracture Mechanics and Fatigue Methods: Applications for Structural Design and Maintenance, ASTM STP 798, p.79-94
American Society for Testing and Materials

[Bernard, P.J., T.C. Lindley and C.E. Richards; 1976]
"Mechanisms of Overload Retardation During Fatigue Crack Propagation"
Fatigue Crack Growth Under Spectrum Loads, ASTM STP 595, p.78-97
American Society for Testing and Matrials

[Bogdanoff, J.L.; 1978a]
"A New Cumulative Damage Model. Part 1"
Journal of Applied Mechanics, Vol.45, No.2, June 1978, p.246-250
American Society of Mechanical Engineers

[Bogdanoff, J.L.; 1978b]
"A New Cumulative Damage Model. Part 3"
Journal of Applied Mechanics, Vol.45, No.4, December 1978, p.733-739
American Society of Mechanical Engineers

[Bogdanoff, J.L. and F. Kozin; 1980]
"A New Cumulative Damage Model. Part 4"
Journal of Applied Mechanics, Vol.47, No.1, March 1980, p.40-44
American Society of Mechanical Engineers

[Bogdanoff, J.L. and F. Kozin; 1985]
"Probabilistic Models of Cumulative Damage"
John Wiley & Sons, Inc.

[Bogdanoff, J.L. and W. Krieger; 1978]
"A New Cumulative Damage Model. Part 2"
Journal of Applied Mechanics, Vol.45, No.2, June 1978, p.251-257
American Society of Mechanical Engineers

[Brincker, R. and J. D. Sørensen; 1990]
"High-Speed Stochastic Fatigue Testing"
Experimental Mechanics, Vol., No., p.4-9
Society of Experimental Mechanics

[Broek, D.; 1985]
"A Similitude Criterion for Fatigue Crack Growth Modeling"
Fracture Mechanics: Sixteenth Symposium, ASTM STP 868, p.347-360
American Society for Testing and Materials

[Chakrabarti, A.K.; 1980]
"Fatigue-Crack-Growth-Retardation Model Based Upon Critical-Damage Approach"
Engineering Fracture Mechanics, Vol.13, No.1, p.1-14
Pergamon Press Ltd.

[Chand, S. and S.B.L. Garg; 1985]
"Crack Propagation Under Constant Amplitude Loading"
Engineering Fracture Mechanics, Vol.21, No.1, p.1-30
Pergamon Press Ltd.

[Cherepanov, G.P. and H. Halmanov; 1972]
"On the Theory of Fatigue Crack Growth"
Engineering Fracture Mechanics, Vol.4, p.219-230
Pergamon Press

[Chow, C.L., C.W. Woo and K.T. Chung; 1986]
"Fatigue Crack Propagation in Mild Steel"
Engineering Fracture Mechanics, Vol.24, No.2, p.233-241
Pergamon Journals Ltd.

[Chu, W.-Y., C.-M. Hsiao and T.-H. Liu; 1984]
"Fatigue Under Cyclic Compressive Load"
Fatigue of Engineering Materials and Structures, Vol.7, No.4, p.279-284
Fatigue of Engineering Materials Ltd

[Corbly, D.M. and P.F. Packman; 1973]
"On the Influence of Single and Multiple Peak Overloads on Fatigue Crack Propagation in 7075-T6511 Aluminum"
Engineering Fracture Mechanics, Vol.5, No.2, p.479-497
Pergamon Press

[Davenport, R.T. and R. Brook; 1979]
"The Threshold Stress Intensity Range in Fatigue"
Fatigue of Engineering Materials and Structures, Vol.1, p.151-158
Fatigue of Engineering Materials Ltd.

[Ditlevsen, O. and R. Olesen; 1985]
"Statistical Analysis of the Virkler Data on Fatigue Crack Growth"
DCAMM Report No.314, December 1985
Technical University of Denmark

[Drew, M.W. and K.R.L. Thompson; 1988]
"The Effect of Overload Cycles on Fatigue Crack Propagation in Two Structural Steels"
Engineering Fracture Mechanics, Vol.30, No.5, p.579-593
Pergamon Press plc.

[Druce, S.G., C.J. Beevers and E.F. Walker; 1979]
"Fatigue Crack Growth Retardation Following Load Reductions In A Plain C-Mn Steel"
Engineering Fracture Mechanics, Vol.11, No.2, p.385-395
Pergamon Press Ltd.

[Elber, W.; 1970]
"Fatigue Crack Closure Under Cyclic Tension"
Engineering Fracture Mechanics, Vol.2, p.37-45
Pergamon Press

[Elber, W.; 1971]
"The Significance of Fatigue Crack Closure"
Damage Tolerance in Aircraft Structures, ASTM STP 486, p.230-242
American Society for Testing and Materials

[Ellyin, F. and C.O.A. Fakinlede; 1986]
"Nonlinear dislocation model of the work-hardening crack-tip field"
International Journal of Fracture, Vol.32, No.1, p.3-20
Martinus Nijhoff Publishers

[Ellyin, F. and C.O.A. Fakinlede; 1987]
"A dislocation model for work hardening material and cyclic J-integral"
International Journal of Fracture, Vol.33, No.2, p.95-110
Martinus Nijhoff Publishers

[Ewalds, H.L and R.J.H. Wanhill; 1984]
"Fracture Mechanics"
Edward Arnold and Delftse Uitgevers
Maatschappij

[Fatigue Handbook; 1985]
"Fatigue Handbook. Offshore Steel Structures"
Tapir

[Fleck, N.A.; 1988]
"Influence of Stress State on Crack Growth Retardation"
Basic Questions in Fatigue: Volume I, ASTM STP 924, p.157-183
American Society for Testing and Materials

[Forman, R.G., V.E. Kearney and R.M. Engle; 1967]
"Numerical Analysis of Crack Propagation in Cyclic-Loaded Structures"
Journal of Basic Engineering, Vol.89, No.3, September 1967, p.459-464
American Society of Mechanical Engineers

[Fuchs, H.O. and R.I. Stephens; 1980]
"Metal Fatigue in Engineering"
John Wiley & Sons, Inc.

[Führing, H. and T. Seeger; 1984]
"Fatigue Crack Growth under Variable Amplitude Loading"
Subcritical Crack Growth Due to Fatigue, Stress Corrosion and Creep, p.109-133
Elsevier Applied Science Publishers

[Gansted, L.; 1991]
"Constant-Amplitude Load on Steel CCT-Specimens"
Fracture and Dynamics, Paper No. , December 1991
University of Aalborg, Denmark

[Gdoutos, E.E. and G. Papakaliatakis; 1987]
"Crack growth initiation in elastic-plastic materials"
International Journal of Fracture, Vol.32, No.3, p.143-156
Martinus Nijhoff Publishers

[Grandt, A.F., Jr.; 1984]
"Introduction to Damage Tolerance Analysis Methodology"
Damage Tolerance of Metallic Structures: Analysis and Applications, ASTM STP 842, p.3-24
American Society for Testing and Materials

[Grosskreutz, J.C.; 1971]
"Fatigue Mechanisms in the Sub-Creep Range"
Metal Fatigue Damage-Mechanism, Detection, Avoidance and Repair, ASTM STP 495, p.5-60
American Society for Testing and Materials

[Gurney, T.R.; 1979]
"Fatigue of welded structures"
Cambridge University Press, 2nd edition

[Hellan, K.; 1985]
"Introduction to Fracture Mechanics"
McGraw-Hill Book Co. - International Student Edition

[Himmelein, M.K.; 1979]
"The Effect of Stress Ratio and Overload Ratio on Fatigue Crack Delay and Arrest Behavior due to Single Peak Overloads"
Ph.D. Thesis, Purdue University
Purdue University

[Hudson, C.M.; 1981]
"A Root-Mean-Square Approach for Predicting Fatigue Crack Growth under Random Loading"
Methods and Models for Predicting Fatigue Crack Growth under Random Loading, ASTM STP 748, p.41-52
American Society for Testing and Materials

[Hudson, C.M. and K.N. Raju; 1970]
"Investigation of Fatigue-Crack Growth under Simple Variable-Amplitude Loading"
International Journal of Nondestructive Testing, Vol.2, p.189-205
Gordon and Breach Science Publishers

[Iwasaki, T., A. Katoh and M. Kawahara; 1982]
"Fatigue Crack Growth Under Random Loading"
Naval Architecture and Ocean Engineering, Vol.20, p.194-216
Nihon Zosen Gakkai, Tokyo

[Jacoby, G.H, and H. Nowack; 1972]
"Comparison of Scatter Under Program and Random Loading and Influencing Factors"
Probabilistic Aspects of Fatigue, ASTM STP 511, p.61-74
American Society for Testing and Materials

[Kanazawa, T., S. Machida and K. Itoga; 1975]
"On the Effect of Cyclic Stress Ratio on the Fatigue Crack Propagation"
Engineering Fracture Mechanics, Vol.7, No.3, p.445-455
Pergamon Press

[Knott, J.F.; 1973]
"Fundamentals of Fracture Mechanics
Butterworths

[Laird, C.; 1967]
"The Influence of Metallurgical Structure on the Mechanisms of Fatigue Crack Propagation"
Fatigue Crack Propagation, ASTM STP 415, p.131-180
American Society for Testing and Materials

[Lemaitre, J.; 1986]
"Local Approach of Fracture"
Engineering Fracture Mechanics, Vol.25, No.5/6, p.523-537
Pergamon Press Ltd.

[Leve, H.L.; 1969]
"Cumulative Damage Theories"
Metal Fatigue: Theory and Design, p.170-203
John Wiley & Sons, Inc.

[Liaw, P.K., T.R. Leax, T.R. Fabis and J.K. Donald; 1987]
"Fatigue Crack Growth Behavior in an Mn-Cr Austenitic Steel"
Engineering Fracture Mechanics, Vol.26, No.1, p.1-13
Pergamon Journals Ltd.

[Lyngbye, J. and R. Brincker; 1990]
"Crack Detection by Digital Image Processing"
Fracture and Dynamics, Paper No.23, June 1990
University of Aalborg, Denmark

[Madsen, H.O.; 1982]
"Deterministic and Probabilistic Models for Damage Accumulation due to Time Varying Loading"
DIALOG 5-82
Danmarks Ingeniørakademi. Bygningsafdelingen, Lyngby

[Madsen, H.O., S. Krenk and N.C. Lind; 1986]
"Methods of Structural Safety"
Printice-Hall, Inc.

[McEvily, A.J. and K. Minakawa; 1988]
"Crack Closure and Variable-Amplitude Fatigue Crack Growth"
Basic Questions in Fatigue: Volume I, ASTM STP 924, p.357-376
American Society for Testing and Materials

[Mughrabi, H., R. Wang, K. Differt and U. Essmann; 1983]
"Fatigue Crack Initiation by Cyclic Slip Irreversibilities in High-Cycle Fatigue"
Fatigue Mechanisms: Advances in Quantitative Measurement of Physical Damage, ASTM STP 811, p.5-45
American Society for Testing and Materials

[Mukherjee, B. and D.J. Burns; 1972]
"Regression Models for the Effect of Stress Ratio on Fatigue Crack Growth Rate"
Probabilistic Aspects of Fatigue, ASTM STP 511, p.43-60
American Society for Testing and Materials

[Papoulis, A.; 1984]
"Probability, Random Variables, and Stochastic Processes"
McGraw-Hill, Inc. - International Student Edition, 2nd Edition

[Paris, P.C.; 1962]
"Crack Propagation Caused by Fluctuating Loads"
Paper from ASME Meeting 3
American Society of Mechanical Engineers

[Paris, P. and F. Erdogan; 1963]
"A Critical Analysis of Crack Propagation Laws"
Journal of Basic Engineering, Trans ASME Series D 85, p.528-534
American Society of Mechanical Engineers

[Paris, P.C., M.P. Gomez and W.E. Anderson; 1961]
"A Rational Analytic Theory of Fatigue"
The Trend in Engineering, Vol.13, No.1, p.9-14
The Office of Engineering Research, University of Washington

[Parzen, E.; 1962]
"Stochasic Processes"
Holden-Day

[Pook, L.P. and R.A. Smith; 1979]
"Theoretical Background to Elastic Fracture Mechanics"
Fracture Mechanics: Current Status, Future Prospects, p.29-67
Proceedings of a Conference, Cambridge University, 16. March 1979
Pergamon Press

[Porter, T.R.; 1972]
"Method of Analysis and Prediction for Variable Amplitude Fatigue Crack Growth"
Engineering Fracture Mechanics, Vol.4, No.4, p.717-736
Pergamon Press

[Priddle, E.K.; 1989]
"The Influence of Test Variables on the Fatigue Crack Growth Threshold"
Fatigue & Fracture of Engineering Materials & Structures, Vol.12, No.4, p.333-345
Fatigue of Engineering Materials Ltd

[Probst, E.P. and B.M. Hillberry; 1974]
"Fatigue Crack Delay and Arrest Due to Single Peak Tensile Overloads"
American Institute of Aeronautics and Astronautics Journal, Vol.12, No.3, p.330-335
Student Journal, Inc.

[Rice, R.C. and R.I. Stephens; 1973]
"Overload Effects on Subcritical Crack Growth in Austenitic Manganese Steel"
Progress in Flaw Growth and Fracture Toughness Testing, ASTM STP 536, p.95-114
American Society for Testing and Materials

[Robin, C., M. Louah and G. Pluvinage; 1983]
"Influence of an Overload on the Fatigue Crack Growth in Steels"
Fatigue of Engineering Materials and Structures, Vol.6, No.1, p.1-13
Fatigue of Engineering Materials Ltd.

[Sabnis, G.M., H.G. Harris, R.N. White and M.S. Mirza; 1983]
"Structural Modelling and Experimental Techniques"
Printice-Hall, Inc.

[Schijve,J.; 1973]
"Effect of Load Sequences on Crack Propagation Under Random and Program Loading"
Engineering Fracture Mechanics, Vol.5, No.2, p.269-280
Pergamon Press

[Schijve, J.; 1976]
"Observations on the Prediction of Fatigue Crack Growth Propagation Under Variable-Amplitude Loading"
Fatigue Crack Growth Under Spectrum Loads, ASTM STP 595, p.3-23
American Society for Testing and Materials

[Schijve, J.; 1979]
"Four Lectures on Fatigue Crack Growth"
Engineering Fracture Mechanics, Vol.11, No.1, p.167-221
Pergamon Press Ltd.

[Schijve, J.; 1980]
"Prediction Methods for Fatigue Crack Growth in Aircraft Material"
Fracture Mechanics: Twelfth Conference, ASTM STP 700, p.3-34
American Society for Testing and Materials

[Shin, C.S. and Fleck, N.A.; 1987]
"Overload Retardation in a Structural Steel"
Fatigue & Fracture of Engineering Materials & Structures, Vol.9, No.5, p.379-393
Fatigue of Engineering Materials Ltd

[Stephens, R.I., D.K. Chen and B.W. Hom; 1976]
"Fatigue Crack Growth with Negative Stress Ratio Following Single Overloads in 2024-T3 and 7075-T6 Aluminum Alloys"
Fatigue Crack Growth Under Spectrum Loads, ASTM STP 595, p.27-40
American Society for Testing and Materials

[Suresh, S.; 1983]
"Micromechanisms of Fatigue Crack Growth Retardation Following Overloads"
Engineering Fracture Mechanics, Vol.18, No.3, p.577-593
Pergamon Press Ltd.

[Sørensen, J.D. and R. Brincker; 1989]
"Simulation of Stochastic Loads for Fatigue Experiments"
Experimental Mechanics, Vol.29, No.2, p.174-182
Society of Experimental Mechanics

[Tanaka, S., M. Ichikawa and S. Akita; 1981]
"Variability of m and C in the Fatigue Crack Propagation Law da/dN = $C(\Delta K)^m$"
International Journal of Fracture, Vol.17, No.5, p.R121-R124
Sijthoff & Noordhoff International Publishers

[Tanaka, S., M. Ichikawa and S. Akita; 1984]
"A Probabilistic Investigation of Fatigue Life and Cumulative Cycle Ratio"
Engineering Fracture Mechanics, Vol.20, No.3, p.501-513
Pergamon Press Ltd.

[Trantina, G.G, and C.A. Johnson; 1983]
"Probabilistic Defect Size Analysis Using Fatigue and Cyclic Crack Growth Rate Data"
Probabilistic Fracture Mechanics and Fatigue Methods: Applications for Structural Design and Maintenance, ASTM STP 798, p.67-78
American Society for Testing and Materials

[Trebules, V.W., Jr., R. Roberts and R.W. Hertzberg; 1973]
"Effect of Multiple Overloads on Fatigue Crack Propagation in 2024-T3 Aluminum Alloy"
Progress in Flaw Growth and Fracture Toughness Testing, ASTM STP 536, p.115-146
American Society for Testing and Materials

[Virkler, D.A., B.M. Hillberry and P.K. Goel; 1979]
"The Statistical Nature of Fatigue Crack Propagation"
Journal of Engineering Materials, Vol.101, No.2, p.148-153, April 1979
American Society of Mechanical Engineers

[Walker, K.; 1970]
"The Effect of Stress Ratio During Crack Propagation and Fatigue for 2024-T3 and 7075-T6 Aluminum"
Effects of Environment and Complex Load History on Fatigue Life, ASTM STP 462, p.1-14
American Society for Testing and Materials

[Wheeler, O.E.; 1972]
"Spectrum Loading and Crack Growth"
Journal of Basic Engineering, Vol.94, Series D, No.1, March 1972, p.181-186
American Society of Mechanical Engineers

[Yao, J.T.P., F. Kozin, Y.-K. Wen, J.-N. Yang, G.I. Schuëller and O. Ditlevsen; 1986]
"Stochastic Fatigue, Fracture and Damage Analysis"
Structural Safety, Vol.3, No.3+4, p.231-267
Elsevier Science Publishers B.V.

[Yokobori, T.; 1979]
"A Critical Evaluation of Mathematical Equations for Fatigue Crack Growth with Special Reference to Ferrite Grain Size and Monotonic Yield Strength Dependence"
Fatigue Mechanisms, ASTM STP 675, p.683-706
American Society for Testing and Materials

[Zheng, X.; 1987]
"A Simple Formula for Fatigue Crack Propagation and a New Method for the Determination of ΔK_{th}"
Engineering Fracture Mechanics, Vol.27, No.4, p.465-475
Pergamon Journals Ltd.

[Zheng, X. and M.A. Hirt; 1983]
"Fatigue Crack Propagation in Steels"
Engineering Fracture Mechanics, Vol.18, No.5, p.965-973
Pergamon Press Ltd.

OTHER LITERATURE

[Allen, R.J., G.S. Booth and T. Jutla; 1988a]
"A Review of Fatigue Crack Growth Characterisation by Linear Elastic Fracture Mechanics (LEFM). Part I - Principles and Methods of Data Generation"
Fatigue & Fracture of Engineering Materials & Structures, Vol.11, No.1, p.45-69
Fatigue of Engineering Materials Ltd

[Allen, R.J., G.S. Booth and T. Jutla; 1988b]
"A Review of Fatigue Crack Growth Characterisation by Linear Elastic Fracture Mechanics (LEFM). Part II - Advisory Documents and Applications Within National Standards"
Fatigue & Fracture of Engineering Materials & Structures, Vol.11, No.2, p.71-108
Fatigue of Engineering Materials Ltd

[ASTM STP 566; 1974]
"Handbook of Fatigue Testing"
Handbook of Fatigue Testing, ASTM STP 566
American Society for Testing and Materials

[Dolinsky, K.; 1987]
"Fatigue Crack Growth with Retardation Under Stationary Stochastic Loading"
Engineering Fracture Mechanics, Vol.27, No.3, p.279-290
Pergamon Journals Ltd.

[Feltner, C.E. and P. Beardmore; 1970]
"Strengthening Mechanisms in Fatigue"
Achievement of High Fatigue Resistance in Metals and Alloys, ASTM STP 467, p.77-112
American Society for Testing and Materials

[Freudenthal, A.M.; 1973]
"Fatigue and Fracture Mechanics"
Engineering Fracture Mechanics, Vol.5, No.2, p.403-414
Pergamon Press

[Hertzberg, R.W.; 1989]
"Deformation and Fracture Mechanics of Engineering Materials" - 3rd ed.
John Wiley & Sons

[McEvily, A.J.; 1988]
"On Crack Closure in Fatigue Crack Growth"
Mechanics of Fatigue Crack Closure, ASTM STP 982, p.35-43
American Society for Testing and Materials

[Morman, K.N., Jr. and R.G. Dubensky; 1976]
"Predicting Fatigue Crack Retardation Under Single and Intermittent Overloading"
Cracks and Fracture, ASTM STP 601, p.245-261
American Society for Testing and Materials

[Nemec, J.; 1982]
"Damage to Structures by High-Cycle Fatigue"
Fatigue of Engineering Materials and Structures, Vol.5, No.3, p.205-214
Pergamon Press Ltd.

[Newman, J.C., Jr.; 1982]
"Prediction of Fatigue Crack Growth under Variable-Amplitude and Spectrum Loading Using a Crack Closure Model"
Design of Fatigue and Fracture Resistant Structures, ASTM STP 761, p.255-277
American Society for Testing and Materials

[Nilsson, F.L.; 1985]
"Fatigue Crack Propagation under Random Loading"
Probabilistic Methods in the Mechanics of Solids and Structures, p.157-164
Proceedings of IUTAM SYMPOSIUM, Stockholm/Sweden, 1984
Springer Verlag

[Qingzhi, H.; 1984]
"A Model for Calculating the Fatigue Crack Opening and its Applications"
Fatigue of Engineering Materials and Structures, Vol.7, No.1, p.41-53
Fatigue of Engineering Materials Ltd

[Schijve, J.; 1962]
"Fatigue Crack Propagation in Light Alloy Sheet Material and Structures"
Advances in Aeronautical Sciences, Vol.3, p.387-408
Pergamon Press Inc.

[Schijve, J.; 1974]
"Fatigue Damage Accumulation and Incompatible Crack Front Orientation"
Engineering Fracture Mechanics, Vol.6, No.2, p.245-252
Pergamon Press

[Sehitoglu, H.; 1985]
"Characterization of Crack Closure"
Fracture Mechanics: Sixteenth Symposium, ASTM STP 868, p.361-380
American Society for Testing and Materials

[Sommer, A.M. and P. Thoft-Christensen; 1990]
"Inspection and Maintenance of Marine Steel Structures - State-of-the-Art"
Structural Reliability Theory Series, Paper No.74, April 1990
University of Aalborg, Denmark

[Stephens, R.I., E.C. Sheets and G.O. Njus; 1977]
"Fatigue Crack Growth and Life Prediction in Man-Tan Steel Subjected to Single and Intermittent Tensile Overloads"
Cyclic Stress-Strain and Plastic Deformation Aspects of Fatigue Crack Growth, ASTM STP 637, p.167-191
American Society for Testing and Materials

[Suresh, S.; 1985]
"Further Remarks on the Micromechanisms of Fatigue Crack Growth Retardation Following Overloads"
Engineering Fracture Mechanics, Vol.21, No.6, p.1169-1170
Pergamon Press Ltd.

[Vecchio, R.S., R.W. Hertzberg and R. Jaccard; 1984]
"On the Overload Induced Fatigue Crack Propagation Behavior in Aluminum and Steel Alloys"
Fatigue of Engineering Materials and Structures, Vol.7, No.3, p.181-194
Fatigue of Engineering Materials Ltd

[Wozumi, J.T., T. Spamer and G.E. Lambert; 1980]
"An Engineering Model for Assessing Load Sequencing Effects"
Effect of Load Spectrum Variables on Fatigue Crack Initiation and Propagtion, ASTM STP 714, p.128-142
American Society for Testing and Materials

SYMBOLS

a	=	crack length
a_0	=	initial crack length
a_{0L}	=	crack length at the time when overload is introduced
a_b	=	failure crack length
a_c	=	critical crack length
a_{eff}	=	effective crack length
a_f	=	failure crack length
a_i	=	crack length at an arbitrary time after introducing an overload
a_N	=	crack length corresponding to N
$\delta a, \Delta a$	=	crack length increase
A	=	Airy's stress function
A_n	=	complex constant
b	=	failure state
B_n	=	complex constant
C	=	material constant
C_{ret}	=	retardation parameter
CD	=	cumulative damage
d	=	empirical coefficient, damage state
da	=	crack length increase
dA_p	=	volume work per unit thickness
dK	=	stress intensity factor increase
dN	=	increase in number of cycles
dW	=	crack work per unit thickness
DC	=	duty cycle
E	=	Young's modulus
E[.]	=	expected value of random variable
f	=	frequency
f[.]	=	probability density function of random variable
f_u	=	ultimate stress
f_y	=	yield stress
F	=	geometry and load dependent factor
G	=	shear modulus
$\mathcal{G}$	=	energy release rate
I_k	=	interval of histogram
k_i	=	constant, $i = 1, 2$
K	=	stress intensity factor
K_{eff}	=	effective stress intensity factor
K_c	=	critical stress intensity factor
K_{Ic}	=	fracture toughness
$K_{\max}$	=	maximum stress intensity factor
$K_{\max,rms}$	=	root mean square maximum stress intensity factor
$K_{\min}$	=	minimum stress intensity factor

$K_{\min,rms}$	=	root mean square minimum stress intensity factor
K_{op}	=	opening stress intensity factor
ΔK	=	stress intensity factor range
ΔK_{eff}	=	effective stress intensity factor range
ΔK_i	=	stress intensity factor range in the i th load cycle
ΔK_{rms}	=	root mean square stress intensity factor range
ΔK_{th}	=	threshold value of ΔK
m	=	material constant
n	=	number of load cycles in a duty cycle
N	=	number of cycles
$\overline{N}$	=	mean value of number of cycles
N_0	=	initial number of cycles
N_c	=	number of cycles to cause fracture
N_f	=	number of cycles to cause failure
δN	=	increase in number of duty cycles
$\overline{\delta N}$	=	mean value of increase in number of duty cycles
$\overline{p}_0$	=	initial state vector
p	=	$1-q$
$\overline{p}_x$	=	state vector
P	=	force
P[.]	=	probability distribution of random variable
$\overline{\overline{P}}$	=	transition matrix
$\overline{\overline{P}}_i$	=	transition matrix for i th duty cycle
$P_{\max}$	=	maximum load
$P_{\min}$	=	minimum load
ΔP	=	load range
q	=	transition probability
q[.]	=	norm value
r	=	p/q
r_{0L}	=	plastic zone size due to a previous overload
r_y	=	plastic zone size
r_y^*	=	fraction of plastic zone size
r_{yi}	=	plastic zone size corresponding to the i th load cycle
R	=	$K_{\min}/K_{\max}$ = stress intensity factor ratio, $\sigma_{\min}/\sigma_{\max}$ = stress ratio
R_{rms}	=	$K_{\min,rms}/K_{\max,rms}$ = root mean square stress intensity factor ratio
S	=	stress range
S[.]	=	deviation of random variable
u	=	displacement
u_i	=	displacement component in Cartesian coordinate system $(i,j=1,2,3)$
U	=	stress range ratio, potential energy
v	=	displacement

$\mathrm{Var}[.]$	=	variance of random variable
x	=	discrete time
x_i	=	Cartesian coordinate $(i, j = 1, 2, 3)$
z	=	complex variable
$\overline{z}$	=	complex conjugate variable
Z	=	Bernoulli random variable
ΔS_i	=	stress range in i th load cycle
α	=	function of $\overline{z}$
α_i	=	dimensionless function, $i = 1, 2, 3$
β	=	function, function of $\overline{z}$
γ	=	surface energy
γ_0	=	initial crack growth rate
δ	=	flexibility
ϵ_{ij}	=	strain component in Cartesian coordinate system $(i, j = 1, 2, 3)$
ϵ_u	=	fracture strain
$\Delta\epsilon_p$	=	plastic strain range
θ	=	angle
κ	=	fracture mechanical parameter
λ	=	number of load cycles in one duty cycle
λ_n	=	eigenvalue
ν	=	Poisson's ratio
π_j	=	probability that damage is initially in state j
σ	=	stress
σ_0	=	stress accounting for pre-loading history
σ_1	=	maximum stress
σ_2	=	minimum stress
σ_{cl}	=	crack closure stress
σ_{ij}	=	stress component in Cartesian coordinate system $(i, j = 1, 2, 3)$
σ_m	=	mean stress
$\sigma_{\max}$	=	maximum stress
$\sigma_{\min}$	=	minimum stress
σ_{op}	=	crack opening stress
$\Delta\sigma$	=	stress range
$\Delta\sigma_c$	=	critical stress range
$\Delta\sigma_{\mathrm{eff}}$	=	effective stress range
τ_y	=	shear yield stress
ϕ	=	analytical function of $\overline{z}$
χ	=	analytical function of $\overline{z}$

RESUMÉ IN DANISH

Analyse af konstruktioner udsat for dynamiske belastinger får stadig større betydning i dimensioneringsfasen bl.a. som følge af øgede krav til konstruktioners størrelse samtidig med ønsker om minimalt materialeforbrug. Dette samt mange andre faktorer, såsom temperatur- og korrosionspåvirkninger, giver en øget risiko for udmattelse af konstruktioner og/eller konstruktionsdele. I tilknytning til anlægs- og byggesektoren har stål en særlig interesse, idet dette materiale i høj grad benyttes i offshore konstruktioner, større brobyggeri m.m..

Disse forhold danner baggrund for projektet, hvor en egentlig projektafgrænsning er givet i kapitel 1. Det overordnede spørgsmål, der danner udgangspunkt for projektet er: "Er det muligt at etablere en simpel, numerisk udmattelsesrevnevækstmodel i hvilken alle parametre kan betragtes som karakteristiske for materialet, og hvor eksisterende viden om udmattelse er inkluderet ?"

De grundlæggende aspekter vedrørende udmattelse som følge af dynamiske belastninger er behandlet i kapitel 2. Hovedvægten er lagt på at give en fysisk forståelse for udmattelsesfænomenet samt at introducere de to mest kendte indgangsvinkler til beskrivelse af udmattelse. Desuden er de forskellige dynamiske belastninger og disses indflydelse på udmattelsesforløbet beskrevet.

Eksisterende, empiriske udmattelsesmodeller og deres anvendelsesmuligheder er diskuteret i kapitel 3, idet kun de vigtigste/mest typiske er medtaget. Resultatet af gennemgangen er, at ingen af modellerne på tilfredsstillende vis er i stand til at beskrive udmattelsesforløbet under en vilkårlig belastning.

Alternativt kan numeriske modeller benyttes til beskrivelse af udmattelsesforløbet. Én af de mest velkendte (B-modellen) er beskrevet og vurderet i kapitel 4. Det konkluderes, at det grundlæggende princip i modellen er godt, men at relationen til den fysiske viden om udmattelse ikke direkte er benyttet.

På grundlag af den numeriske model i kapitel 4, er der udviklet en ny numerisk model, der inkluderer de fysiske egenskaber i udmattelse. Modellen er baseret på, at revnevækstprocessen kan beskrives ved en diskret Markov teori. Modellen, der er beskrevet i kapitel 5, kan anvendes ved såvel deterministisk som stokastisk belastning. Når model-parametrene er fastlagt for et givet materiale kan modellen benyttes på enhver konstruktion af det givne materiale, idet blot geometrifunktionen skal kendes.

Introduktion af en ny model kræver, at den er testet med henblik på at vurdere dens anvendelighed. To tests er blevet udført, én hvor eksisterende revnevækstdata for en aluminiumslegering er benyttet, se kapitel 6, og én for blødt stål for hvilket der er etableret eksperimentelle revnevækstdata i forbindelse med projektet, se kapitel 7.

Analyserne i kapitel 6 af de simulerede revnevækstdata sammenlignet med de eksisterende data viser, at for passende valg af modelparametre opnås særdeles god overensstemmelse. Sammenligningen er baseret på såvel kvalitative som kvantitative krav såsom form af kurverne og statistiske egenskaber. Sidstnævnte er sammenlignet

på baggrund af en norm, ligesom en diskussion af hvilken egenskab, der er mest betydningsfuld, er foregået.

Tilsvarende analyser af de kvalitative og statistiske egenskaber af de eksperimentelt fastlagte udmattelsesdata og de simulerede data er foretaget i kapitel 7 med lignende resultater.

Det skulle således være muligt for et givet materiale, for hvilket nogle få materialeparametre fastlægges eksperimentelt, at benytte den udviklede model til simulering af udmattelsesdata.

Endelig konkluderes det i kapitel 8, at afhandlingens resultater er: På basis af eksisterende viden om udmattelse og udmattelsesmodeller er en ny, simpel, numerisk udmattelsesmodel udviklet og testet med tilfresstillende resultat; et stort antal udmattelsesdata er for et blødt stål etableret eksperimentelt og arbejdet levner mulighed for videre forskning.

I appendix A gives en introduktion til lineær-elastisk brudmekanik. Udledning af spændings- og flytningsfelter er inkluderet.

Sammenligning af to tællemetoder er udført i appendix B i form af et illustrativt eksempel.

Oversigt over programmer udviklet i tilknytning til afhandlingen forefindes i appendix C.

De simulerede kurver for udmattelsesrevnevækst, som er benyttet i kapitel 6, fremgår af appendix D. Kun ét typisk sæt af kurver er medtaget for hver simuleringsserie. De resterende kurver er tilgængelige hos forfatteren.

I appendix E er de simulerede kurver for udmattelsesrevnevækst baseret på de i kapitel 7 eksperimentelt fastlagte parametre vist.

A. LINEAR ELASTIC FRACTURE MECHANICS

On the basis of the connection of fracture mechanics with the phenomenon of fatigue an overview of linear elastic fracture mechanics is given in this appendix. The linear elastic fracture mechanics, which requires isotropic, homogeneous, linear elastic materials, assumes the existence of material defects in the form of initial cracks in the continuum considered. Further, only plane stress state or plane strain state at the crack tip is considered.

Fracture mechanics deals with the local state of the material at the crack tip. The state is described in terms of global load and geometry parameters under which the crack propagates.

In the first section, a brief introduction to linear elastic fracture mechanics (LEFM) is given. The following two sections contain more detailed descriptions of some of the subjects mentioned.

A.1 INTRODUCTION

A characteristic feature of a continuum containing a crack is the development of a local singular stress field. To describe the stress field around a crack tip the load at the crack tip as a result of given external loads can be divided in three parts and later superimposed.

It is common to use the following distinction in mode I, mode II and mode III actions, see figure A.1. respectively, see figure A.1. Under the assumption of linear elasticity division of the total action into 3 basic cases is permissible.

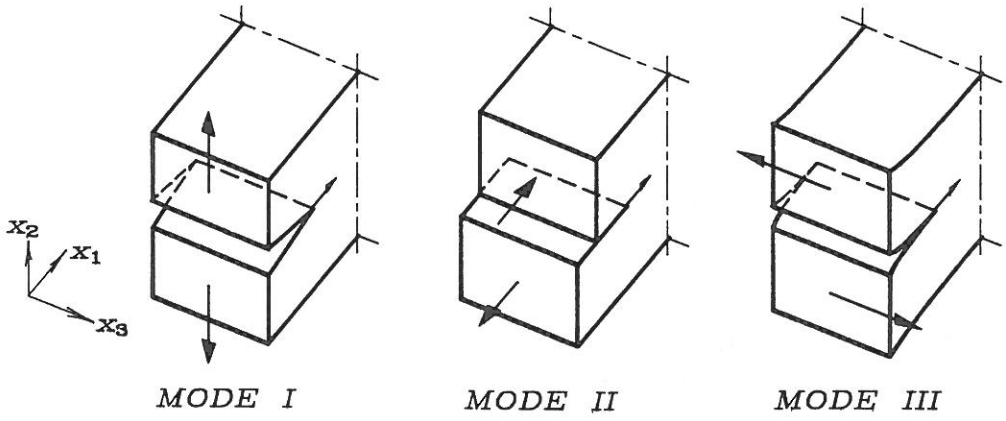

Figure A.1: Illustration of the mode I, mode II and mode III.

The mode I acting consists of a displacement which is symmetrical with regard to the x_1-x_3-plane and which is parallel with the x_2-direction. This mode is named the opening mode and is the dominant mode. The mode II acting, known as the shear mode, corresponds to a displacement which is asymmetrical with regard to the x_1-x_3-

plane and where the displacement is in the x_1-direction. Finally, a displacement which is asymmetrical with regard to the x_1-x_3-plane and which goes in the x_3-direction, performs a mode III acting, the antiplane shear mode.

Based on the first-order theory of elasticity the stress and displacement fields have to fulfil the equations of equilibrium, the kinematic relations, the constitutive relations and the boundary conditions. The governing equations for the three modes of action are derived in detail in section A.2. The expressions, which assume a straight and sharp crack front, are only valid near the crack tip ($r \to 0$).

MODE I

$$\begin{bmatrix} \sigma_{11} \\ \sigma_{22} \\ \sigma_{12} \end{bmatrix} = K_I(2\pi r)^{-\frac{1}{2}} \begin{bmatrix} 1 - \sin\frac{\theta}{2}\sin\frac{3\theta}{2} \\ 1 + \sin\frac{\theta}{2}\sin\frac{3\theta}{2} \\ \cos\frac{3\theta}{2}\sin\frac{\theta}{2} \end{bmatrix} \cos\frac{\theta}{2} \tag{A.1}$$

$$\sigma_{33} = \begin{cases} 0 & \text{in plane stress} \\ \nu(\sigma_{11} + \sigma_{22}) & \text{in plane strain} \end{cases} \tag{A.2}$$

$$\begin{bmatrix} u_1 \\ u_2 \end{bmatrix} = \frac{K_I}{4G}(2\pi)^{-\frac{1}{2}} r^{\frac{1}{2}} \begin{bmatrix} (2\kappa - 1)\cos\frac{\theta}{2} - \cos\frac{3\theta}{2} \\ (2\kappa + 1)\sin\frac{\theta}{2} - \sin\frac{3\theta}{2} \end{bmatrix} \tag{A.3}$$

MODE II

$$\begin{bmatrix} \sigma_{11} \\ \sigma_{22} \\ \sigma_{12} \end{bmatrix} = K_{II}(2\pi r)^{-\frac{1}{2}} \begin{bmatrix} -\sin\frac{\theta}{2}\{2 + \cos\frac{\theta}{2}\cos\frac{3\theta}{2}\} \\ \sin\frac{\theta}{2}\cos\frac{\theta}{2}\cos\frac{3\theta}{2} \\ \cos\frac{\theta}{2}\{1 - \sin\frac{\theta}{2}\sin\frac{3\theta}{2}\} \end{bmatrix} \tag{A.4}$$

$$\sigma_{33} = \begin{cases} 0 & \text{in plane stress} \\ \nu(\sigma_{11} + \sigma_{22}) & \text{in plane strain} \end{cases} \tag{A.5}$$

$$\begin{bmatrix} u_1 \\ u_2 \end{bmatrix} = \frac{K_{II}}{4G}(2\pi)^{-\frac{1}{2}} r^{\frac{1}{2}} \begin{bmatrix} (2\kappa + 3)\sin\frac{\theta}{2} + \sin\frac{3\theta}{2} \\ (-2\kappa + 3)\cos\frac{\theta}{2} - \cos\frac{3\theta}{2} \end{bmatrix} \tag{A.6}$$

MODE III

$$\begin{bmatrix} \sigma_{31} \\ \\ \sigma_{32} \end{bmatrix} = K_{III}(2\pi r)^{-\frac{1}{2}} \begin{bmatrix} -\sin\frac{\theta}{2} \\ \\ \cos\frac{\theta}{2} \end{bmatrix} \tag{A.7}$$

$$[u_3] = 2\frac{K_{III}}{G}(2\pi)^{-\frac{1}{2}} r^{\frac{1}{2}} [\sin\tfrac{\theta}{2}] \tag{A.8}$$

where

K_I = stress intensity factor in mode I
K_{II} = stress intensity factor in mode II
K_{III} = stress intensity factor in mode III
G = $\frac{E}{2(1+\nu)}$ = shear modulus
E = Young's modulus
ν = Poisson's ratio

$$\kappa = \begin{cases} \dfrac{3-\nu}{1+\nu} & \text{in plane stress} \\ \\ 3-4\nu & \text{in plane strain} \end{cases}$$

and the remaining symbols are shown in figure A.2.

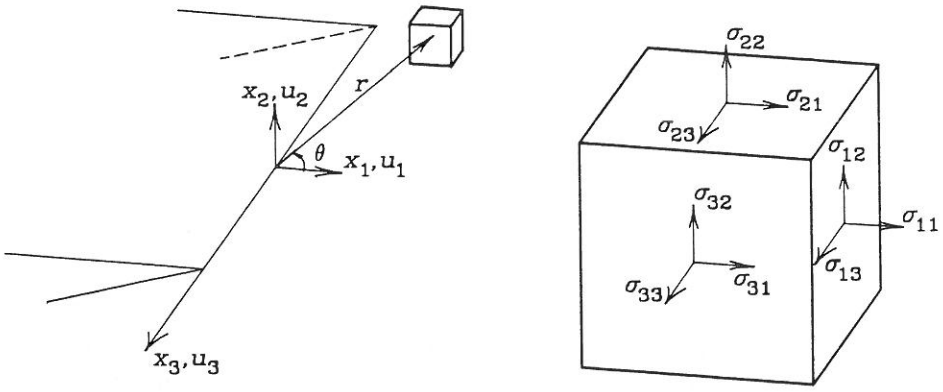

Figure A.2: Coordinate system used for stresses and displacements near a crack tip.

The expressions (A.1)-(A.8) are only valid in the immediate vicinity of the crack tip because less important parts are neglected, see appendix A.2.

The stress expressions in (A.1), (A.4) and (A.7) are derived without any assumptions on the geometry of the cracked structure and the placing of the crack in the structure as well as the size and direction of the external action is unknown. This shows that the *distribution* of the stresses in (A.1), (A.4) and (A.7) only depends on the coordinates (r, θ).

On the other hand, the *magnitude* of the stresses is depending on the geometry of the structure and the crack together with the external action. This dependence finds expression through K_I, K_{II} and K_{III}, respectively, which consequently is named the stress intensity factor for mode I, mode II and mode III action, respectively.

As it is seen from (A.1), (A.4) and (A.7) the stresses at the crack tip are assuming infinite values for $r \to 0$, which, due to the definition of stress, corresponds to applying an infinite force that no real materials can support. Yielding in a certain scale will thus appear near a crack tip. If the plastic zone is of small extension, small scale yielding is said to occur. In this case LEFM can be applied. Otherwise, i.e. if large scale yielding occurs, elastic plastic fracture mechanics (EPFM) is demanded.

Therefore, it is important to examine the size of the plastic zone, which has been performed in appendix A.3.

On the assumption of an approximate σ_{22}-stress distribution, where the stresses do not take on values greater than the yielding stress of the material, f_y, and which has the same vertical projection as the linear-elastic stress distribution, the extension of the plastic zone is found as

$$r_y = \begin{cases} \frac{1}{\pi}\left(\frac{K_i}{\sigma}\right)^2 & \text{in plane stress yielding} \\ \\ \frac{1}{3\pi}\left(\frac{K_i}{\sigma}\right)^2 & \text{in plane strain yielding} \end{cases} \qquad i = \text{I, II, III} \tag{A.9}$$

where

$$\sigma = \begin{cases} f_y & \text{in mode I and mode II} \\ \tau_y & \text{in mode III} \end{cases}$$

and r_y is shown in figures A.3 and A.4 for plane stress yielding and plane strain yielding, respectively.

Depending on the dimension of the two dimensional continuum in the x_3-direction two extreme situations occur. If the dimension in the x_3-direction is small compared to the dimensions in the x_1-x_2-plane (thin plate) the the material near the crack tip is said to be in a state of plane stress ($\sigma_{31} = \sigma_{32} = \sigma_{33} = 0$). If the dimension in the x_3-direction is sufficiently large the the material near the crack tip will be in a state of plane strain ($\epsilon_{31} = \epsilon_{32} = \epsilon_{33} = 0, \sigma_{31} = \sigma_{32} = 0$ and $\sigma_{33} = \nu(\sigma_{11} + \sigma_{22})$) except for a thin layer near the boundaries.

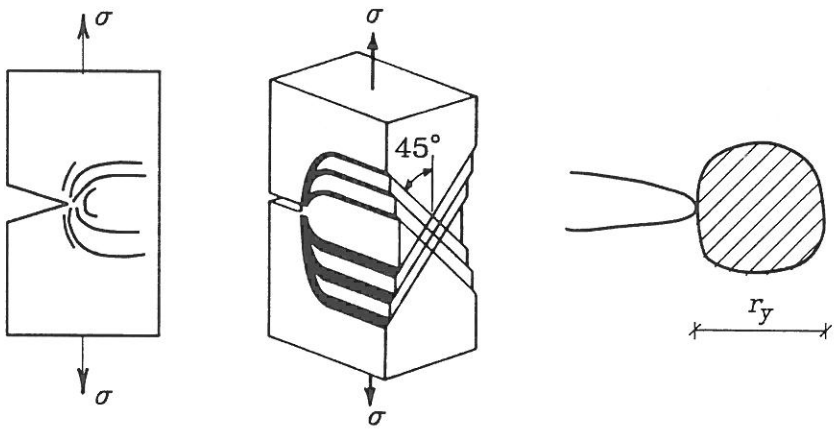

Figure A.3: Definition of r_y in plane stress yielding.
Based on [Ewalds, H.L. and R.J.H. Wanhill; 1984, p.71].

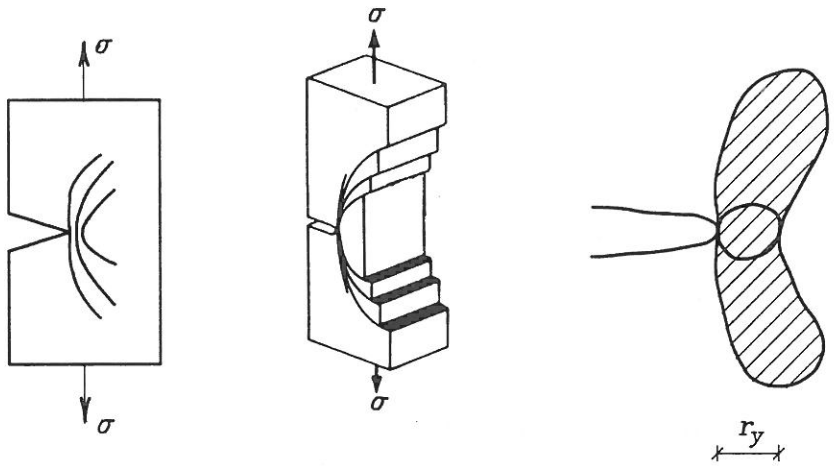

Figure A.4: Definition of r_y in plane strain yielding.
Based on [Ewalds, H.L. and R.J.H. Wanhill; 1984, p.71].

In small scale yielding, the stress distribution (A.1), (A.4) and (A.7) can still be used or a correction for the crack tip plasticity can be performed.

The stress intensity factors K_I, K_{II} and K_{III}, which are part of (A.1)-(A.8), can be determined by the so-called flexibility method. This method, which is an energy method, expresses the change of the potential energy per unit thickness with the crack length, $(\partial\delta/\partial a)$ of a body, i.e.

$$\frac{\partial U}{\partial a} = f(\frac{\partial \delta}{\partial a}) \tag{A.10}$$

where

∂U = change of potential energy
∂a = increase of crack length

$\partial\delta$ = increase of flexibility per unit thickness

To determine the connection a plane, linear elastic, cracked body acted upon by the external force P per unit thickness is considered. The forced point is exposed to the displacement u in the force direction, see figure A.5.

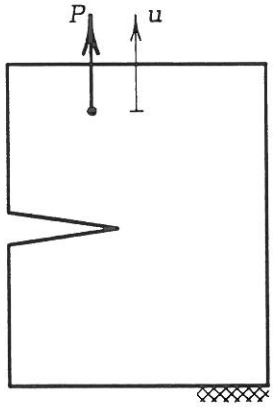

Figure A.5: Linear elastic body exposed to plane stress or plane strain. The body is acted upon by the external force per unit thickness P, which causes a displacement u in the force direction.

The potential energy per unit thickness, U see (A.10), can be expressed as the sum of the strain energy of the body and the potential of the external force both calculated per unit thickness of the body. Hereby, see [Hellan, K.; 1985, ch.3],

$$U = \begin{cases} \frac{1}{2}Pu - Pu = -\frac{1}{2}Pu & \text{prescribed force} \\ \\ \frac{1}{2}Pu & \text{prescribed displacement} \end{cases} \tag{A.11}$$

Because of the assumption of linear elasticity, the connection between the force P per unit thickness and the displacement u can be expressed as

$$u = \delta P \tag{A.12}$$

where

δ = the flexibility of one unit thickness of the body

By this (A.11) can be rewritten as

$$U = \begin{cases} -\dfrac{\delta P^2}{2} & \text{prescribed force} \\ \\ \dfrac{-u^2}{2\,\delta} & \text{prescribed displacement} \end{cases} \tag{A.13}$$

The work, $\mathcal{G}$, which is used for formation of a unit area new crack surface, can according to e.g. [Hellan, K.; 1985, p.55] be expressed as

$$\mathcal{G} = -\frac{\partial U}{\partial a} \tag{A.14}$$

$\mathcal{G}$ is denoted the energy release rate (some references use crack driving force).

From (A.13) and (A.14) the desired connection between $(\partial U/\partial a)$ and $(\partial \delta/\partial a)$ is found.

$$\mathcal{G} = \begin{cases} \dfrac{P^2}{2}\dfrac{\partial \delta}{\partial a} & \text{prescribed force} \\ \dfrac{u^2}{2}\dfrac{1}{\delta^2}\dfrac{\partial \delta}{\partial a} & \text{prescribed displacement} \end{cases} \tag{A.15}$$

It is seen from (A.12) that the two expressions in (A.15) are identical, i.e. the crack driving force does not depend on whether the force or the displacement is prescribed.

The following connections between the crack driving force and the stress intensity factor in respectively mode I, mode II and mode III action are found in e.g. [Hellan, K.; 1985, p.58]

MODE I

$$\mathcal{G} = \begin{cases} \dfrac{K_I^2}{E} & \text{plane stress} \\ \dfrac{1-\nu^2}{E} K_I^2 & \text{plane strain} \end{cases} \tag{A.16}$$

MODE II

$$\mathcal{G} = \begin{cases} \dfrac{K_{II}^2}{E} & \text{plane stress} \\ \dfrac{1-\nu^2}{E} K_{II}^2 & \text{plane strain} \end{cases} \tag{A.17}$$

MODE III

$$\mathcal{G} = \frac{1+\nu^2}{E} K_{III}^2 \tag{A.18}$$

The expressions (A.15) and (A.16)-(A.18) constitute the analytical foundation for the flexibility method.

Since the calculations are performed per unit thickness of the body the involved quantities are stated in the following units:

$$\begin{aligned} [P] &= \mathrm{Nmm}^{-1} \\ [\delta] &= \mathrm{mm}^2\mathrm{N}^{-1} \\ [U] &= \mathrm{N} \\ [\mathcal{G}] &= \mathrm{Nmm}^{-1} \\ [K] &= \mathrm{MPa}\sqrt{\mathrm{mm}} \end{aligned}$$

It is seen from (A.15)-(A.18) that an experimental or numerical determination of K can be made by registering connected values of the force per unit thickness, P, the displacement in the force acting point, u, and the crack length, a. An experimental determination of the stress intensity factor K is from (A.15) seen to be independent of the flexibility of the loading arrangement if only the loading arrangement is assumed to be in the linear region.

By establishing the above set of formulas the most important expressions and conceptions in the linear fracture mechanics are introduced.

A.2 STRESS AND DISPLACEMENT FIELDS NEAR A CRACK TIP

In this section a description of the stress field and displacement field around the crack tip is given for a mode I, a mode II and a mode III influenced body.

It is assumed that the crack is through-going and that the crack front is straight and sharp. Furthermore, it is assumed that the body, in which the crack appears, consists of a homogeneous, isotropic, linear-elastic material. Provided these assumptions are fulfilled two extreme cases in the 3-dimensional situation exists, i.e. plane stress condition and plane strain condition.

The stresses and displacements are referred to the local coordinate system shown in figure A.2.

For the description of the stress field around the crack tip it is required that the equations of equilibrium, the kinematics relations and the constitutive relations are fulfilled. This can be expressed in Beltrami-Michell's compatibility condition for a body in a state of plane stress or plane strain, see [Rathkjen, A.; 1984, p.11].

$$(\sigma_{11} + \sigma_{22})_{,x_1x_1} + (\sigma_{11} + \sigma_{22})_{,x_2x_2} = 0$$

or

$$\nabla^2(\sigma_{11} + \sigma_{22}) = 0 \tag{A.19}$$

where subscript , means differentiated with respect to, and where

$$\nabla^2 = \frac{\partial^2}{\partial x_1^2} + \frac{\partial^2}{\partial x_2^2} \tag{A.20}$$

Expressing the stresses as

$$\sigma_{11} = A_{,x_2x_2} \qquad \sigma_{22} = A_{,x_1x_1} \qquad \sigma_{12} = -A_{,x_1x_2} \tag{A.21}$$

where

$A(x_1, x_2) =$ Airy's stress function

(A.19) becomes

$$\begin{aligned} \nabla^2(\sigma_{11} + \sigma_{22}) &= \nabla^2(A_{,x_1x_1} + A_{,x_2x_2}) \\ &= A_{,x_1x_1x_1x_1} + 2A_{,x_1x_1x_2x_2} + A_{,x_2x_2x_2x_2} \\ &= \nabla^4 A = 0 \end{aligned} \tag{A.22}$$

where

$$\nabla^4 = \frac{\partial^4}{\partial x_1^4} + \frac{\partial^4}{\partial x_2^4} + 2\frac{\partial^4}{\partial x_1^2 \partial x_2^2}$$

Since the compatibility condition (A.19) is thus satisfied the strains related to the stresses uniquely determine the displacements in case the boundary conditions for the displacements are fulfilled. The plane problem consists of finding solutions of the biharmonic equation given by (A.22) where, furthermore, A has to satisfy the boundary conditions in the actual problem.

It is not possible to mention a general form of A as a function of x_1 and x_2 but, for the stress field near a crack tip solutions can be obtained by introduction of the complex variable

$$z = x_1 + ix_2 \tag{A.23}$$

and its complex conjugated

$$\overline{z} = x_1 - ix_2 \tag{A.24}$$

By inserting, see [Rathkjen, A.; 1984, p.13],

$$A_{,x_1x_1x_1x_1} = A_{,zzzz} + 4A_{,zzz\overline{z}} + 6A_{,zz\overline{zz}} + 4A_{,z\overline{zzz}} + A_{,\overline{zzzz}}$$

$$A_{,x_1x_1x_2x_2} = -A_{,zzzz} + 2A_{,zz\overline{zz}} - A_{,\overline{zzzz}}$$

$$A_{,x_2x_2x_2x_2} = A_{,zzzz} - 4A_{,zzz\overline{z}} + 6A_{,zz\overline{zz}} - 4A_{,z\overline{zzz}} + A_{,\overline{zzzz}}$$

into the biharmonic equation (A.22) the following is obtained

$$A_{,x_1x_1x_1x_1} + 2A_{,x_1x_1x_2x_2} + A_{,x_2x_2x_2x_2} = 0$$

$$A_{,zz\overline{zz}} = 0 \tag{A.25}$$

Integrating (A.25) leads to

$$\begin{aligned} 2A_{,zz\overline{z}} &= \phi''(z) \\ 2A_{,zz} &= \overline{z}\phi''(z) + \chi''(z) \\ 2A_{,z} &= \overline{z}\phi'(z) + \chi'(z) + \alpha(\overline{z}) \\ 2A &= \overline{z}\phi(z) + \chi(z) + z\alpha(\overline{z}) + \beta(\overline{z}) \end{aligned} \tag{A.26}$$

where superscript $'$ means differentiated with respect to, and where

ϕ, χ = analytical functions of z, i.e differentiable at every point and continuous derivatives

α, β = functions of $\overline{z}$

Since A is a real function, i.e. a function which assumes real values for every x_1 and x_2 and thus for every value of z and $\overline{z}$, it can be shown (see [Rathkjen, A.; 1984, p.18]) that

$$\alpha(\overline{z}) = \overline{\phi}(z) \tag{A.27}$$

and

$$\beta(\overline{z}) = \overline{\chi}(z) \tag{A.28}$$

so (A.26) is reduced to

$$2A = \overline{z}\phi(z) + z\overline{\phi}(z) + \chi(z) + \overline{\chi}(z) \tag{A.29}$$

Inserting (A.29) into (A.21) the fundamental combinations of stresses can be generated:

$$\sigma_{11} + \sigma_{22} = 2[\phi'(z) + \overline{\phi}\,'(z)] = 4\Re\phi'(z)$$

$$\sigma_{22} - \sigma_{11} + 2i\sigma_{12} = 2[\overline{z}\phi''(z) + \chi''(z)] \tag{A.30}$$

in which it is used that

$$f(z) + \overline{f}(z) = 2\Re f(z)$$

$$f_{,z}(z) = f'(z)$$

$$f_{,x_1}(z) = f_{,z}(z)z_{,x_1} = f'(z)$$

$$f_{,x_2}(z) = f_{,z}(z)z_{,x_2} = if'(z)$$

The analytical functions $\phi(z)$ and $\chi(z)$ can, cf. [Owen, D.R.J. and A.J. Fawkes; 1983, p.9], be written as complex eigenvalue functions in the form of

$$\phi(z) = \sum_{n=0}^{\infty} A_n z^{\lambda_n} \qquad \chi(z) = \sum_{n=0}^{\infty} B_n z^{(\lambda_n+1)} \qquad n = 0, 1, 2, \ldots \tag{A.31}$$

where

λ_n = real eigenvalue

A_n = $(a_{n1} + ia_{n2})$ =complex constant

B_n = $(b_{n1} + ib_{n2})$ =complex constant

(A.30) leads to

$$\sigma_{22} + i\sigma_{12} = \phi'(z) + \overline{\phi}\,'(z) + \overline{z}\phi''(z) + \chi''(z)$$

which by inserting (A.31) and

$$z = x_1 + ix_2 = re^{i\theta} \tag{A.32}$$

gives

$$\sigma_{22}+i\sigma_{12}=\sum_{n=0}^{\infty}\lambda_n A_n(re^{i\theta})^{(\lambda_n-1)}+\sum_{n=0}^{\infty}\lambda_n\overline{A}_n(re^{-i\theta})^{(\lambda_n-1)}+$$

$$(re^{-i\theta})\sum_{n=0}^{\infty}\lambda_n(\lambda_n-1)A_n(re^{i\theta})^{(\lambda_n-2)}+$$

$$\sum_{n=0}^{\infty}\lambda_n(\lambda_n+1)B_n(re^{i\theta})^{(\lambda_n-1)}$$

which is reduced to

$$\sigma_{22}+i\sigma_{12}=\sum_{n=0}^{\infty}\lambda_n r^{(\lambda_n-1)}\{A_n[e^{i\theta(\lambda_n-1)}+(\lambda_n-1)e^{i\theta(\lambda_n-3)}]+$$

$$\overline{A}_n e^{-i\theta(\lambda_n-1)}+B_n(\lambda_n+1)e^{i\theta(\lambda_n-1)}\} \tag{A.33}$$

The stresses on the crack surface are zero, cf. figure A.5

$$\sigma_{22}=\sigma_{12}=0 \quad \text{for } \theta=\pm\pi$$

Inserting $\theta=\pi$, (A.33) becomes

$$\sum_{n=0}^{\infty}\lambda_n r^{(\lambda_n-1)}\{A_n\lambda_n+\overline{A}_n[\cos(2\pi\lambda_n)-i\sin(2\pi\lambda_n)]+B_n(\lambda_n+1)\}=0 \tag{A.34}$$

where it is used that

$$e^{i\theta}=\cos\theta+i\sin\theta \quad \text{and} \quad e^{-i\theta}=\cos\theta-i\sin\theta \tag{A.35}$$

For $\theta=-\pi$, (A.33) becomes

$$\sum_{n=0}^{\infty}\lambda_n r^{(\lambda_n-1)}\{A_n\lambda_n+\overline{A}_n[\cos(2\pi\lambda_n)+i\sin(2\pi\lambda_n)]+B_n(\lambda_n+1)\}=0 \tag{A.36}$$

Subtracting (A.34) from (A.36) gives

$$\sin(2\pi\lambda_n)=0 \quad \Rightarrow \quad 2\pi\lambda_n=n\pi$$

and thus

$$\lambda_n = \tfrac{1}{2}n \qquad n = 0, 1, 2, ... \tag{A.37}$$

which inserted into (A.34) and (A.36) gives

$$\frac{1}{2}nA_n + (-1)^n\overline{A}_n + B_n(\frac{1}{2}n + 1) = 0$$

By inserting the expressions for A_n, $\overline{A}_n$ and B_n in the above and by separation in real and imaginary part,

$$-b_{n1} = \frac{a_{n1}(\frac{1}{2}n + (-1)^n)}{\frac{1}{2}n + 1} \qquad -b_{n2} = \frac{a_{n2}(\frac{1}{2}n - (-1)^n)}{\frac{1}{2}n + 1} \tag{A.38}$$

Using (A.38) in (A.33) the real part and the imaginary part of the expression forms σ_{22} and σ_{12}, respectively.

$$\begin{aligned}\sigma_{22} = \sum_{n=1}^{\infty} \tfrac{1}{2}nr^{(\frac{1}{2}n-1)}\{a_{n1}[(2 - \tfrac{1}{2}n - (-1)^n)\cos(\tfrac{1}{2}n - 1)\theta + \\ (\tfrac{1}{2}n - 1)\cos(\tfrac{1}{2}n - 3)\theta] - a_{n2}[(2 - \tfrac{1}{2}n + (-1)^n)\sin(\tfrac{1}{2}n - 1)\theta + \\ (\tfrac{1}{2}n - 1)\sin(\tfrac{1}{2}n - 3)\theta]\}\end{aligned} \tag{A.39}$$

$$\begin{aligned}\sigma_{12} = \sum_{n=1}^{\infty} \tfrac{1}{2}nr^{(\frac{1}{2}n-1)}\{a_{n1}[(\tfrac{1}{2}n - 1)\sin(\tfrac{1}{2}n - 3)\theta - \\ (\tfrac{1}{2}n + (-1)^n)\sin(\tfrac{1}{2}n - 1)\theta] + a_{n2}[(\tfrac{1}{2}n - 1)\cos(\tfrac{1}{2}n - 3)\theta - \\ (\tfrac{1}{2}n - (-1)^n)\cos(\tfrac{1}{2}n - 1)\theta]\}\end{aligned} \tag{A.40}$$

Finally (A.30) becomes

$$\sigma_{11} - i\sigma_{12} = 2\Re\phi'(z) - [\overline{z}\phi''(z) + \chi''(z)]$$

and thus from (A.31), (A.37) and (A.38)

$$\sigma_{11} = \sum_{n=1}^{\infty} \tfrac{1}{2} n r^{(\frac{1}{2}n-1)} \{ a_{n1}[(2 + \tfrac{1}{2}n + (-1)^n)\cos(\tfrac{1}{2}n - 1)\theta -$$

$$(\tfrac{1}{2}n - 1)\cos(\tfrac{1}{2}n - 3)\theta] - a_{n2}[(2 + \tfrac{1}{2}n - (-1)^n)\sin(\tfrac{1}{2}n - 1)\theta -$$

$$(\tfrac{1}{2}n - 1)\sin(\tfrac{1}{2}n - 3)\theta]\} \tag{A.41}$$

The displacements u_1 and u_2 in the direction of x_1 and x_2, respectively, are determined from the constitutive equations which by inserting (A.21) become

$$\begin{aligned} E u_{1,x_1} &= \sigma_{11} - \nu\sigma_{22} = A_{,x_2x_2} - \nu A_{,x_1x_1} \\ E u_{2,x_2} &= \sigma_{22} - \nu\sigma_{11} = A_{,x_1x_1} - \nu A_{,x_2x_2} \\ G(u_{1,x_2} + u_{2,x_1}) &= \sigma_{12} = -A_{,x_1x_2} \end{aligned} \tag{A.42}$$

where

$$\begin{aligned} G &= \tfrac{E}{2(1+\nu)} = \text{shear modulus} \\ E &= \text{Young's modulus} \\ \nu &= \text{Poisson's ratio} \end{aligned}$$

By integrating the two first equations in (A.30), see for example [Rathkjen, A.; 1984, p.28-33], the following is obtained

$$2G(u_1 + iu_2) = \kappa\phi(z) - z\overline{\phi}'(z) - \overline{\chi}'(z) \tag{A.43}$$

where

$$\kappa = \begin{cases} \dfrac{3-\nu}{1+\nu} & \text{factor in plane stress} \\ 3 - 4\nu & \text{factor in plane strain} \end{cases} \tag{A.44}$$

The third equation in (A.42) determines the arbitrary functions in x_1 and x_2, respectively, as a result of the integrations. It turns out that the functions correspond to rigid body motions, see [Rathkjen, A.; 1984, p.31]. The stresses do not change due to rigid body motions, wherefore the latter is neglected in (A.43).

The equations (A.31), (A.37) and (A.38) and separation in a real and an imaginary part gives

$$u_1 = \frac{1}{2G}\sum_{n=1}^{\infty} r^{\frac{1}{2}n}\{a_{n1}[(\kappa + \tfrac{1}{2}n + (-1)^n)\cos(\tfrac{1}{2}n\theta) - \tfrac{1}{2}n\cos(\tfrac{1}{2}n-2)\theta] - a_{n2}[(\kappa + \tfrac{1}{2}n - (-1)^n)\sin(\tfrac{1}{2}n\theta) - \tfrac{1}{2}n\sin(\tfrac{1}{2}n-2)\theta]\} \tag{A.45}$$

$$u_2 = \frac{1}{2G}\sum_{n=1}^{\infty} r^{\frac{1}{2}n}\{a_{n1}[(\kappa - \tfrac{1}{2}n - (-1)^n)\sin(\tfrac{1}{2}n\theta) + \tfrac{1}{2}n\sin(\tfrac{1}{2}n-2)\theta] + a_{n2}[(\kappa - \tfrac{1}{2}n + (-1)^n)\cos(\tfrac{1}{2}n\theta) + \tfrac{1}{2}n\cos(\tfrac{1}{2}n-2)\theta]\} \tag{A.46}$$

For $n = 1$ (A.41), (A.39), (A.40), (A.45) and (A.46) are reduced to

$$\begin{aligned}
\sigma_{11} &= a_1^1 r^{-\frac{1}{2}}(1 - \sin\tfrac{\theta}{2}\sin\tfrac{3\theta}{2})\cos\tfrac{\theta}{2} + a_1^2 r^{-\frac{1}{2}}(2 + \cos\tfrac{\theta}{2}\cos\tfrac{3\theta}{2})\sin\tfrac{\theta}{2} \\
\sigma_{22} &= a_1^1 r^{-\frac{1}{2}}(1 + \sin\tfrac{\theta}{2}\sin\tfrac{3\theta}{2})\cos\tfrac{\theta}{2} - a_1^2 r^{-\frac{1}{2}}\cos\tfrac{\theta}{2}\cos\tfrac{3\theta}{2}\sin\tfrac{\theta}{2} \\
\sigma_{12} &= a_1^1 r^{-\frac{1}{2}}\cos\tfrac{\theta}{2}\cos\tfrac{3\theta}{2}\sin\tfrac{\theta}{2} - a_1^2 r^{-\frac{1}{2}}(1 - \sin\tfrac{\theta}{2}\sin\tfrac{3\theta}{2})\cos\tfrac{\theta}{2} \\
u_1 &= \tfrac{1}{4G}a_1^1 r^{\frac{1}{2}}\{(2\kappa-1)\cos\tfrac{\theta}{2} - \cos\tfrac{3\theta}{2}\} - \tfrac{1}{4G}a_1^2 r^{\frac{1}{2}}\{(2\kappa+3)\sin\tfrac{\theta}{2} + \sin\tfrac{3\theta}{2}\} \\
u_2 &= \tfrac{1}{4G}a_1^1 r^{\frac{1}{2}}\{(2\kappa+1)\sin\tfrac{\theta}{2} - \sin\tfrac{3\theta}{2}\} + \tfrac{1}{4G}a_1^2 r^{\frac{1}{2}}\{(2\kappa-3)\cos\tfrac{\theta}{2} + \cos\tfrac{3\theta}{2}\}
\end{aligned} \tag{A.47}$$

In front of the crack tip, i.e. $\theta = 0$, the stresses and displacements cf. (A.47) become

$$\begin{aligned}
&\sigma_{11} = a_{11}r^{-\frac{1}{2}} \quad \sigma_{22} = a_{11}r^{-\frac{1}{2}} \quad \sigma_{12} = -a_{12}r^{-\frac{1}{2}} \\
&u_1 = \tfrac{1}{2G}a_{11}r^{\frac{1}{2}}(\kappa-1) \quad u_2 = \tfrac{1}{2G}a_{12}r^{\frac{1}{2}}(\kappa-1)
\end{aligned} \tag{A.48}$$

As σ_{11} and σ_{22} have to be symmetrical about the x_1-axis ($\theta = 0$) and σ_{12} has to be

antimetrical about the same axis in a mode I influenced body is it seen from figure A.6 that (A.47) hereby is reduced to

$$\begin{bmatrix} \sigma_{11} \\ \sigma_{22} \\ \sigma_{12} \end{bmatrix} = a_{11} r^{-\frac{1}{2}} \begin{bmatrix} 1 - \sin\frac{\theta}{2}\sin\frac{3\theta}{2} \\ 1 + \sin\frac{\theta}{2}\sin\frac{3\theta}{2} \\ \cos\frac{3\theta}{2}\sin\frac{\theta}{2} \end{bmatrix} \cos\frac{\theta}{2} \tag{A.49}$$

The displacements u_1 and u_2 are symmetrical about the x_1-axis as well so

$$\begin{bmatrix} u_1 \\ u_2 \end{bmatrix} = \frac{1}{4G} a_{11} r^{\frac{1}{2}} \begin{bmatrix} (2\kappa - 1)\cos\frac{\theta}{2} - \cos\frac{3\theta}{2} \\ (2\kappa + 1)\sin\frac{\theta}{2} - \sin\frac{3\theta}{2} \end{bmatrix} \tag{A.50}$$

see also figure A.7.

For a mode II influenced body the stresses σ_{11} and σ_{22} are found as the antimetrical parts of (A.47), whereas σ_{12} is formed by the symmetrical part of (A.47) with respect to the x_1-axis. By this

$$\begin{bmatrix} \sigma_{11} \\ \sigma_{22} \\ \sigma_{12} \end{bmatrix} = a_{12} r^{-\frac{1}{2}} \begin{bmatrix} \sin\frac{\theta}{2}\{2 + \cos\frac{\theta}{2}\cos\frac{3\theta}{2}\} \\ -\sin\frac{\theta}{2}\cos\frac{\theta}{2}\cos\frac{3\theta}{2} \\ -\cos\frac{\theta}{2}\{1 - \sin\frac{\theta}{2}\sin\frac{3\theta}{2}\} \end{bmatrix} \tag{A.51}$$

The displacements u_1 and u_2 are antimetrical and symmetrical, respectively, about the x_1-axis and from figure A.7 and (A.39) the following is found

$$\begin{bmatrix} u_1 \\ u_2 \end{bmatrix} = \frac{1}{4G} a_{12} r^{\frac{1}{2}} \begin{bmatrix} -(2\kappa + 3)\sin\frac{\theta}{2} - \sin\frac{3\theta}{2} \\ (2\kappa - 3)\cos\frac{\theta}{2} + \cos\frac{3\theta}{2} \end{bmatrix} \tag{A.52}$$

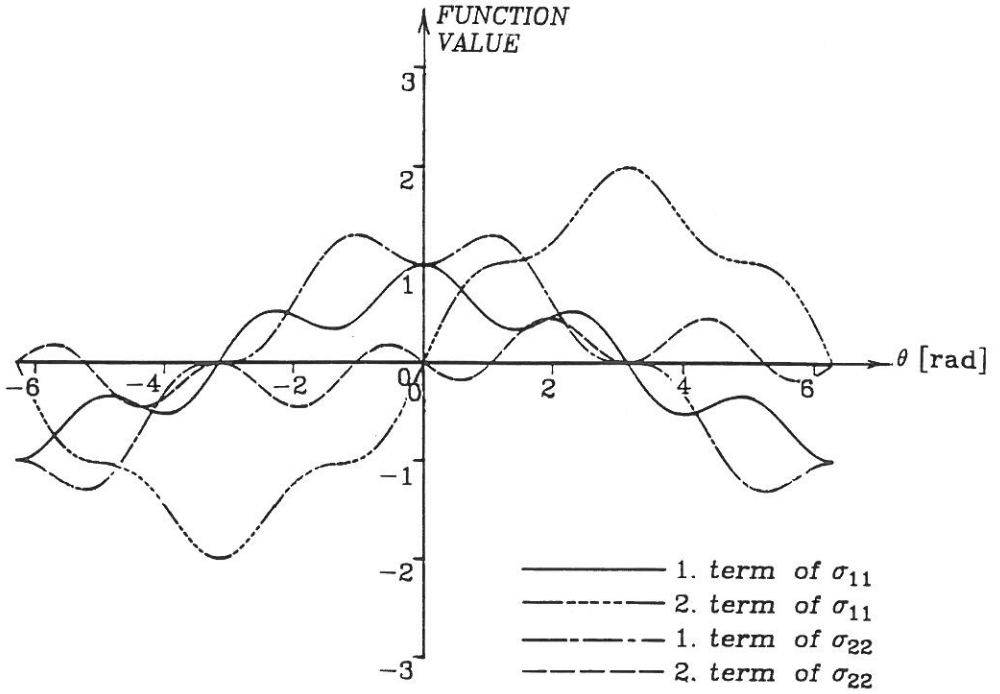

Figure A.6: 1st and 2nd term in σ_{11} and σ_{22} as a function of θ.

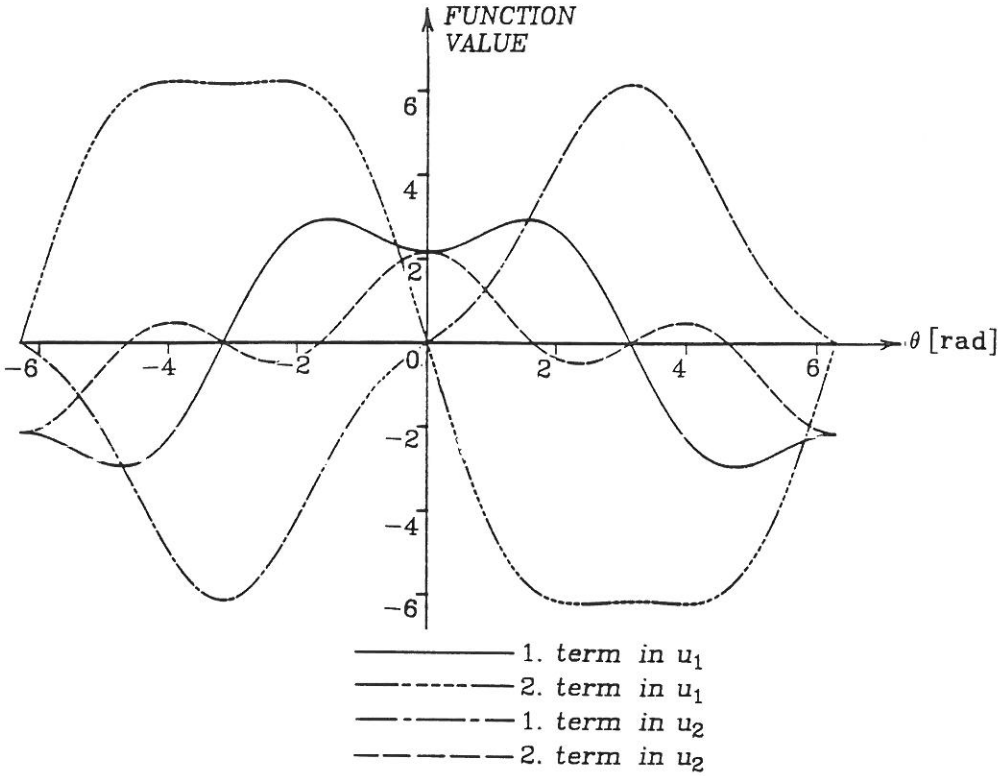

Figure A.7: 1st and 2nd term in u_1 and u_2, respectively, as a function of θ

The stresses σ_{ij} are desired on the form

$$\sigma_{ij} = K_k(2\pi r)^{-\frac{1}{2}} f(\theta) \quad k = \text{I,II} \quad i,j = 1,2$$

For $\theta = 0$ the following is found from from (A.48)

$$a_{11} = K_I(2\pi)^{-\frac{1}{2}} \quad a_{12} = -K_{II}(2\pi)^{-\frac{1}{2}} \tag{A.53}$$

where

K_I = stress intensity factor in mode I
K_{II} = stress intensity factor in mode II

Finally,

MODE I

$$\begin{bmatrix} \sigma_{11} \\ \sigma_{22} \\ \sigma_{12} \end{bmatrix} = K_I(2\pi r)^{-\frac{1}{2}} \begin{bmatrix} 1 - \sin\frac{\theta}{2}\sin\frac{3\theta}{2} \\ 1 + \sin\frac{\theta}{2}\sin\frac{3\theta}{2} \\ \cos\frac{3\theta}{2}\sin\frac{\theta}{2} \end{bmatrix} \cos\frac{\theta}{2} \tag{A.54}$$

$$\begin{bmatrix} u_1 \\ u_2 \end{bmatrix} = \frac{K_I}{4G}(2\pi)^{-\frac{1}{2}} r^{\frac{1}{2}} \begin{bmatrix} (2\kappa - 1)\cos\frac{\theta}{2} - \cos\frac{3\theta}{2} \\ (2\kappa + 1)\sin\frac{\theta}{2} - \sin\frac{3\theta}{2} \end{bmatrix} \tag{A.55}$$

MODE II

$$\begin{bmatrix} \sigma_{11} \\ \sigma_{22} \\ \sigma_{12} \end{bmatrix} = K_{II}(2\pi r)^{-\frac{1}{2}} \begin{bmatrix} -\sin\frac{\theta}{2}\{2 + \cos\frac{\theta}{2}\cos\frac{3\theta}{2}\} \\ \sin\frac{\theta}{2}\cos\frac{\theta}{2}\cos\frac{3\theta}{2} \\ \cos\frac{\theta}{2}\{1 - \sin\frac{\theta}{2}\sin\frac{3\theta}{2}\} \end{bmatrix} \tag{A.56}$$

$$\begin{bmatrix} u_1 \\ u_2 \end{bmatrix} = \frac{K_{II}}{4G}(2\pi)^{-\frac{1}{2}} r^{\frac{1}{2}} \begin{bmatrix} (2\kappa + 3)\sin\frac{\theta}{2} + \sin\frac{3\theta}{2} \\ (-2\kappa + 3)\cos\frac{\theta}{2} - \cos\frac{3\theta}{2} \end{bmatrix} \tag{A.57}$$

The above expressions are only valid close to the crack tip.

Finally, the stress and displacement fields for a mode III loaded body are derived. As mentioned in section A.1, the only displacement component different from zero

is $u_3 = u_3(x_1, x_2)$. The following is inspired by [Kanninen, M.F. and C.H. Popelar; 1985].

The strains in a homogeneous, isotropic material can be written as,

$$\epsilon_{ij} = \tfrac{1}{2}(u_{i,j} + u_{j,i}) \quad i,j = 1,2,3 \tag{A.58}$$

which in mode III acting is reduced to

$$\epsilon_{3j} = \tfrac{1}{2}u_{3,j} \quad j = 1,2 \tag{A.59}$$

The stresses are given by Hookes' law,

$$\sigma_{ij} = 2G(\epsilon_{ij} + \frac{\nu}{1-2\nu}\delta_{ij}\epsilon_{kk}) \quad i,j,k = 1,2,3 \tag{A.60}$$

The only ϵ_{ij} value different from zero is given by (A.59), so (A.60) becomes

$$\sigma_{3j} = 2G\epsilon_{3j} \quad j = 1,2 \tag{A.61}$$

Since body forces are neglected, the equations of equilibrium are

$$\sigma_{ij,j} = 0 \quad i,j = 1,2,3$$

which can likewise be reduced to

$$\sigma_{3j,j} = 0 \quad j = 1,2 \tag{A.62}$$

and inserting (A.61) and (A.59) gives

$$u_{3,jj} = \nabla^2 u_3 = 0 \tag{A.63}$$

where the Laplace operator ∇^2 is given by (A.20).

In order to find the solution of (A.63) an analytic function,

$$f(z) = u(x_1, x_2) + i\, v(x_1, x_2) \tag{A.64}$$

is introduced. The complex variable is given by (A.23). Since f is analytic, it has to fulfil the Cauchy-Rieman equations,

$$\frac{\partial u}{\partial x_1} = \frac{\partial v}{\partial x_2} \qquad \frac{\partial u}{\partial x_2} = -\frac{\partial v}{\partial x_1} \tag{A.65}$$

From (A.65) it is easily seen that

$$\nabla^2 u = \nabla^2 v = 0$$

Thus, the real and imaginary parts of any analytical function are solutions of (A.63).

Since the displacement field is real it may be expressed as

$$u_3(z) = \frac{1}{G}[f(z) + \overline{f}(z)] \tag{A.66}$$

where $\overline{f}(z)$ is the complex conjugate of $f(z)$.

Inserting (A.66) in (A.59) the following expressions are found

$$\begin{aligned} \epsilon_{31} &= \frac{1}{2G}[f'(z) + \overline{f}\,'(z)] \\ \epsilon_{32} &= \frac{i}{2G}[f'(z) - \overline{f}\,'(z)] \end{aligned} \tag{A.67}$$

Using (A.61) and inserting (A.67), the following expression is obtained,

$$\sigma_{31} - i\sigma_{32} = 2f'(z) \tag{A.68}$$

In the following $f(z)$ is sought to describe the stress and displacement fields near the crack tip shown in figure A.2.

The analytic function

$$f(z) = Cz^{\lambda+1} \qquad C = A + iB \tag{A.69}$$

is tested as a possible solution. A, B and λ are real constants.

Using the coordinate system shown in figure A.1, it is seen from (A.66) that $\lambda > -1$ to ensure finite displacements for $|z| = r = 0$.

Inserting (A.69) in (A.68) yields

$$\sigma_{31} - i\sigma_{32} = 2(\lambda+1)z^{\lambda}C = 2(\lambda+1)r^{\lambda}(A+iB)(\cos\lambda\theta + i\sin\lambda\theta) \tag{A.70}$$

where (A.32) is used.

Separation in real and imaginary part gives,

$$\sigma_{31} = 2(\lambda+1)r^{\lambda}(A\cos\lambda\theta - B\sin\lambda\theta)$$
$$\sigma_{32} = -2(\lambda+1)r^{\lambda}(A\sin\lambda\theta + B\cos\lambda\theta) \tag{A.71}$$

Since (A.69) fulfils all governing equations it is a solution of the problem if the boundary conditions also are fulfilled. The present boundary conditions are

$$\sigma_{32} = 0 \quad \text{for } \theta = \pm\pi$$

Inserting this gives,

$$A\sin\lambda\pi + B\cos\lambda\pi = 0$$
$$A\sin\lambda\pi - B\cos\lambda\pi = 0 \tag{A.72}$$

To obtain a non-trivial solution the determinant of the coefficients of the equations (A.72) must equal zero. This requirement leads to

$$\sin 2\lambda\pi = 0$$

with solutions for $\lambda > -1$ given as

$$\lambda = \tfrac{n}{2} \quad n = -1, 0, 1, 2, \ldots$$

All these possible values of λ give an infinite set of functions of the form (A.69) that fulfils the boundary conditions at the crack surface. The dominant terms are obtained for $\lambda = -\frac{1}{2}$ for which (A.72) gives $A = 0$ so (A.71) becomes

$$\begin{bmatrix} \sigma_{31} \\ \\ \sigma_{32} \end{bmatrix} = Br^{-\frac{1}{2}} \begin{bmatrix} \sin\frac{\theta}{2} \\ \\ -\cos\frac{\theta}{2} \end{bmatrix} \tag{A.73}$$

Stating the stresses in the same form as (A.54) and (A.56), (A.73) becomes

$$\begin{bmatrix} \sigma_{31} \\ \\ \sigma_{32} \end{bmatrix} = K_{III}(2\pi r)^{-\frac{1}{2}} \begin{bmatrix} -\sin\frac{\theta}{2} \\ \\ \cos\frac{\theta}{2} \end{bmatrix} \tag{A.74}$$

where the stress intensity factor in mode III, K_{III}, has been introduced for B as

$$B = -K_{III}(\sqrt{2\pi})^{-\frac{1}{2}}$$

Setting $\lambda = -\frac{1}{2}$, $A = 0$ and $B = -K_{III}(2\pi)^{-\frac{1}{2}}$, (A.66) gives,

$$[u_3] = 2\frac{K_{III}}{G}(2\pi)^{-\frac{1}{2}} r^{\frac{1}{2}} [\sin\tfrac{\theta}{2}] \tag{A.75}$$

Thus, the stress and displacement fields in the three modes are established, see (A.54)-(A.57), (A.74) and (A.75).

A.3 EXTENT OF THE PLASTIC ZONE NEAR A CRACK TIP

Assuming linear-elasticity, the derivation of the stress field near a crack tip will result in infinite stress at the tip, see section A.1 and A.2. However, in real materials such stresses cannot appear. If the crack appears in a material with yielding capacity, a plastic zone around the crack tip will be enforced, see figure A.8.

In the present section, an evaluation of the size of the plastic zone is performed. Further, it is described how to make a compensation of the small-scale yielding behaviour of the material.

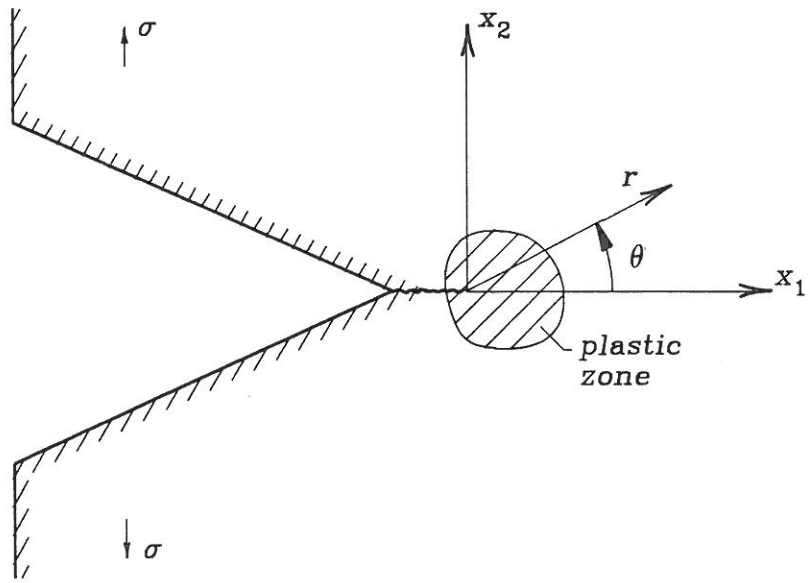

Figure A.8: Illustration of plastic zone near crack tip.

The evaluation of the size of the plastic zone in mode I acting is performed by equivalizing of the elastically determined σ_{22}-stress distribution with the approximate elastic-plastic distribution. The variation of the normal stress σ_{22} along the x_1-axis is shown in figure A.9.

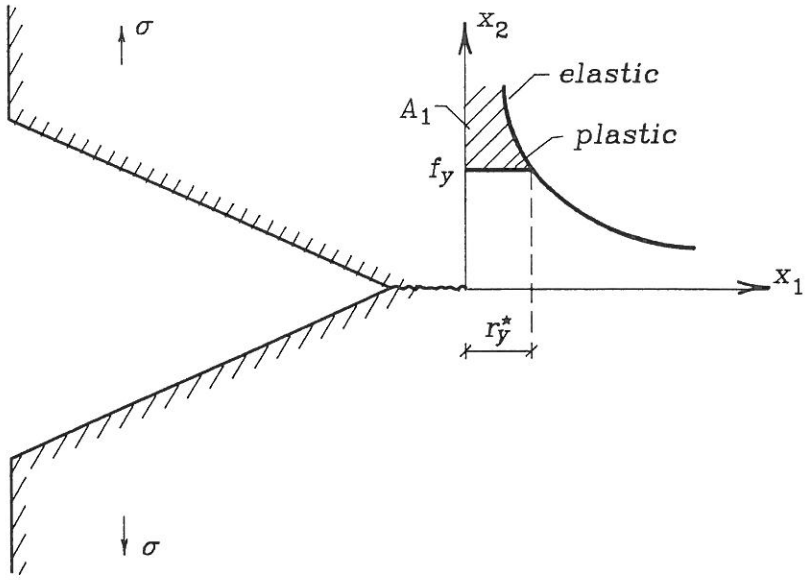

Figure A.9: Variation of σ_{22} along the x_1-axis ($\theta = 0$) in mode I acting. r_y^* = the distance at which the elastic determined σ_{22}-stress exceeds the yielding stress of the material, f_y.

From figure A.9 it is seen that σ_{22} exceeds the yielding stress f_y at a distance of the length r_y^*, where r_y^* is used as the first approximation of the extent of the yielding zone in the x_1-direction. Inserting f_y and r_y^* in the expression for σ_{22} (see section A.1, (A.1)) it is found for $\theta = 0$ that

$$\sigma_{22} = f_y = \frac{K_I}{\sqrt{2\pi r_y^*}}$$

$$\Downarrow$$

$$r_y^* = \frac{1}{2\pi}\left(\frac{K_I}{f_y}\right)^2 \tag{A.76}$$

Since, the hatched area in figure A.9 is avoided in the assumed plastic stress distribution, the size of r_y^*, given as (A.76), is not large enough. The extent of the plastic zone is determined by calculating the total area A_1 under the curve for the elastic σ_{22} over the interval $[0\,;\, r_y^*]$. This area is to be equivalent to the area $A_2 = f_y\, r_y$, where r_y is the second approximation of the extent of the plastic zone. r_y is determined from the demand

$$A_1 = A_2$$

$$\Downarrow$$

$$\int_0^{r_y^*} \frac{K_I}{\sqrt{2\pi r}} dr = f_y r_y$$

$$\Downarrow$$

$$(2r_y^*)^{\frac{1}{2}}(\pi)^{-\frac{1}{2}}K_I = f_y r_y \tag{A.77}$$

Substitution of K_I by use of (A.76) gives

$$2f_y r_y^* = f_y r_y$$

$$\Downarrow$$

$$r_y = 2r_y^* \tag{A.78}$$

Thus, approximate determination of the extent of the plastic zone in mode I acting is performed by use of

$$r_y = \frac{1}{\pi}\left(\frac{K_I}{f_y}\right)^2 \tag{A.79}$$

The distribution of σ_{22} is found by a parallel displacement of the elastic curve (see figure A.9) the distance r_y^* to the right and afterwards cutting off the curve at $\sigma_{22} = f_y$, see figure A.10

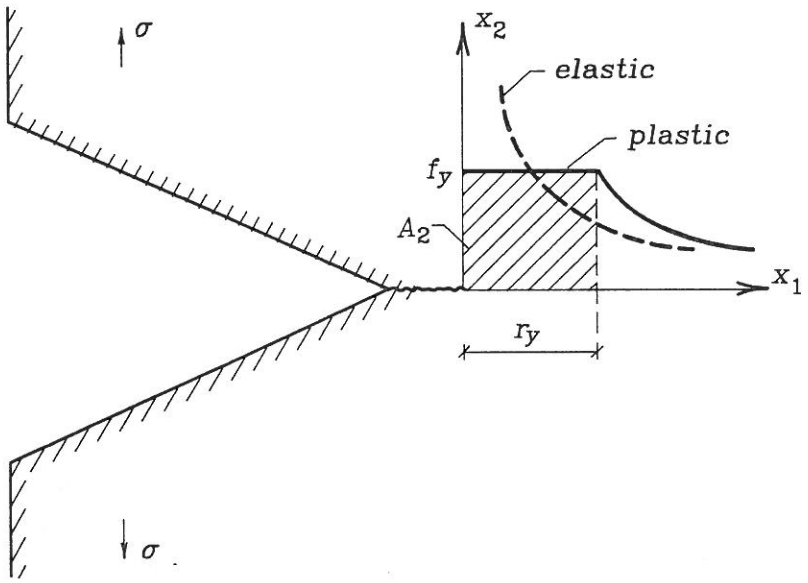

Figure A.10: Distribution of σ_{22} for $\theta = 0$ in mode I acting.

The size of the plastic zone in mode II can be determined in exactly the same way as in mode I. The only difference is that σ_{22} for mode II, see section A.1 (A.4), has to be used. Thus,

$$r_y = \frac{1}{\pi}\left(\frac{K_{II}}{f_y}\right)^2 \tag{A.80}$$

Finally, in mode III the shear stress σ_{32}, see section A.1 (A.7), cannot exceed the shear yield stress τ_y. Using the same arguments as before, the extent of the plastic zone in mode III is

$$r_y = \frac{1}{\pi}\left(\frac{K_{III}}{\tau_y}\right)^2 \tag{A.81}$$

The extent of the plastic zone in the three modes is established under the assumption of plane stress. The extent of the plane strain plastic zone is one-third of the plane stress values because, it requires three times the yield stress in plane stress to obtain a plane strain plastic zone. Thus, (A.70)-(A.81) are reduced by a factor three in plane strain.

B. EXAMPLE OF THE USE OF THE RAIN-FLOW COUNTING METHOD AND THE RANGE PAIR COUNTING METHOD

This appendix serve as an illustation of how the two counting methods, the Rainflow Counting Method and the Range Pair Counting Method, are used. The discussion of the methods are performed in section 2.3.

The example is based on figure B.1 showing a relization of a random load.

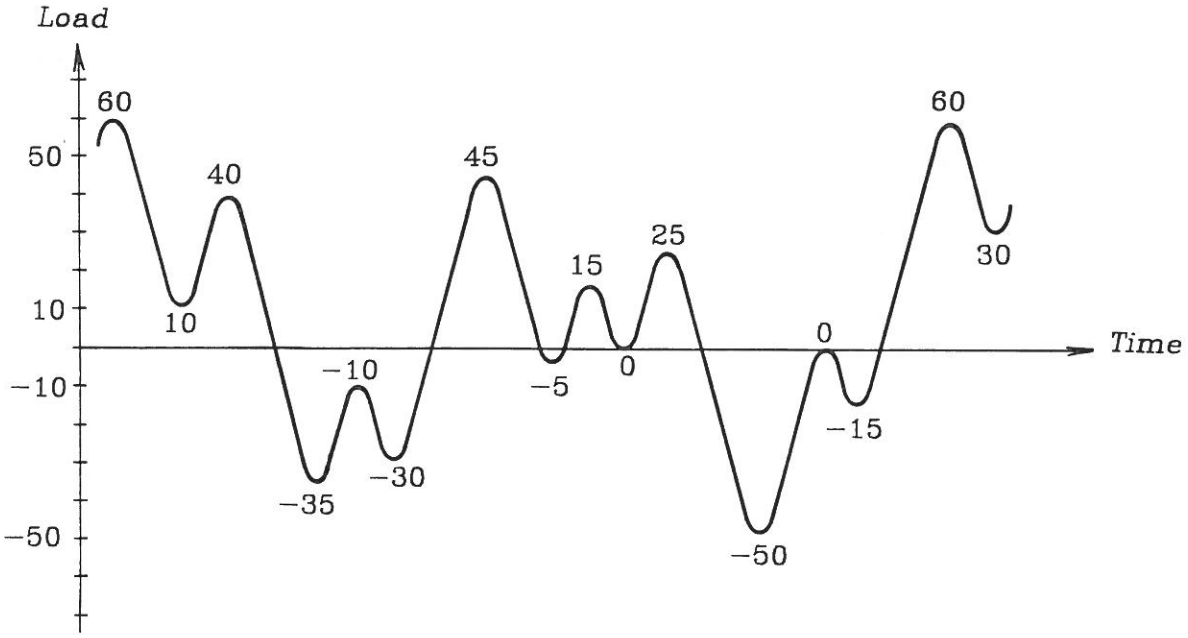

Figure B.1: Realization of a random load.

The procedure in the Rainflow Counting Method appears from the following and figure B.2.

1. The realization of the stochastic process is replaced by a sawtooth pattern with the magnitude of the peaks and troughs unchanged. (Figure B.1 → figure B.2(a)).
2. The load is rearranged to start with the highest peak, (Figure B.2(b): 60).
3. Start from the highest peak and go down to the next reversal, (60 → 10). Proceed horizontally to the next downward range and go down to the next reversal, (10 → -35) and (-35 → -50). If there is no range going down from the level of the trough at which was stopped, proceed upward to the next reversal, (-50 → 0).
4. Repeat the same procedure upward instead of downward, (0 → 60) and continue these steps to the end.
5. Repeat the procedure 2-4 for all parts that were not used in previous procedures. (Figure B.2(c): 60 → 30, 45 → -5 → -35, -35 → -10 → 45, 0 → -15, -15 → 0, 10 → 40, 40 → 10, figure B.2(d): 25 → -5, -5 → 15 → 25, -10 → -30, -30 → -10 and figure B.2(e): 15 → 0 → 15).

Thus, it is assumed that the numerical greatest peak value is positive. If this is not the case, start from the smallest trough and go upward instead.

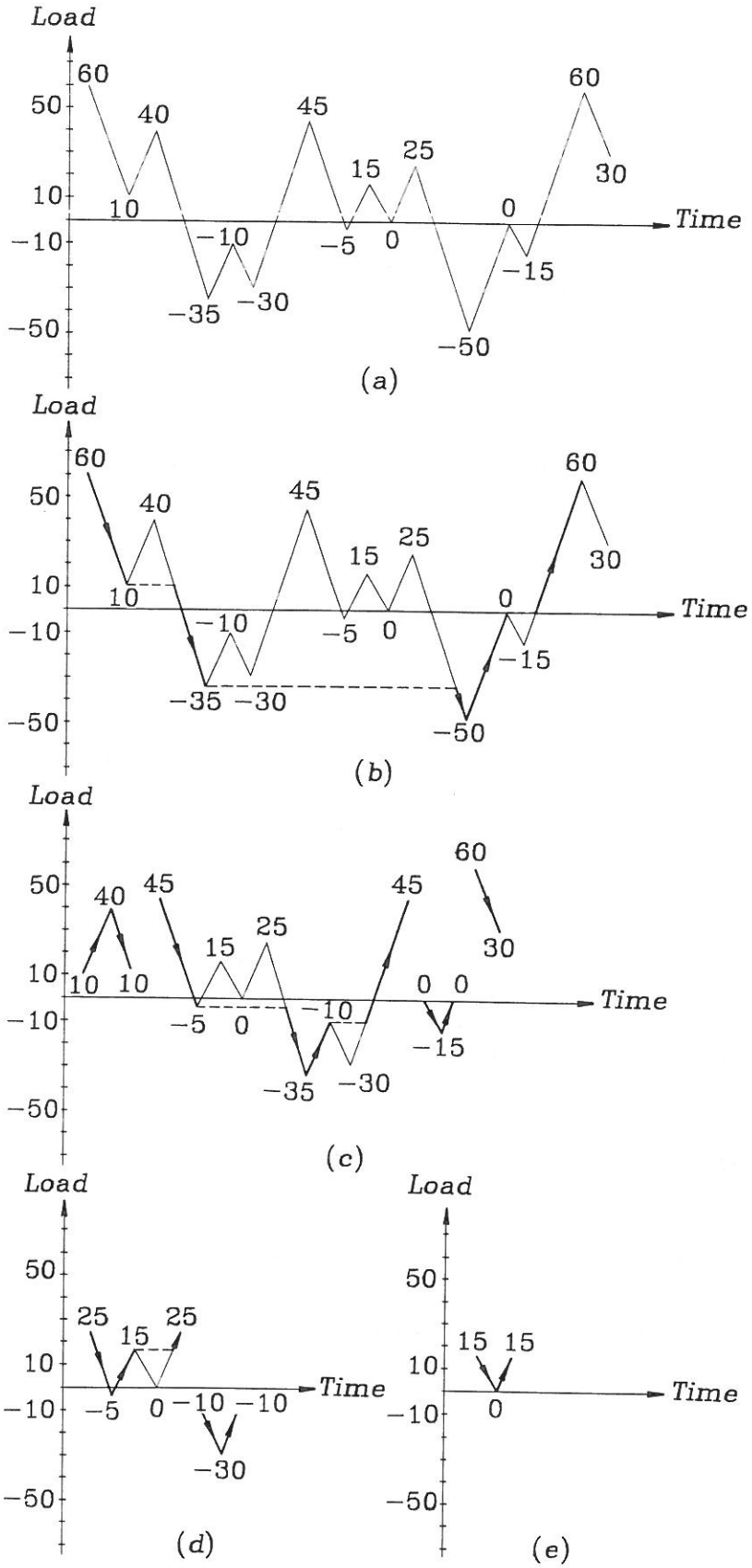

Figure B.2: The principle in the Rainflow Counting Method.

Each complete path, e.g. (60 → 10 → -35), is regarded as a half cycle (simple range). The half cycles are counted and the result for the realization in figure B.1 and figure B.2 is given in table B.3.

Range	Positive half-cycles	Negative half-cycles	Total cycles
110	-50 → 0 → 60	60 → 10 → -35 → -50	1
80	-35 → -10 → 45	45 → -5 → -35	1
30	10 → 40, -5 → 15 → 25	40 → 10, 60 → 30, 25 → -5	$2\frac{1}{2}$
20	-30 → -10	-10 → -30	1
15	-15 → 0, 0 → 15	0 → -15, 15 → 0	2

Table B.3: Rainflow Counting corresponding to figures B.1 and B.2.

In the Range Pair Counting Method, a range is defined as the part of the realization between two adjacent points of reversal. Both the positive (ascending) and the negative (descending) ranges are counted. The cycles are formed by pairing positve and negative ranges of the same size. The results for the realization in figure B.1 is given in tabel B.4.

Range	Positive half-cycles	Negative half-cycles	Total cycles
75	-30 → 45, -15 → 60	40 → -35, 25 → -50	2
50	-50 → 0	60 → 10, 45 → -5	$1\frac{1}{2}$
30	10 → 40	60 → 3	1
25	-35 → -10, 0 → 25		1
20	-5 → 15	-10 → -30	1
15		15 → 0, 0 → -15	1

Table B.4: Range Pair Counting corresponding to figure B.1.

C. C-PROGRAMS

In this appendix an overview of the most important programs developed in connection with the thesis are given. All the programs are made in the programming language "C" by the author.

SIMULA

SIMULA is used to simulate FMF-data, i.e. (N, a)-data corresponding to the FMF-model.

On the basis of the input parameters, which are the initial and the failure crack length (a_0 and a_f), the stress range ($\Delta\sigma$), the number of cycles in each duty cycle (λ) and the step length δa besides the experimentally determined material constants C and m, the program calculates the probability of remaining in the given crack state.

A random generator, see [Brincker, R. and J.D. Sørensen; 1990], decides if the crack remains in the same crack state or propagates to the next state after applying a duty cycle. Thus, only if the random number is larger than the transition probability of the given crack state, the crack will propagate. Otherwise, the crack remains in the given state. This procedure is continued until the failure crack length is reached. Every time the crack propagates, the present (N, a)-value is written in the output file. Parameters which are varied are λ and δa.

SORT

SORT sorts the simulated FMF-data (VSIM) so only crack lengths corresponding to the Virkler data are selected

VNORM

VNORM is used to make a quantitative comparison of the Virkler data and the FMF-data (VSIM) using the following norm

$$q_X = \left[\sum_{j=0}^{n} (x_{\text{VSIM}} - x_{\text{VIRKLER}})^2 \right]^{\frac{1}{2}} \tag{C.7}$$

where

X	=	the statistical property in consideration
n	=	162 for δN_j and 163 for N_j
x_{VSIM}	=	statistical value of VSIM 2-4 and VSIM 6-8
x_{VIRKLER}	=	statistical value of the Virkler data

INI

INI transforms the observed crack growth data into (N, a)-data changing them so they obtain the same initial values (N_0, a_0).

PARIS

PARIS applies linear regression analysis to experimental data for calculating the material constants C and m. The program has been used on the Virkler data and on the experimental data from the CA-load tests.

STAT-PACK

The programs in **STAT-PACK** calculates the mean value, the standard deviation and the probability density function value of the number of cycles applied in each crack state to reach the successive state and of the total number of cycles applied to reach a given crack state, i.e.

$$\overline{\delta N_j} = \frac{1}{n}\sum_{i=1}^{n}(\delta N_j)_i \tag{C.1}$$

$$S_{\delta N_j} = \left[\frac{1}{n-1}\sum_{i=1}^{n}((\delta N_j)_i - \overline{\delta N_j})^2\right]^{\frac{1}{2}} \tag{C.2}$$

$$f_{\delta N_j} = \sum_{i=1}^{n}(\delta N_j | \delta N_j \in]k\cdot 250; (k+1)\cdot 250]) \qquad k = 0,1,2,\ldots,39 \tag{C.3}$$

$$\overline{N_j} = \frac{1}{n}\sum_{i=1}^{n}(N_j)_i \tag{C.4}$$

$$S_{N_j} = \left[\frac{1}{n-1}\sum_{i=1}^{n}((N_j)_i - \overline{N_j})^2\right]^{\frac{1}{2}} \tag{C.5}$$

$$f_{N_j} = \sum_{i=1}^{n}(N_j | N_j \in]k\cdot 10000; (k+1)\cdot 10000]) \qquad k = 0,1,2,\ldots,39 \tag{C.6}$$

where

$$\begin{aligned} i &= 1,2,\ldots,n \\ j &= 0,1,2,\ldots,n \end{aligned}$$

n = number of crack states
δN_j = number of load cycles applied at the crack state j
$\overline{\delta N_j}$ = mean value of the number of load cycles applied at the crack state j
$S_{\delta N_j}$ = standard deviation of the number of load cycles applied at crack state j
$f_{\delta N_j}$ = probability density function value of the number of load cycles applied at crack state j
N_j = total number of load cycles applied to reach the crack state j
$\overline{N_j}$ = mean value of the total number of load cycles applied to reach the crack state j
S_{N_j} = standard deviation of the total number of load cycles applied to reach the crack state j
f_{N_j} = probability density function value of total number of load cycles applied to reach crack state j

The probability density is found by dividing the sample space into 40 intervals and then at each crack state counting the number of events in each interval.

The **STAT-PACK** consists of 4 programs

- **VSTAT** used on the Virkler data ($n = 68$, $j = 164$)
- **STAT** used on the FMF-data from simulation series VSIM ($n = 500$, $j = 164$)
- **CASTAT** used on the experimental data ($n = 34$, $j = 145$)
- **ESIMSTAT** used on the FMF-data from simulation series ESIM ($n = 500$, $j = 145$)

Besides, **CASTAT** performs interpolation so the (N, a)-data are known for fixed values of the crack length a. Likewise, **ESIMSTAT** performs interpolation on the FMF-data from ESIM in order to select the same a-values as in **CASTAT**.

D. SIMULATED FATIGUE CRACK GROWTH CURVES WITH VIRKLER PARAMETERS

In this appendix, the fatigue crack growth curves obtained by simulations with the Virkler parameters are shown. The simulations are performed by the program **SIMULA** (see appendix C). The input parameters are outlined in tables 6.8 and 6.9 in chapter 6 in which the evaluation of the curves is found.

The number of data set in each simulation series is 500, but for simplicity only 100 data sets are shown in each plot. Further, only one typical plot from each simulation series is shown, see figure D.1-D.8. The remaining plots and the data are obtainable from the author.

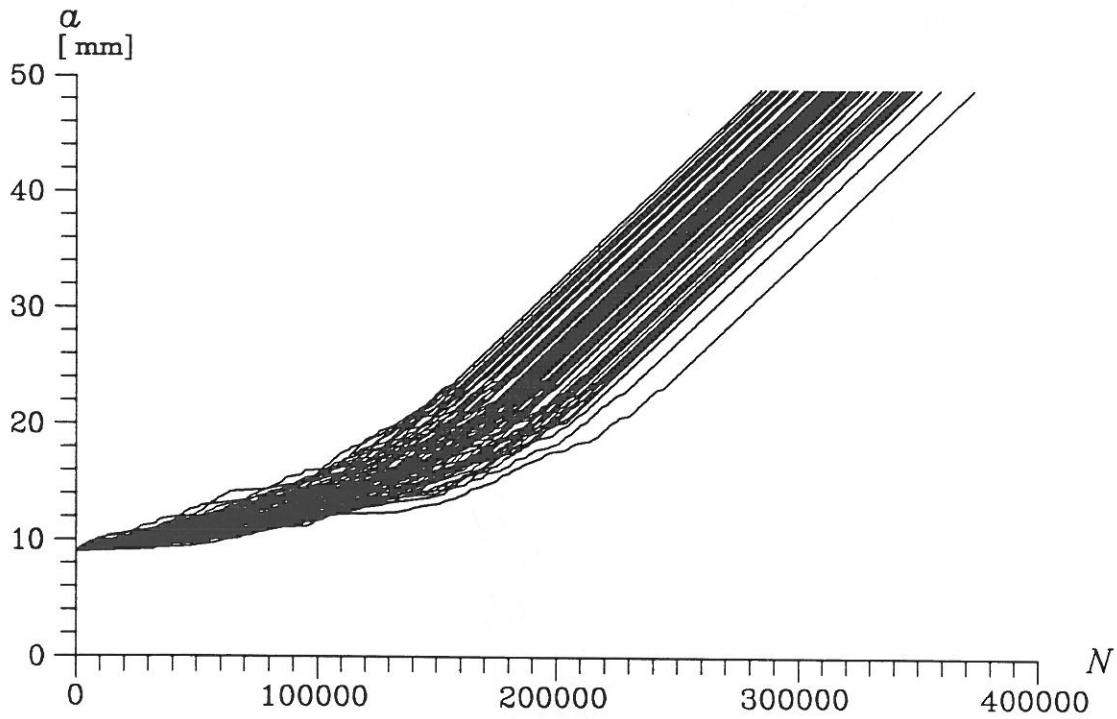

Figure D.1: Typical plot of (N, a)-curves from simulation series VSIM 1.
N = number of load cycles, a = crack length.

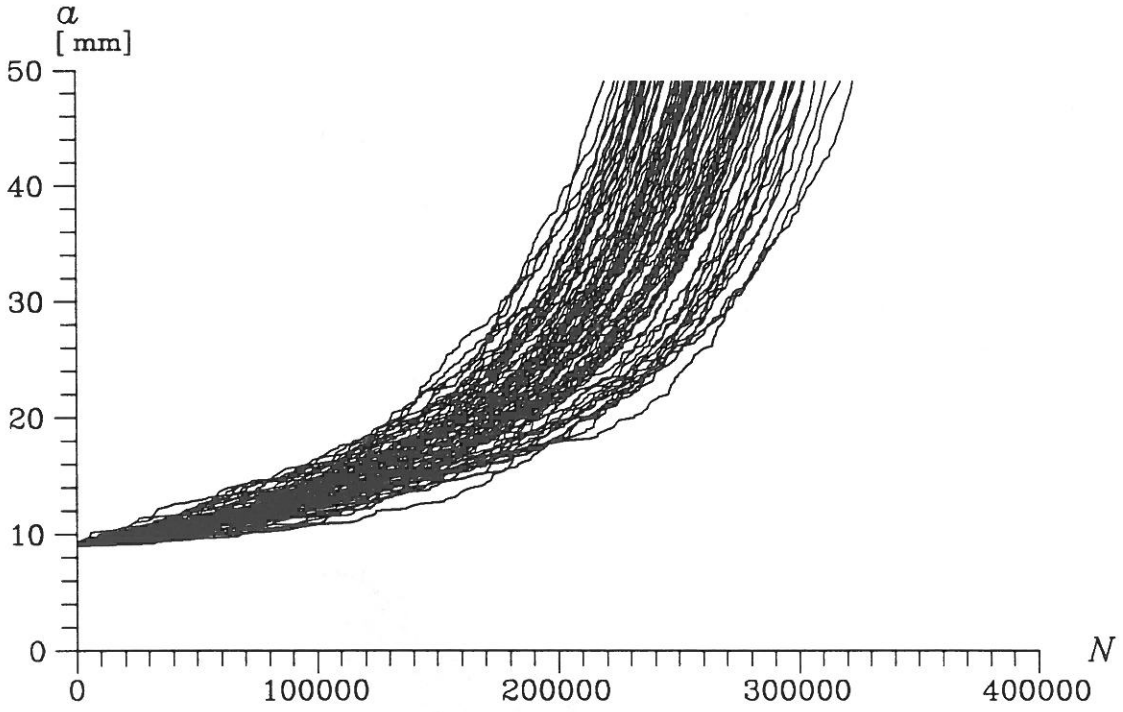

Figure D.2: Typical plot of (N, a)-curves from simulation series VSIM 2.
N = number of load cycles, a = crack length.

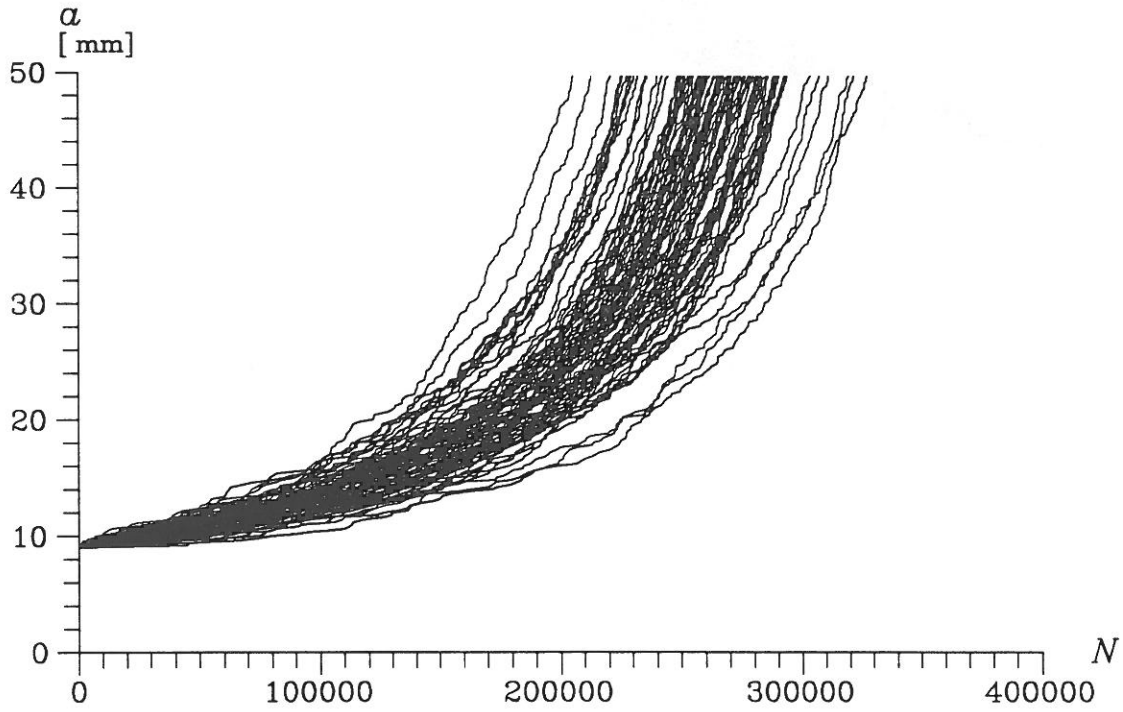

Figure D.3: Typical plot of (N, a)-curves from simulation series VSIM 3.
N = number of load cycles, a = crack length.

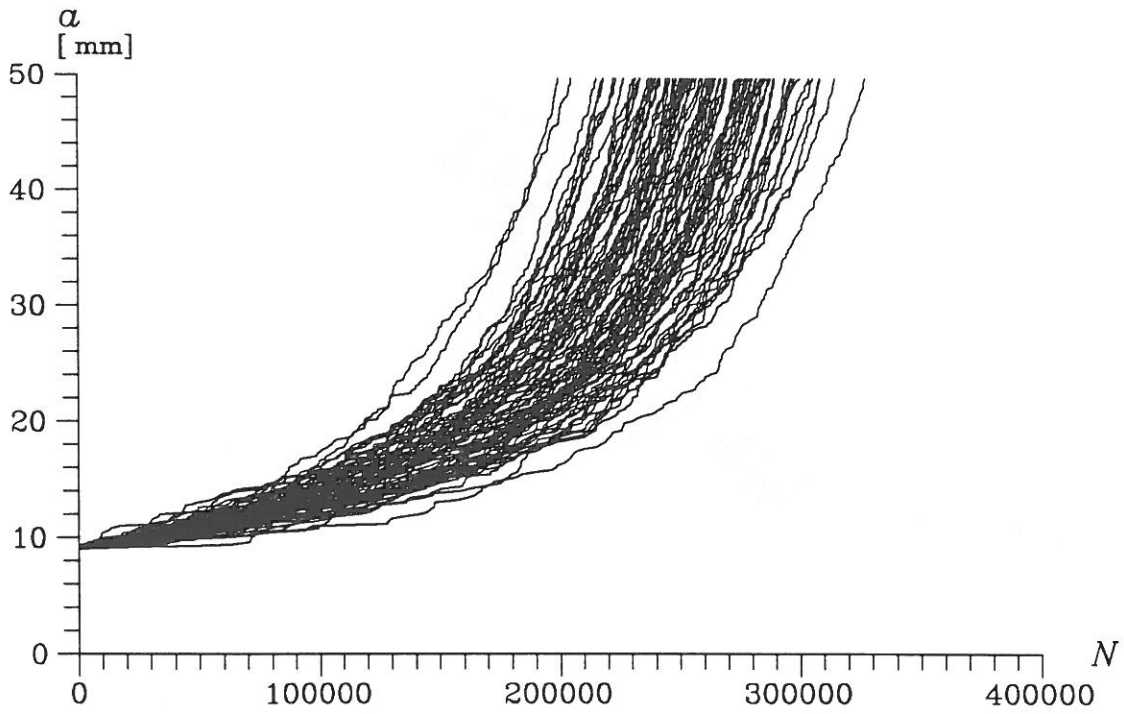

Figure D.4: Typical plot of (N, a)-curves from simulation series VSIM 4.
N = number of load cycles, a = crack length.

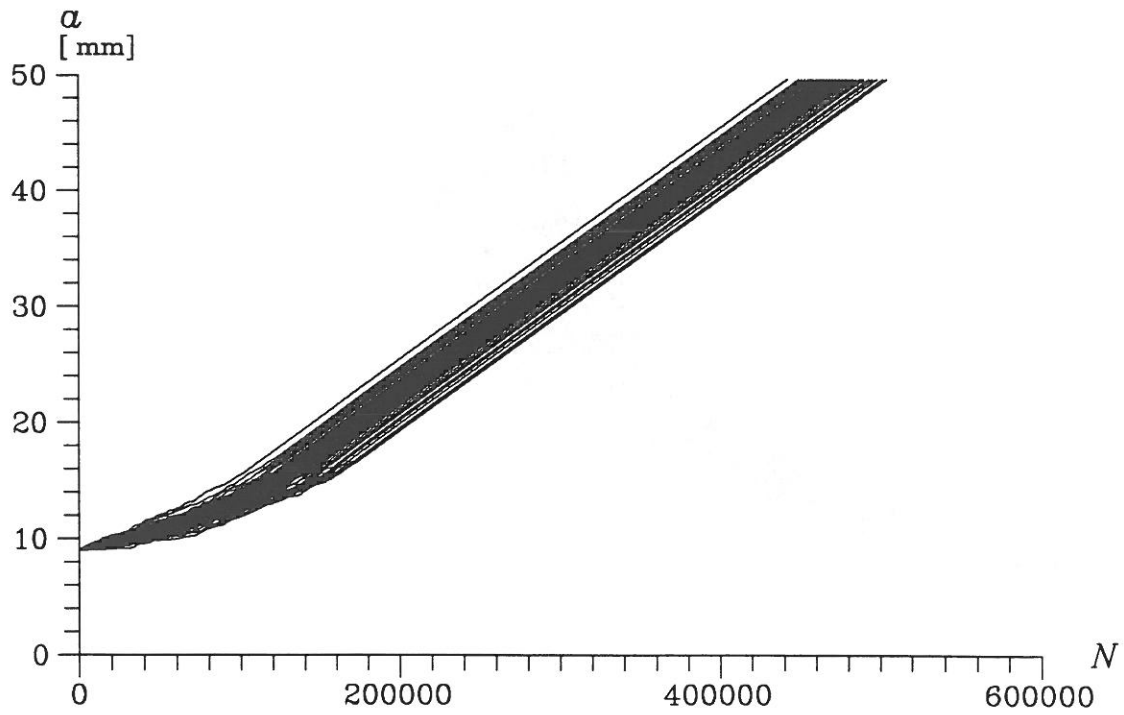

Figure D.5: Typical plot of (N, a)-curves from simulation series VSIM 5.
N = number of load cycles, a = crack length.

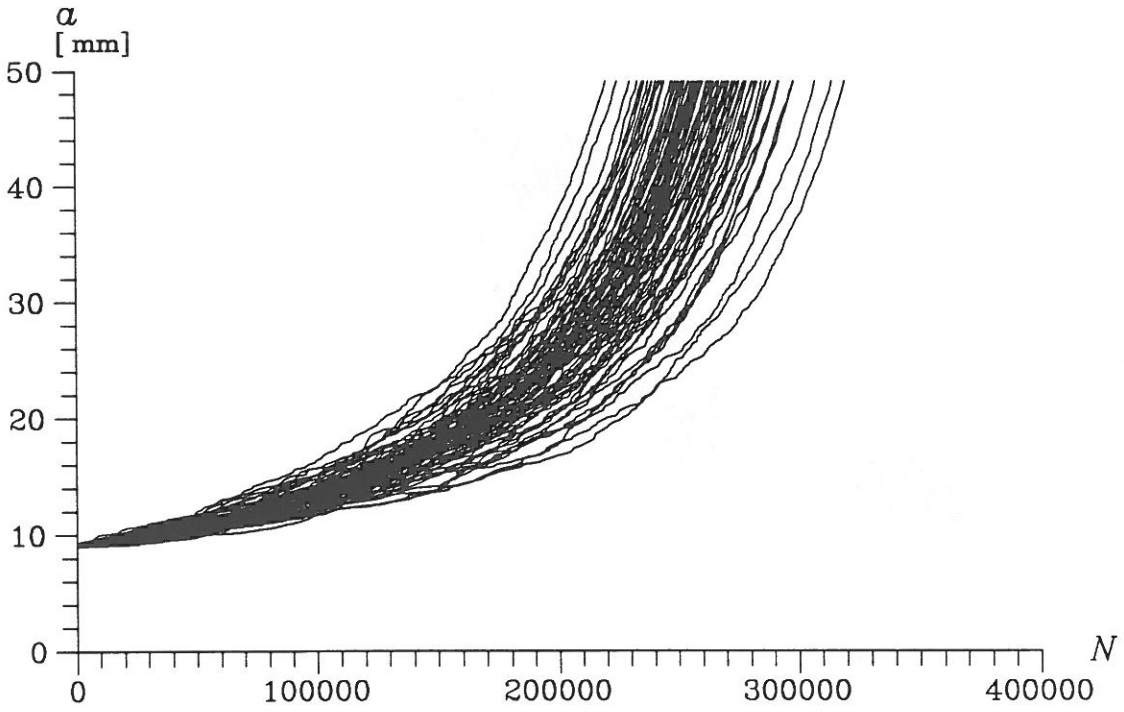

Figure D.6: Typical plot of (N, a)-curves from simulation series VSIM 6.
N = number of load cycles, a = crack length.

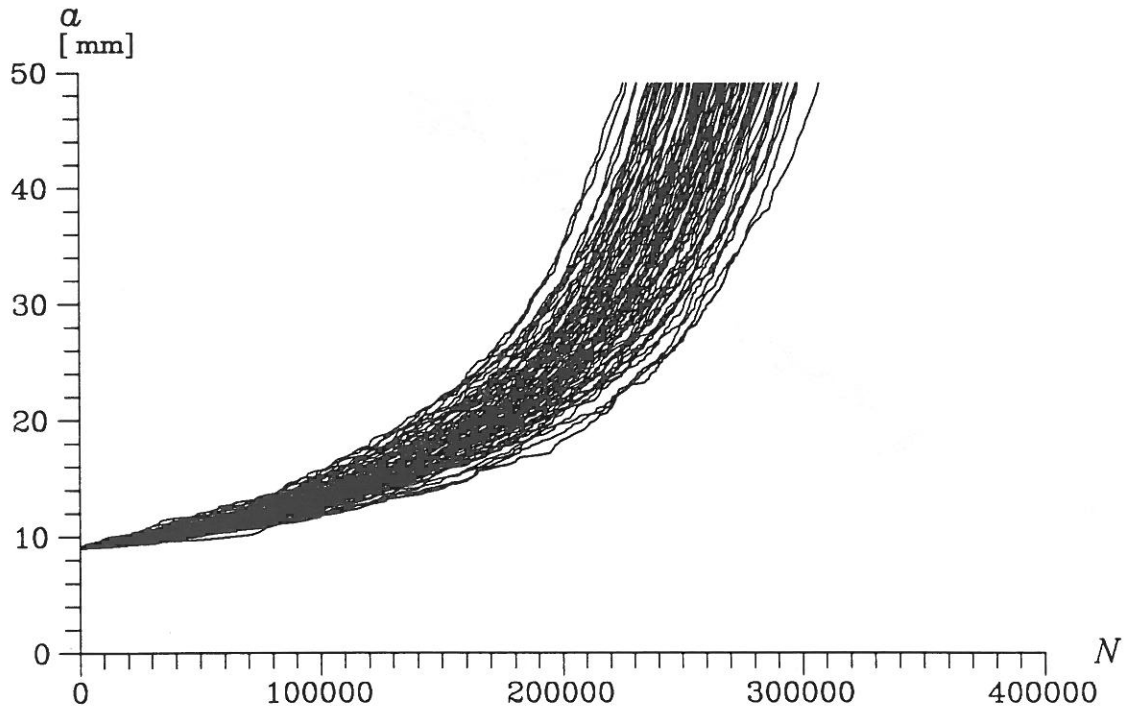

Figure D.7: Typical plot of (N, a)-curves from simulation series VSIM 7.
N = number of load cycles, a = crack length.

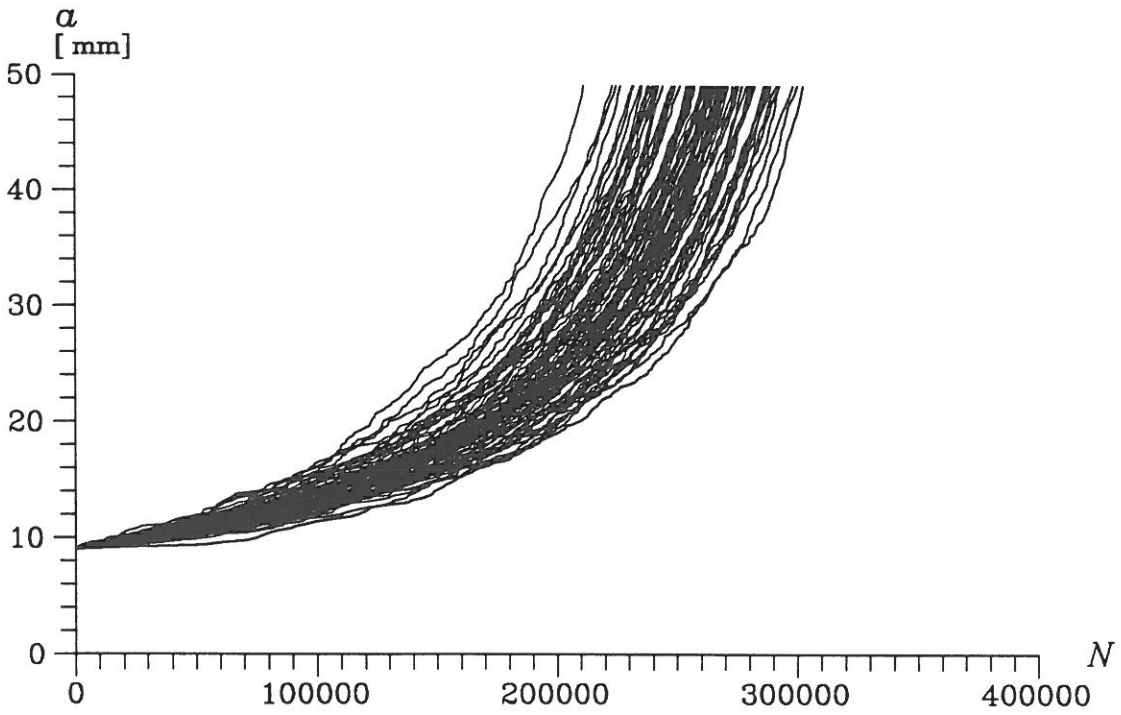

Figure D.8: Typical plot of (N, a)-curves from simulation series VSIM 8.
N = number of load cycles, a = crack length.

E. SIMULATED FATIGUE CRACK GROWTH CURVES WITH EXPERIMENTAL PARAMETERS

In this appendix, the fatigue crack growth curves obtained by simulations with the experimental parameters are shown. The simulations are performed by the program **SIMULA** (see appendix C). The input parameters are outlined in section 7.2 in which the evaluation of the curves is found.

The number of data set in the simulation series is 500, but for simplicity only 100 data sets are shown in each plot. The data are obtainable from the author.

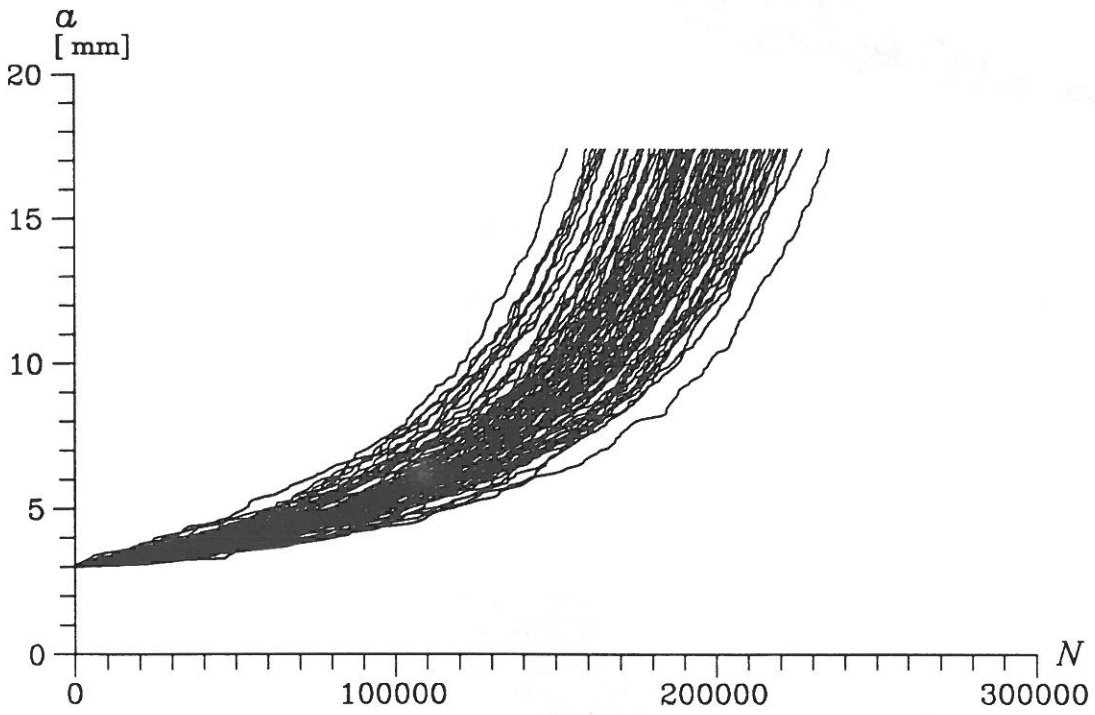

Figure E.1: Plot of (N, a)-curves 1-100 from simulation series ESIM.
N = number of load cycles, a = crack length.

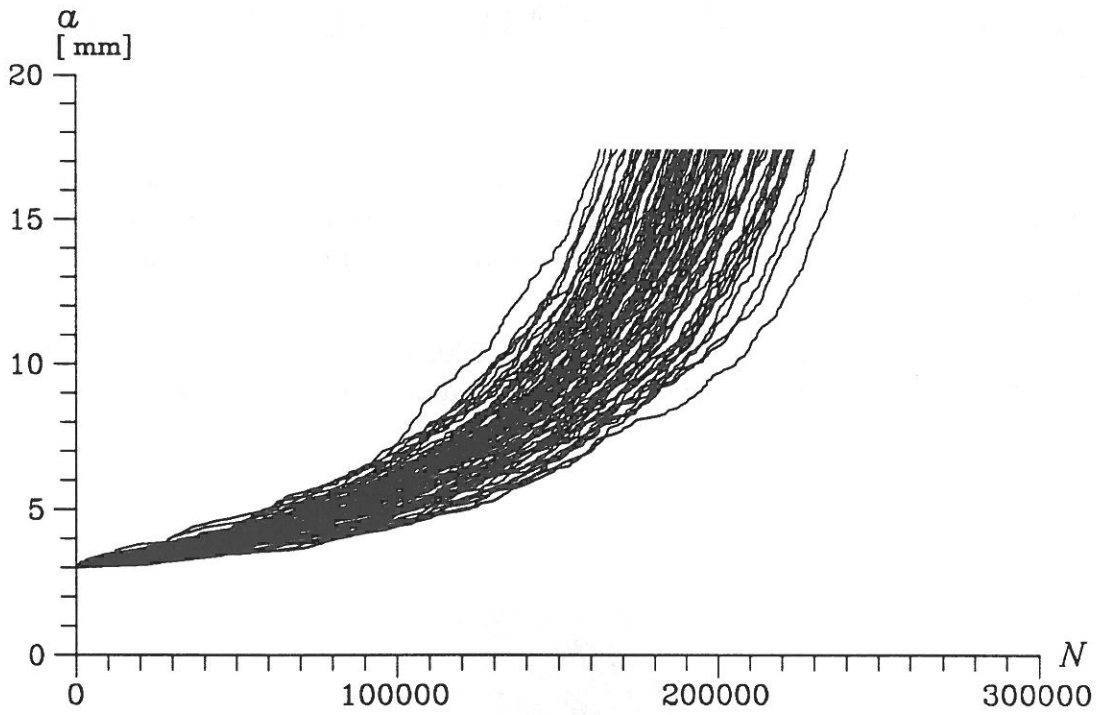

Figure E.2: Plot of (N, a)-curves 101-200 from simulation series ESIM.
N = number of load cycles, a = crack length.

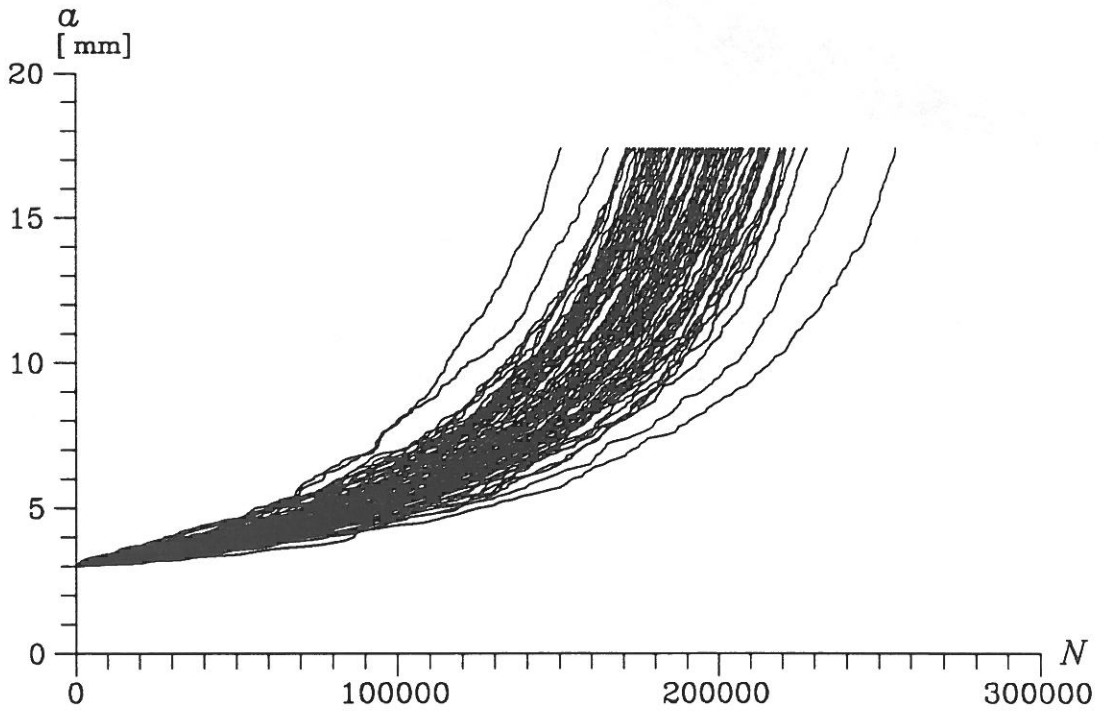

Figure E.3: Plot of (N, a)-curves 201-300 from simulation series ESIM.
N = number of load cycles, a = crack length.

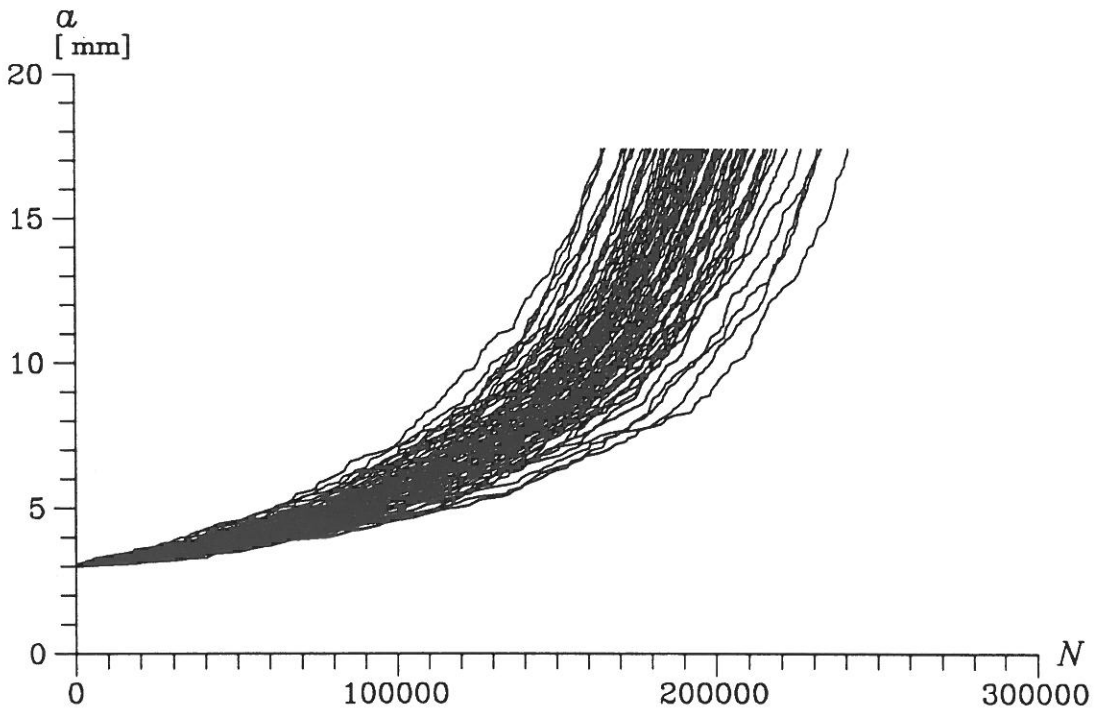

Figure E.4: Plot of (N, a)-curves 301-400 from simulation series ESIM.
N = number of load cycles, a = crack length.

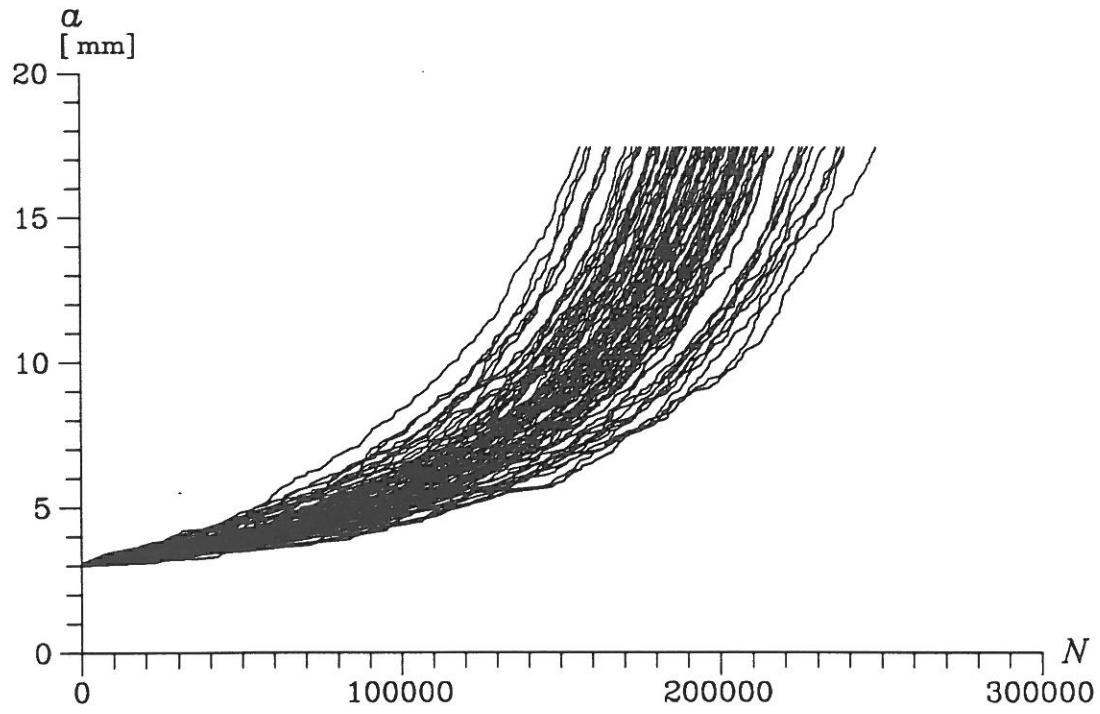

Figure E.5: Plot of (N, a)-curves 401-500 from simulation series ESIM.
N = number of load cycles, a = crack length.